SYNTHESIS OF POLYANILINE HYBRIDS OF GRAPHENE/MWNT FOR PHOTOCURRENT GENERATION AND OPTICAL LIMITING APPLICATIONS

A Thesis submitted

in partial fulfillment for the Degree of

Doctor of Philosophy

by

REMYAMOL T.

Department of Chemistry

INDIAN INSTITUTE OF SPACE SCIENCE AND TECHNOLOGY

THIRUVANANTHAPURAM

MARCH, 2014

CERTIFICATE

This is to certify that the thesis entitled **Synthesis of polyaniline hybrids of graphene/MWNT for photocurrent generation and optical limiting applications** submitted by **Remyamol T** to the Indian Institute of Space Science and Technology, Thiruvananthapuram, in partial fulfillment for the award of the degree of **Doctor of Philosophy** is a *bona fide* record of research work carried out by her under our supervision. The contents of this thesis, in full or in parts, have not been submitted to any other Institution or University for the award of any degree or diploma.

Dr. Honey John
Supervisor
Department of Chemistry

Dr. Pramod Gopinath
Co-supervisor
Department of Physics

Thiruvananthapuram
March, 2014

Counter signature of HOD with seal

DECLARATION

I declare that this thesis entitled **Synthesis of polyaniline hybrids of graphene/MWNT for photocurrent generation and optical limiting applications** submitted in partial fulfillment of the degree of **Doctor of Philosophy** is a record of original work carried out by me under the supervision of Dr. Honey John and Dr. Pramod Gopinath, and has not formed the basis for the award of any other degree or diploma, in this or any other Institution or University. In keeping with the ethical practice in reporting scientific information, due acknowledgements have been made wherever the findings of others have been cited.

Remyamol T.
SC10D002

Thiruvananthapuram – 695547
28/03/2014

AKNOWLEDGEMENTS

This dissertation would not have been possible without many people who were always there when I needed them the most.

I would first like to express my sincere thanks to my thesis supervisor Dr. Honey John for her strong motivation, great patience and constructive criticism apart from invaluable guidance to me. I am blessed and privileged to finish my thesis under her guidance, who trusted me completely and gave freedom to explore ideas of my own. Rather than as a supervising guide, I am deeply indebted to her motherly affection in taking utmost care to listen to my professional and personal hardships. I am thankful to the encouragement showered upon me by her family especially her husband. Without her continuous encouragement, I could not imagine this thesis ever becoming a reality.

I am thankful to Dr. Pramod Gopinath, my co-supervisor for his encouragement and wise advices for the research work. I am fortunate enough to work under a personality like him, a perfectionist who took much pain and patience to go through our papers and this dissertation, checking each word and punctuations, giving suggestions and corrections which helped me improve it immeasurably.

I take this opportunity to thank Director, IIST and Department of Space for providing me the prestigious IIST-ISRO research fellowship. My thanks to Dr. V. Adimurthy, former Dean R & D and Dr. Thomas Kurien, Dean R& D, for their support and timely review to finish this thesis. My special thanks to Prof. Kuruvilla Joseph, HOD, Chemistry who always took keen interest in rendering good laboratory facilities. I am indebted to the support extended to me by Dr. K.N. Ninan, faculty members of Department of Chemistry, and my fellow research students. I would also like to thank Dileepettan and all the staff members of Department of Chemistry for their whole hearted support.

I remember with sincere gratitude, the positive suggestions and corrections given to my work by the doctoral committee members. I would like to express my sincere gratitude and appreciation to Dr. Reji Philip, Raman Research Institute, Bangalore and his students for providing their open aperture Z scan facility. During the finishing stage of my work, I enjoyed the benefit of excellent discussions with Jinesh sir. My sincere gratitude for all his help, valuable suggestions and corrections during thesis writing. Many thanks to Gigy Mam for all the support and prayers she extended to me while writing this thesis. In spite of her busy schedule she was kind enough to go through my thesis, checking each word and sentences, giving suggestions etc.

I cannot forget my intimate and gratifying relationship with my fellow researchers, Kavitha, Haripadmam, Jalaja, Sarah, Sarika and Dhanyechi. Special thanks to Ms. Kavitha M. K. for the fruitful discussions during the research work. Special thanks go to Library and Reprographic facility, IIST for printing facilities, IITM for XRD and SEM measurements, NIIST for TEM measurements and AIMS for Raman and XPS measurements.

The support of my family gave me immense strength and determination to complete the research programme. I am grateful to my parents, achachan, dearest brother and other family members who encouraged and listened to me throughout my studies. Without them I would not be where I am now. The remarkable love, patience, understanding and continuous encouragement of my husband Mr. Susil Raj K. kept me going during the research programme. He was with me through the thick and thin and patiently suffered along with me without a word of grudge or impatience. I wish to take this opportunity to thank my in laws for their constant support to finish my research work.

Last but not least, I praise God almighty for inspiring me to pursue research and for helping me to overcome the hurdles that I faced along the way.

Remyamol T.

ABSTRACT

In the last few years polyaniline, an environmentally and thermally stable, easily processable conducting polymer, in nano regime attracted enormous interest of the researchers owing to its lightweight, flexibility, ease of device fabrication in large areas and control over electrical and optical properties. Also there has been a notable enthusiasm in graphene research since the discovery of graphene in 2004 by the mechanical exfoliation of graphite using scotch tape. The combination of polyaniline and graphene/carbon nanotubes offers an attractive way for the generation of new hybrid materials that find a range of applications such as photovoltaics, optical limiters, sensors, actuators, transistors, etc.

This thesis focuses on the synthesis, characterization and property evaluation of polyaniline in nano dimensions and its hybrids with graphene and multiwalled carbon nanotubes. Polyaniline nanostructures with cube-like morphology are synthesized by a novel inverse microemulsion polymerization technique using ammonium oleate as the surfactant and toluene sulphonic acid as the dopant. The formation mechanism of cube-like nanostructures by the self assembly of polyaniline nanorods inside the inverse micelles of ammonium oleate in the paraffin–oil water system is proposed with the support of experimental techniques. The suitability of cube-like polyaniline for optical limiting and photocurrent generation applications are studied (This part of the work is published in *Synthetic Metals* 2013). The optical limiting device applications require easy fabrication of films of nonlinear optical materials in a transparent host. In this respect, films of cube-like polyaniline in transparent polymer matrix (polymethyl methacrylate) are fabricated by *in situ* free radical polymerization of methyl methacrylate in the presence of cube-like polyaniline. Detailed studies on the nonlinear optical properties of the films are carried out using open aperture Z scan technique by varying the polyaniline loading and also by varying the laser energy. A switchover from saturable absorption to reverse saturable absorption is observed in the film (0.1 wt % polyaniline loading in the monomer) as the energy of laser beam increases from 5 μJ to 100 μJ (This part of the work is published in *Materials Chemistry and Physics* 2014).

Both applications (optical limiting and photocurrent generation) under study can be improved by the combination of electron donating polyaniline with an electron acceptor material. Stable carbon allotropes like carbon nanotubes and graphene are well known electron acceptor materials and photoinduced electron transfer from conjugated polymer to these materials are already reported. To initiate the study, polyaniline is hybridized with graphite oxide by *in situ* polymerization of aniline in the presence of synthesized graphite oxide. The hybrid shows photoluminescence quenching compared to pure polyaniline. The hybrid also shows strong optical limiting (high nonlinear absorption coefficient, β=19 cm/GW and low saturation intensity, I_{sat}=0.4 GW/cm^2) than individual components due to the photoinduced electron transfer between polyaniline and graphite oxide and the synergetic combination of reverse saturable absorption of polyaniline and nonlinear scattering of graphite oxide. The hybrid shows stable photocurrent cycles upon repetitive switching (on/off) of illumination with white

light for 30 second duration (intensity of light is 100 mW/cm^2). The photocurrent generated by this class of hybrid (9.1 μA) is higher than that of pristine polyaniline (4.6 μA) and it increases as the graphite oxide loading increases (published in *Materials Research Express 2014*).

With the aim of improving the properties of polyaniline/graphite oxide hybrid through covalent connection, phenylene diamine functionalized reduced graphene oxide is synthesized. By this modification of graphite oxide, significant reduction and exfoliation is achieved and aniline monomer is introduced on the reduced graphene oxide layers. The presence of phenylene diamine groups on reduced graphene oxide results in the formation of hybrids with covalent connections during the *in situ* polymerization of aniline. Photoluminescence quenching is more significant in this hybrid compared to unfunctionalized graphite oxide-polyaniline hybrid, revealing better electron transfer through the direct covalent linkage between polyaniline and reduced graphene oxide. This covalently connected hybrid shows better optical limiting (β=25 cm/GW, I_{sat}=0.2 GW/cm^2) compared to pristine polyaniline (β=5.8 cm/GW, I_{sat}=2.5 GW/cm^2) and polyaniline-graphite oxide hybrid (published in *Carbon* 2013). The hybrid also shows dc conductivity (6.3 S/cm), 200 times higher than that of polyaniline-graphite oxide hybrid (0.03 S/cm). Moreover, this hybrid shows a photocurrent of 29 μA, while the corresponding polyaniline-graphite oxide hybrid and pristine polyaniline shows only 9.1 and 4.6 μA, respectively. This large improvement in dc conductivity and photocurrent is attributed to the formation of direct conducting pathways by the covalent connection and may be due to the photoinduced electron transfer from polyaniline to reduced graphene oxide (Published in *RSC Advances 2014*).

To study the optical limiting and photocurrent generation properties of polyaniline/carbon nanotube hybrids, polyaniline-phenylene diamine functionalized multiwalled carbon nanotube hybrids through covalent connections are synthesized by the same methodology adopted for polyaniline-phenylene diamine functionalized reduced graphene oxide hybrid. This hybrid also shows photoluminescence quenching, improved optical limiting (β=23 cm/GW, I_{sat}=0.3 GW/cm^2) and photocurrent generation (10 μA) compared to pristine polyaniline.

Finally, the synthesized cube-like polyaniline is grafted on reduced graphene oxide layers by utilizing acylation chemistry of graphite oxide followed by amide bond forming reaction between amine groups of polyaniline and acid chlorides of graphite oxide. Significant reduction and exfoliation of graphite oxide is achieved in the hybrid and the cube-like morphology of pristine polyaniline is disturbed by the weakening of the interaction between polyaniline nanorods due to the introduction of reduced graphene oxide layers (published in *Synthetic Metals* 2013). The hybrid shows a dc conductivity of 6.6 S/cm. Considerable quenching of the photoluminescence of cube-like polyaniline is observed after covalent grafting on reduced graphene oxide layers due to the photoinduced electron transfer between polyaniline and reduced graphene oxide. The cube-like polyaniline grafted reduced graphene oxide hybrid shows improved optical limiting (β=20 cm/GW, I_{sat}=0.25 GW/cm^2) and photocurrent generation (31 μA) compared to pristine cube-like polyaniline (4.5 μA). The films of this hybrid in polymethyl methacrylate matrix are also fabricated and studied the nonlinear optical properties in comparison with cube-like polyaniline-polymethyl

methacrylate film with the same linear transmittance. The hybrid film shows significant contribution of reverse saturable absorption at laser energy of 5 μJ, while cube-like polyaniline film shows only saturable absorption at the same laser energy. At 45 μJ, both the films show reverse saturable absorption, but large improvement in optical limiting behaviour is observed in the hybrid film (β=320 cm/GW, I_{sat}=0.2 GW/cm^2) compared to pristine cube-like polyaniline film ((β=70 cm/GW, I_{sat}=3 GW/cm^2).

In conclusion, this thesis gives an insight into the synthesis strategies, properties, and fabrication methods which can be used for utilizing polyaniline hybrids in various applications like optical limiting devices and photovoltaics.

TABLE OF CONTENTS

LIST OF FIGURES

LIST OF TABLES

ABBREVIATIONS

µA	Microampere
µJ	Microjoule
µl	Microlitre
µm	Micrometre
0D	Zero Dimensional
1D	One Dimensional
2D	Two Dimensional
2PA	Two Photon Absorption
3D	Three Dimensional
Å	Angstrom
ABSA	Azobenzenesulphonic Acid
AFM	Atomic Force Microscope
Ag	Silver
Al	Aluminium
APS	Ammonium Persulfate
ATRP	Atom Transfer Radical Polymerization
C	Carbon
cm	Centimetre
CNTs	Carbon Nanotubes
Cu	Copper
CVD	Chemical Vapour Deposition
D_1	Detector 1
D-10-CSA	Dextro-10-Camphorsulphonic Acid
D_2	Detector 2
DBSA	Dodecylbenzenesulphonic Acid
DC/dc	Direct Current
DMF	Dimethylformamide
Eq.	Equation
ESCA	Electron Spectroscopy for Chemical Analysis

eV	Electron Volt
FCA	Free Carrier Absorption
Fig.	Figure
FTIR	Fourier Transform Infrared
FTO	Fluorine doped Tin Oxide
g	Gram
GO	Graphite Oxide
GW	Giga Watt
h	Hour
HOMO	Highest Occupied Molecular Orbital
HRTEM	High Resolution Transmission Electron Microscope
Hz	Hertz
I_b	Intensity of benzenoid C=C stretching vibration in FTIR spectrum
I_D	Intensity of D band in Raman spectrum
I_{dark}	Dark current
I_G	Intensity of G band in Raman spectrum
I_{light}	Current generated after light illumination
Iq	Intensity of quinonoid C=C stretching vibration in FTIR spectrum
IR	Infrared
K	Kelvin
kV	Kilo Volt
L-10-CSA	Leavo-10-Camphorsulphonic Acid
LUMO	Lowest Unoccupied Molecular Orbital
M	Molar
m	Meter
mg	Milligram
min	Minute
ml	Millimetre
MPA	Multi Photon Absorption
MV	Mega Volt

MWNT	Multi Walled Carbon Nanotube
N	Nitrogen
Nd:YAG	Neodymium-doped Yitrium Aluminum Garnet
NIR	Near Infrared
NLO	Nonlinear Optical
nm	Nanometer
NS	Nobel Symposium
ns	Nanosecond
O	Oxygen
^{o}C	Degree Celsius
P3HT	Poly-3-hexyl thiophene
pH	Potential of Hydrogen
PMMA	Polymethyl Methacrylate
PmPV	Poly (m-phenylenevinylene-co-2,5-dioctoxy-p-phenylenevinylene)
PMT	Photomultiplier Tube
Pt	Platinum
PVK	Polyvinyl Carbazole
rpm	Revolutions Per Minute
RSA	Reverse Saturable Absorption
S	Sulphur
S/cm	Siemens per centimetre
SA	Saturable absorption
SAED	Selected Area Diffraction Pattern
SAN	o-aminobenzenesulphonic acid
SEM	Scanning Electron Microscopy
SWNT	Single Walled Carbon Nanotube
TEM	Transmission Electron Microscope
TGA	Thermogravimetric Analysis
TPa	Terapascal
TSA	Toluenesulphonic Acid
UV	Ultraviolet

W	Watts
wt %	Weight percentage
XPS	X-ray Photoelectron Spectroscopy
XRD	X-ray Diffraction
β-NSA	β-Naphthalenesulphonic Acid

NOTATIONS

λ	Wavelength
d	Crystal lattice spacing
θ	Angle of diffraction
α	Absorption coefficient
B	Fitting parameter in Tauc equation
h	Planks constant
ρ	Resistivity
E_g	Band gap
L	Thickness of the sample of Z scan experiment
ω_0	Beam waist
Z_0	Diffraction length of the focussed laser beam
I	Current
α_0	Linear absorption coefficient
α_2	Two photon absorption coefficient
z	Position
υ	Frequency
R	Reflectance
t	Thickness of the pellet for DC conductivity measurements
I_i	Incident beam intensity
I_e	Intensity of the beam at the exit surface of the sample
I_0	Intensity of the beam at the focus
T	Transmittance
V	Voltage
s	Spacing of four point probes
ln	Natural logarithm
λ_{max}	Absorption maximum
E(z)	Input fluence at each z position
E_{in}	Input laser energy

β	Nonlinear absorption coefficient
I_{sat}	Saturation intensity
$\omega(z)$	Beam radius

NOMENCLATURE

C_{60}	Fullerene
SiC	Silicon Carbide
NH_3	Ammonia
H_2SO_4	Sulfuric acid
HNO_3	Nitric acid
$KMnO_4$	Potassium permanganate
H_2O_2	Hydrogen peroxide
NaOH	Sodium hydroxide
$NaNO_3$	Sodium nitrate
NO_2	Nitrogen dioxide
N_2O_4	Dintrogen tetroxide
$SOCl_2$	Thionyl chloride
NH_4OH	Ammonium hydroxide
PbS	Lead sulphide
AgCl	Silver chloride
Na_2SO_4	Sodium sulphate
$–COONH_4$	Ammonium salt of carboxylic acid
CO_2	Carbon dioxide
ZnO	Zinc oxide
HCl	Hydrochloric acid
$(NH_4)_2S_2O_8$	Ammonium persulfate
–COOH	Carboxylic acid group
KBr	Potassium bromide

CHAPTER 1
INTRODUCTION

This chapter gives a background on conducting polymers and nanohybrids of conducting polymers with graphene and carbon nanotubes. The section of conducting polymers focuses on polyaniline with various morphologies and its wide range of applications especially optical limiting and photocurrent generation applications. The general features of graphene and carbon nanotubes, their electronic properties and the importance of their hybrids are discussed along with main objectives of the thesis.

Conjugated polymer based photonics and electronics have developed enormously in recent years as a result of interdisciplinary studies. Organic and polymeric materials are replacing the traditional inorganic materials due to their numerous advantages. The attractive features of these materials are ease of device fabrication, large area applications, lightweight, mechanical flexibility, control over electrical and optical properties, etc. Other interests include ease of large scale preparation, high environmental stability, possibility of making hybrids with other polymers and inorganic materials. Scientists have been enthusiastic to explore the possibility of transforming conjugated polymers by chemical doping into highly conducting materials with inherent characteristics of polymers, which make them capable of meeting the requirements of modern technology. The desirable properties can be achieved by tailoring the structure, size and shape of the polymer and also by making composites with conducting materials like graphene, carbon nanotubes (CNTs), etc.

1.1. Conducting Polymers

The discovery of conducting polymers (Shirakawa et al., 1977) opened a new era in materials science and technology. The important discovery of high conductivity of iodine doped conjugated polymer (polyacetylene) led to the Nobel Prize in Chemistry for 2000 being awarded to Alan Heeger, A. J. Mac Diramid and Hideki Shirakawa for their pioneering development of electrically conducting polymers (Heeger, 2001; MacDiarmid, 2001; Shirakawa, 2001). Since the

revolutionary discovery of polyacetylene, the development of the field of conducting polymers has continued to accelerate at an unexpectedly rapid rate and a variety of other conducting polymers and their derivatives have been discovered. Fig. 1.1 shows examples of few conducting polymers.

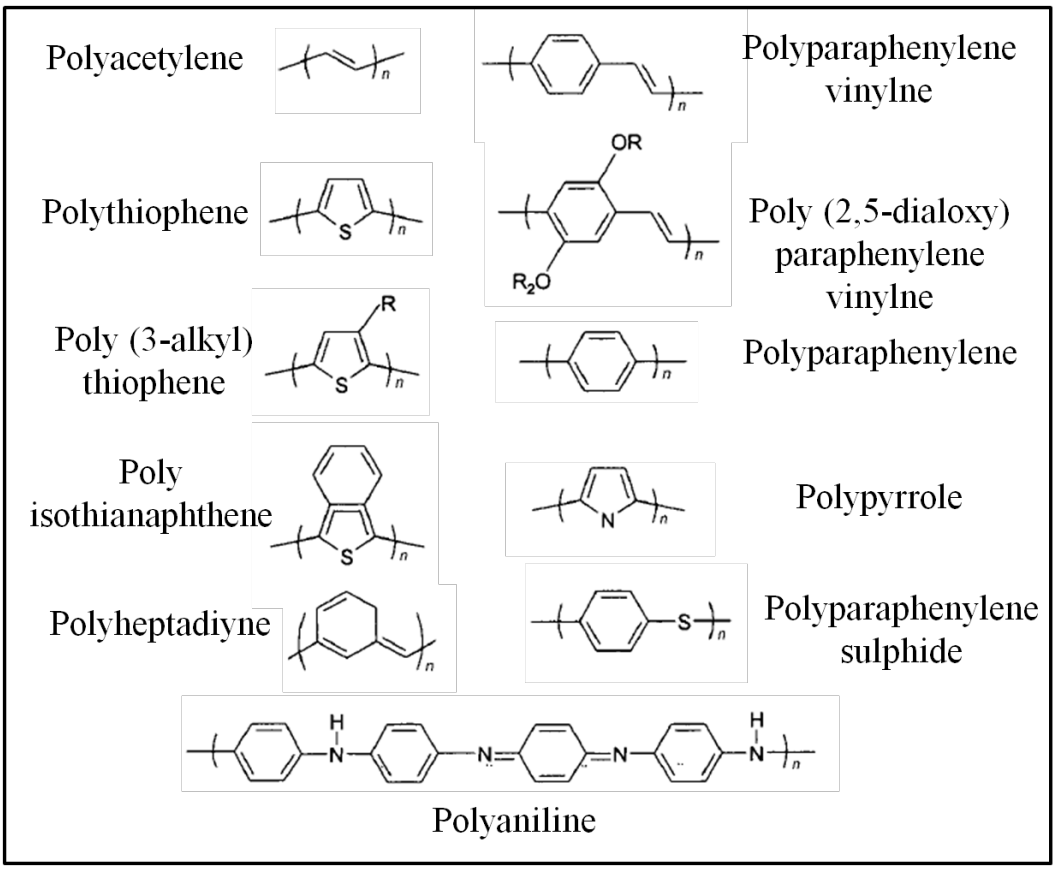

Figure 1.1 Examples of few conducting polymers

Professor Rånby B. (1993) designated conducting polymers as the 'fourth generation of polymeric materials' in his lecture at the Nobel Symposium (NS-81). Conducting polymers are macromolecules with conjugated π bonds in the main chain. The overlapping between the molecular orbitals in the polymer back bone leads to the delocalization of the electrons along the polymer chain and these delocalized π electron system is responsible for the interesting electronic and optical properties of the conducting polymers. The properties of conducting polymers are very different from other polymers in conductivity, but similar in their lightweight, low cost, moldability, etc. This class of polymer can undergo drastic change in conductivity during the interaction with acid or alkaline

materials. Due to the chemical versatility of conducting polymers, researchers around the globe are motivated to investigate their applications in many areas including light emitting diodes (Burroughes et al., 1990; Chen B. et al., 2014; Gustafsson et al., 1992; Kuik et al., 2014; Sessolo et al., 2013; Tsai et al., 2014), sensors (Dong L. et al., 2013; Gopalakrishnan and Dichtel, 2013; Hua et al., 2014; Liao et al., 2013; McQuade et al., 2000), field effect transistors (Huang H. et al., 2014; Sirringhaus et al., 2000; Tseng et al., 2014; Zhou et al., 2014), batteries (Guo et al., 2011; Zhang Q. et al., 2013), super capacitors (Kumar et al., 2012; Snook et al., 2011; Sun M. et al., 2014), actuators (Han and Shi, 2004; Jager et al., 2000; Nguyen et al., 2012), solar cells (Chen Z. et al., 2014; Hoppe et al., 2004; Huynh et al., 2002; Kim et al., 2006; Li W. et al., 2014; Price et al., 2011), electromagnetic shielding materials (Koul et al., 2000; Varshney et al., 2014; Wang Y. and Jing, 2005), etc.

Generally conducting polymers are conjugated polymers, which are organic semiconductors. Analogous to semiconductors, electrons in conjugated polymers are also organized in bands rather than discrete levels. The ground state bands are either completely filled or completely empty (Skotheim, 1997; Nalwa, 2007). This band structure originates from the splitting of interacting molecular orbitals of the constituent monomer units in a manner reminiscent of the band structure of solid-state semiconductors. The highest occupied band is known as valance band and the lowest unoccupied band is known as conduction band. The difference in energy between these bands is the band gap of the polymer. The control of the band gap by manipulating chemical structure of the polymer can tune the electrical and optical properties of the polymer (Roncali, 1997). In metals, valance band overlaps the conduction band and all the electrons are available for conduction. But in insulators, the electrons in the valence band are separated by a large gap from the conduction band and hence the entry of electrons from valance band to conduction band is restricted at ordinary temperatures. In semiconductors, the band gap is small enough so that the thermal energy can bridge the gap for a small fraction of electrons.

Conjugated polymer is a semiconductor with finite band gap, hence transforming it into a conductor requires the introduction of charge carriers in the polymer chain. This can be achieved by addition (reduction) or removal of electron (oxidation) from the polymer chain and this process is known as doping of conjugated polymers. Doping induces conductivity in conjugated polymers because of two reasons; (i) doping introduces more number of charge carriers into the electronic structure of the polymer, and (ii) the carrier delocalization along the polymer chain is achieved by the attraction of the electron in one repeat unit to the nucleus of the other repeat unit and it is extended to three dimensions through inter chain electron transfer (Heeger, 2001). When an electron is removed from the polymer chain by oxidation, a radical cation is created, but it does not delocalize completely. Partial delocalization occurs over several monomer units and thus the monomer units deform structurally. The partially delocalized radical cation is known as polarons. The distortion produced by these polarons is of high energy than remaining portion of the chain and this high energy states are known as polaron states formed in between the band gap. Hence doping creates new localized electronic states in the band gap with the lower energy levels being occupied by a single unpaired electron (Bredas and Street, 1985). A second electron can be removed from the polymer chain in two ways; it can be either from the polaron or from anywhere in the polymer chain. If an electron is removed from the polaron, it generates a bipolaron. Bipolarons can be defined as a pair of like charges associated with a strong local distortion and it is of high energy and thus short lived. Conduction by polarons and bipolarons is the dominant mechanism of charge transport in polymers with nondegenerate ground states. The conductivity of the doped polymer depends on many factors like nature and concentration of dopants, homogeneity of doping, crystallinity and morphology of the polymer.

1.1.1. Polyaniline

Among the conjugated polymers, polyaniline is the most studied conducting polymer. Polyaniline exhibits diversity in its backbone structure. It has amine and imine segments in the backbone of the polymer chain. The protonation,

deprotonation and various other physicochemical properties of the polyaniline is due to the presence of the chemically flexible –NH– group flanked either side by phenyl rings. Polyaniline exists in four oxidation states, namely, leucoemeraldine base, emeraldine base, emeraldine salt and pernigraniline. Among these, emeraldine salt, as shown in Fig. 1.2, is the only conducting form of polyaniline.

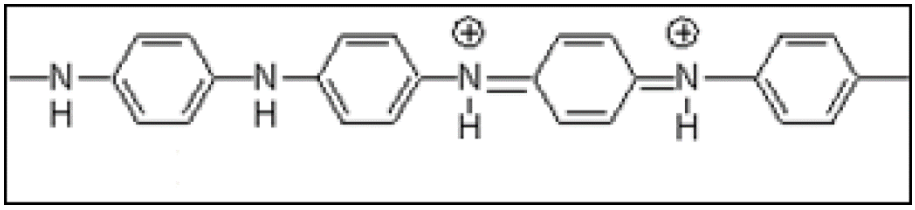

Figure 1.2 Structure of polyaniline emeraldine salt

Polyaniline emeraldine salt of mineral acids is having high conductivity, but they are mostly insoluble. This lack of solubility and processability is related to the rigidity of the polymer chain, which is a direct consequence of the high level of conjugation of the polymer. The use of organic acids as dopants is recognized as one important solution for improving the processability of polyaniline. Cao and co-workers (1992) were the first group to notice a large improvement in the solubility of polyaniline doped with organic acids and such improvement in processability are termed as 'counter ion-induced processability'.

Several efforts have been directed towards functionalization, copolymerization and blending of polyaniline to enhance its solubility. Yue et al. (1991) introduced sulphonic acid groups in the polyaniline chain to make it a self doped polymer and the solubility of polyaniline is improved significantly. Chan et al. (1995) synthesized water soluble self doped conducting polyaniline from poly (o-aminobenzylphosphonic acid) and its sodium salt. Ruiz et al. (2013) improved the processability of polyaniline by treating with different thermoplastic matrices such as polycaprolactone and polybutylene terephthalate using compression and extrusion methods. Cooper and Vincent (1989) prepared electrically conducting organic films by casting aqueous dispersions of mixed polymer lattices (one lattice is the conducting polypyrrole or polyaniline and other is the film-forming

lattice of 1:1 co-polymer of polymethyl methacrylate and polybutyl acrylate) on supporting glass microscope slides.

Preparation of colloidal dispersion is another method of improving processability of polyaniline. Dispersions have been prepared by emulsion polymerization of aniline in the presence of steric stabilizers such as surfactants, water soluble polymers or silica colloids (Stejskal and Sapurina, 2004; Tadros et al., 1992). Since these dispersions are mixtures of polymer and steric stabilizers, it will affect the properties of polyaniline. If polyaniline is doped with a protonic acid the backbone of the emeraldine form of polyaniline will be positively charged (Fig. 1.2). So a stable colloid could be formed through electrostatic repulsion without using steric stabilizers if the particle size is sufficiently small. Li and Kaner (2005) provided a simple and environment friendly synthesis of self stabilized polyaniline colloids by simply purifying chemically prepared nanofibers and controlling the pH. The stable colloids were formed at around pH=2.6 through electrostatic repulsion without any chemical modification or steric stabilizer. Li X. et al. (2008) also prepared stabilizer free colloids of polyaniline nanofibers in the presence of β-cyclodextrin and the colloid was found to be stable for 60 days without any steric or electrostatic stabilizer.

Synthesis in nano dimension is another important method of improving the solubility and processability of polyaniline. Various methods have been reported for the synthesis of polyaniline micro or nanostructures including electrochemical, template, enzymatic, plasma, heterophase, solution, interfacial, seeding, metathesis, sonochemical, self assembling polymerizations, etc. Out of these methods, template synthesis is extensively investigated. The templates can be mainly classified as hard or soft. In hard template method, the desired material with the desired shape is synthesized within the pores of a template and the template is removed after the synthesis. One of the important features of this method is the possibility for the synthesis of one dimensional micro/nanostructured polyaniline with controllable diameter, length and orientation (Wu and Bein, 1994). However, there are several disadvantages for

this method. Tedious post treatments are required for the removal of the external template and these post treatments may destroy the nanostructures. Also the size and morphology of the available templates are limited. The soft template method is another simple, cheap and powerful method for the synthesis of polyaniline nanostructures. It does not require any external template or the complex post treatments. In this approach, polyaniline is synthesized in the environment of a template formed by a surfactant or any other material organized in a particular nanostructure.

The accidental discovery of polyaniline nanotubes by a conventional *in situ* doping polymerization in the presence of β-naphthalene sulphonic acid (β–NSA) later lead to the development of a new method for the synthesis of polyaniline nanostructures (Qiu et al., 2001). This method is called as template-free method because no external templates are used. Organic dopants like β–NSA, azobenzene sulphonic acid (ABSA), D-10 camphor sulphonic acid (D-10-CSA), etc., have been used for the synthesis of self assembled polyaniline nanostructures by template-free approach. Wei et al. (2002) synthesized polyaniline micro/nanostructures (microtubes, nanotubes and nanofibers) using β–NSA as the dopant and found that the formation mechanism is different when the [NSA]/[aniline] ratio is changed. They reported that NSA-aniline salt precipitate is acting as a template. Huang and Wan (2002) used ABSA as the dopant to synthesize nanotubes and nanofibers of polyaniline with photoisomerization function. Lijuan and Meixiang (2002) synthesized self assembled polyaniline nanotubes with 80-100 nm diameters by the template-free method using D-10-CSA as the dopant. Wei et al. (2003) reported the formation mechanism of sub micrometer sized tubes of conducting polymers (polyaniline and polypyrrole) and their junctions and dendrites, through a self assembly approach. This result provides a new method to synthesize complicated nanotubular structures by simple self assembly. Zhang L. et al. (2004) systematically studied the effect of hydrogen bonding on self assembled polyaniline nanotubes in the presence of different carboxylic acids such as propionic acid, lactic acid, succinic acid, malic acid, tartaric acid, and citric acid. The nanotubes aggregated to dendrites when

carboxylic acids with a hydroxyl group are used. The research group of Zhang and Wan (2003) studied the self assembly of polyaniline nanotubes to hollow microspheres by simply changing the molar ratio of the dopant (salicylic acid) to monomer. The same group also reported the chiral nanotubes of polyaniline synthesized by a self assembly process in the presence of dopants L-CSA and D-CSA. Polyaniline microtubes with hexagonal cross-section are formed in the presence of 8-hydroxy quinoline as the dopant (Liu et al., 2011). Yang et al. (2005) synthesized polyaniline nanofibers of diameter 120-370 nm by self assembly process using a self doping monomer (*o*-aminobenzenesulphonic acid-SAN) along with aniline. Here SAN acts both as self doping monomer and surfactant. Chiou et al. (2007) demonstrated that excess oxidant (ammonium persulfate) preferentially forms highly uniform, extra long nano fibers/nanotubes. The formation of aniline dimer cation radicals can act as an effective surfactant to shape the polyaniline morphology. In general, the morphology and size of the nanostructures synthesized by the template free method can be altered by the reaction conditions, monomer to dopant ratio, the amount of the oxidants, etc.

Various applications of polyaniline like light emiting diodes (Chen et al., 1996), electrode materials (Domingues et al., 2011; Dong Y. P. et al., 2013; Li Q. et al., 2008), sensors (Huang et al., 2002; Huang et al., 2004), CO_2 adsorption (Kemp et al., 2013), EMI shielding (Koul, et al., 2000), electrochemical actuators (Sansiñena et al., 2003), super capacitors (Wang et al., 2009), etc. are extensively studied in the past years because of its excellent characterestics. Among the wide range of applications, the electronic state of the polyaniline leads to potential applications like optical limiting, and photocurrent generation applications, etc.

1.2. Optical Limiting Applications

Following the demonstration of first functioning laser (Maiman, 1960), optical limiting materials are thoroughly investigated. As the power of laser increases, demand for the protection from lasers becomes greater. Protection from high intense laser beams is one of the great apprehensions from public safety and technological perspective. Various materials including organic dyes,

organometallics, fullerenes, semiconductors, etc. are studied for optical limiting applications (Balapanuru et al., 2010; Krishna et al., 2011; Zhang et al., 2009a; Zhu et al., 2011). Other than laser protection, optical limiting materials can also be used for pulse shaping and smoothing, pulse compression, etc. (Band et al., 1986).

Optical limiting is a nonlinear optical process in which the transmittance of a material decreases as the incident light intensity increases. An optical limiting material will attenuate high intensity laser beams while exhibiting transmittance under low intensity regime. A good optical limiter should satisfy the following conditions: large nonlinear absorption coefficient, low limiting threshold, high damage threshold, wide dynamic range, low scattering losses, ultrafast response time, broad band response, high linear transmittance and good mechanical and thermal stability. A single material cannot provide all these requirements and hence the devices are assembled by the combination of various optical limiters with these properties.

Optical limiting in a material arises through various nonlinear optical mechanisms like nonlinear absorption, nonlinear refraction, nonlinear scattering, etc. The common mechanisms leading to nonlinear absorption are reverse saturable absorption (RSA), multi photon absorption (MPA), free carrier absorption (FCA), etc. RSA is observed for the first time by Giuliano and Hess, (1967) while studying the Q-switching of a laser cavity with organic dye molecules. RSA occurs when the excited state absorption cross-section of a molecule is larger than the ground state absorption cross-section at the input wavelength. In the case of MPA, an electron is excited from the ground state to excited state by simultaneous absorption of two or more photons through a virtual intermediate state. Free carrier absorption (FCA) is mainly observed in semiconductors, where absorption of photon promote electron to conduction band. The generated free carriers can be excited to higher lying states by the absorption of additional photons and it is known as free carrier absorption. Optical limiting is also possible by nonlinear refraction due to the change in refractive index induced

by high external electric field. Nonlinear refraction may arise from molecular reorientation, the electronic Kerr effect, excitation of free carriers, photorefraction, or optically-induced heating of the material (Marrucci et al., 1998).

Optical limiting can also be achieved by nonlinear scattering. Nonlinear scattering is possible through two ways; by the laser induced formation of new scattering centers or by the laser induced changes in the refractive index difference between existing scatter centers and their surroundings. Optical limiters based on nonlinear scattering in dispersions depend upon the liquid media because the process in such media is often reversible. In solids the scattering centers are generated due to irreversible decomposition processes that can lead to degradation in the linear operation of the device (Tutt and Boggess, 1993).

Wide varieties of materials are studied for optical limiting applications based on different mechanisms. Recently, researchers are focusing on the synthesis of optical limiting materials and the design of laser protecting devices. Materials like semiconducting and metal nanoparticles, organic molecules like porphyrins, phthalocyanines, etc. are extensively studied for optical limiting applications. Polyaniline emerged as a widely studied group of nonlinear optical material (Chen et al., 1994; de Souza et al., 1995; Mattes et al., 1991; Osaheni et al., 1992; Pandey et al., 2009; Sezer et al., 2009). Interest in the nonlinear optical properties of polyaniline for potential applications in photonic devices has grown tremendously due to its fast response time (sub picosecond), high damage threshold and ease of fabrication. Optical nonlinearity of polyaniline is due to its nonlinear absorption. Carbon nanomaterials like fullerene, carbon nanotubes and graphene are another interesting class of optical limiting materials. Discovery of optical limiting in C_{60} is one of the most important developments for the scientific community and it is considered as the bench mark material for optical limiting applications.

1.3. Photocurrent Generation Applications

Conducting polymer electronics has become an attractive field in recent years because of its potential applications as light emitting diodes (Braun and Heeger, 1991), transistors (Paloheimo et al., 1990), photodiodes (Admassie et al., 2006), photovoltaic devices (Huynh, et al., 2002; Zhang et al., 2002) etc. Polyaniline, owing to its high absorption in the visible range, good charge carrier mobility and stability, is an attractive candidate for photocurrent generation applications. Desilvestro and Haas (1991) examined the occurrence of two types of photoinduced currents in polyaniline under illumination with visible light. Kilmartin and Wright (1996) studied the photo effects in polyaniline electrode in insulating state as well as in conducting state. Bubb et al. (2005) studied the persistent photoconductivity in polyaniline thin films. But the photocurrent generated by conducting polymers is relatively low because of the high exciton binding energies. So strategies are adopted to make bilayer or bulk heterojuction donor-acceptor system by blending or hybridizing conjugated polymers with efficient and stable acceptor materials like carbon nanomaterials (Chatterjee et al., 2013; Kymakis et al., 2007; Liu Q. et al., 2009; Liu et al., 2010).

Hybrids of p-type conducting polymers with n-type graphene or CNT facilitate the formation of bulk heterojuction structures. Such materials are promising candidate for photocurrent generation and hence suitable for photo detector or solar cell applications. The bulk heterojuction structures have a lot of advantages over layered structures. In the case of a single layered device, an organic semiconductor is sandwiched between two electrodes with different work functions (Marks et al., 1994) and electrons from the low-work-function electrode will flow to the high-work-function electrode until the Fermi levels are equalized. This built in electric field developed by the asymmetric work function of electrodes is not sufficient to achieve the exciton dissociation because of the high binding energy of excitons (0.1-0.4 eV) in polymer semiconductors. In the devices, the exciton dissociation happens only at the interfaces between polymer and the cathode and most of the excitons generated are recombining before it reaches the interface. The low mobility of charge carriers in conducting polymers

is another disadvantage, which increases the chance of recombination. These problems can be overcome by fabricating bilayer devices, i.e., by inserting an acceptor layer in between donor layer and the electrodes (Tang, 1986). In the bilayer structure, the energy difference between the donor and acceptor provides a sufficient energy to overcome the intrinsic exciton binding energy and excitons can be efficiently separated. However, such a structure has limited interfacial areas for dissociation of excitons, which led to the development of bulk heterojuction structures. In bulk heterojuction hybrid structures each donor site is within a distance less than the exciton diffusion length of donor-acceptor interface.

The above discussed advantages of bulk heterojuction system prompted us to study the photocurrent generation of the polyaniline hybrids of carbon nanotubes and graphene. General properties and applications of carbon nanotubes and graphene are discussed in the following sections.

1.4. Carbon Nanotubes

Carbon nanotube, an important carbon allotrope, exists in two forms namely, single walled carbon nanotube (SWNT) and multiwalled carbon nanotube (MWNT) as shown in Fig.1.3.

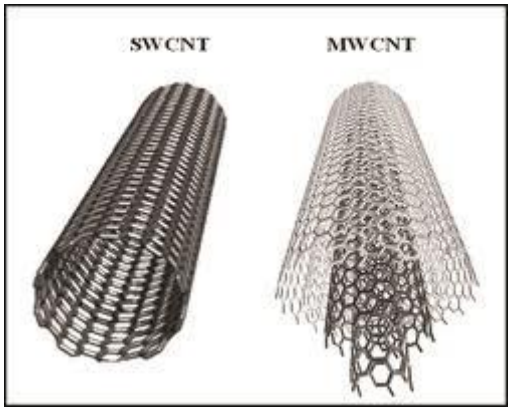

Figure 1.3 Structure of single walled and multiwalled carbon nanotubes.

The inherent electrical properties of carbon nanotubes are determined by the chiral vector, along which the graphene is hypothetically rolled to form the nanotube. Carbon nanotubes have excellent mechanical properties (high stability, strength and stiffness) combined with low density and elastic deformability with special surface properties (selectivity, surface chemistry). CNT can be metallic or semiconducting depending on the crystal structure of the material. Superior optical limiting action of CNTs than carbon black and fullerenes is reported for the first time by a research group from National University of Singapore (Chen, 1999). The optical limiting performance, dynamics and mechanism of CNT suspensions are studied in detail by many research groups (Anglaret et al., 2000; Sun et al., 2000; Vivien et al., 2000a; Vivien et al., 2000b; Vivien et al., 2002). Carbon nanotubes show optical limiting behaviour by nonlinear scattering due to the laser induced formation of new scattering centers. The new scattering centers may be thermally induced solvent bubbles or the micro plasmas generated by the sublimation of carbon nanotubes. However, the large surface energy of nanotubes restricts the dispersion in most of the solvents. So polymers or organic molecules can be employed to covalently or noncovalently solubilize CNTs. The conjugated polymer PmPV is studied as an appropriate polymer to disperse CNTs while retaining the optical response (Curran et al., 1998). O'Flaherty et al. (2003) studied the optical limiting applications of carbon nanotube dispersions in PmPV. Recent research in this field focuses on the synergetic combination of nonlinear scattering carbon nanotubes with reverse saturable absorbing materials for enhanced optical limiting action.

Carbon nanotubes also have widespread applications in the field of optoelectronics. The conjugated polymer-CNT hybrids will act as interpenetrating bulk heterojunction and thus facilitate charge separation and transport of carriers to electrodes. The high electric field at the junction can split up the excitons, while carbon nanotube can act as a pathway for the electrons (Kymakis et al., 2003). The common strategy to utilize carbon nanotube for photocurrent generation applications is the dispersion of carbon nanotubes in electron donating conjugated polymers like P3HT or P3OT. Various researchers reported the combination of

carbon nanotubes with conjugated polymers for organic photovoltaic applications (Ago et al., 1999; Miller et al., 2006; Kazaoui et al., 2005; Kymakis and Amaratunga, 2002; Landi et al., 2005a; Landi et al., 2005b). Even though polythiophene based hybrids of CNT are investigated for photocurrent generation, the other conjugated polymer hybrids are not explored widely.

1.5. Graphene

Graphene is a 2D carbon allotrope having a honey comb lattice structure with carbon-carbon distance of 0.142 nm (Geim, 2007). Graphene is isolated by the scientists Andre Geim and Konstantin Novoselov at the University of Manchester (Novoselov et al., 2004). They used a simple but effective mechanical exfoliation method for extracting thin layers of graphene from a graphite crystal with Scotch tape. The Nobel Prize in Physics 2010 was awarded to them for successfully producing, isolating, identifying and characterizing graphene (Katsnelson et al., 2006; Nair et al., 2008; Novoselov et al., 2005). Graphene is the 2D building material for carbon nanomaterials of all other dimensionalities as shown in Fig. 1.4.

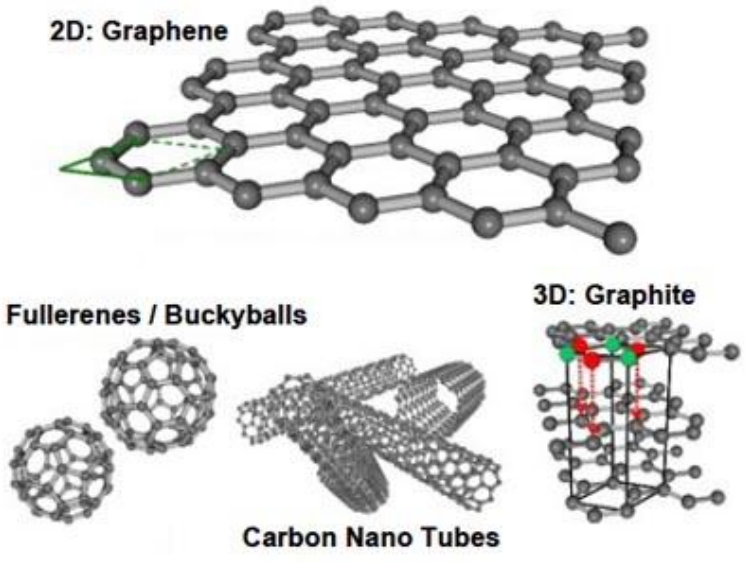

Figure 1.4 Graphene and its descendants- Graphite (stacked graphene), Carbon nanotubes (rolled graphene), and Fullerenes (wrapped graphene)

Graphene is the thinnest and strongest material known. Monolayer graphene is a good transparent conductor, as it possesses higher transparency of 97.7% in the visible region (Nair, et al., 2008). Even though graphene is almost transparent, it is so dense that even the smallest helium atom cannot pass through it. The research based on graphene materials has increased exponentially due to its extraordinary electronic and optical properties, high carrier mobility, large specific surface area (~2630 m^2/g), superior mechanical strength (Young's modulus of (~1 TPa) and excellent electrical ($0.96x10^6$ S/cm) and thermal conductivity (~5000 Wm/K). They can behave like relativistic particles and can be described by Dirac's equation for mass less fermions (Castro Neto et al., 2009).

The production of graphene by mechanical exfoliation of graphite is limited to small scale applications. So, various CVD techniques and epitaxial techniques have been developed for the large scale production of single layered or few layered graphene on metal and SiC substrates (Li et al., 2009; Mattevi et al., 2011; Yang et al., 2013). However, the use of metal substrates often necessitates a transfer of the graphene onto other substrates. Moreover, these high temperature techniques are not compatible for large area flexible electronics. A possible solution to overcome this problem is to utilize solution based techniques for the synthesis of graphene materials. Oxidative exfoliation of graphene followed by the chemical reduction of graphite oxide (GO) is the most common and economical method for the large scale production of reduced graphene oxide or chemically functionalized graphene (Si and Samulski, 2008). The oxidation of graphite leads to its exfoliation by the weakening the van der Waals interaction between the layers and renders hydrophilic nature by the introduction of various oxygen functionalities (He et al., 1998; Lerf et al., 1998). Although the GO itself is an insulator, its graphitic network can be restored by the chemical reduction or thermal annealing. The microscopic and electrical characterization of the reduced graphene oxide reveal the formation of nanometer sized graphene sheets separated by defect rich regions. The electrical characterestics of graphene are preserved because the defect regions are small. Another advantage of this method is the ability of GO with expanded d-spacing and large number of oxygen

functionalities to act as a template for the formation of hybrids with various inorganic and organic nanomaterials.

Graphene materials like graphene oxide (Liu Z. et al., 2009), graphene fluoride (Bourlinos et al., 2012), etc. are known to exhibit important broad band optical limiting action, making them an interesting candidate for optical limiting devices. Lim et al. (2011) demonstrated giant broad band nonlinear optical absorption in dispersed graphene sheets and Wang (2009) demonstrated the broad band nonlinear optical behaviour of graphene dispersions. Feng et al. (2010) investigated optical limiting properties of graphene families including graphene and graphene oxide nanosheets and ribbons. Jiang et al. (2012) studied the broad band optical limiting of graphene oxide thin films and found an enhanced nonlinear absorption coefficient upon laser induced reduction. So the combination of graphene with various reverse saturable absorbing materials is a recent strategy to obtain very good optical limiting behaviour.

A major challenge in developing light harvesting devices is the effective separation of photogenerated electron-hole pairs and the transfer of electron to electrode. Graphene is a promising acceptor material (Liu Z. et al., 2008) and charge carrier for the photocurrent generating devices due to its high specific surface area, high mobility, tunable bandgap and the higher linear in-plane dimensions (approximately 5 μm) compared to the thickness (0.34 nm) (Charlier et al., 1991; Schedin et al., 2007; Williams et al., 2007). Hence graphene hybrids of p-type conjugated polymers are considered as an important class of hybrid materials for the fabrication of donor/acceptor based devices for photocurrent generation.

1.6. Scope and Objectives of the Thesis

As outlined in the above mentioned research outlooks, the combination of donor/acceptor nanosystem is required for getting very good optical limiting and photocurrent generation. The purpose of this research is to enhance the optical limiting and photocurrent generation properties of conducting polyaniline by

synthesizing nanostructures of polyaniline and hybrids of polyaniline with graphene and multiwalled carbon nanotube. The main objectives of the research work are summarized below:

1. Synthesis of polyaniline nanostructures by a novel inverse microemulsion polymerization technique, its spectroscopic and microscopic characterization, prediction of mechanism for the formation of nano polyaniline with experimental support and the property evaluation based on optical limiting and photocurrent generation.

2. Transparent film fabrication of polyaniline nanostructures using polymethyl methacrylate (PMMA) as matrix, its characterization and optical limiting property (energy dependant and concentration dependant) studies.

3. Synthesis of polyaniline-graphite oxide hybrid with noncovalent interactions (by *in situ* polymerization of aniline in the presence of synthesized graphite oxide), its characterization and evaluation of nonlinear optical (NLO) and photocurrent generation properties.

4. Modification of graphite oxide by phenylene diamine grafting and synthesis of polyaniline-phenylene diamine functionalized reduced graphene oxide (GONH2) hybrid by *in situ* polymerization of aniline in the presence of GONH2 (aiming covalent interaction between polyaniline and GONH2), its characterization and studies on NLO and photocurrent generation applications.

5. Synthesis of phenylene diamine functionalized MWNT (MWNTCONH2), hybridization with polyaniline by the *in situ* polymerization of aniline in the presence of MWNTCONH2, its characterization, NLO and photocurrent generation property studies.

6. Covalent grafting of polyaniline synthesized by inverse microemulsion polymerization on reduced graphene oxide, its characterization and studies on NLO and photocurrent generation properties.

1.7. Organization of the Thesis

Chapter 1 covers the background of the thesis specially focusing on morphological effect of conducting polymers, the importance of graphene and CNT hybrid systems for optical limiting and photocurrent generation applications.

Chapter 2 discusses the conceptual basis and details of the experimental methods and characterization techniques like scanning electron microscopy (SEM), transmission electron microscopy (TEM), X-ray diffraction (XRD), Fourier transform infrared spectroscopy (FTIR), X-ray photoelectron spectroscopy (XPS), Raman spectroscopy, Thermogravimetric analysis (TGA), etc. Experimental set up for the NLO studies, dc-conductivity and photocurrent measurements are also highlighted in chapter 2.

Chapter 3 describes the synthesis of nanostructured and processable cube-like polyaniline by a novel inverse microemulsion polymerization technique and its characterization. The formation mechanism for the cube-like polyaniline is discussed with experimental support. The suitability of cube-like polyaniline for optical limiting and photocurrent generation is reported. NLO properties of the cube-like polyaniline film in PMMA matrix are also discussed.

Chapter 4 details the synthesis and characterization of graphite oxide, preparation of polyaniline-GO hybrid with non-covalent interactions by *in situ* chemical oxidative polymerization of aniline in the presence of GO and the improved optical limiting and photocurrent generation of the hybrid compared to pure polyaniline.

Chapter 5 deals with the design and synthesis of phenylene diamine functionalized reduced graphene oxide (GONH2) and the preparation of

polyaniline-GONH2 hybrid with covalent connections by simple *in situ* polymerization of aniline in the presence of GONH2. Improved optical limiting, dc conductivity and photocurrent generation of the hybrid compared to pristine polyaniline and polyaniline-GO hybrid are also discussed.

Chapter 6 discusses the synthesis of phenylene diamine functionalized multiwalled carbon nanotube (MWNTCONH2), preparation of polyaniline-MWNTCONH2 hybrids with covalent connections and the optical limiting, dc-conductivity and photocurrent generation of the hybrid.

Chapter 7 outlines the direct covalent grafting of the synthesized cube-like polyaniline on reduced graphene oxide layers and the improved optical limiting, dc conductivity and the photocurrent generation of the hybrid compared to pristine cube-like polyaniline.

Chapter 8 summarizes the research work and results of this thesis. Future work to improve the performance of the hybrid system studied and the promising applications to be evaluated are suggested in this chapter.

CHAPTER 2
EXPERIMENTAL

This chapter details the synthesis of polyaniline and polyaniline hybrids of graphene and MWNT and their film fabrication methods. Various characterization techniques, techniques for nonlinear optical studies, DC conductivity measurements and photocurrent generation studies are also discussed.

2.1. Synthesis

2.1.1. Materials

Toluenesulphonic acid (TSA), oleic acid, paraffin oil (light), 25% ammonia solution (NH_3), redox initiator ammonium persulphate (APS), 98% sulfuric acid (H_2SO_4), 70% nitric acid (HNO_3), potassium permanganate ($KMnO_4$), 30% hydrogen peroxide (H_2O_2), benzoyl peroxide, methyl methacrylate monomer, sodium sulfate, sodium hydroxide (NaOH), acetone, methanol, m-cresol, and 2-propanol from Merck, India were used as received. Monomer aniline, thionyl chloride and dimethylformamide (DMF), received from Merck, India, were used after reduced pressure distillation. Phenylene diamine was purchased from Spectrochem and used as such. Auxisol was used as the stabilizer for the emulsion. Graphite powder (particle size < 20 μm), nafion solution (5 wt % in water and lower aliphatic alcohols) and fluorine doped tin oxide (FTO) coated glasses were purchased from Sigma Aldrich. Multiwalled carbon nanotube (MWNT, 95 wt %, 5-15 nm diameter, 1-10 um length) was purchased from Bucky USA.

2.1.2. Synthesis of cube-like polyaniline by inverse microemulsion polymerization technique

Polyaniline cube-like nanostructures were synthesized by introducing a novel inverse microemulsion polymerization technique. Paraffin oil-water microemulsion was prepared by mixing oil and oleic acid in the presence of ammonia solution and *in situ* generated ammonium oleate was acting as a

surfactant. Aniline was polymerized in oil-water emulsion using 1 M TSA as dopant, APS as initiator and auxisol as the stabilizer. The reaction was carried out for 12 h with constant stirring at room temperature. For a detailed study on the structure of polyaniline formed in the above mentioned emulsion, the reaction was repeated by keeping the reaction time as 4 h and 8 h. In order to understand the effect of inverse micelles of ammonium oleate for the formation of nanocube-like structures, polyaniline was synthesized by chemical oxidative polymerization in the absence of the emulsion system using TSA (1 M) as dopant and APS as initiator.

2.1.3. Synthesis of graphite oxide (GO)

GO was synthesized by a novel strategy adopted by simplifying Hummers method (Hummers and Offeman, 1958). In Hummers method graphite oxide was prepared by stirring powdered graphite and 50 g of sodium nitrate into 2.3 litres of sulphuric acid at 0 ^{o}C. Then 300 g of potassium permanganate was added to the suspension. The temperature is increased to 35±3 ^{o}C, where it was maintained for 30 min. At the end of 30 min., 4.6 litres of water was added and the temprerature in increased to 98 ^{o}C and it is maintained at the same temperature for 15 min.The suspension was further diluted to approximately 14 litres and treated with 3% H_2O_2 and the suspension was filtered to get graphite oxide. In our procedure , the commonly used $NaNO_3$ treatment was avoided so that the generation of toxic gases like NO_2 and N_2O_4 were avoided and the reaction was carried out at low temperature (less than 10 ^{o}C).

2.1.4. Synthesis of polyaniline-GO hybrid

Polyaniline-GO hybrids were synthesized by the *in situ* polymerization of aniline in the presence of synthesized GO using 1 M TSA as the dopant and APS as the initiator at room temperature. Aniline:GO ratio chosen for the synthesis were 4:1, 2:1, 1:1, and 1:2 and the samples were named as PxGy, where x is the proportion of aniline and y is the proportion of GO. Pure polyaniline was also synthesized in the absence of GO, while maintaining all other experimental conditions the same.

2.1.5. Synthesis of polyaniline-phenylene diamine functionalized reduced graphene oxide hybrid

At first, GO was treated with catalytic amount of dry DMF and excess amount of freshly distilled $SOCl_2$ under inert atmosphere at 80±2 ^oC for the formation of acid chlorides and then phenylene diamine was grafted on it by the amidation reaction to form phenylene diamine reduced graphene oxide (GONH2). Polyaniline-GONH2 hybrids were synthesized by the *in situ* polymerization of aniline in the presence of synthesized GONH2 using 1 M TSA as the dopant and APS as the initiator at room temperature. Aniline:GONH2 ratios, 2:1, 1:1, and 1:2 were selected for the synthesis of hybrids and the samples were named as PxNH2Gy, where x is the proportion of aniline and y is the proportion of GONH2. In this methodology, covalent bonds between polyaniline and reduced graphene oxide are achieved because of the participation of phenylene diamine groups attached to the reduced graphene oxide layers during the polymerization reaction of aniline.

2.1.6. Synthesis of polyaniline-phenylene diamine functionalized MWNT hybrid

Initially, carboxylic acid groups were introduced in MWNT by refluxing pristine MWNT with 65% HNO_3 at 110±2 ^oC for 6 h. The powder obtained was filtered, washed with distilled water, and dried at 80 ^oC. The acid functionalized MWNT was then treated with excess amount of dry DMF and freshly distilled $SOCl_2$ under inert atmosphere at 80±2 ^oC for the formation of acid chlorides. Phenylene diamine was then grafted on it by the amidation reaction to form phenylene diamine functionalized MWNT (MWNTCONH2). Polyaniline-MWNTCONH2 hybrids were synthesized by the *in situ* polymerization of aniline in the presence of synthesized MWNTCONH2 using 1 M TSA as the dopant and APS as the initiator at room temperature. Aniline:MWNTCONH2 ratios chosen for the synthesis of hybrids were 2:1, 1:1, and 1:2 and the samples were named as PxNH2Cy, where x is the proportion of aniline and y is the proportion of

MWNTCONH2. Covalent bonds between polyaniline and MWNT are formed by this methodology .

2.1.7. Synthesis of cube-like polyaniline grafted reduced graphene oxide hybrid (polyaniline-g-rGO)

The synthesized cube-like polyaniline was grafted on reduced graphene oxide by a two step approach. First GO was treated with catalytic amount of dry DMF and excess amount of freshly distilled $SOCl_2$ under inert atmosphere at 80±2 ^oC for the formation of acid chlorides. Then the dedoped cube-like polyaniline dispersed in dry DMF was grafted on it through amidation reaction. The dedoping of cube-like polyaniline was carried out by stirring the polyaniline in the presence of NH_4OH(1 M) for 24 h.

2.2. Film Fabrication

2.2.1. Fabrication of cube-like polyaniline and polyaniline-g-rGO film in PMMA host for NLO studies

Weighed amount of cube-like polyaniline was dispersed in the monomer (methyl methacrylate) by means of ultrasonication. The monomer/polyaniline dispersion was then polymerized using benzoyl peroxide as the initiator. The viscous polymer formed was immediately casted on a glass plate and dried in air. By varying the concentration of polyaniline (0.02 to 0.1 wt % with respect to the monomer), free-standing and flexible films with an average thickness of 0.25 mm were fabricated. Polyaniline-g-rGO films in PMMA host were also fabricated by the same method as discussed above.

2.2.2. Fabrication of films for photocurrent generation studies

Thin films of the samples were fabricated on clean FTO glasses. The FTO glasses were cleaned by ultrasonication in acetone, methanol and distilled water. The samples in cresol/nafion mixture were spin coated on FTO at 1500 rpm for 1 min. After spin coating, the films were baked at 100 ^oC for 30 min.

2.3. Characterization Techniques

A combination of spectroscopic, thermal and microscopic techniques were employed to analyze the properties of materials synthesized for this research work. Fourier transform infrared spectroscopy (FTIR) was used to understand the structural features of the samples. Raman spectroscopy was used to analyze the percentage defects in samples containing graphene and carbon nanotubes. Crystallinity of the samples were analyzed using X-ray diffraction studies (XRD). X-ray photoelectron spectroscopy (XPS) was used to analyze the elemental composition of the samples. Characterestic absorption and emission of the samples were studied using UV-visible absortion spectroscopy and fluorescence spectroscopy respectively. Thermal decomposition pattern of the samples was studied using thermogravimetric analysis (TGA). Zeta potential of the polyaniline samples were measured using Malvern Zetasizer. Size, morphology and surface features of the samples were studied by various microscopic techniques like scanning electron microscopy (SEM), transmission electron microscopy (TEM) and atomic force microscopy (AFM).

2.3.1. Spectroscopic techniques

2.3.1.1. Fourier transform infrared spectroscopy

Infrared spectroscopy is the most popular chemical characterization technique for structural analysis. An infrared spectrum gives characteristic absorption peaks corresponding to the vibrational frequency of bonds between the atoms in the material. In an infrared spectrometer, infrared radiation of successively increasing wavelength is passed through the sample and the percentage of absorbance is measured. During exposure to the radiation, some of the incident frequencies will be in resonance with the molecular vibrations. This resonance allows the exchange of energy between the incident electromagnetic wave and the molecular vibrations and the absorbed frequencies are recorded as a spectrum. The Fourier transform spectrometer contains an interferometer that produces a Fourier spectrum which gives the distinct frequencies absorbed from the IR spectrum. By utilizing the FTIR spectroscopy a significant improvement in the quality of the infrared spectra and acquisition time is achieved (Griffiths and

Hasseth, 2007; Robert, 1990).

The instrument used for the present study was Perkin Elmer 100 FTIR spectrometer with diffuse reflectance accessory. Spectral range and optical resolution of the instrument is 4500-450 cm^{-1} and 0.5 cm^{-1} respectively. The samples were diluted with KBr before the measurement and each sample was scanned 32 times.

2.3.1.2. Raman spectroscopy

Raman spectroscopy is a spectroscopic technique based on inelastic scattering of a monochromatic light, usually from a laser source (Gardiner, 1989). When light of a certain wavelength interacts with a molecule, most of the photons are elastically scattered and therefore have the same energy of the incident photons. However, a very small fraction is inelastically scattered, hence the energy of scattered photons is different from that of the incident photon. In Raman spectroscopy, the incident photons have much greater energy than that of the molecular vibrations, because a very small fraction of the incident photons gains energy from the molecular vibrations. This shift in energy gives information about the molecular vibrational modes in the system. Raman spectroscopy is a powerful tool to study the sp^2 and sp^3 hybridizations of carbon atoms in carbon nanostructures and it is largely utilized for analyzing the defects in graphene and CNTs.

The Raman spectrum of the powder samples under study was recorded in WiTech alpha 300 Raman system excited with 488 nm.

2.3.1.3. X-ray diffraction studies

XRD is a very useful tool to identify crystalline phases and orientation, hence helps in determining the structural properties of the crystalline materials. In a typical X-ray diffractometer, X-rays generated by a cathode ray tube, is filtered to produce monochromatic X-rays, collimated to concentrate and direct towards the sample. The dominant effect that occurs when an incident beam of

monochromatic X-rays interacts with a target material is the scattering of the X-rays from atomic lattices within the target material. In crystalline materials, the scattered X-rays undergo constructive and destructive interference. The diffraction of X-rays by crystals is described by Bragg's Law, $n\lambda=2d \sin\theta$ (Bragg, 1912). The directions of possible diffractions depend on the size and shape of the unit cell of the material. The intensities of the diffracted waves depend on the kind and arrangement of atoms in the crystal structure. When a powder with randomly oriented crystallites are placed in an X-ray beam, the beam will see all possible inter atomic planes. If the scanning angle of the detector is systematically changed, all possible diffraction peaks from the powder will be detected. Calculation of d-spacing from diffraction peaks allows the identification of the material, because each material has a set of unique d-spacings. Material identification is achieved by the comparison of calculated d-spacings with standard reference data.

Bruker AXS D8 advance X-ray diffractometer with Cu Kα (λ=1.54 Å) radiation was used for XRD studies of the synthesized powder samples. XRD pattern was recorded in the range $2\theta = 5^{o}$ to $2\theta = 50^{o}$.

2.3.1.4. X-ray photoelectron spectroscopy

XPS is a quantitative spectroscopic technique that measures the surface elemental composition at parts per thousand range. It also gives information about chemical and electronic state of the elements. The spectrum is recorded by measuring the kinetic energy and number of electrons ejecting from the material by irradiating with a beam of soft X-rays (with a photon energy of 200-2000 eV). The characterestics of the electrons escaping from the top 0 to 10 nm of the material being analyzed can be obtained by this technique. Each core atomic orbitals of elements are associated with a characteristic binding energy, hence each element will give a set of peaks in the photoelectron spectrum. Moreover, the intensity of the peaks is related to the concentration of the element. Thus, the technique provides a quantitative analysis of the surface composition and is known by the alternative acronym, ESCA (Electron Spectroscopy

for Chemical Analysis). The shape and binding energy of each peak can be changed by the chemical state of the emitting atom. Hence XPS also provides chemical bonding informations. (Kai et al., 1967). XPS can detect all the elements except hydrogen or helium.

In our studies, Kratos Axis ultra photoelectron spectrometer with a monochromatic Al Kα X-ray source (1486.6 eV) was used to study the elemental compositions of the sample. The samples under study were in the powder form.

2.3.1.5. Ultraviolet-visible absorption spectroscopy

UV-visible absorption spectroscopy is the measurement of the attenuation of a beam of light in the visible, near-UV and near-infrared ranges after transmitting or reflecting from a sample surface. In this region of the electromagnetic spectrum, the energies are sufficient for electronic transitions (Skoog et al., 2007). Various kinds of electronic excitations are possible in organic molecules such as n-π*, π-π*, n-σ*, π-σ*, σ-π* and σ-σ *. Out of these six transitions, only two lowest energy transitions (n-π*, π-π*) are possible by the energies available in the 200 to 800 nm spectrum.

The light source commonly used is deuterium discharge lamp for UV measurements and a tungsten-halogen lamp for visible and NIR measurements. A combination of photomulplier tube and a Peltier-cooled PbS IR detector is used in UV-visible-NIR spectrometers.

Optical absorption measurements of the powder samples were recorded in 2-propanol using Cary 100 Bio UV-visible spectrophotometer.

2.3.1.6. Fluorescence spectroscopy

Fluorescence spectroscopy analyzes fluorescence from a sample. Fluorescence occurs when a fluorophore is excited into a higher electronic state by absorbing an incident photon and returning to the ground state by emitting a

photon. A fluorescence emission spectrum is recorded by scanning the emission beam as a function of wavelength at a particular excitation wavelength.

A typical fluorescence spectrometer (spectrofluorometer) contains a sample holder, a xenon lamp, monochromators, focussing optics and a detector. The detector is commonly kept at 90 degrees to the light source. Jobin Yvon Flurolog 3-11 spectrofluorometer was used for the measurements of the samples under study. The samples were dispersed in 2-propanol (1 mg in 5 ml).

2.3.2. Thermogravimetric analysis

TGA is a technique which records the weight loss of a substance as a function of temperature, when it is subjected to an environment heated or cooled at a controlled rate (Coats and Redfern, 1963). TGA provides information about physical phenomena as well as chemical phenomena.

A thermogravimetric analyzer consists of a sample pan with a precision balance. The pan is heated or cooled in a furnace during the experiment. Usually a null type balance with a sensing element is used to detect change in mass. The sample environment is controlled by a purge gas, which may be inert or reactive. The heating can be programmed in a controlled rate. Usual sample size is between 1 mg to 10 mg.

Thermal studies of the samples were done using thermogravimetric analyzer (TGA Q50, TA instruments) at a heating rate of 10 ^{o}C/min under nitrogen atmosphere from room temperature to 800 ^{o}C.

2.3.3. Zeta potential measurements

Zeta potential analysis determines the magnitude of surface charge of the particles in a colloidal dispersion. It measures the degree of repulsion between similar charges in a colloid. It is the fundamental parameter affecting the stability of a dispersion. The Zeta potential values usually range from -100 mV to +100 mV. Stable dispersion usually have a zetapotential values greater than +25 mV or

less than -25 mV. The dispersion of particles with zeta potential outside this range will eventually aggregate due to van der waals attractions.

To get insight into the self assembled nanostructures of polyaniline, the Zeta potential values of polyaniline dispersions in 2-propanol was studied using Malvern Zetasizer Nano ZS.

2.3.4. Microscopic techniques

2.3.4.1. Scanning electron microscopy

Similar to an optical microscope SEM provides topographical information of the specimen being investigated, but with a nanoscale resolution. Conventional light microscopes use a series of glass lenses to create a magnified image, where as an electron microscope creates magnified image by using electrons instead of light waves. SEM is an electron microscope that images sample by scanning it with high energy beam of electrons. The electrons interacts with the atoms of the sample and produces signals with information about sample surface topography, composition, etc. SEM produces signals including secondary electrons, backscattered electrons (Goldstein, et al., 1981), characteristic X-rays, cathodoluminescence, transmitted electrons etc. The most common detector is secondary electron detectors. Using secondary electron detector, SEM can produce very high resolution images of a sample surface, revealing details about less that 1 to 5 nm in size. SEM images have a large depth of field, hence a characteristic 3 D appearance due to the very narrow electron beam. A wide range of magnification is possible from about 10 times to more than 500000.

For SEM imaging, the specimen must be electrically conductive at least at the surface to prevent the accumulation of electrostatic charge on the surface. When scanned by the electron beam, nonconducting specimens tend to charge and this causes scanning faults. So the specimens are usually coated with conducting materials like gold.

In our work, the specimen for SEM were prepared by drop casting the

dispersion of the samples in 2-propanol on a piece of carbon tape and the morphology of the samples were analyzed using FEI Quanta FEG 200 high resolution scanning electron microscope.

2.3.4.2. Transmission electron microscopy

In this technique, a beam of electrons accelerated with 100 kV potential or higher (up to 1 MV) is transmitted through an ultra thin specimen (usually less than 200 nm in thickness). TEM provides information on the sample morphology at a resolution of 1nm or even smaller, crystallography and its elemental composition. The scattering of the electrons during the transmission determines the kind of information about the sample. Through elastic scattering, electrons do not lose energy during the transmission and diffraction patterns of the samples can be observed. Whereas, inelastic interaction between the primary electrons and the electrons from the sample at the heterogeneities of the nanostructures causes a complex absorption and scattering effects and produces spatial variations in the intensity of the transmitted electrons, which can be distinguished by the detector during image formation.

For imaging using TEM, samples dispersed in 2-propanol was placed on the inner meshed area of TEM grid made up of Cu. It has a diameter of 3 mm with a thickness and mesh size ranging from few to 100 μm. The sample was dried under vacuum before imaging. TEM imaging was done using FEI Quanta high resolution transmission electron microscope.

2.3.4.3. Atomic force microscopy

AFM is a high resolution scanning probe microscope. AFM scan the specimen using a sharp tip (a couple of microns long and less than 100 Å diameter) located at the free end of a cantilever. When the tip is brought closer to the sample surface, the van der Waals interaction between the tip and sample lead to a deflection of the cantilever according to Hooke's Law (Cappella and Dietler, 1999). The deflection of the cantilever is measured using a laser spot reflected from the top surface of the cantilever in an array of photodiodes.

Depending on the applications, there are number of modes of operation in AFM. Most common are contact or non-contact modes (Binnig and Quate, 1986). In contact mode, the cantilever is scanned across the surface of the sample and the surface features of the sample are measured directly using the deflection of the cantilever. The tip is held at a distance less than few Å from the sample surface and the force between the tip and sample is repulsive. When the cantilever pushes the tip against the sample, it bends and the position of the laser beam on the detector changes. The position sensitive photodetector can measure displacements of light due to cantilever deflections as small as 10 Å. Generally in non-contact mode, the tip of the cantilever is oscillated at its resonant frequency or just above (Gross et al., 2009). The van der Waals forces between the sample and tip decreases the resonance frequency of the cantilever. Then by adjusting the average tip-to-sample distance, the feedback loop system maintains a constant oscillation frequency or amplitude. Measuring the tip-to-sample distance at each data point constructs the topographic image of the sample.

The samples for AFM were prepared by dropcasting the dispersion in isopropyl alcohol on freshly cleaved mica surface and imaging was done using Agilent technologies N9451A atomic force microscope (AFM) in non contact mode.

2.3.5. NLO studies

Open aperture Z scan technique developed by Sheik Bahae et al. (1990) was used to study the third order NLO properties of the samples. The rapid acceptance of Z scan technique as as a standard technique for separately determining the nonlinear changes in the index and changes in absorption is primarily due to the simplicity of the technique as well as the simplicity of the interpretation.

A Q-switched Nd:YAG laser (Minilite continuum) with pulse width of 5 ns at the excitation wavelength of 532 nm operating at 10 Hz was used as a source

and a lens of 10 cm focal length was used to focus the laser. The sample dispersed in DMF at a linear transmittance of 75% was mounted on a computer controlled translation stage. While moving the sample through the focus along the laser direction, the input energy as well as the transmitted energy were measured by two similiar pyroelectric energy probes (RjP 735, Laser Probe Corp.), which were connected to an energy meter (RJ7600, Laser Probe Corp.). The experimental set up for the open aperture Z scan technique is sketched in Fig. 2.1.

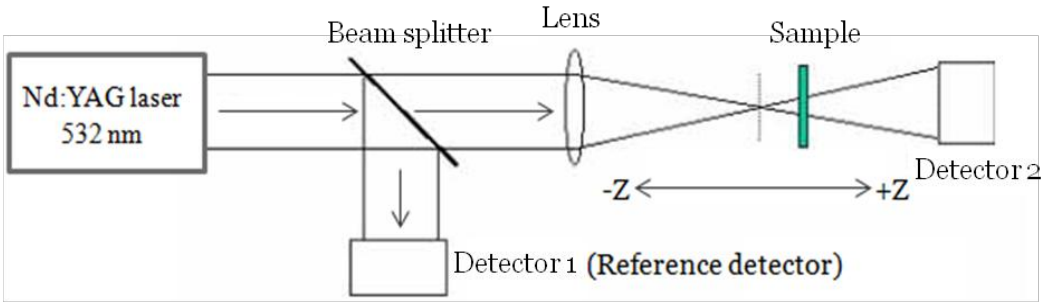

Figure 2.1 Open aperture Z scan experiment set-up for measuring the nonlinear absorption properties of the materials (Sutherland, 2003).

The incoming beam was first split by a beam splitter. The reflected light was recorded by detector 1 (D_1), as a reference. The transmitted light was focused by a convex lens and the power of the light transmitted through the sample was measured by detector 2 (D_2). Then the information of the nonlinearity can be derived from the ratio of D_2 to D_1 as a function of the position z (relative to the focal plane). In open aperture Z scan technique, the entire energy transmitted through the sample is collected. So the reduction in transmittance measured is independent of the nonlinear refraction and thus can be used to determine the nonlinear absorption coefficient. The nonlinear absorption coefficient can be extracted by fitting the experimental data with the Z scan theory.

In the Z scan experiment, the thickness of the sample L should be smaller than the diffraction length of the focused beam ($L < Z_0 = \pi\omega_0^2 / \lambda$, ω_0 is the beam waist). In this case, the sample length is small enough that changes in the beam diameter within the sample due to either diffraction or nonlinear refraction can be

neglected, the sample can be regarded as thin sample, in which the self-refraction process can be referred to as "external self-activity" (Yang H., 2012).

Data Analysis

For the nonlinear absorption, material satisfies the attenuation equation,

$$\frac{dI}{dz'} = -(\alpha_0 + \alpha_2 I)I \tag{2.1}$$

where α_0, α_2 are the linear absorption and two photon absorption coefficients respectively. Integrating Eq. (2.1) over z´, we obtain the irradiance at the exit surface of the sample as follows:

$$I_e(z,r,t) = \frac{(1-R)^2 I_i(z,r,t)e^{-\alpha_0 L}}{1+q(z,r,t)} \tag{2.2}$$

where $q(z,r,t) = (1-R)\alpha_2 I_i(z,r,t)L_{eff}$, $L_{eff} = (1-e^{-\alpha_0 L})/\alpha_0$, R is the reflectance, L is the sample thickness, incident beam intensity $I_i(z,r,t)$ can be expressed as:

$$(1-R)I_i(z,r,t) = I_0(z)\exp\left[-2r^2/w^2(z)\right]\exp\left[-(t/t_0)^2\right] \tag{2.3}$$

Where $I_0(z) = I_0 \Big/ \left(1+\frac{z^2}{z_0^2}\right)$, $w^2(z) = w_o{}^2\left(1+\frac{z^2}{z_0^2}\right)$, $z_0 = \pi w_0^2/\lambda$, w_o is the minimum beam waist at the focal plane.

The normalized transmittance can be obtained by integrating the Eq. 2.2 over the space and temporal Gaussian pulses. The result is expressed as

$$T(z) = \frac{1}{q_0\sqrt{\pi}}\int_{-\infty}^{+\infty}\ln\left[1+q_0\exp(-x^2)\right]dx \tag{2.4}$$

where $q_o = \alpha_2 I_0 L_{eff}$, $L_{eff} = (1 - e^{-\alpha_0 L}) / \alpha_0$

2.3.6. DC conductivity measurements

The DC conductivity of the samples were measured using four-probe method. The four-probe method is one of the standard and most widely used methods for the measurement of resistivity.

The four-point-probe contains four thin collinearly placed tungsten wire probes. Current I is forced to flow between the outer probes, and voltage drop (V) was measured between the two inner probes. If the sample is of semi-infinite volume and if the inter probe spacings are equal (s), then it can be shown that the resistivity of the semi-infinite volume is given by,

$$\rho = (2\pi s)(V / I) \tag{2.5}$$

But practically samples are of finite size. Hence correction factors for six different boundary configurations have been introduced by Valdes (1954). According to this, if the distance from any probe to the nearest boundary is at least 5s, no correction is required. For the cases when the sample thickness is ≤5s, the true resistivity can be computed by using the thickness correction factor as given in Eq. 2.5. If the t/s ≤0.5, the resistivity can be calculated by the equation;

$$\rho = (\pi / \ln 2)(V / I)t \tag{2.6}$$

Both the equations, 2.5 and 2.6 can be applied only if the sample size is large compared to the probe spacing. In order to get accurate measurements correction for the edge effects is required. If the ratio of the pellet diameter to the spacing is greater than 40, no edge corrections are needed. For our studies, we used circular pellets of the samples with diameter 13 mm and thickness less than 0.5 mm. The pellets of the samples were prepared by applying a pressure of 4 tons using a

hydraulic press (PCI Analytics Pvt. Ltd, Mumbai). The probe spacing used was 2 mm. So the thickness correction factor is not needed and edge correction of 0.82 was applied to the Eq. 2.7. The correction factor is obtained from the National Bureau of Standards Technical Note 199 – "Correction Factor Tables for Four-Point Probe Resistivity Measurements on Thin, Circular Semiconductor Samples".

In the present study, the current from a DC-source meter (Keithley, 2182A) was allowed to pass through the outer probes of the four-probe and voltage across the two inner probes was measured using nanovoltmeter (Keithley, 6221). The resistance was obtained from the slope of the I-V plot.

2.3.7. Photocurrent generation studies

Photocurrent experiments were conducted using Autolab electrochemical work station in a conventional three electrode electrochemical cell comprising of the thin film sample as the working electrode, platinum wire as counter electrode and Ag/AgCl as a reference electrode. 0.2 M Na_2SO_4 taken in a quartz beaker was used as the electrolyte solution. The electrolyte was bubbled with nitrogen before and during the measurement. The active area of the working electrode was 0.25 cm^2. The potential of the working electrode was set at 3 V against the Pt counter electrode. An incandescent lamp operating at 300 W was used as the illumination source. The photointensity was measured using digital solar meter (Daystar meter, USA) which uses polycrystalline silicon photovoltaic cell as the sensor. The light intensity chosen for the measurement was 100 mW/cm^2. The photoresponse property of the samples under white light illumination was studied by measuring the photocurrent growth and decay of the samples by repetitive switching of the illumination (on/off) at an interval of 30 s using a stop watch. The photocurrent was calculated by taking difference between the observed current after the illumination of the sample and the dark current.

$$Photocurrent = I_{light} - I_{dark} \tag{2.8}$$

Schematic representation of the experimental set up is given as Fig. 2.2.

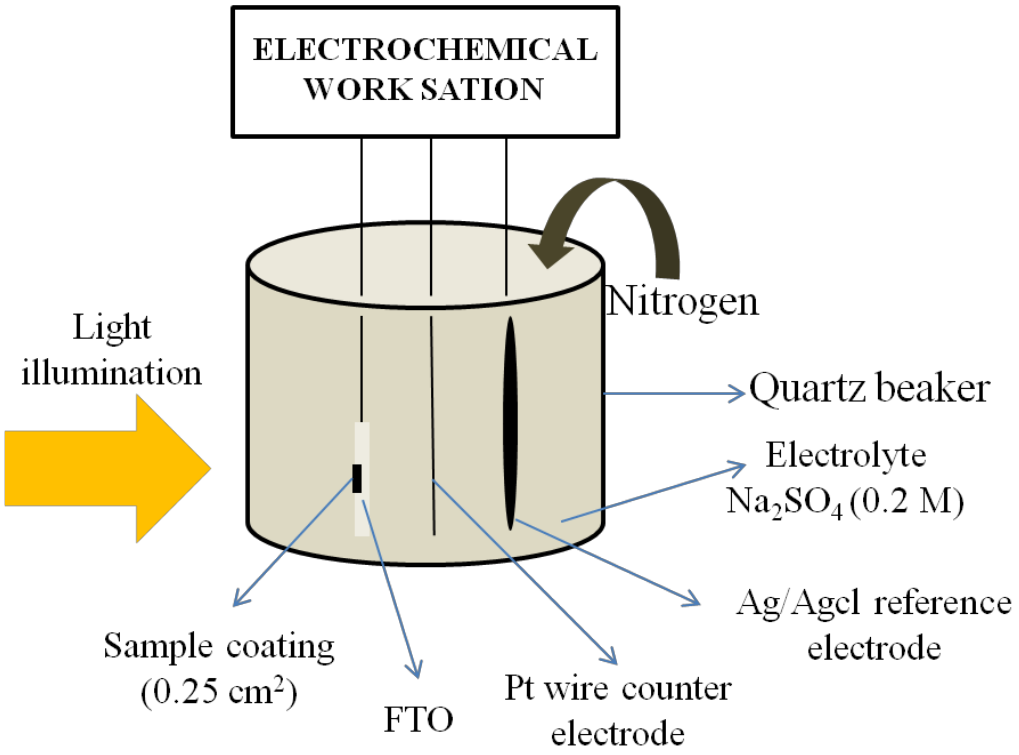

Figure 2.2 Experimental set-up for measuring the photocurrent generation

CHAPTER 3
STUDIES ON POLYANILINE: SYNTHESIS BY INVERSE MICROEMULSION POLYMERIZATION

In this chapter, a novel inverse microemulsion polymerization technique is discussed for the synthesis of nanostructured and processable cube-like polyaniline. The polyaniline is well characterized using FTIR, XRD, XPS, SEM, TEM, etc. and the formation mechanism is identified. Open aperture Z scan studies of polyaniline dispersion in DMF shows the suitability of cube-like polyaniline for optical limiting, and hence polyaniline-PMMA films are fabricated and the nonlinear optical properties are studied in detail. The photocurrent generation in polyaniline is also discussed in this chapter.

3.1. Introduction

Polyaniline, one of the highly pursued conducting polymer has attracted great attention in wide variety of research areas like, lightweight batteries (Karami et al., 2003), electrochromic displays (Akhtar et al., 1988), electroluminescent devices (Chen et al., 1996), electrochemical actuators (Sansiñena et al., 2003), sensors (Huang et al., 2004; Huang et al., 2002), supercapacitors (Gupta and Miura, 2006), Schottky diodes (Narasimhan et al., 1998), photonic devices (Englebienne and Van Hoonacker, 2005), etc., because of its good environmental stability, ease of synthesis, low cost, lightweight, and tunable electrical conductivity. It also shows a particular sensitivity to proton activity on the environment. Polyaniline has a flexible –NH– group in the polymer chain flanked by phenyl rings on both sides. The difference in composition of amine and imine segments of polyaniline generates several oxidation states ranging from completely reduced leucoemeraldine to completely oxidized pernigraniline states as shown in Fig. 3.1.

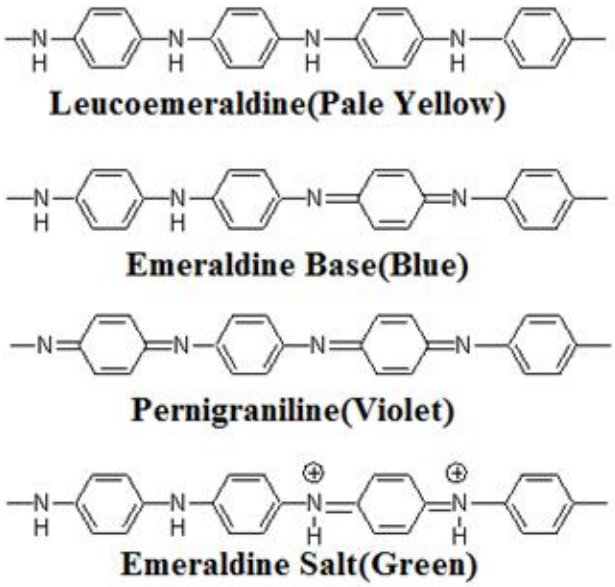

Figure 3.1 Various possible oxidation states of polyaniline

Out of several possible oxidation states, 50% oxidised emeraldine salt shows electrical conductivity. The uniqueness of polyaniline is the sensitivity of the emeraldine oxidation state of polyaniline to pH, which yields emeraldine base and emeraldine salt. Nonconducting emeraldine base form can be easily converted to highly conducting emeraldine salt by simple protonation using mineral or organic protonic acids. The protonation is accompanied by a drastic change in electronic structure, crystallinity, solubility, etc. Eventhough protonation improves the conductivity, inorganic mineral acid doped polyaniline is mostly insoluble. Counter ion-induced processability by the use of organic acids as dopants is one important solution for improving the processability of polyaniline.

Synthesis in nano dimensions is an important aspect of improving the solubility and processability of polyaniline. The nanostructured and processable polyaniline can be easily fabricated as thin films for a variety of applications. Especially optical limiting and photocurrent generation applications demand easy fabrication of films of polyaniline. The control of the size and shape of polyaniline nanostructures has gained wide attention due to their superior surface and electron transport properties (Gao et al., 2011; Zhang Y. S. et al., 2009).

The most widely employed polyaniline synthesis is the chemical oxidation of aniline in aqueous acidic media using APS as the oxidant. This conventional solution polymerization of polyaniline is known to produce agglomerates with irregular shape due to secondary growth. Hence several methods have been developed for the synthesis of nanostructures of polyaniline. The common method for the synthesis of polyaniline nanostructures includes chemical, electrochemical, template, enzymatic, plasma methods, etc. Chemical methods can be subdivided into heterophase, solution, interfacial, seeding, metathesis, sonochemical, self assembling polymerizations, etc. The heterophase polymerization method includes different methods like precipitation, suspension, emulsion, and so on. In comparison with conventional polyaniline aggregates, polyaniline micro/nano architectures including spheres (Dhand et al., 2010; Fu et al., 2007; Lei et al., 2009), rods (Bhadra and Sarkar, 2009; Ding et al., 2008; Kuila et al., 2009) and fibers (Huang and Kaner, 2003; Huang et al., 2002; Zhang X. et al., 2004) combine the advantages of both organic conductors and low dimensional systems (e.g. large surface area, quantum effect) and yields many interesting physicochemical properties and useful applications.

Template synthesis using hard templates like anodic aluminium oxide, channels of zeolites, etc. and soft templates like surfactant or any other material organized in a particular nanostructure is another interesting method adopted by researchers to develop nanostructured polyaniline. Qiu et al., (2001) synthesized polyaniline nanotubes by *in situ* doping polymerization using β–NSA as the dopant, called as template free method. Organic dopants like β–NSA, ABSA, D-10-CSA, etc. also have been used for the synthesis of self assembled polyaniline nanostructures by template-free approach.

In recent years, emulsion polymerization (macroemulsion, mini emulsion, microemulsion) of aniline (Kane and Krafcik, 2013) has come the forefront. The concept of emulsion polymerization of aniline is introduced by Österholm et al. (1993) wherein DBSA is used as a surfactant and dopant. The chemical oxidative polymerization of aniline in water-oil microemulsions has

been intensively investigated. Emulsion polymerization is a compartmentalized polymerization reaction taking place in a large number of micelles dispersed in a continuous external phase. This method has several advantages over other polymerization techniques. The physical state of the emulsion makes it easier to control the polymerization. Thermal and viscosity problems are less significant than in bulk polymerization. High molecular weight and high reaction rates can be achieved by this method. The emulsions are divided into two types; direct (oil in water) and inverse (water in oil). The type of the emulsion depends on the choice of emulsifier, water to oil ratio, temperature of the polymerization, etc.

Polyaniline is an attractive candidate for NLO applications, because of its good nonlinear absorption coefficient, high damage threshold and ultrafast response (Osaheni et al., 1992). Various materials including organic dyes, organometallics, fullerenes, semiconductors, and conjugated polymers are studied for optical limiting applications (Balapanuru et al., 2010; Krishna et al., 2011; Zhu et al., 2011). Several scientific publications reported that many materials exhibit different nonlinear absorption processes simultaneously depend upon the wavelength or intensity of the laser beam, concentration of the active material, etc. (Gao et al., 2007; Gurudas et al., 2008; Notaras et al., 2007). Zheng et al. (2010) reported both saturable absorption (SA) and reverse saturable absorption (RSA) in silica gel composites of silver nanowires depending upon the intensity of the laser beam. Sreekumar et al. (2009) found the transition from SA to RSA for nanoclustered amido black dye–polymer films while increasing the dye content. Among the conjugated polymers, polyaniline is widely studied for NLO applications (Pandey et al., 2009; Sezer et al., 2009; Chen et al., 1994; de Souza et al., 1995). Most of the studies on polyaniline for NLO applications are done in the form of dispersions in solvents. But the real application of optical limiting requires easy fabrication of films without compromising its optical limiting properties. Very few publications reported NLO properties of polyaniline films in inert matrices (Mattes et al., 1991). One of the main difficulties in using polyaniline for optical application is its low solubility in common solvents, resulting in aggregation and thereby causing the decay of optical properties.

Immobilization of NLO material in a transparent host is needed for device fabrication.

One of the key properties of polyaniline is the presence of conjugated double bonds in polymer backbone and hence a wide energy gap between 2-3.5 eV. But this conjugation in itself is not enough to induce desired electronic properties in the polymer. It is reported that any wide gap semiconducting material can be made more photo-absorbing by creating mid gap energy levels by doping (Kurmaev et al., 2001). The physics of photocurrent generation in organic and polymer materials have some fundamental differences with that of the inorganic counterparts. Major difference is the short exciton diffusion lengths and relatively large exciton binding energies. This short exciton diffusion lengths in the range of 10 nm and exciton binding energies of ~0.5 eV are the major cause of comparatively reduced efficiencies for organic and polymeric materials (Friend et al., 1997). Moreover the devices made of single conjugated polymers have very low efficiencies, since the electric field provided by the asymmetrical work functions of the electrodes being insufficient in dissociating the excitons produced. The p type acid doping in polyaniline will introduce sub-bands within the band gap and brings a strong light absorption band in polyaniline. Due to this high absorption coefficients in the visible range along with high mobility of charge carriers and good environmental stability, polyaniline is a very attractive material for photocurrent generation and hence for solar cell applications (Jeon et al., 2012).

With this background, in this chapter, we are introducing a novel inverse microemulsion polymerization technique for the synthesis of nanostructured and processable polyaniline. Inspired from the template–like action of TSA for the growth of polyaniline and also from the recognition of bulky organic acids for improving the processability of polyaniline, we selected TSA as the dopant. We are also reporting the open aperture Z scan studies of polyaniline in DMF, which shows the suitability of the synthesized polyaniline for optical limiting applications. Thin films of polyaniline in transparent PMMA host are also

fabricated and its NLO properties are studied in detail. Photocurrent generation studies of the synthesized polyaniline films under white light irradiation are also included in this chapter.

3.2. Experimental

3.2.1. Synthesis of polyaniline

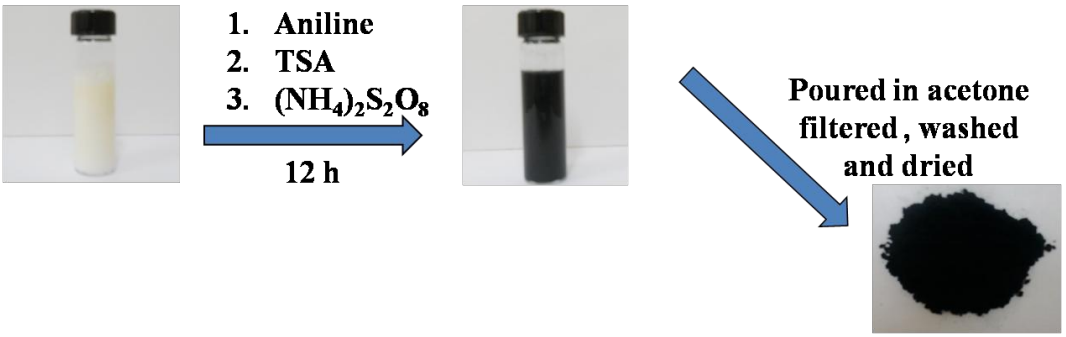

Figure 3.2 Schematic representation of the synthesis of polyaniline by inverse microemulsion polymerization

Polyaniline nanostructures are synthesized by introducing a novel inverse microemulsion polymerization technique. The scheme for the synthesis is shown in Fig. 3.2. In a typical inverse microemulsion polymerization technique, two steps are involved, namely the generation of an inverse emulsion, and the synthesis of polymer inside the inverse emulsion. Paraffin oil-water microemulsion is prepared by mixing oil (1 g) and oleic acid (5.65 g) in the presence of ammonia solution (0.1 M, 20 ml)). The *in situ* generated ammonium oleate is acting as the surfactant. Aniline (1 g) is polymerized in this oil-water emulsion using toluenesulphonic acid (1 M, 25 ml) as dopant, ammonium per sulphate (2 M, 7 ml) as the initiator and auxisol as the stabilizer. Freshly distilled aniline is added to the newly prepared oil-water emulsion and it is stirred in the presence of auxisol stabilizer. TSA is added dropwise to the emulsion system and finally aniline in emulsion is polymerized by the slow addition of the initiator in 30 minutes. Here TSA acts both as dopant and structure directing agent. The reaction is carried out for 12 h with constant stirring at room temperature. After polymerization, polyaniline is precipitated by using acetone. The dark green polyaniline formed is washed with excess acetone, methanol and distilled water. It

is then dried under vacuum at 60 ^{o}C for 24 h. For a detailed study on the structure of polyaniline formed in the above mentioned emulsion, the reaction is repeated by keeping the reaction time as 4 h and 8 h. Polyaniline is also synthesized by chemical oxidative polymerization in the absence of the emulsion system to study the effect of inverse emulsion polymerization on the structure and properties of polyaniline.

3.2.2. Fabrication of polyaniline-PMMA films for optical limiting studies.

Polyaniline-PMMA films are prepared by the *in situ* polymerization technique. The monomer methyl methacrylate is washed with 20% NaOH three times to remove the inhibitor prior to polymerization. The excess NaOH is washed out using distilled water and the inhibitor free monomer is dried over sodium sulphate. Weighed amount of polyaniline is dispersed in the monomer (5 ml) by means of ultrasonication. The monomer/polyaniline dispersion is then polymerized using benzoyl peroxide (0.025 g) as initiator at 80 ^{o}C in an oil bath. The viscous polymer formed is immediately casted on a glass plate and dried in air at room temperature. By varying the concentration of polyaniline (0.02 to 0.1 wt % with respect to the monomer), free-standing and flexible films with an average thickness of 0.25 mm are fabricated. The schematic representation of the film fabrication is given Fig. 3.3. The photograph shown in the scheme reveals the good quality of the film.

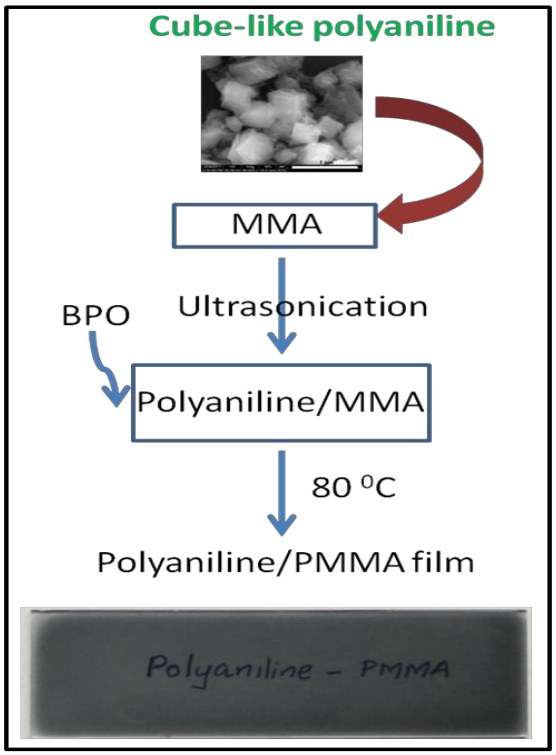

Figure 3.3 Schematic representation of the film fabrication

3.2.3. Fabrication of polyaniline films for photocurrent measurements

Thin films of polyaniline for photocurrent measurement are fabricated on clean FTO glasses. The FTO glasses are cleaned by ultrasonication in acetone, methanol and distilled water. The polyaniline (10 mg) dispersion is made in cresol/nafion (2:1 ratio, 3 ml) mixture. 300 µl of the dispersion is spin coated on FTO glasses (2 cm^2) at 1500 rpm for 1 min. After spin coating, the films are dried at room temperature for 15 min and baked at 100 ^oC for 30 min. For the photocurrent measurements, active area of the film is fixed as 0.25 cm^2 by masking the remaining portion with black tape.

3.3. Results and Discussion

3.3.1. Characterization

Molecular structure of polyaniline is analyzed using Fourier Transform Infrared (FTIR) spectrum as shown in Fig. 3.4. The characteristic peaks obtained are in good agreement with the previously reported results (Jang et al., 2007). The

out-of-plane bending vibration of C-H on 1,4-disubstituted rings are found at 823 cm^{-1} and the bands at 1580 and 1497 cm^{-1} are attributed to the stretching vibrations of C=C quinonoid rings and benzenoid rings respectively. Aromatic C-H in-plane bending vibration is observed at 1156 cm^{-1}. The vibration band at 1249 cm^{-1} corresponds to the C-$N^{+\cdot}$ stretching modes of the polaronic charge carriers in the doped polyaniline, while the peak at 1309 cm^{-1} is due to the stretching vibration of the C-N bond.

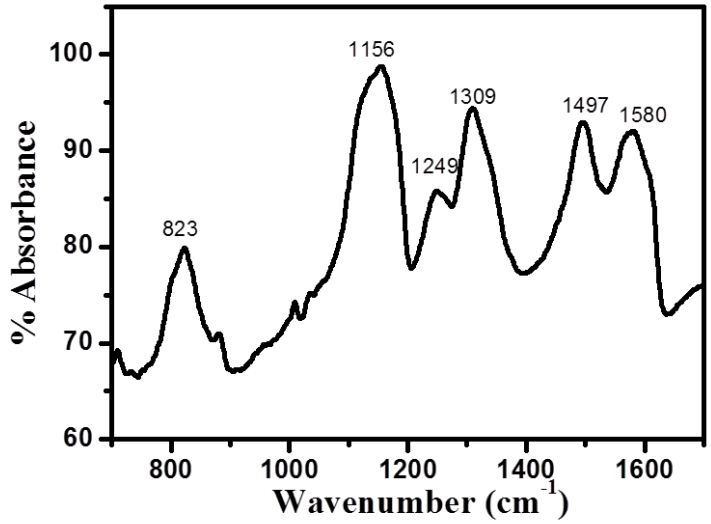

Figure 3.4 FTIR spectrum of polyaniline

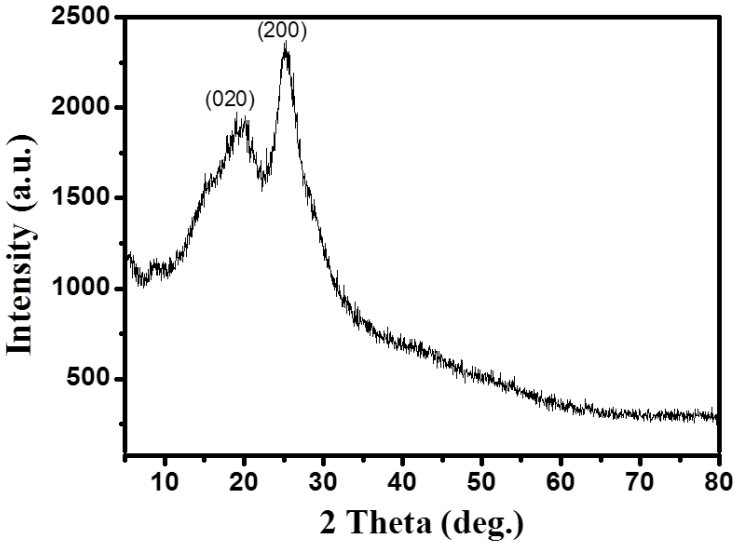

Figure 3.5 XRD spectrum of polyaniline

Fig. 3.5 represents the X-ray diffraction (XRD) pattern of polyaniline, showing typical peaks at 20 and 25°. These peaks are ascribed to the periodicity parallel and perpendicular to the polymer chains, respectively (Pouget et al., 1991) and these crystalline peaks are assigned to (020) and (200) reflection of polyaniline in emeraldine salt form. The strong peak at 25° indicates a very good π-π inter chain stacking between the phenyl rings leading to the effective conjugation.

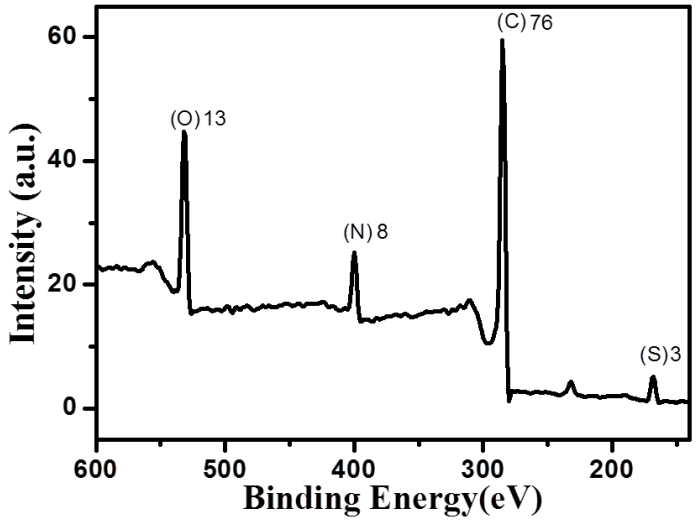

Figure 3.6 XPS spectrum of polyaniline

A typical X-ray photoelectron spectrum (XPS) of polyaniline is shown in Fig. 3.6. It reveals four peaks at 532, 400, 285 and 168 eV corresponding to the presence of O, N, C, and S respectively in polyaniline. The percentage of each element is quantified as 76 % carbon, 13 % oxygen, 8 % nitrogen and 3 % sulphur.

Thermo gravimetric analysis (TGA) of polyaniline is carried out under nitrogen atmosphere with a heating rate of 10 °C and the decomposition pattern is given in Fig. 3.7. The first weight loss observed from 200 to 350 °C is due to the loss of oligomers and bounded dopant TSA. The weight loss in the temperature range 350-600 °C is due to the main chain degradation of polyaniline (Chan et al.,1989). Polyaniline retains approximately about 57% of its original weight at

temperature as high as 600 °C. The strong dipole-dipole interaction between the polymer network may be the prime reason for higher thermal stability of polyaniline (Freshour, 1995).

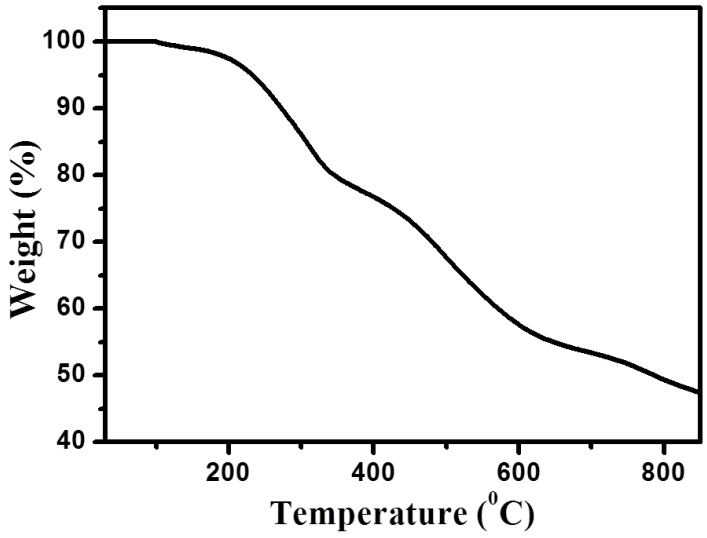

Figure 3.7 TGA pattern of polyaniline

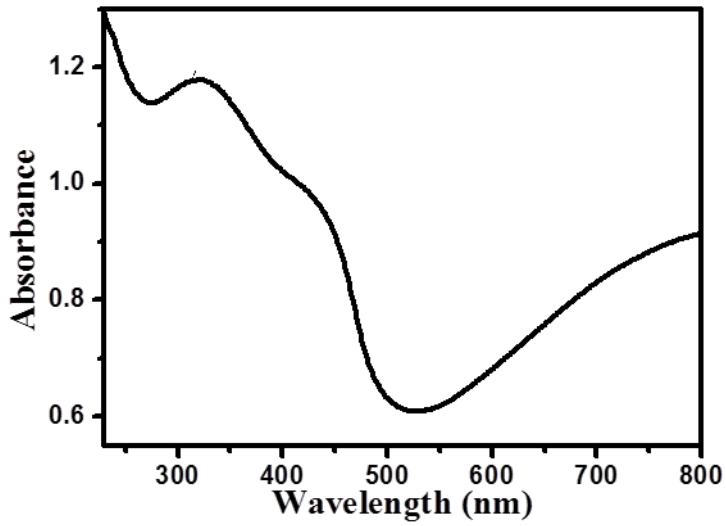

Figure 3.8 UV-visible spectrum of polyaniline

UV-visible spectrum of the polyaniline recorded in 2-propanol is shown in Fig. 3.8 (a). It reveals a λ_{max} at 325 nm due to the π-π^* transition of the benzenoid rings, a shoulder around 435 nm and a tail extending to the NIR region due to the wellknown polaron transitions (Stejskal et al., 1993). Hence the UV-

visible spectrum clearly shows the presence of broad polaronic band deep in the band gap of doped polyaniline.

Fig. 3.9 shows the photoluminescence spectrum of polyaniline in 2-propanol excited at 360 nm, showing a broad emission centered at 480 nm. The π-π* transition of the benzenoid units are responsible for the photoluminescence in polyaniline (Shimano and MacDiramid, 2001). The excitation wavelengh is chosen as 360 nm, since it falls inside the π–π* absorption envelope centered at 325 nm.

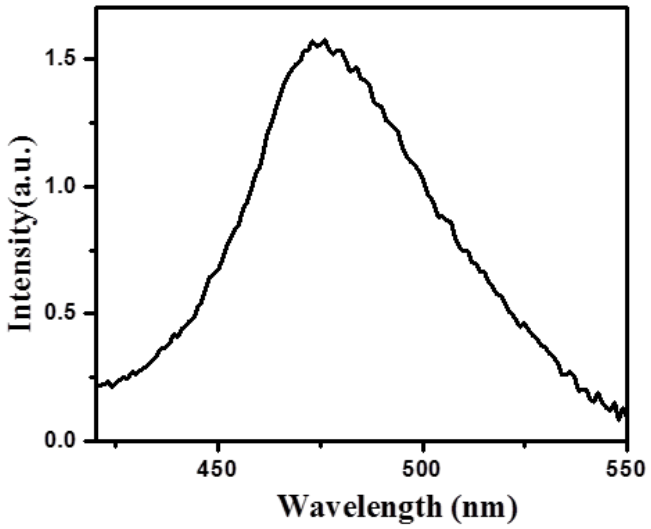

Figure 3.9 Photoluminescence spectrum of polyaniline

The morphology of polyaniline is investigated using SEM and the images are shown in Fig. 3.10 (a-d). It reveals a cube-like morphology of polyaniline with an average size of 320 nm. The high magnification image (Fig. 3.10 d) reveals the formation of cube-like nanostructures by the self assembly of polyaniline nanorods. The cube-like morphology is again confirmed using TEM images as shown in Fig. 3.11.

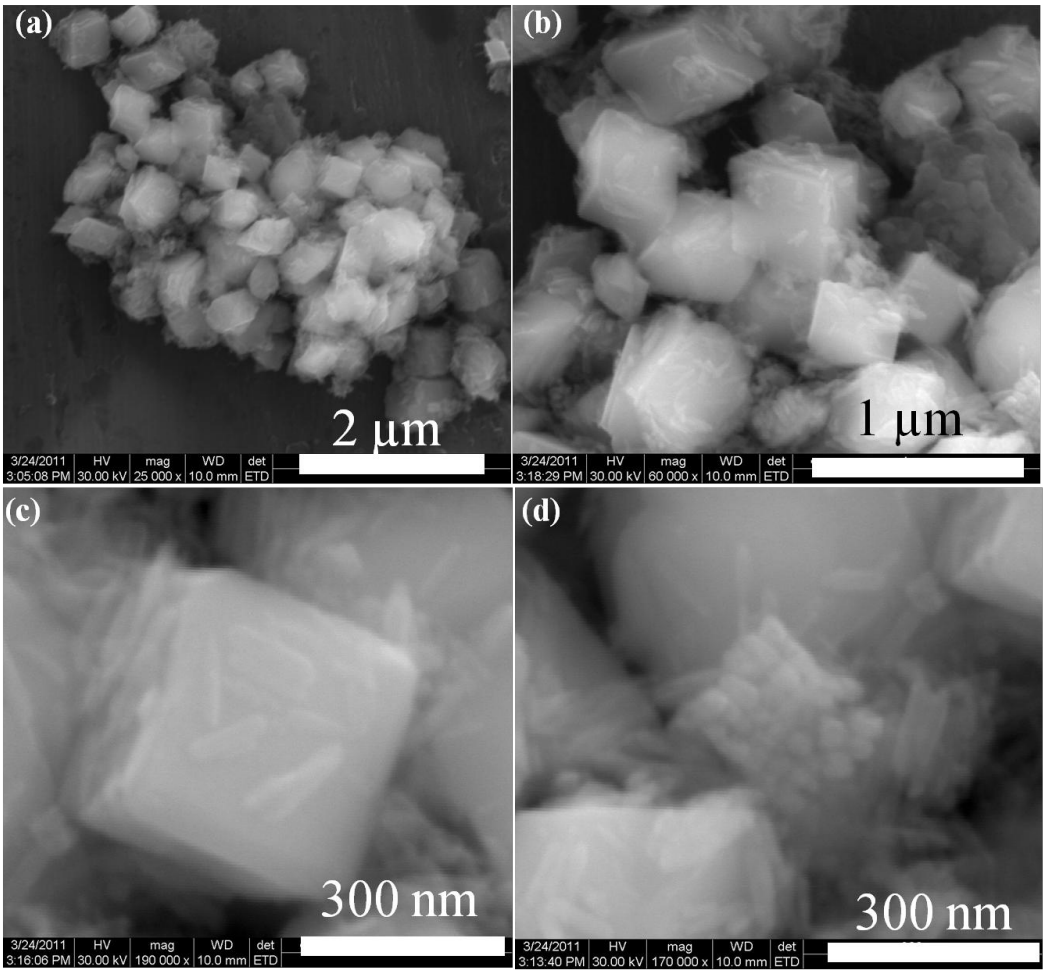

Figure 3.10 SEM image of polyaniline with different magnifications; (a) 25000x, (b) 60000x, (c) 190000x and (d) 170000x

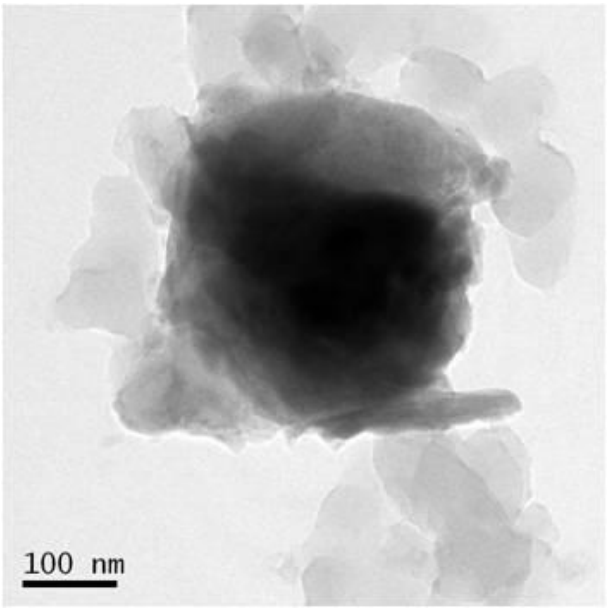

Figure 3.11 TEM image of polyaniline

3.3.2. Formation mechanism

In order to get an insight into the transformation from 1D nanorods to the 3D cube-like nanostructures, the polymerization is repeated by changing the polymerization time to 4 h and 8 h, while keeping all other conditions the same.

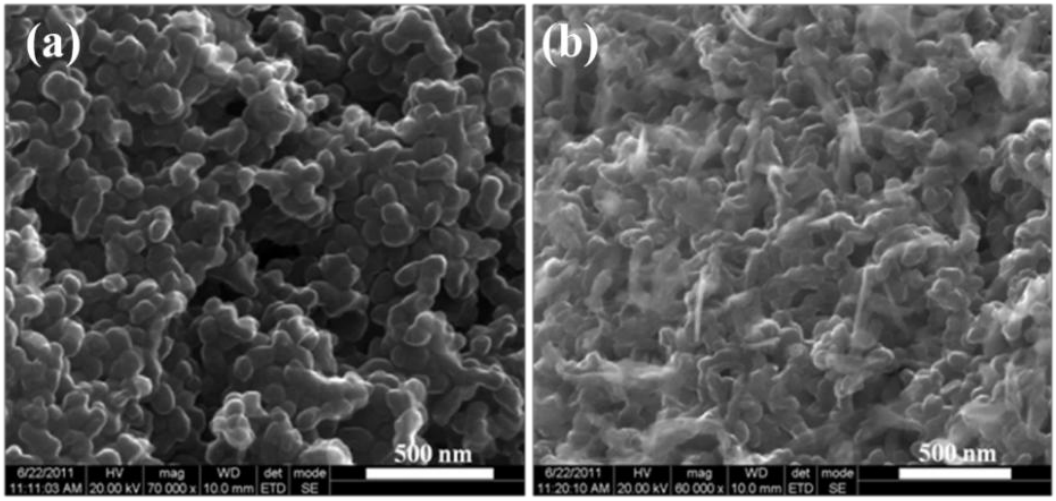

Figure 3.12 SEM image of polyaniline after (a) 4 h and (b) 8 h reaction. Magnification of (a) and (b) are 70000x and 60000x respectively

When the polymerization time is 4 h, polyaniline nanospheres are formed as shown in Fig. 3.12 (a) and when the polymerization time is 8 h, nanorods begins to appear (Fig. 3.12 (b)). As the time proceeds to 12 h, these nanorods get self assembled to form cube-like nanostructures (Fig. 3.10).

Based on these experimental evidences, the formation mechanism is proposed for the cube-like nanostructures of polyaniline. In the inverse microemulsion polymerization technique, the surfactant ammonium oleate is generated by the reaction of oleic acid with ammonia solution in the presence of paraffin oil. The structure of ammonium oleate is given in Fig. 3.13.

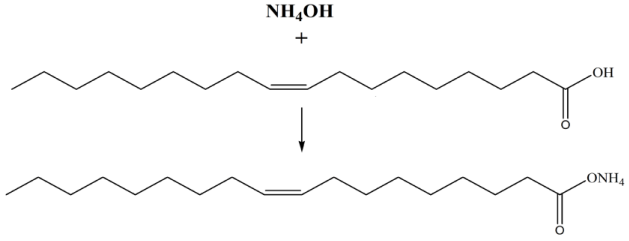

Figure 3. 13. Structure of ammonium oleate

Due to the amphiphilic nature, the ammonium oleate is acting as a surfactant and it form inverse micelles in oil-water system as shown in the inset of Fig. 3.14. The hydrophobic part (long hydrocarbon chain) of ammonium oleate extends to the oil phase and hydrophilic group ($–COONH_4$) lies in the water phase. When aniline is added to the emulsion, initially it will stay outside the micelle, i.e., in the oil phase and when the TSA is added, it will protonate a part of aniline into anilinium cations. These anilinium cations along with toluenesulphonate counter anions enter into the inverse micelles and it will self assemble to normal micelles inside the inverse micelles. The free aniline existing outside the inverse micelles will then diffuse into the normal micelles to form aniline filled micelles. This aniline filled micelles might be regarded as a template for the formation of nanorods (Huang and Wan, 2002; Wei, et al., 2003; Yang, et al., 2005; Zhang and Wan, 2005). At the initial stages, the micelles might have a spherical morphology due to the lower surface energies and the formation is represented in Fig. 3.14.

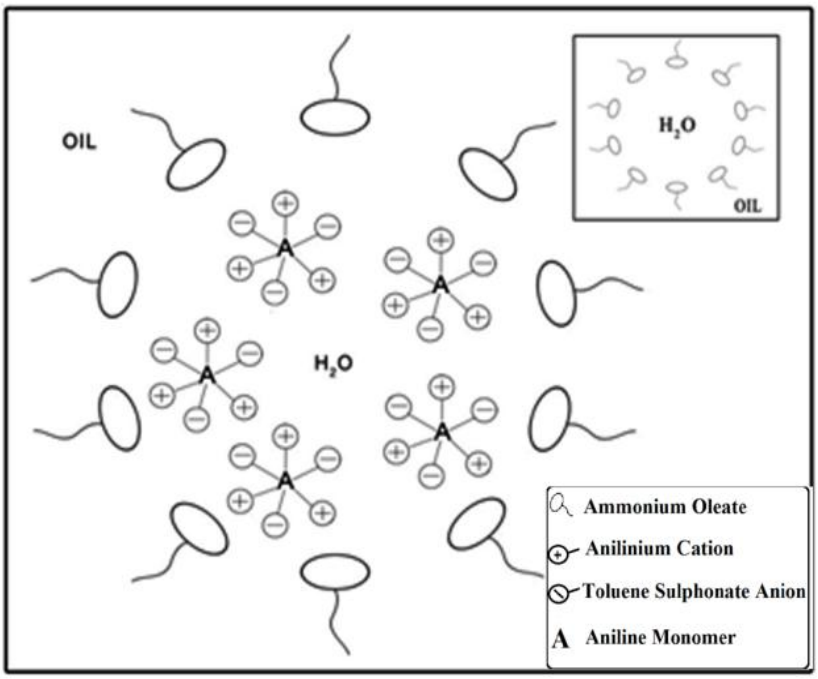

Figure 3.14 Representation of formation of normal micelles inside the inverse micelles. Inset shows the formation of inverse micelles.

When water soluble initiator (APS) is added, polymerization starts at the normal micelle/water interface and proceeds inwards. As the polymerization proceeds, the spherical micelles tend to join along the direction of polymer chain and gets elongated and forms nanorods. After a particular percentage of monomer conversion, the normal micelles burst out and the individual nanorods coming out gets aligned by the combined interactions of π-π stacking and inter/intra molecular H-bonding inside the inverse micelles and form cube-like polyaniline nanostructures as shown in Fig. 3.15.

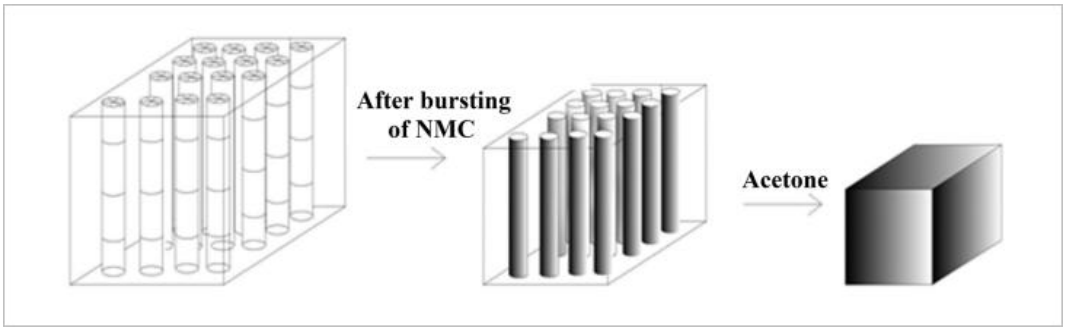

Figure 3.15 Representation of the formation and self assembly of nanorods into nanocube-like structures.

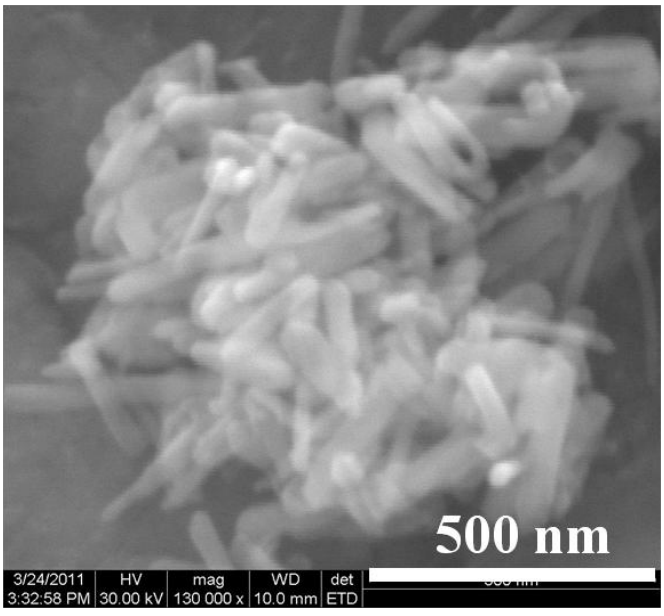

Figure 3.16 SEM image of polyaniline synthesized in the absence of inverse emulsion. Magnification of the image is 130000x

To confirm the influence of inverse micelles for the self assembly of nanorods, polyaniline is synthesized in the absence of inverse emulsion. In the absence of emulsion system, randomly oriented nanorods are formed as expected by the proposed mechanism and it is shown in Fig. 3.16. (Remyamol et al. 2013).

Zeta potential measurements also supported the bundling of nanorods to form cube-like nanostructures. Aliquots of the polymerization mixture after 4 h and 8 h show zeta potential values 29.8 and 28.2 mV respectively. But after 12 h, zeta potential value is drastically reduced to 2.66 mV due to the lowering of surface charge after bundling of nanorods to cube-like structures.

3.3.3. Optical limiting properties

Optical limiting properties of polyaniline are studied by employing open aperture Z scan technique using Nd:YAG laser of wavelength 532 nm and pulse width 5 ns. The samples are prepared in DMF with a linear transmittance of 0.75. Laser energy chosen is 25 µJ. The Z scan curve in Fig. 3.17 (a) reveals a normalized transmittance valley indicating optical limiting behaviour due to overall nonlinear absorption. The nonlinear absorption may be due to RSA and/or effective two photon absorption. RSA occurs when the excited state absorption cross-section of a molecule is larger than the ground state absorption cross-section at the input wavelength.

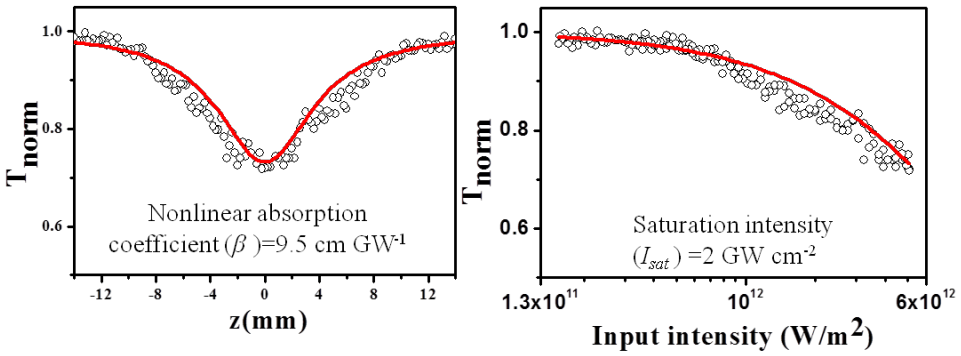

Figure 3.17 (a) Open aperture Z scan curve and (b) Optical limiting plot

The Z scan experimental data is found to fit well to two-photon type absorption. For two- photon absorption (2PA), the normalized transmittance is given by

$$T(z,S=1)=\frac{1}{q_0(z,0)\sqrt{\pi}}\int_{-\infty}^{+\infty}\ln\left[1+q_0(z,0)e^{-t^2}\right]dt \qquad (3.1)$$

Where $q_0(z,0)=\beta(1-R)I_0L_{eff}/[1+(z^2/z_0^2)]$ and z_0 is the Rayleigh length. R is the Fresnel reflectance of the sample surface, L_{eff} is given by $[1-e^{-\alpha L}]/\alpha$, α is the linear absorption coefficient and L is the thickness of the sample. In order to investigate optical limiting, input intensity versus normalized transmittance graph is drawn as given in Fig. 3.17 (b). For a Gaussian beam, input fluence at each z position is

$$E(z)=\frac{4\sqrt{\ln 2}E_{in}}{\pi^{3/2}\omega(z)^2} \qquad (3.2)$$

where E_{in} is the input laser pulse energy and ω (z) is the beam radius (Sutherland, 2003). The NLO parameters are evaluated by fitting the experimental data with the theoretical plot. The cube-like polyaniline dispersion shows nonlinear absorption coefficient (β) of 9.5 cm/GW with a saturation intensity (I_{sat}) of 2 GW/cm^2. Low saturation intensity and high nonlinear absorption coefficient are the desirable attributes of an optical limiter.

The preliminary open aperture Z scan analysis discussed above reveals the suitability of cube-like polyaniline for optical limiting applications. However, for the application point of view, immobilization of NLO material in a transparent host without compromising the optical limiting properties is needed. Use of transparent polymers as the host is advantageous for device fabrication because of their low cost and flexibility. In this study, PMMA is chosen as the host polymer owing to its good optical transparency, compatibility of the monomer with polyaniline and ease of polymerization. Several films are fabricated by varying the polyaniline loading (0.02 to 0.1 wt % with respect to monomer).

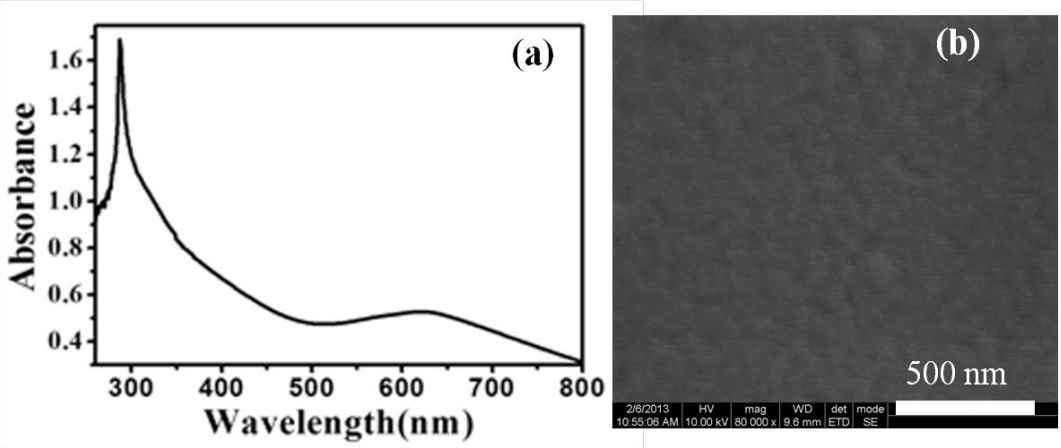

Figure 3.18 (a) UV-vis absorption spectrum of the film (0.1 wt %) and (b) SEM image of the film (0.1 wt %). Magnification of the image is 80000x

Fig. 3.18 (a) shows the characteristic UV-visible spectrum of polyaniline-PMMA film with highest polyaniline loading. It shows a peak at 640 nm due to the excitonic transition in polyaniline (Stejskal et al., 1993). The π-π* transition in polyaniline is overlapped with the absorption corresponding to PMMA at 300 nm (Capan et al.,2007). The uniform surface morphology in SEM image (Fig. 3.18 (b)) indicates the good quality of the film. The nanostructure of polyaniline along with the presence of toluenesulphonate counter ions improved the miscibility of polyaniline with the monomer and hence, upto 0.1 wt % polyaniline is dispersed in the monomer without adding any dispersing agent.

Figs. 3.19 and 3.20 and displays the open aperture Z scan curve and optical limiting plots respectively of various films for a laser energy of 150 μJ. It is clear from the figure that all the films exhibit a decrease in transmittance with increasing input laser intensity and hence good optical limiting behaviour. The β and I_{sat} values of various films are listed in Table 3.1.

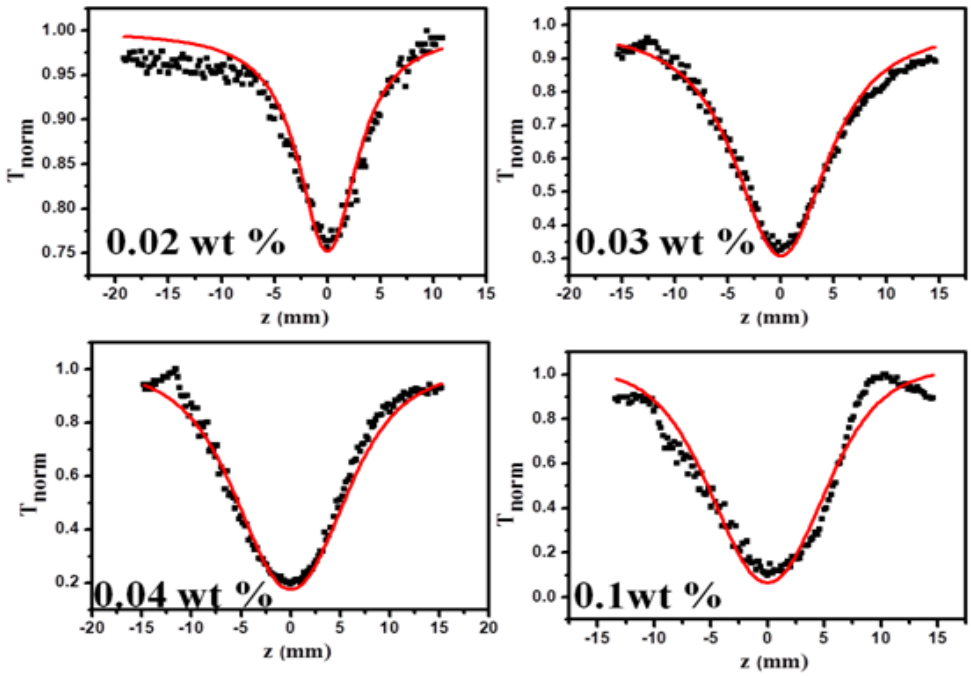

Figure 3.19 Open aperture Z scan plots of polyaniline/PMMA films with different polyaniline loading

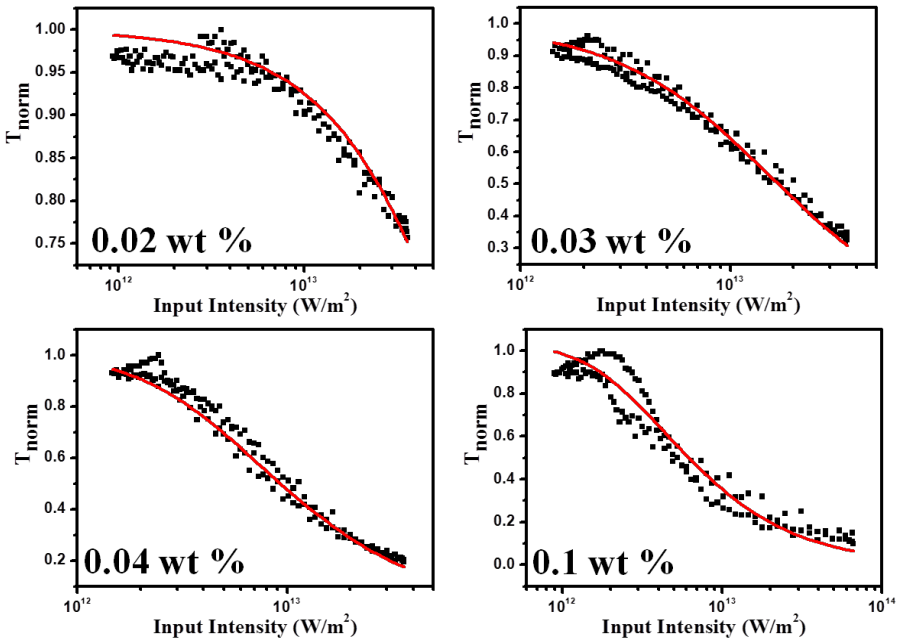

Figure 3.20 Optical limiting plots of polyaniline/PMMA films with different polyaniline loading

Table 3.1 Estimated values of β and I_{sat} for polyaniline/PMMA film with different polyaniline loading.

Polyaniline loading (wt% in monomer)	Linear transmittance	β (cm/GW)	I_{sat} (GW/cm^2)
0.02	0.78	5.5	4.5
0.03	0.72	35	0.8
0.04	0.39	120	0.3
0.1	0.31	230	0.15

When comparing the films with different polyaniline loading, β value is found to increase with polyaniline loading because of the presence of more molecules per unit volume, which will interact with the laser beam and hence improve the optical nonlinearity. The pure PMMA film is also investigated by Z scan analysis to determine its contribution to nonlinearity and it is observed that host PMMA matrix is not contributing to the nonlinearity of the composite film.

The film with the highest polyaniline loading (0.1 wt %) is selected as a representative sample for studying the NLO properties in detail. To assess the behaviour of nonlinear absorption of the film as a function of input energy, open aperture Z scan are performed for five different laser energies, namely 5 μJ, 20 μJ, 30 μJ, 45 μJ and 100 μJ as shown in Fig. 3.21.

A switch over from saturable absorption to reverse saturable absorption is observed, as the energy of the laser beam increases from 5 μJ to 100 μJ. At lower input energies, Z scan curve exhibits a peak at the focus, implying that SA plays a dominant role for the NLO properties. With the increase of laser energy (20 μJ), the peak disappears and a valley appears with two humps. Similar observation has been reported by Philip et al. (2000). When the film is far away from the focus, the pump intensity is too low to induce nonlinearity and the transmittance is equal to unity. When the film is moved near to the focus, intensity of light on the sample is increased and the ground state gets depleted causing absorption saturation, so that the transmittance increases. On the other hand as the film reaches the focus, still higher intensities are seen by the film and RSA dominates causing strong optical limiting and hence transmittance decreases effectively and falls to a value

less than unity. As the energy of laser beam continues to increase (30 and 45 μJ), the valley depth enhances and the peaks are reduced gradually as shown in Fig. 3.21. At higher energy (100 μJ), the nonlinear absorption overrides the ground state bleaching completely and shows deep valley indicating only RSA. Hence these flexible films with intensity dependent SA and RSA at the same wavelength, offers significant design flexibility apart from the inherent nonlinear absorption properties and leading to applications like efficient laser pulse narrowing and optical switching (Remyamol et al., 2014).

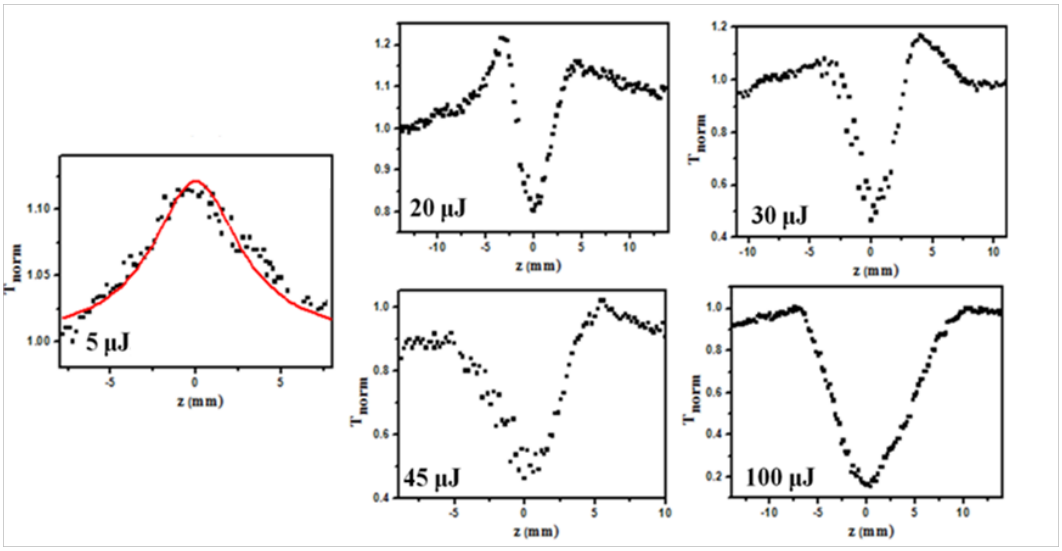

Figure 3.21 Open aperture Z scan curves of polyaniline-PMMA film (0.1 wt %) measured at different input laser energies.

3.3.4. Photocurrent generation studies

For the photocurrent measurements, thin film samples of polyaniline are fabricated on clean FTO by spin coating technique. Photocurrent experiments are performed with Autolab electrochemical work station in a conventional three electrode electrochemical cell. The light intensity selected for the measurement is 100 mW/cm^2. The photoresponse property is studied by recording the photocurrent growth (30 s) and decay (30 s) with white light irradiation. Fig. 3.22 shows the photocurrent cycles of polyaniline for repetitive switching (on/off) of the light. It indicates that the samples can be reversibly turned 'on' and 'off' by switching of the irradiation. The photocurrent is calculated from the difference between current generated after illumination of the

film for 30 seconds and the dark current. The cube-like polyaniline shows an average photocurrent of 4.5 µA.

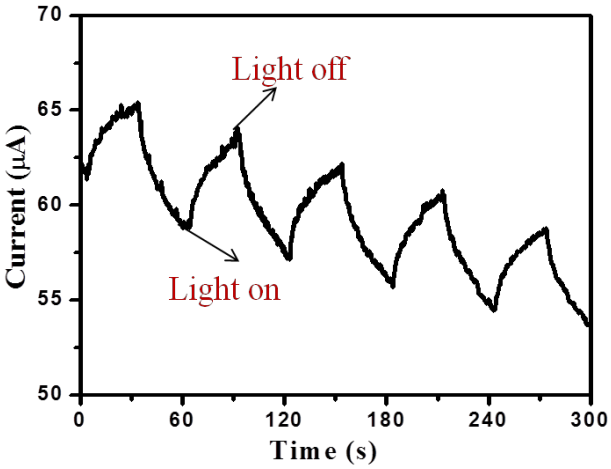

Figure 3.22 Photocurrent cycles of polyaniline film

When the film is irradiated, absorption of photon causes the excitation of electron from the highest molecular orbital (HOMO) of polyaniline to the lowest unoccupied molecular orbital (LUMO). Polaron transition may also be possible. This results in the formation of photogenerated excitons. But the exciton binding energy is high because of the comparatively low dielectric constant of polymer (Friend et al., 1997). This may be one of the reason for the low photocurrent in pure polyaniline. Fast recombination of the separated electrons and holes can also contributes to the low photocurrent. The photocurrent can be improved by facilitating electron transfer to an acceptor material before recombination of the separated electrons and holes. The efficient electron transfer can be achieved by making bulk heterojunction devices of polyaniline with good acceptor materials like graphene, CNT, fullerenes etc. In the following chapters we are discussing the hybrids of polyaniline with graphene and CNT.

3.4. Conclusions

Nanostructured polyaniline with a novel cube-like morphology is synthesized by introducing an inverse microemulsion polymerization technique using *in situ* generated ammonium oleate as the surfactant and organic acid TSA

as the dopant. The interesting cube-like morphology of polyaniline is formed by the self assembly of polyaniline nanorods in the inverse microemulsion. Corresponding formation mechanism is proposed based on experimental evidences. This new structures are examined for their nonlinear optical activities. From the preliminary open aperture Z scan studies, polyaniline is found to be a good candidate for optical limiting applications. It shows nonlinear absorption coefficient 9.5 cm/GW and saturation intensity 2 GW/cm^2. Polyaniline films are fabricated in a transparent PMMA host by an *in situ* free radical polymerization of methyl methacrylate followed by the solution casting of the polymerization mixture. The films show strong optical limiting behaviour. The β and I_{sat} values of film with highest polyaniline loading (0.1 wt % with respect to monomer) at a laser energy of 150 µJ are observed to be 230 cm/GW and 0.15 GW/cm^2 respectively. Moreover, it shows a switch over from SA to RSA as the energy of laser beam increases. The cube-like polyaniline shows a photocurrent of 4.5 µA after illumination of white light (intensity 100 mW/cm^2) for 30 seconds duration. Even though polyaniline is a good candidate for photocurrent generation, fast recombination of charge carriers is a major disadvantage and it can be overcome by facilitating electron transfer to a good acceptor material. Bulk heterojuction devices can be made by hybridizing polyaniline with stable carbon allotropes like graphene, CNT, fullerenes, etc for improving the photocurrent generation of pure polyaniline.

CHAPTER 4
STUDIES ON POLYANILINE-GRAPHITE OXIDE HYBRID

In this chapter, the synthesis and characterization of graphite oxide (GO) and polyaniline-GO hybrid with non-covalent interactions are discussed. The improved optical limiting behaviour and photocurrent generation of the hybrid, compared to the pure polyaniline is demonstrated. The significant photoluminescence quenching of polyaniline in the hybrid suggests photoinduced electron transfer from polyaniline to GO, hence improving nonlinear optical properties and photocurrent generation.

4.1. Introduction

The hybrids of nanostructured conducting polymers with carbon nanomaterials are one of the successfully exploited classes of materials. Carbon nanomaterials are often cited as a potential successor to conventional semiconducting materials in electronic and optoelectronic applications because of the highly delocalized electronic structure. Among conducting polymers, polyaniline is an excellent organic conductor with good environmental stability and low cost and has been used to make hybrids with carbonaceous materials. Hybrids of polyaniline with various carbon nanomaterials like carbon black, fullerene, graphite, graphene, CNT, etc. are reported for potential applications in diverse areas (Ali et al., 2007; Feng et al., 2003; Sapurina et al., 2000; Sotzing et al., 2000; Wu et al., 2005; Xiong et al., 2012). Out of the carbonaceous hybrids of polyaniline, its graphene hybrids are the most interesting and attractive class of hybrids with several applications in different fields, because of the interesting combination of the unique redox property and excellent environmental stability of polyaniline with the superior properties of graphene like high electron mobility, large specific surface area, very good thermal and electrical conductivity, excellent electronic and mechanical properties, etc. (Ansari et al., 2014; Dong Y. P. et al., 2013; Murugan et al., 2009; Su et al., 2014; Wang G. et al., 2012a; Xu et al., 2010; Zhang et al., 2010).

Graphene has been established as a viable candidate for next generation electronics and photonics owing to its excellent properties and thus drawn enormous attention of researchers (Blake et al., 2008; Bunch et al., 2007; Geim, 2007; Gilje et al., 2007; Huang et al., 2012; Wang et al., 2007). The use of graphene is promising because of its high optical transparency, ultra high charge carrier mobility, low resistance and high chemical and mechanical stability (Berger et al., 2006; Bolotin et al., 2008; Novoselov et al., 2004). However, the applications of pure graphene sheets are limited despite its excellent characteristics and face many challenges to induce controlled functionality. Various synthetic methods like mechanical exfoliation, epitaxial growth, chemical and electrochemical reduction of graphite oxide (GO), etc. have been developed for producing high quality graphene (Guo H.-L. et al., 2009; Li et al., 2008; Li et al., 2009; Zhou et al., 2009; Zhu et al., 2010). Among them the chemical reduction of GO is proven to be an effective method because of the low cost and possibility of mass production. Heavy oxygenation of graphite during GO synthesis (Hummers and Offeman, 1958) results in different functional groups (hydroxyl, carboxy, epoxy and alkoxy groups) on the basal planes and the edge sites. It makes GO sheets strongly hydrophilic and easily dispersible (Niyogi et al., 2006; Si and Samulski, 2008; Stankovich et al., 2006a), and thereby open up a way to introduce various functional materials. Recently graphene based composite materials of metal and metal oxide nanoparticles (Chen et al., 2010; Guo S., et al., 2009; Huang et al., 2010; Kong et al., 2009), nanoparticles of semiconducting oxides (Kavitha et al., 2013; Nayak et al., 2013), quantum dots (Cao et al., 2010), conducting polymers (Alvi et al., 2011; Jianhua et al., 2012; Liu et al., 2012), etc. are gaining more attraction due to the synergetic combination of the properties of different components. The challenge in designing composite systems is the requirement to obtain defect free individual graphene oxide or graphene sheets in the reduced form. One of the possible ways to harness the properties of graphene for future applications is the incorporation of graphene sheets into conjugated polymers like polyaniline, polypyrrole, polythiophene, polyphenylene vinylene etc.

Many authors (Chen et al., 2012; Fan et al., 2013; Gómez et al., 2011; Li J. et al., 2011; Li et al., 2012; Wang et al., 2009; Yan et al., 2010; Zhang, et al., 2010; Zhou et al., 2013; Zhu et al., 2012) synergetically combined polyaniline and graphene materials like graphene nanosheets, graphite oxide, graphene oxide, etc. for supercapacitor applications. Polyaniline-graphene composites are demonstrated for several other extensive applications in diverse areas like anticorrosion coatings (Chang et al., 2012), biosensor (Ameen et al., 2012; Feng et al., 2011; Hai Binh et al., 2012), electrochemical sensor (Fan et al., 2011; Qiu et al., 2012), field emission devices (Goswami et al., 2011), thermoelectric devices (Du et al., 2012), transparent conductive electrodes for optoelectronic devices (Domingues et al., 2011), electrorheological smart materials (Zhang et al., 2012), CO_2 absorption (Mishra and Ramaprabhu, 2012), dye sensitized solar cells (Wang G. et al., 2012a, Wang G. et al., 2012 b) and so on.

The functionalized graphene nanocomposites with tunable bandgap have potential application as optical limiters. Liu Y. et al. (2009) synthesized oligothiophene functionalized graphene material with superior optical limiting properties. Kavitha et al. (2013) recently reported the enhanced optical limiting properties of reduced graphene oxide–ZnO hybrid material. The broadband optical limiting performance of a graphene oxide–zinc phthalocyanine nanocomposite was demonstrated by Zhu et al. (2011). Several research groups have studied the scope of graphene materials functionalized with porphyrin for optical limiting applications (Xu Y. et al., 2009; Wang et al., 2013; Krishna et al., 2011; Liu Z.-B. et al., 2009). Balapanuru et al. (2010) synthesized a graphene oxide–dye (4-(1-pyrenylvinyl)-N-butylpyridinium bromide) charge-transfer complex by a simple ion-exchange process and studied the broad band optical limiting action. Even though the combination of graphene materials with various materials discussed above are explored for synergetic improvement in the nonlinear optical properties, polyaniline-graphene hybrids are not known in this context.

The optoelectronic and light harvesting applications of graphene are of particular interest for academic, technological and industrial sectors. Graphene based materials are anticipated to be used for effective charge separation and carrier transport, when blended with conjugated polymers due to the large surface area for donor acceptor interfaces and continuous pathway for electron transfer (Huang et al., 2012; Liu Z. et al., 2008). Intramolecular charge transfer in hybrid materials is one of the important reasons for the enhancement of optoelectronic properties of hybrid systems. Various authors (Liu Q. et al., 2009; Yu et al., 2010) reported the strong electron/energy transfer from the conjugated polymer P3HT to graphene and the resulting improvement in photovoltaic properties. But the application of polyaniline-graphene hybrids for photocurrent generation is relatively unexplored.

Therefore, by the introduction of polyaniline into graphene sheets either through covalent grafting or noncovalent mixing/adsorption, the optoelectronic properties can be expected to rival that of individual components. Both methods have its own advantages and disadvantages. The noncovalent modification based on van der Waals forces or π-π interactions without destroying the electronic structure of graphene could be considered as a good way to investigate the properties of hybrid materials. Small molecules such as 1-pyrene butyrate, sodium dodecyl benzene sulfonate, 1-pyrene carboxylic acid, dendronized perylene bisimides, 3,4,9,10-perylene tetracarboxylic diimide bisbenzenesulfonic acid, etc. (An et al., 2010; Su et al., 2009; Xu Y. et al., 2008) and polymers like polystyrene, polyaniline, polypyrrole, (Bai et al., 2009; Choi et al., 2010) etc. are widely used to make graphene composites by noncovalent interactions for a variety of applications. Inspired by these encouraging findings, herein we report the noncovalent functionalization of polyaniline with graphite oxide and the improved nonlinear optical properties as well as the photocurrent generation of the hybrid compared to the individual components.

4.2. Experimental

4.2.1. Synthesis of graphite oxide

For the synthesis of GO, the Hummers method (Hummers and Offeman, 1958) is modified by avoiding the heating procedure and carrying out the reaction at lower temperature (less than 10 ^{o}C). The scheme for the synthesis is given in Fig. 4.1.

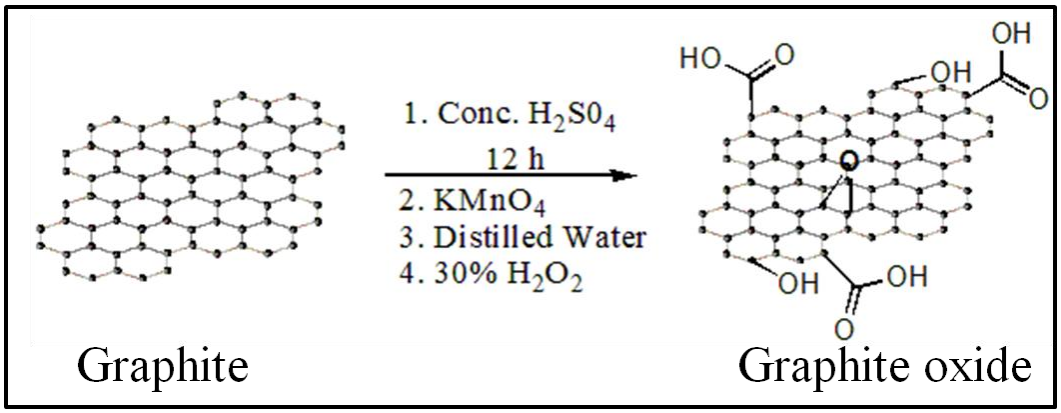

Figure 4.1 Scheme of the synthesis of graphite oxide

Initially, graphite (1 g) is mixed with concentrated H_2SO_4 (100 ml) and stirred for 12 h. The mixture is then cooled in an ice bath, and while maintaining vigorous stirring, $KMnO_4$ (2 g) is added slowly to the suspension and stirred for 2.5 h. It is then diluted with distilled water (50 ml) and the stirring is continued for 1 h. The mixture is then allowed to cool to room temperature and finally treated with 150 ml distilled water followed by 10ml of 30% H_2O_2. The product obtained is filtered through nylon cloth to remove unreacted graphite if any, and further purified by centrifuging and washing with dilute hydrochloric acid (HCl) and excess water until the pH remains neutral. Finally the sample is dried under vacuum at 80 ^{o}C for 24 h.

4.2.2. Synthesis of pristine polyaniline

Freshly distilled aniline monomer (200 µl) is dissolved in 1 M TSA (40 ml) and the initiator ammonium persulfate (APS) is added to the solution with stirring. The polymerization reaction is continued for 9 h at room temperature.

The polyaniline formed is then filtered, washed with distilled water, methanol and acetone and vacuum dried at 60 ^{o}C for 24 h.

4.2.3. Synthesis of polyaniline-graphite oxide hybrid

Polyaniline-GO hybrids are synthesized by the *in situ* polymerization of aniline in the presence of synthesized GO using 1 M TSA as the dopant and APS as the initiator. The synthesis scheme is given in Fig. 4.2.

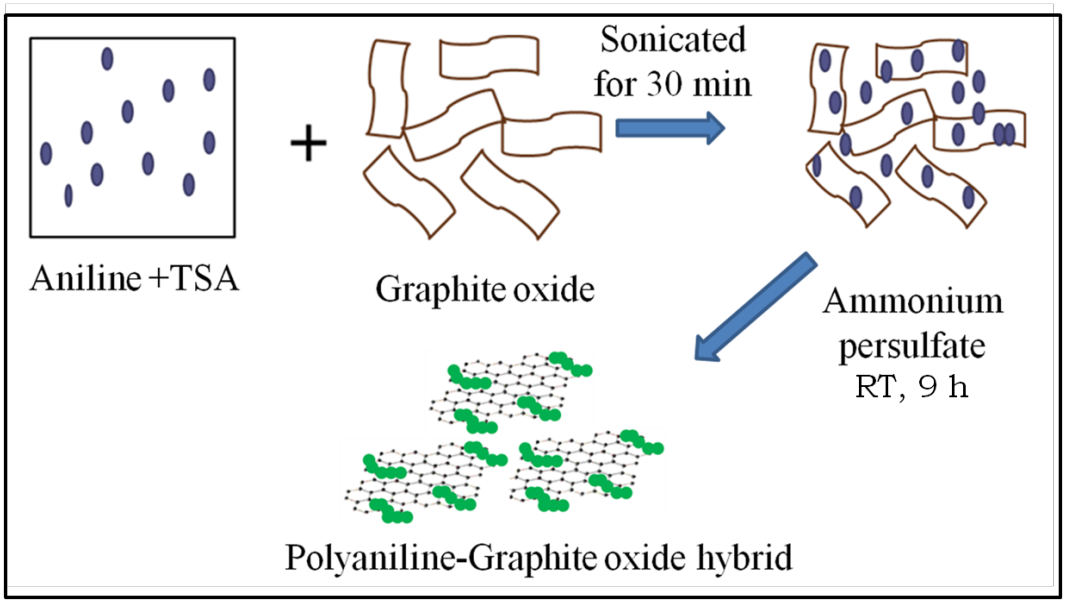

Figure 4.2 Scheme of the synthesis of polyaniline-graphite oxide hybrid

Weighed amount of GO is dispersed in TSA by ultrasonication for 30 minutes. Freshly distilled aniline is added to it and stirred for 10 minutes for the adsorption of monomer on GO sheets. Aniline can be adsorbed on the surface of GO through a strong electrostatic interaction between amino group of aniline and oxygen functionalities of GO. Therefore a homogeneous mixture of GO and aniline can be easily achieved. Freshly prepared aqueous solution of ammonium persulfate is added drop-wise to the dispersion and stirring is continued for 9 h. The hybrid formed is filtered through Millipore 0.45 μm filter, washed with water and methanol and dried under vacuum at 60 ^{o}C for 24 h. A series of hybrids are synthesized by varying aniline:GO ratio as 4:1, 2:1, 1:1 and 1:2 and the samples are named as P4G1, P2G1, P1G1 and P1G2 respectively.

4.3. Results and Discussion

4.3.1. Characterization of GO

The presence of oxygen functionalities in GO is analyzed using FTIR spectrum as shown in Fig. 4.3.

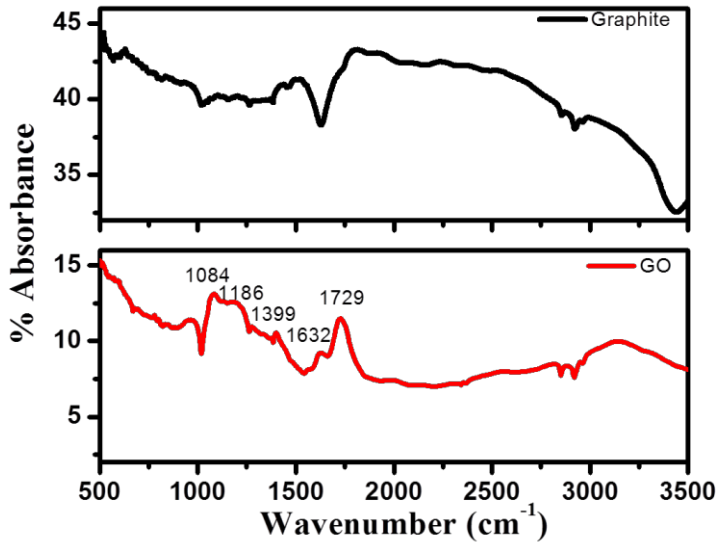

Figure 4.3 FTIR spectra of graphite and GO

The strong absorption at 1729 cm^{-1} is attributed to the C=O stretching vibrations of carboxylic acid group. The bands due to the carboxy (C–O), epoxy (O–C–O), and alkoxy (C–O) groups are also found at 1399, 1186 and 1084 cm^{-1}, respectively, as reported elsewhere (Kumar et al., 2012). The peak at 1632 cm^{-1} is due to the unoxidized C=C stretching vibrations and the broad band after 3000 cm^{-1} depicts the O-H stretching vibrations (Sun et al., 2011).

GO exhibits layered morphology with the oxygen functionalities disrupting the carbon hexagonal plane and increasing the interlayer spacing. The increased d spacing from 0.34 nm (graphite) to 0.86 nm (GO) by weakening van der Waals forces between the layers is clearly evident from the XRD pattern as given in Fig. 4.4. After oxidation, the characteristic graphitic plane at $2\theta=26.7^{o}$ shifts towards $2\theta=10.3^{o}$ corresponding to the (001) plane. The disappearance of

0.34 nm inter-graphene spacing indicates the complete oxidation of graphite into graphite oxide.

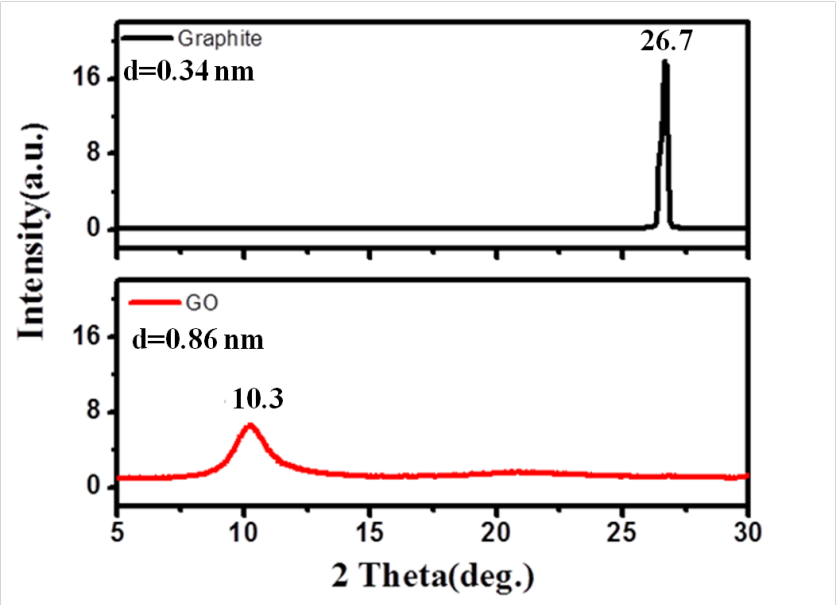

Figure 4.4 XRD spectra of graphite and GO

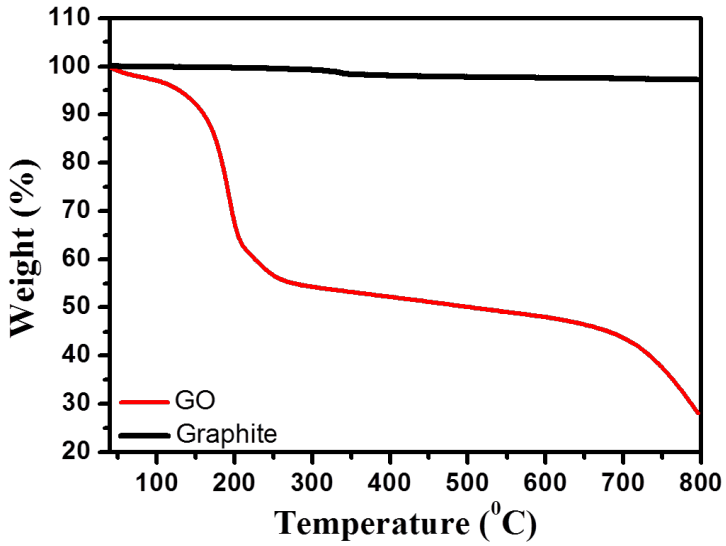

Figure 4.5 TGA patterns of graphite and GO

The TGA analysis of graphite and GO is shown in Fig. 4.5. Graphite is found to be stable in the temperature range studied, whereas GO shows a major weight loss starting from 150 °C, due to the loss of labile oxygen containing functional groups (Wang G. et al., 2005). The increased inter layer spacing also promotes the easy removal of oxygen functionalities. Weight loss after 680 °C is

due to the degradation of sp^3 carbon atom. The 8% weight loss up to 150 ^oC is due to the loss of adsorbed water molecules. From the TGA analysis, oxygen percentage is calculated as 47 % (weight loss in the temperature range 150-680 ^oC).

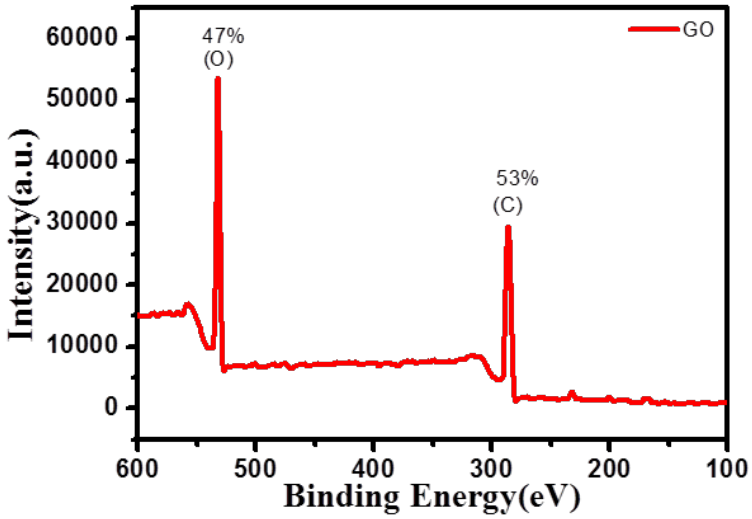

Figure 4.6 XPS spectrum of GO

The oxygen percentage is again confirmed with XPS spectrum shown in Fig. 4.6. The XPS spectrum of GO shows peaks at 285 and 531 eV corresponding to C 1s and O 1s respectively. The percentage of oxygen and carbon are quantified as 47% and 53% respectively.

Fig. 4.7 shows the Raman spectra of graphite and GO. Graphite shows a broad G band representing the in-plane bond stretching of sp^2 carbon atoms and a very small D band (defect band) corresponds to the breathing mode of the rings or K-point phonons of A_{1g} symmetry (Cançado et al., 2004; Ferrari and Robertson, 2000). The I_G/I_D ratio in this case is 7.1. After oxidation, the intensity of defect band increases and I_G/I_D ratio decreases to 0.91. Since I_G/I_D ratio is a measure of disorder, it is clearly understood that oxidation induces defects in GO sample.

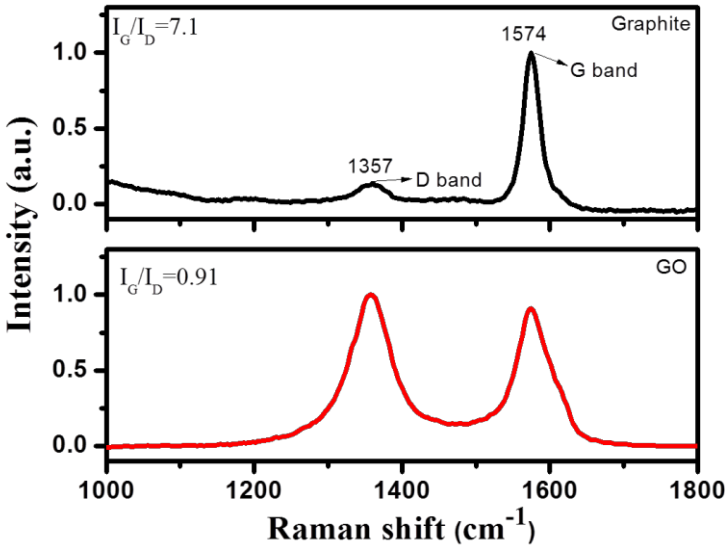

Figure 4.7 Raman spectra of graphite and GO

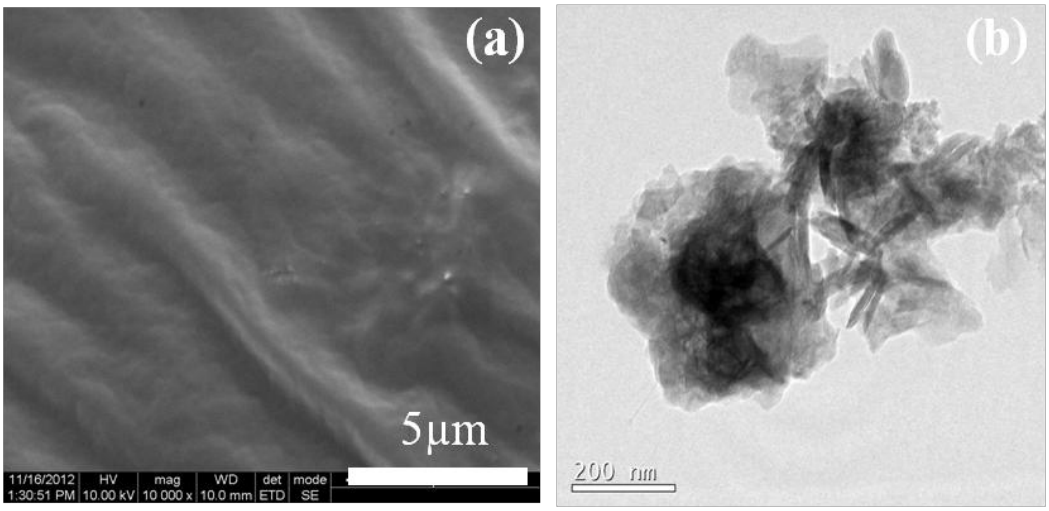

Figure 4.8 (a) SEM image and (b) TEM image of GO. Magnification of the SEM image is 10000x

The SEM and TEM images of GO shown in Fig. 4.8 depict the layered and aggregated morphology of GO. The bumpy texture of the flat regions in SEM images can be related to the presence of isolated epoxy and hydroxyl reaction sites. The wrinkles can be attributed to the defects in the carbon lattice as remnants of the epoxy reaction strings (Schniepp et al., 2006).

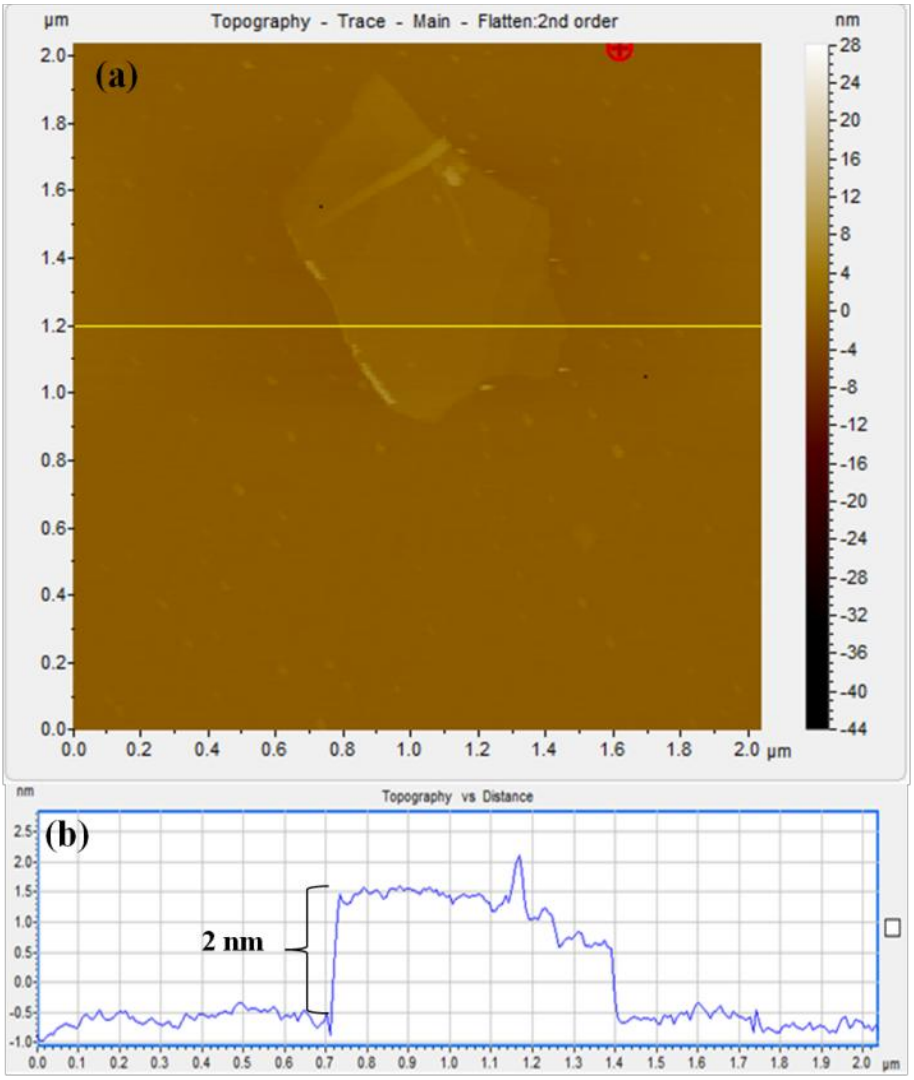

Figure 4.9 (a) AFM image and (b) Horizontal cross-section line scan of AFM image of GO

AFM images of GO as shown in Fig. 4.9 (a) confirms the layered morphology. The corresponding cross-sectional analysis given in Fig. 4.9 (b) indicates that the average thickness of the GO layers is around 2 nm. It should be noted that the thickness of a single graphene sheet is equal to the interlayer spacing in graphite (0.34 nm), but a GO sheet is approximately 1 nm thick due to the presence of functional groups, structural defects and adsorbed water molecules (Eda et al., 2008; McAllister et al., 2007; Stankovich et al., 2007). So the obtained GO layer may have 2 sheets of GO.

4.3.2. Characterization of polyaniline-GO hybrid

A series of polyaniline-GO hybrids are synthesized by varying the aniline:GO ratio. The structure of the hybrids is characterized by FTIR spectroscopy. Fig. 4.10 shows the FTIR spectra of hybrid P1G2 along with that of pure polyaniline.

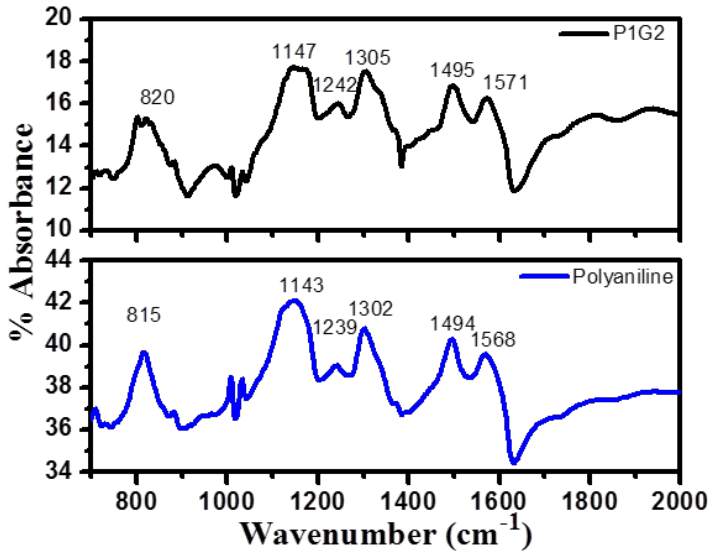

Figure 4.10 FTIR spectra of hybrid (P1G2) and polyaniline

In polyaniline, the out-of-plane bending vibration of C-H on 1,4-disubstituted rings are found at 815 cm^{-1} and the bands at 1568 and 1494 cm^{-1} are attributed to the C=C stretching vibrations of quinonoid rings and benzenoid rings respectively. Aromatic C-H in-plane bending vibration is observed at 1143 cm^{-1}. The vibration band at 1239 cm^{-1} corresponds to the $C\text{-}N^{\cdot+}$ stretching modes of the polaronic charge carriers in the doped polyaniline, while the peak at 1302 cm^{-1} is due to the stretching vibration of the C-N bond. The hybrid shows all the characteristic peaks of polyaniline, but the peaks are shifted to higher wavenumber side due to the π-π interaction of polyaniline with the aromatic region of GO. The peaks corresponding to GO are significantly reduced in the hybrid indicating the removal of functional groups of GO during the hybrid formation.

XRD spectrum of polyaniline as shown in Fig. 4.11 (a) reveals three characteristic peaks at 15, 20, and 25^{o} corresponding to the (011), (020), and (200) planes respectively. The peak at 20 and 25^{o} are ascribed to periodicity parallel and perpendicular to the polymer chain respectively. The XRD pattern of hybrid P1G2 (Fig. 4.11 (b)) shows all the characteristic peaks of polyaniline along with a peak at 10.3^{o} corresponding to the (001) planes in GO.

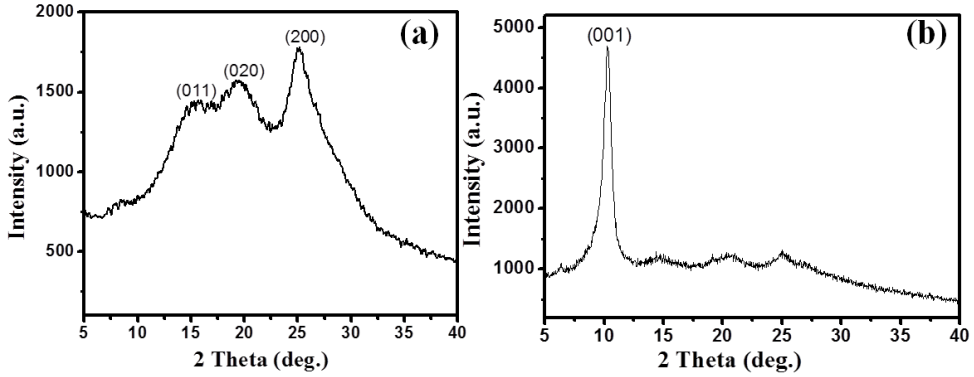

Figure 4.11 XRD spectra of (a) polyaniline and (b) hybrid (P1G2)

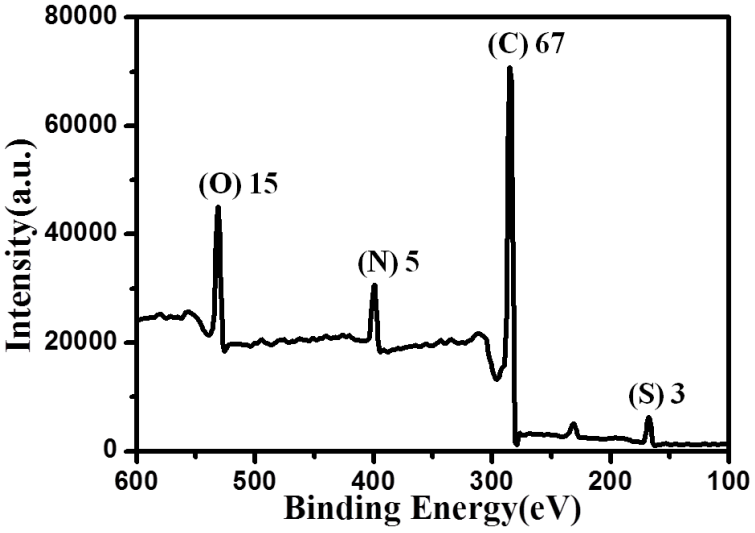

Figure 4.12 XPS spectrum of the hybrid (P1G2)

XPS spectrum is used to study the elemental composition of the hybrids. The XPS spectrum of the hybrid P1G2 is given in Fig. 4.12. Compared to GO, the percentage of oxygen in the hybrid is reduced to 15 and that of carbon is increased to 67, indicating the removal of most of the oxygen functionalities in GO during

the hybrid formation. Two new peaks centered at 399 and 168 eV corresponding to N1s and S2p are confirming the formation of toluenesulphonic acid doped polyaniline hybridized with GO.

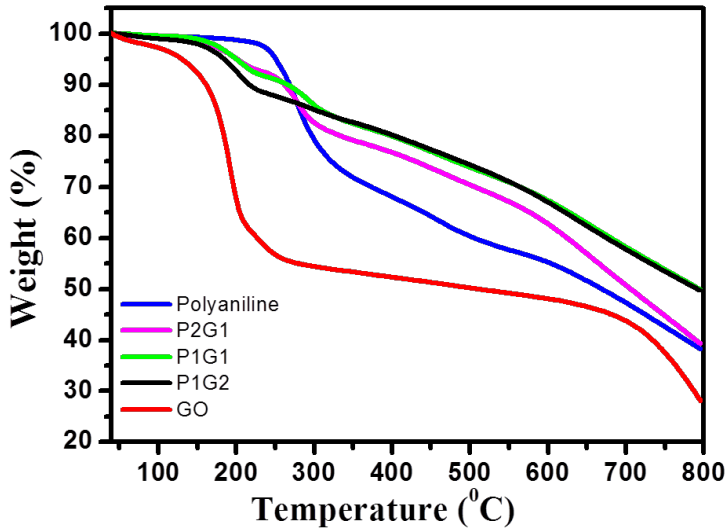

Figure 4.13 TGA pattern of the samples

The decomposition patterns of the samples are studied using thermo gravimetric analysis. As shown in Fig. 4.13, GO loses 42% of its weight from 150 to 200 ^oC, whereas all the hybrids loses less than 10% of its weight at the same temperature range, indicating the removal of oxygen containing groups during hybrid formation. The gradual weight loss of the hybrid starting from 250 ^oC is due to the loss of the dopant molecules in polyaniline. The hybrid samples give more residues compared to the pure polyaniline and GO.

Raman spectrum of the hybrid P1G2 is shown in Fig. 4.14. The I_G/I_D ratio is found to be 1.03, which is higher compared to that of GO as disussed in Fig.4.7. This increase in I_G/I_D ratio indicates fewer defects in the hybrid and suggests significant defect repairing during hybridization resulting in larger sp^2 domain and extended conjugation.

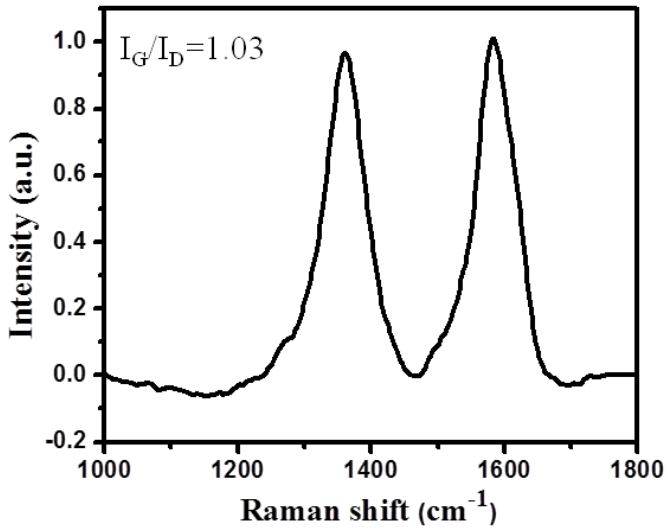

Figure 4.14 Raman spectrum of the hybrid (P1G2)

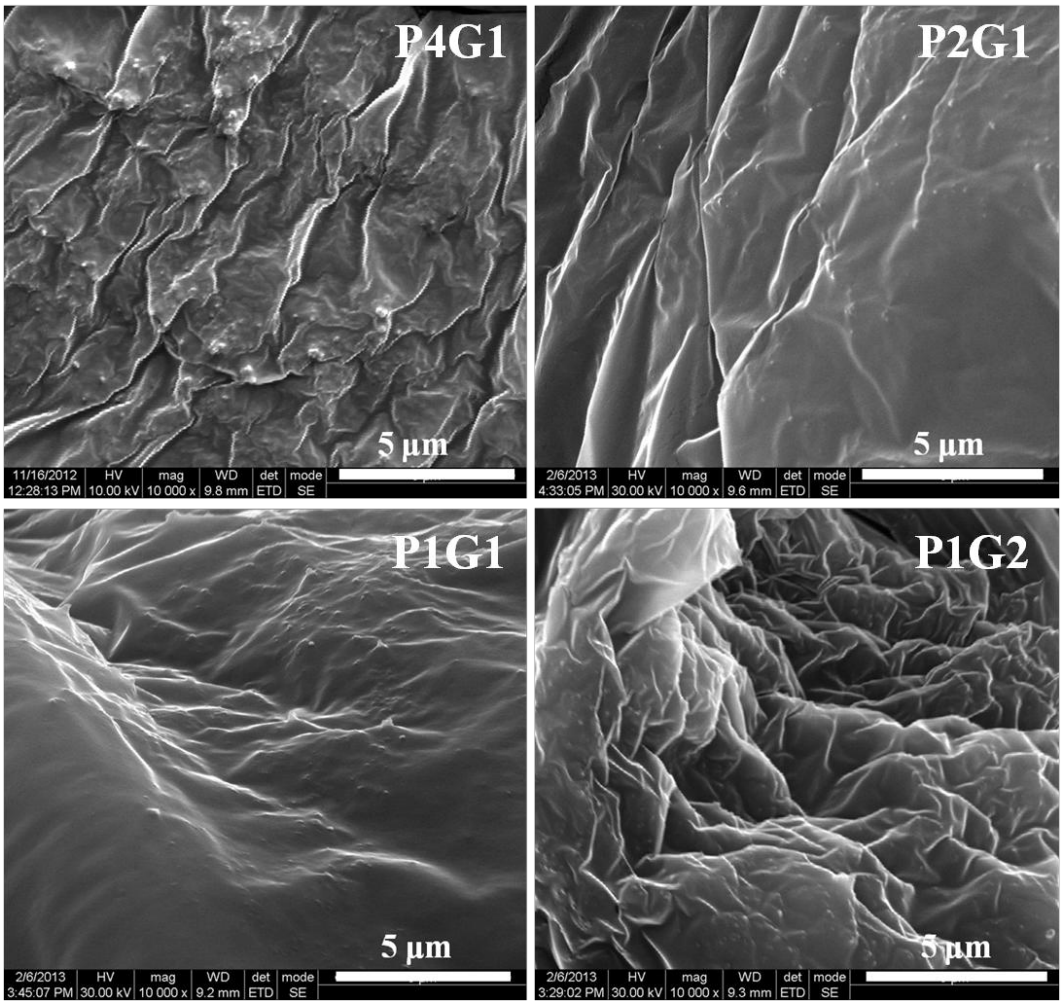

Figure 4.15 SEM image of the hybrids at a magnification of 10000x

The morphology of the hybrids is analyzed using SEM and images are shown in Fig. 4.15. When polyaniline is hybridized with GO, large wrinkled paper-like structure appears and the morphology of the hybrids are observed as uniform. No individual polyaniline agglomerates can be observed, indicating nucleation and growth processes occur only on the surface of GO. The morphology and crystallinity of the hybrid P1G2 is further investigated by TEM analysis. TEM image of P1G2 shown in Fig. 4.16 (a) confirms the formation of polyaniline covered with GO layers. HRTEM image of P1G2 (Fig. 4.16 (b)) clearly shows the distinction between crystalline GO from the amorphous polyaniline layer. The lattice fringes observed in the HRTEM image of P1G2 and the SAED pattern shown in Fig. 4.16 (c) reveals that the crystallinity of GO is maintained in the hybrid.

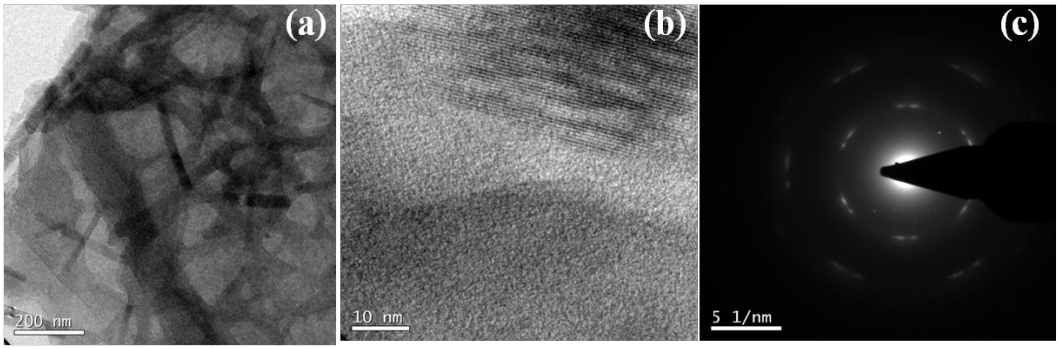

Figure 4.16 (a) TEM image (b) HRTEM image and (c) Selected area diffraction pattern of the hybrid (P1G2)

Fig. 4.17 (a) shows the AFM topographic image of the hybrid sample. It is observed that except the unoccupied substrate areas, two different surface features are appeared. As per the horizontal cross-sectional analysis given in Fig. 4.17 (b), the line goes through two features with average thickness 1 nm and 3.2 nm. The regions with 1 nm thickness may be GO sheet and the other regions may be polyaniline covered with GO layers.

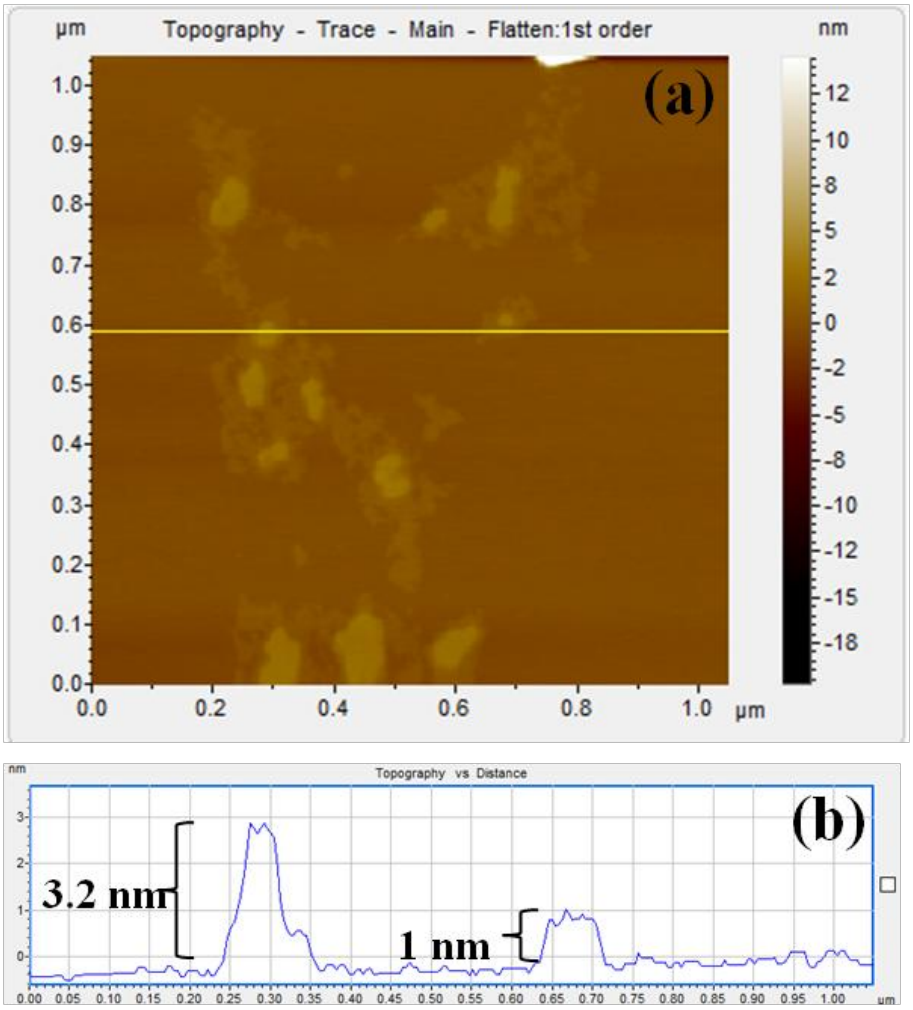

Figure 4.17 (a) AFM image and (b) Horizontal cross-section line scan of AFM image of the hybrid (P1G2)

Fig. 4.18 (a) shows the UV-visible spectra of GO, polyaniline and P1G2 hybrid in 2-propanol. The spectrum of GO shows a peak at 244 nm corresponding to π-π* transition of C=C bond and a shoulder around 290-300 nm due to the n-π* transition of C=O bond. Polyaniline shows λ_{max} at 344 nm, a shoulder around 440 nm and a free carrier tail extending to NIR region corresponding to π-π* and polaron transitions respectively. Compared to polyaniline, spectrum of the hybrid is red shifted and it shows a peak at 262 nm due to the π-π* transition of GO in the hybrid. The red shift of this peak with respect to GO is due to the partial restoration of C=C bond of GO in the hybrid (Li D. et al., 2008).

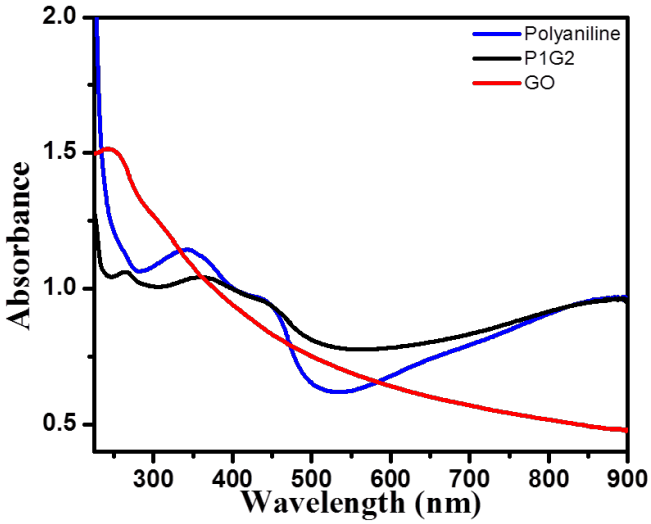

Figure 4.18 UV-visible spectra of polyaniline, GO and the hybrid

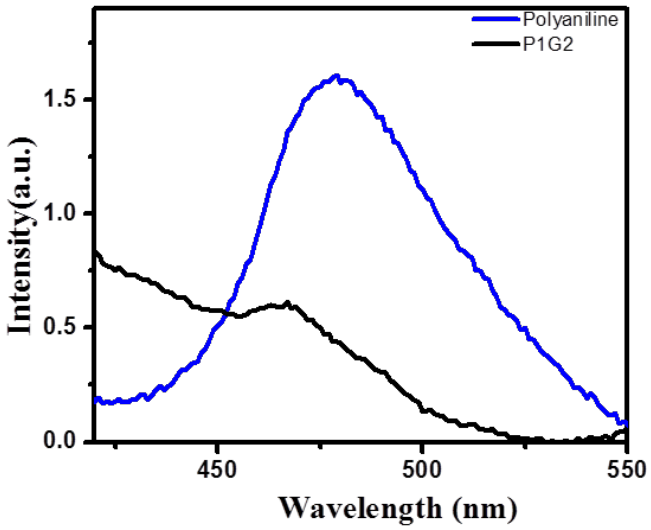

Figure 4.19 Photoluminescence spectra of polyaniline and the hybrid (P1G2)

Fig. 4.19 shows the photoluminescence spectra of polyaniline and P1G2 dispersed in 2-propanol in equal weights. The excitation wavelength is 360 nm. Polyaniline shows a broad emission centered at 480 nm. Photoluminescence of polyaniline is quenched significantly when it is hybridized with GO, suggesting photoinduced electron transfer from polyaniline to GO layers. Similiar observation of photoluminescence quenching due to photoinduced electron transfer from P3HT to graphene is reported by Liu Q. et al. (2009).

4.3.3 Optical limiting properties

Open aperture Z scan technique is employed to measure third order nonlinear optical properties of the samples. All the Z scan curves shown in Fig. 4.20 exhibits normalized transmittance valley, indicating optical limiting behaviour.

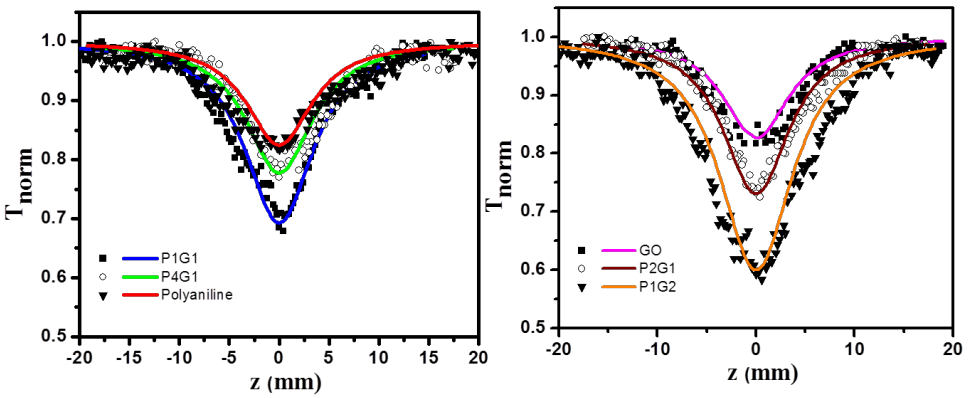

Figure 4.20 Open aperture Z scan plot of the samples

Transmittance valley exists due to different nonlinear mechanisms like reverse saturable absorption, two photon absorption, nonlinear scattering, etc. Compared to polyaniline and GO, the hybrids show enhanced optical limiting property due to the synergetic combination of nonlinear mechanisms of polyaniline and GO. Excited state absorption is the major nonlinear optical mechanism of GO (Liu Z. et al., 2009) at 532nm when nanosecond pulses are used, whereas polyaniline is known to exhibit reverse saturable absorption and/or two photon absorption. The photoinduced electron transfer also may have a significant effect for the enhanced optical limiting response of the hybrid compared to individual components (Liu Z.-B. et al., 2009).

The optical limiting plots are given in Fig. 4.21. The open aperture Z scan experimental data fits well with two photon absorption theoretical plot. The nonlinear absorption coefficient as well as the saturation intensity extracted from the theoretical fit is listed in table 4.1.

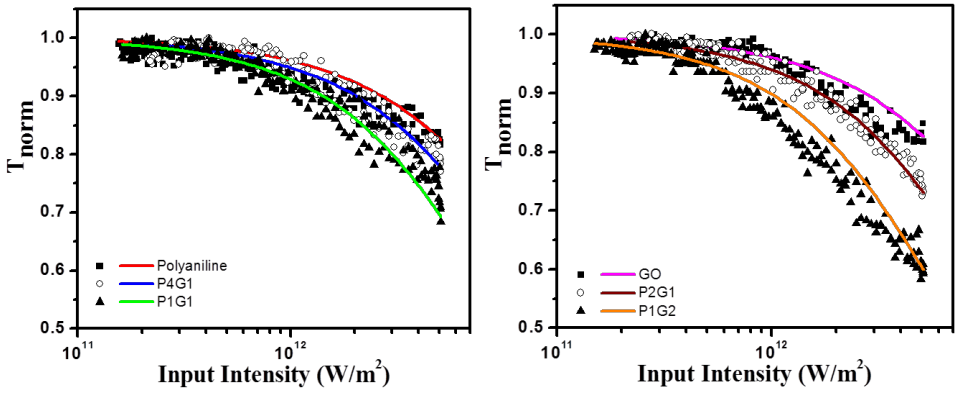

Figure 4.21 Optical limiting behaviour of polyaniline and hybrid samples

Table 4.1 Nonlinear absorption coefficient (β) and saturation intensity (I_{sat}) of the samples

Sample name	β (cm/ GW)	I_{sat} (GW/cm^2)
Polyaniline	5.8	2.5
GO	5.5	3.5
P4G1	8	1.5
P2G1	11	0.7
P1G1	13	0.6
P1G2	19	0.4

The increased percentage of GO enhances the nonlinear absorption coefficient and decreases the limiting threshold, hence the hybrid P1G2 is the best optical limiter among the hybrids.

4.3.4 Photocurrent generation studies

The thin films of polyaniline and polyaniline-GO hybrids were prepared by the experimental methods given in Chapter 2 (section 2.2.2.). Fig. 4.22 shows photocurrent cycles of polyanilne and the hybrids measured as per the procedure given in 2.3.7 by repetitive switching (on/off) of the light. It indicates that the samples can be reversibly turned 'on' and 'off' by switching of the irradiation. Pure polyaniline shows a photocurrent of 4.6 µA. Photocurrent generated increases gradually as the percentage of GO in the hybrid increases and when the aniline to GO ratio is 1:2, the film exhibits a photocurrent of 9.1 µA, almost twice

as that of pure polyaniline, indicating the enhanced separation efficiency of photogenerated excitons through the electronic interaction of polyaniline and GO (Huang, et al., 2012; Liu Z., et al., 2008). The polyaniline-GO hybrid film is acting as a bulk heterojunction device. In such devices, the interfacial areas are large, hence the potential differences are strong enough for efficient exciton dissociation. The photocurrent responses of the hybrids are quite reproducible during the repeated on-off cycles, whereas for pure polyaniline current decay is observed.

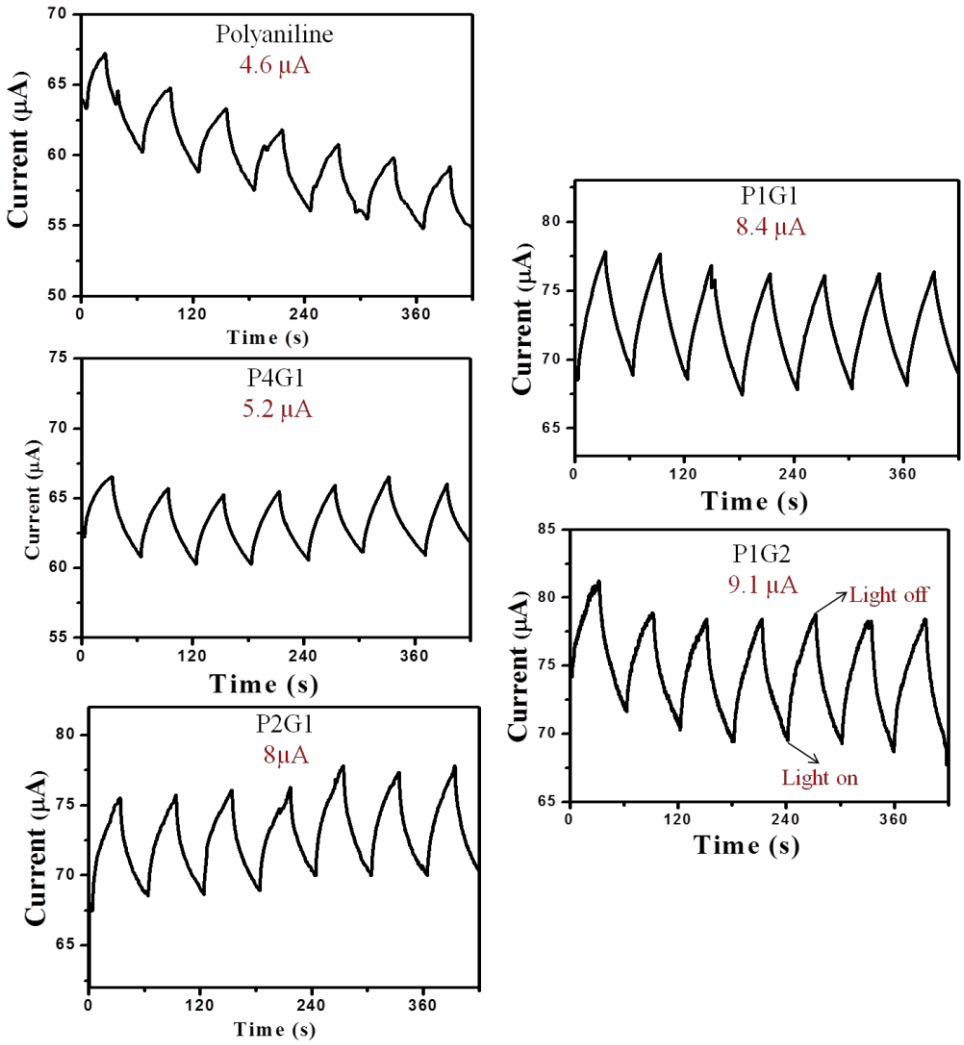

Figure 4.22 Photocurrent cycles of the samples

4.4. Conclusions

A series of polyaniline-GO hybrids with noncovalent interactions are synthesized by the *in situ* polymerization of aniline in the presence of synthesized GO using TSA as the dopant and APS as the initiator. GO is synthesized by modified Hummers method. The GO as well as the hybrids are characterized by various spectroscopic, thermal and microscopic techniques. Photoluminescence quenching is observed in the hybrid compared to pure polyaniline as a result of photoinduced electron transfer. Significant improvement in optical limiting behaviour and photocurrent generation is observed for the hybrids compared to individual components. Both the optical limiting and photocurrent generation of the hybrid increases as the percentage of GO in the hybrid increases. The hybrid P1G2 shows higher β value (19 cm/GW) with lower saturation intensity (0.4 GW/cm^2) compared to that of pure polyaniline (β=5.8 cm/GW, I_{sat}=2.5 GW/cm^2). The improved optical limiting behaviour is due the synergetic combination of NLO mechanisms of polyaniline and GO and light induced electron transfer within the hybrid. The photocurrent generated by P1G2 is 9.1 μA, while pure polyaniline shows only 4.6 μA. The efficient dissociation of excitons at the interface between polyaniline and GO and the photoinduced electron transfer to GO before recombination of the dissociated carriers are contributing to the increased photocurrent of the hybrid compared to pure polyaniline.

CHAPTER 5
STUDIES ON POLYANILINE-PHENYLENE DIAMINE FUNCTIONALIZED REDUCED GRAPHENE OXIDE HYBRID

This chapter discusses about covalent funtionalization of polyaniline with reduced graphene oxide. A novel synthesis route is adopted to achieve covalent connections. GO is modified with phenylene diamine functional groups and the phenylene diamine functionalized reduced graphene oxide is polymerized along with aniline monomer to achieve covalently connected polyaniline-reduced graphene oxide hybrid. The GO, phenylene diamine functionalized reduced graphene oxide and the hybrids are characterized in detail. The improved optical limiting behaviour, dc-conductivity, and photocurrent generation of the hybrid compared to the individual components are also discussed.

5.1. Introduction

The chemical functionalization of graphene is started for the improvement in solubility/processability in both water and organic solvent by introducing different soluble groups (Englert et al., 2011; Si and Samulski, 2008; Stankovich et al., 2006 (a); Stankovich et al., 2006 (b); Yang et al., 2009a; Zhu et al., 2009). Later multifunctional hybrids of graphene with covalent connections having both the superior properties of graphene and the advantages of functional materials have been widely studied. Chandrasekar and Pradeep (2012) were able to attach luminescent silver quantum clusters to graphene through a covalent linker and thus provided a gateway for further experimental and theoretical exploration on the electronic, optical, catalytic, and biological properties of the new material. Lee et al. (2010) introduced a new method for attaching polymer brushes to graphene oxide using surface-initiated atom transfer radical polymerization (ATRP). The method involves the covalent attachment of an initiator to graphene oxide followed by the polymerization of styrene, methyl methacrylate, or butyl acrylate using ATRP. Feng et al. (2013) presented reduced

graphene oxide-azobenzene hybrids via covalent functionalization for long-term solar thermal storage. Xiaoming et al. (2011) demonstrated the synthesis and fluorescence quenching properties of soluble graphene-indolizine hybrid with covalent connections. Graphene materials covalently functionalized with various other functional materials have been reported for a variety of applications like structural reinforcement (Fang et al., 2009; Pramoda et al., 2010; Yang et al., 2009b), dye adsorbents (He et al., 2010), electrocatalysts for oxygen reduction reactions (Liang et al., 2012), optical applications (Tuan et al., 2010), electrorheological applications (Hu et al., 2011) and many more.

Covalent functionalization of graphene materials with other nonlinear optical materials is a valid way to enhance the optical limiting properties due to the formation of effficient donor acceptor system and the combination of NLO mechanisms. Zhang et al. (2009a) synthesized covalently connected graphene-C_{60} hybrid and observed an enhancement in nonlinear optical performance compared to the benchmark material C_{60} and graphene. The conjugation of delocalized π-electron system of the graphene with conjugated organic molecules or polymers can open up a new window for nonlinear optical applications. Liu Y. et al. (2009) and Zhang et al. (2009b) demonstrated superior optical limiting of graphene material covalently functionalized with oligothiophene compared to the individual components and C_{60}. Li P. P. et al. (2011) studied the excellent broad band optical limiting of charm-bracelet type poly (N-vinyl carbazole) (PVK) functionalized with thermally reduced graphene oxide in contrast to the pure PVK.

Xu Y. et al. (2009) reported the first covalently bonded and organic soluble graphene hybrid of porphyrin with superior optical limiting compared to the bench mark material. Liu Z.-B. et al. (2009) reported an enhancement in nonlinear optical properties of two different graphene hybrid materials covalently functionalized with porphyrin and fullerene at 532 nm. The enhanced optical nonlinearity of these hybrids are attributed to the combination of a nonlinear mechanism and the photoinduced electron or energy transfer between porphyrin or fullerene moiety and graphene. Krishna et al. (2011) investigated the nonlinear

optical and optical limiting properties of covalently linked graphene-zinc porphyrin composite materials. The same authors (Krishna et al., 2012) studied structural, spectroscopic and nonlinear optical properties of graphene oxide and its composites with various metal and metal free porphyrins. They observed that the metal free porphyrins with graphene oxide show enhanced nonlinear absorption properties compared to graphene oxide with metal porphyrins in nanosecond time scales. Wang et al. (2013) reported the increase in optical nonlinearity of graphene nanohybrids axially coordinated to two different porphyrins; tin cored porphyrin and phosphourous cored porphyrin compared to graphite oxide and free porphyrins.

Zhu et al. (2011) synthesized a soluble graphene oxide covalently functionalized with zinc phthalocyanine exhibiting much larger nonlinear optical coefficients and broadband optical limiting performance than graphene oxide at 532 and 1064 nm. Soluble graphite oxide axially substituted with gallium phthalocyanine with improved nonlinear absorption coeffient compared to GO, pristine gallium phthalocyanine and C_{60} has been reported by Yong-Xi et al. (2011). Zhao et al. (2013) compared the optical limting behaviour of zinc pthalocyanine covalently functionalized with three different graphene materials; pure graphene, graphene oxide and reduced graphene oxide. In nanosecond regime, reduced graphene oxide–phthalocyanine hybrid shows better optical limiting effect than the other two hybrids.

The covalently connected graphene-porphyrin hybids have been recently studied for photocurrent generation applications. Karousis et al. (2011) electrophoretically deposited graphene oxide with covalently linked porphyrin antennae on tin oxide and the electrode exhibit an incident photon-to-photocurrent-efficiency of 1.3% in a standard photoelectrochemical cell. Tang et al. (2014) synthesized porphyrin hybrid covalently functionalized with graphene and studied the improved photocurrent generation compared to free porphyrin. Chatterjee et al. (2013) studied the role of aminofunctionalized GO for changing

the morphology of polyaniline during *in situ* polymerization and the improved photocurrent generation of the polyaniline-reduced graphene oxide hybrid.

Eventhough covalently grafted hybrids of graphene are known in the literature, the advantages of covalently connected polyaniline–graphene hybrids are not highly explored. Recently few papers are published specially aiming supercapacitor applications (An et al., 2012; Jianhua et al., 2012; Kumar et al., 2013; Kumar et al., 2012; Li Z. F. et al., 2014) and memory effect (Zhang B. et al., 2013) of polyaniline-graphene hybrids with covalent interactions. The optical limiting applications and photocurrent generation of the covalently connected graphene hybrids of polyaniline are highly unexplored.

With this background, polyaniline is covalently connected with reduced graphene oxide by a novel 3 step approach. GO is first functionalized with phenylene diamine by facilitating acylation chemistry of GO, where concominant reduction and exfoliation of GO occurs due to the refluxing of GO with thionyl chloride vapours. Polyaniline-reduced graphene oxide hybrids with covalent connections are synthesized by the *in situ* polymerization of aniline in the presence of GONH2. The improved nonlinear absorption, dc-conductivity and photocurrent generation compared to the individual components and the noncovalently connected polyaniline-GO hybrid (Chapter 4) are discussed here.

5.2. Experimental

5.2.1. Functionalization of graphite oxide with phenylene diamine

Scheme for the phenylene diamine functionalization of GO is shown in Fig. 5.1. At first, the synthesized GO (500 mg) is treated with a catalytic amount of dry DMF and excess amount of freshly distilled $SOCl_2$ under inert atmosphere at 80 ^{o}C for the conversion of carboxylic acid groups to acid chlorides. The excess $SOCl_2$ is removed by distillation under reduced pressure and the obtained cake is redispersed in excess amount of dry DMF. Then phenylene diamine (500 mg) is added to the dispersion and the reaction is continued for 72 h at 120 ^{o}C under inert atmosphere. The obtained mixture is filtered using Millipore 0.45 μm filter,

washed with DMF, distilled water and methanol, and dried under vacuum at 80 ^{o}C for 24 h. During the phenylene diamine functionalization, reduction and exfoliation of GO is achieved, hence the sample is named as phenylene diamine functionalized reduced graphene oxide (GONH2).

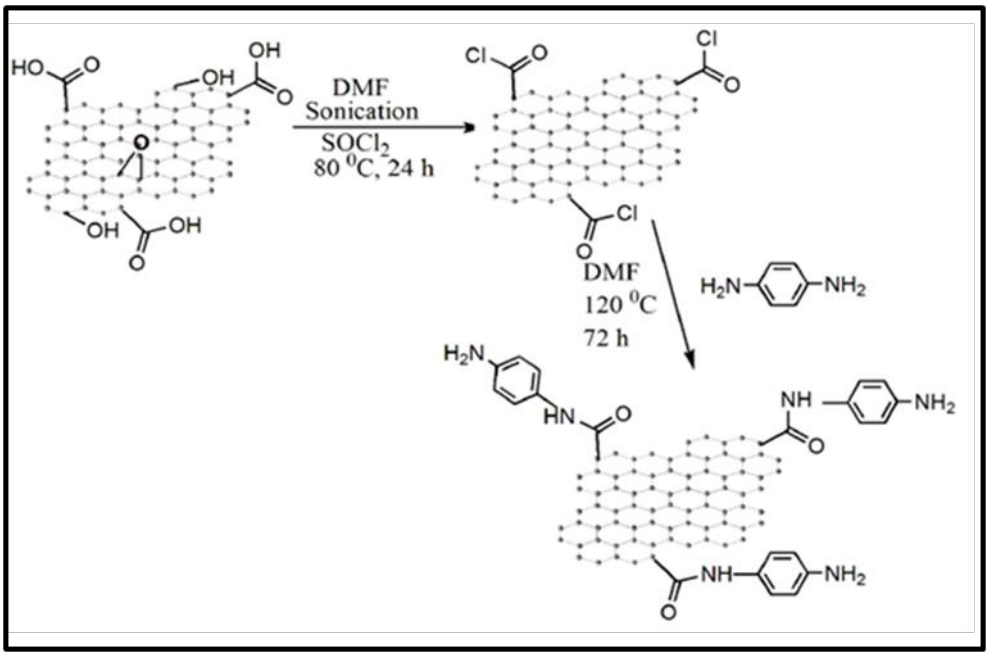

Figure 5.1 Scheme of the functionalization of GO by phenylene diamine

5.2.2. Synthesis of polyaniline-GONH2 hybrid

The hybrids are synthesized by the *in situ* polymerization of aniline in the presence of GONH2 using TSA as the dopant and APS as the initiator as shown in Fig. 5.2. GONH2 (50 mg) is first dispersed in 1 M TSA (40 ml) by ultrasonication. Aniline monomer (200 µl) is added to the dispersion and stirred for 30 min for the adsorption of the monomer on graphene sheets. Freshly prepared aqueous solution of the initiator (APS, 1.4 ml, 2.9 mmol) is added drop wise to the dispersion and stirring is continued for 9 h. The green colored hybrid formed is then filtered through Millipore 0.45 µm filter paper, washed with distilled water, methanol and acetone and vacuum dried at 60 ^{o}C for 24 h. Various hybrids are synthesized by varying the aniline:GONH2 ratio as 2:1, 1:1, and 1:2 and the samples are named as P2NH2G1, P1NH2G1and P1NH2G2, respectively.

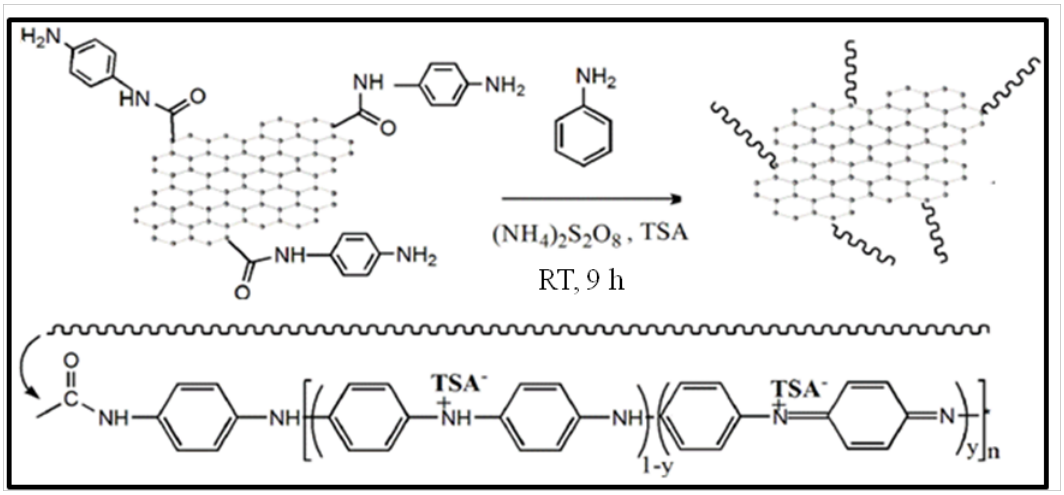

Figure 5.2 Scheme of the synthesis of polyaniline-GONH2 hybrid

During this *in situ* polymerization, the reduced graphene oxide sheets act as a support material and also participate in the polymerization of aniline by the formation of GONH2 radical cation. Using the initiator $(NH_4)_2S_2O_8$, two types of cation radicals are formed namely, phenylene diamine radical cation covalently linked on redued graphene oxide sheets and aniline radical cation physically adsorbed on reduced graphene oxide sheets. The chains initiated by the former will be covalently grafted on the graphene sheets and those initiated by the adsorbed aniline radical cation will get entrapped in the reduced graphene oxide sheets by noncovalent interactions.

5.3. Results and Discussion

5.3.1. Characterization of phenylene diamine functionalized reduced graphene oxide

Fig. 5.3. shows the FTIR spectra of phenylene diamine functionalized reduced graphene oxide and unfunctionalized GO. The spectrum of the GONH2 clearly reveals the presence of amide linkages. After phenylene diamine functionalization, because of the formation of amide bonds, the C=O stretching vibration of GO at 1729 cm^{-1} is shifted to lower wavelength 1711 cm^{-1} (GONH2). The characteristic –NH bending vibration at 1546 cm^{-1} is also observed.

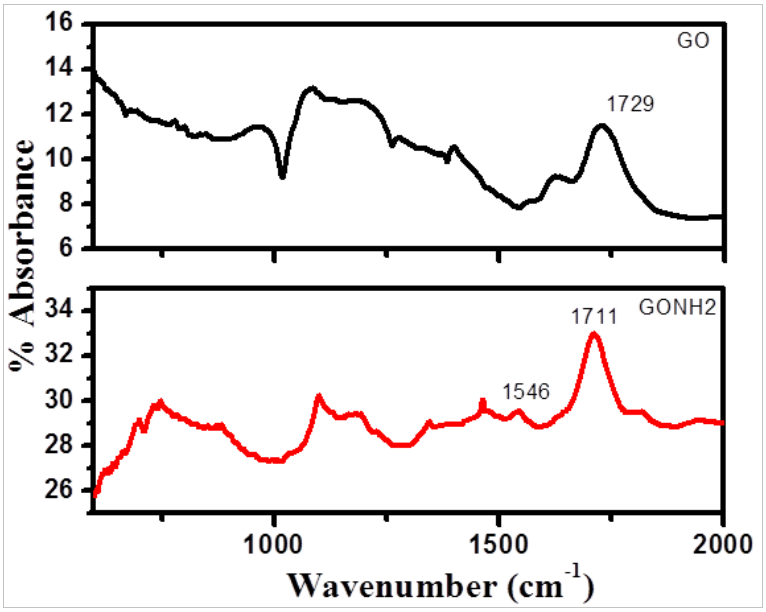

Figure 5.3 FTIR spectra of GO and GONH2

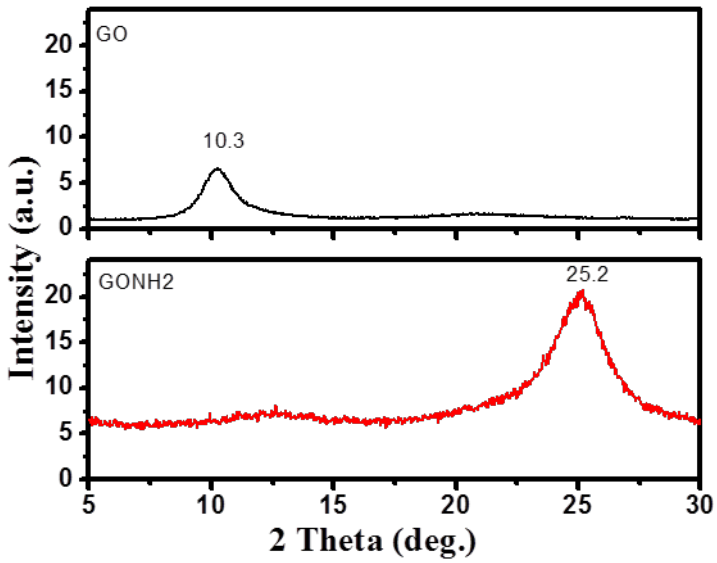

Figure 5.4 XRD spectra of GO and GONH2

Fig. 5.4 shows the XRD spectra of GO and GONH2. After phenylene diamine functionalization of GO, the peak at $2\theta=10.3^{o}$ corresponding to (001) plane in GO disappears and a new broad peak appears at $2\theta=25.2^{o}$. This is due to the decrease of interlayer spacing by the removal of intercalated oxygen functional groups, hence indicating the reduction of GO after phenylene daimine functionalization. The broadening of the peak around $2\theta=25.2^{o}$ in GONH2 compared to the graphitic peak ($2\theta=26.7^{o}$, Fig. 4.4) indicates poor ordering of

sheets in the stacking direction, hence indicating destacking of GO after phenylene diamine functionalization.

Thermal decomposition of GO after phenylene diamine functionalization is investigated by thermogravimetric analysis under nitrogen atmosphere and the decomposition pattern is given in Fig. 5.5. In GO mass reduction starts from 150 ^{o}C due to the pyrolysis of labile oxygen containing groups, whereas GONH2 shows considerable weight loss only after 250 ^{o}C. This indicates that most of the oxygen containing groups are removed during the functionalization.

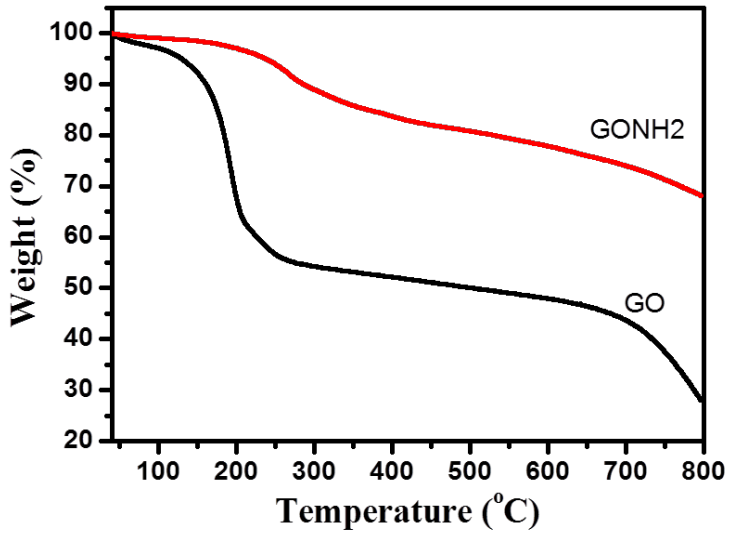

Figure 5.5 TGA pattern of GO and phenylene diamine functionalized reduced graphene oxide

Elemental composition of the samples are studied using XPS analysis as shown in Fig. 5.6. GO shows 47% oxygen and 53% carbon. But after functionalization the intensity of the peak corresponding to oxygen reduces to 8 %, where as that of carbon increases to 86%. This clearly reveals the significant reduction of GO after functionalization with phenylene diamine. Moreover, the spectrum of GONH2 shows a new peak corresponding to N1s at 400 eV due to the anchoring of phenylene diamine groups on reduced graphene oxide.

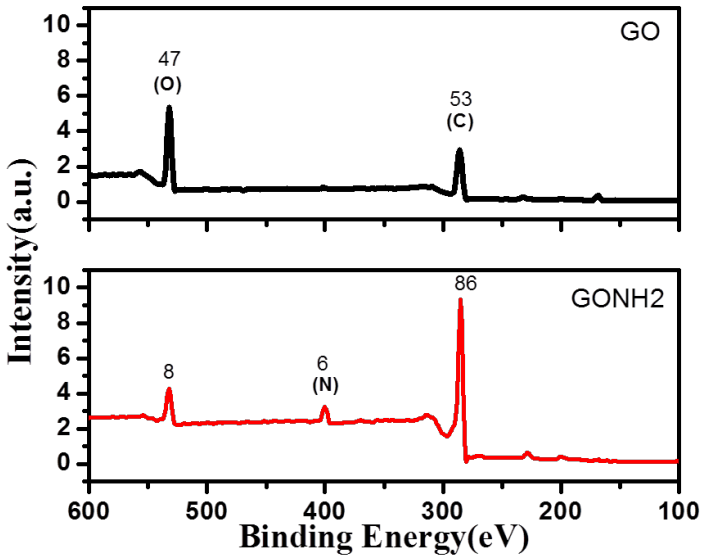

Figure 5.6 XPS spectra of GO and GONH2

Fig. 5.7 shows the Raman spectra of GO and GONH2. Here the I_G/I_D ratio is found to be 0.81, which is less than that of unfunctionalized GO (0.91) as given in Fig. 4.7. This increased intensity of D band is due to the introduction of more defects in reduced graphene oxide after functionalization with phenylene diamine.

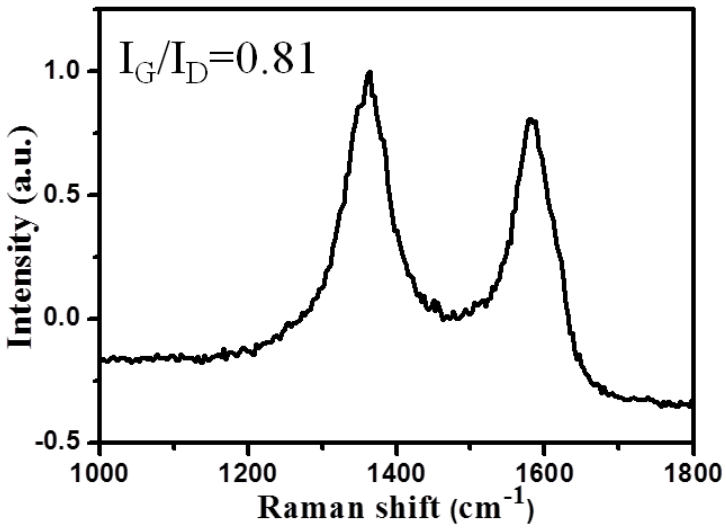

Figure 5.7 Raman spectrum of GONH2

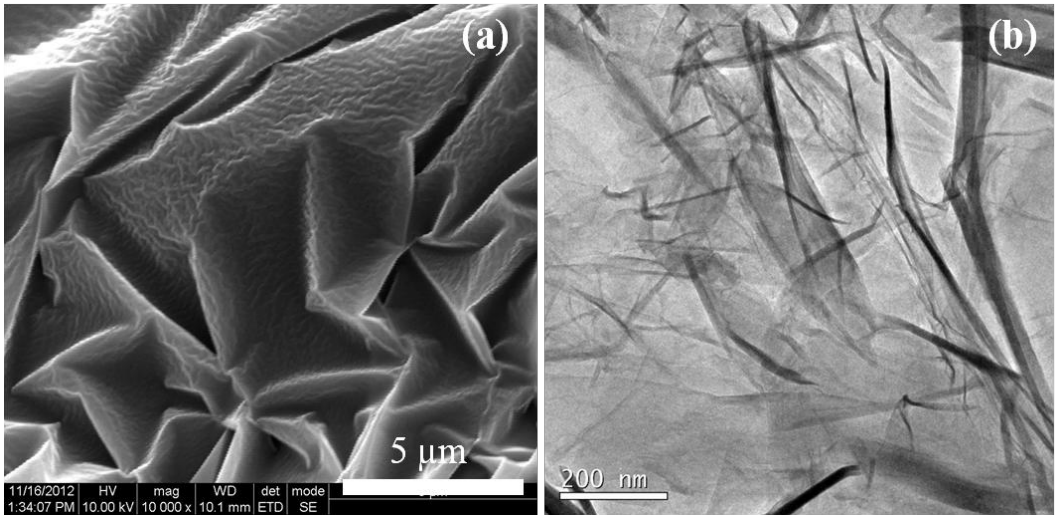

Figure 5.8 (a) SEM image and (b) TEM image of GONH2. Magnification of SEM iamge is 10000x

SEM and TEM image shown in Fig. 5.8 clearly depicts the layered and wrinkled morphology of GONH2. As shown in the SEM image, the surface of GONH2 became very rough due to the introduction of phenylene diamine on the reduced graphene oxide. TEM image of GONH2 clearly shows the considerable exfoliation of GO after phenylene diamine functionalization.

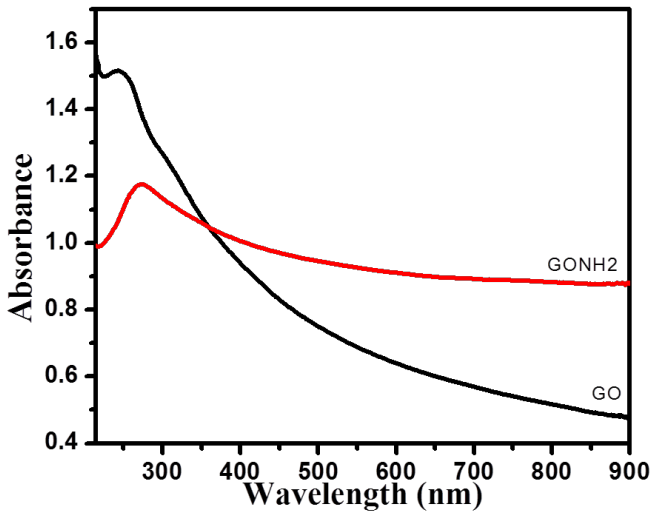

Figure 5.9 UV-visible spectra of GO and GONH2

Fig. 5.9 shows the UV-visible spectra of GO and GONH2. The absorption of GO at 244 nm is red shifted to 274 nm after diamine functionalization, indicating that the electronic conjugation is revived after

phenylene diamine functionalization due to the reduction of GO (Li D. et al., 2008). All the above characterization techniques reveal the significant reduction and exfoliation of GO after phenylene diamine grafting, hence it is named as phenylene diamine functionalized reduced graphene oxide.

5.3.2. Characterization of polyaniline-GONH2 hybrid

Fig. 5.10 shows the FTIR spectrum of the hybrid (P1NH2G2) with highest GO percentage. The hybrid shows all the characteristic peaks of polyaniline (Fig. 4.10), but the peaks are shifted to higher wavenumber side because of the π-π interaction of polyaniline with the aromatic region of the GONH2.

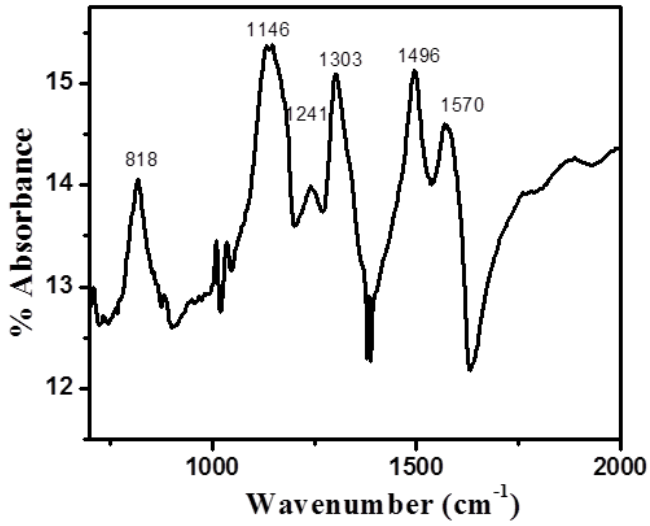

Figure 5.10 FTIR spectrum of the hybrid (P1NH2G2)

The XRD spectrum of the hybrid shown in Fig. 5.11 reveals the characteristic peaks of polyaniline at 15^o and 25^o corresponding to (011) and (200) planes respectively. The characteristic peak of polyaniline at $2\theta=20^o$ (Fig. 4.11 (a)) corresponds to the periodicity parallel to the polymer chain is almost disappeared in the hybrid spectrum because of the better π-π stacking in the hybrid. Moreover, the peak corresponding to GO at 10.3^o is completely disappeared in the spectrum of polyaniline-GONH2 hybrid. This clearly indicates the successful reduction of GO in the hybrids synthesized by this novel methodology.

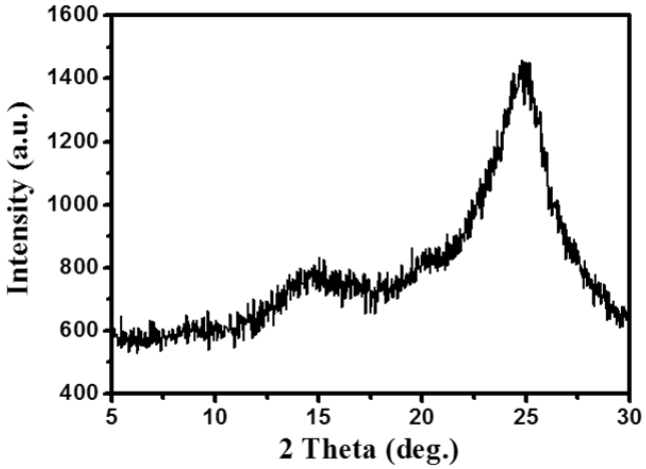

Figure 5.11 XRD spectrum of the hybrid (P1NH2G2)

Fig. 5.12 shows the XPS spectrum of the hybrid P1NH2G2. The composition of the elements in the hybrid are quantified as 15% oxygen, 8% nitrogen, 73% carbon and 4% sulphur. Increased intensity of the N 1s peak of the hybrid compared to that of GONH2 (Fig. 5.6), and the appearance of a new peak at 168 eV corresponding to S 2p in the hybrid confirms the formation of TSA doped polyaniline-GONH2 hybrid.

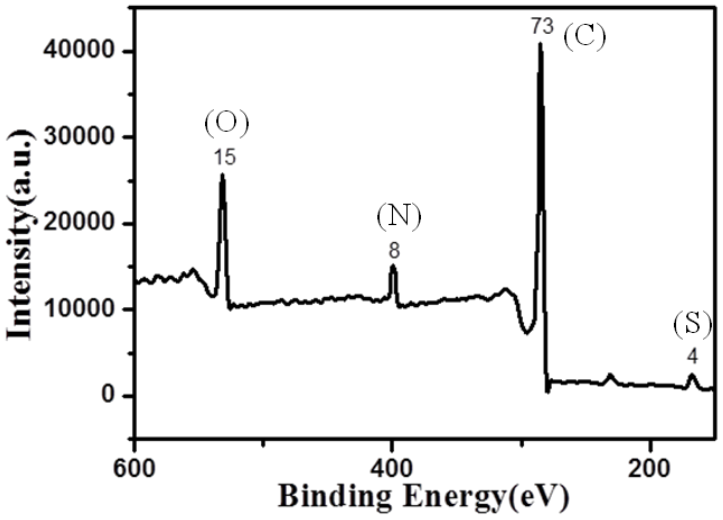

Figure 5.12 XPS spectrum of the hybrid (P1NH2G2)

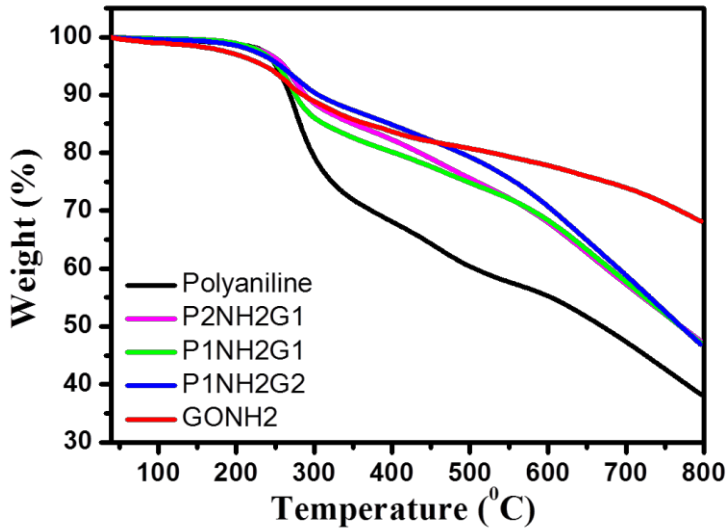

Figure 5.13 TGA patterns of the samples

TGA results given in Fig. 5.13 shows the decomposition patterns of pure polyaniline, GONH2 and the hybrids. Compared to pure polyaniline (38%), the hybrids show more residue (47%) because of the presence of stable GONH2.

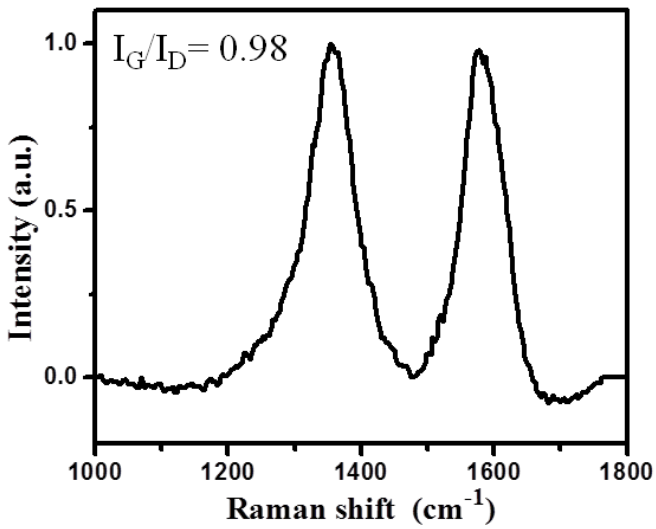

Figure 5.14 Raman spectrum of the hybrid (P1NH2G2)

I_G/I_D ratio of the hybrid is higher (0.98) compared to pristine GONH2 (0.81, Fig. 5.7) as indicated by the Raman spectrum of the hybrid shown in Fig. 5.14, and hence indicating reduced disorder in P1NH2G2 hybrid. This

suggests defect repairing of GONH2 after hybrid formation with polyaniline resulting in larger sp^2 domain and extended π-conjugation.

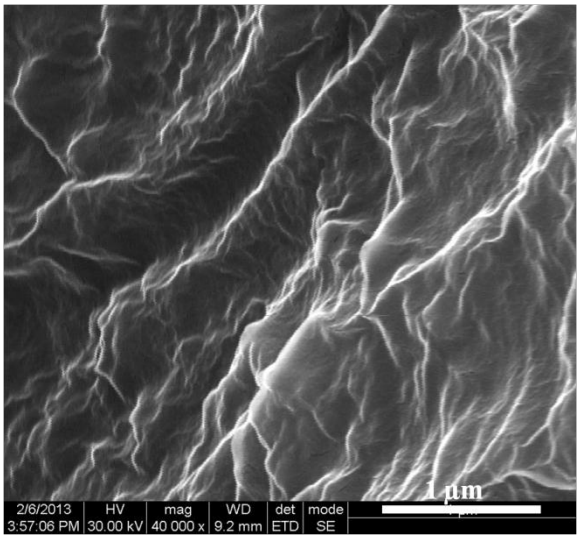

Figure 5.15 SEM image of the hybrid (P1NH2G2) at a magnification of 40000x

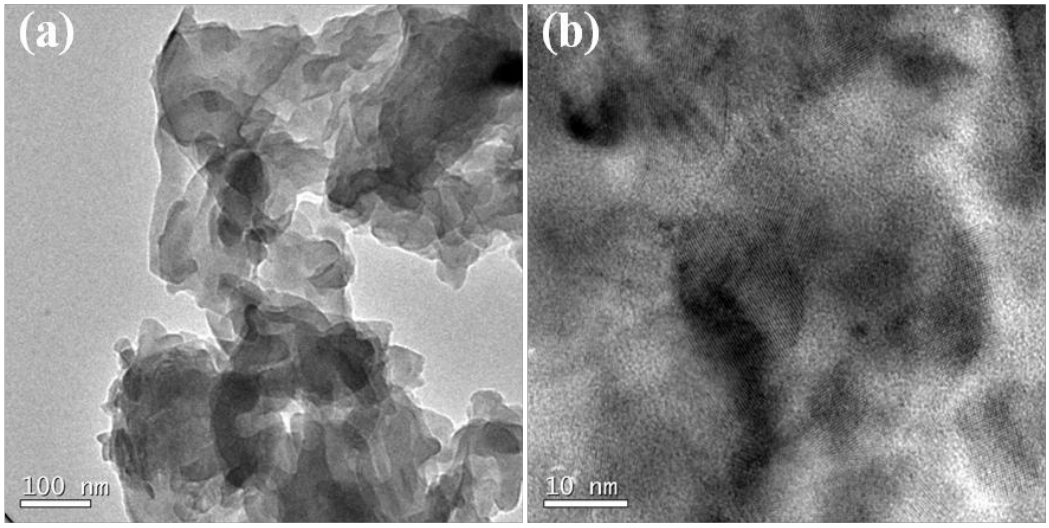

Figure 5.16 (a) TEM image and (b) HRTEM image of the hybrid (P1NH2G2)

SEM and TEM images of P1NH2G2 shown in Figs. 5.15 and 5.16 respectively reveal the presence of polyaniline covered with reduced graphene oxide sheets. HRTEM image shown in Fig. 5.16 (b) shows the crystalline fringes of reduced graphene oxide sheets of the hybrid.

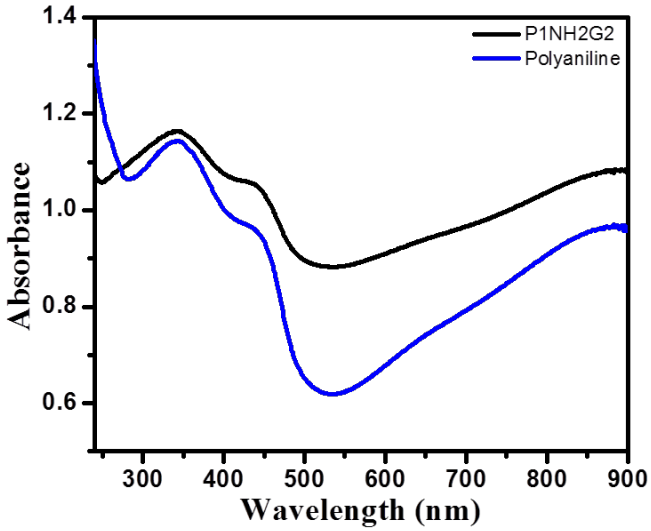

Figure 5.17 UV-visible spectra of polyaniline and the hybrid (P1NH2G2)

Fig. 5.17 (a) shows the UV-visible spectra of polyaniline and the hybrid P1NH2G2 recorded in 2-propanol. The hybrid spectrum shows all the three characteristic peaks of polyaniline.

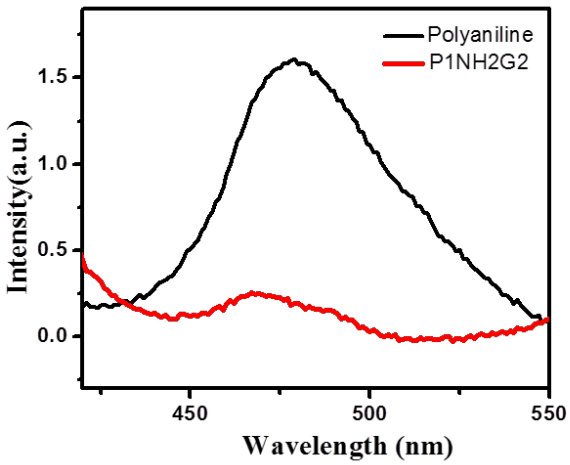

Figure 5.18 Photoluminescence spectra of polyaniline and the hybrid (P1NH2G2)

Photoluminescence spectra of polyaniline and P1NH2G2 dispersions in 2-propanol (1 mg in 5 ml) are recorded at the excitation wavelength of 360 nm as shown in Fig. 5.18. Polyaniline shows a broad emission centered at 480 nm. After hybridization with GONH2, the photoluminescnce is significantly quenched due to the efficient electron transfer between polyaniline and GONH2 facilitated

by the covalent interactions. Because of the reduction of GO, sp^2 domains are increased, which results in the improvement to accept and transfer electrons.

5.3.3 Optical limiting properties

Optical limiting properties of the samples are measured using open aperture Z scan technique. Fig. 5.19 shows Z scan plots of the hybrids, pure polyaniline and GONH2. All the curves exhibit normalized transmittance valley indicating strong optical limiting behaviour. Optical limiting curves plotted using Z scan data are given in Fig. 5.20. Compared to pristine GONH2 and polyaniline, the hybrids show deep valley, hence better optical limiting behavior. The hybrid with highest GONH2 percentage (P1NH2G2) is showing the strongest optical limiting bahaviour among this class of hybrids.

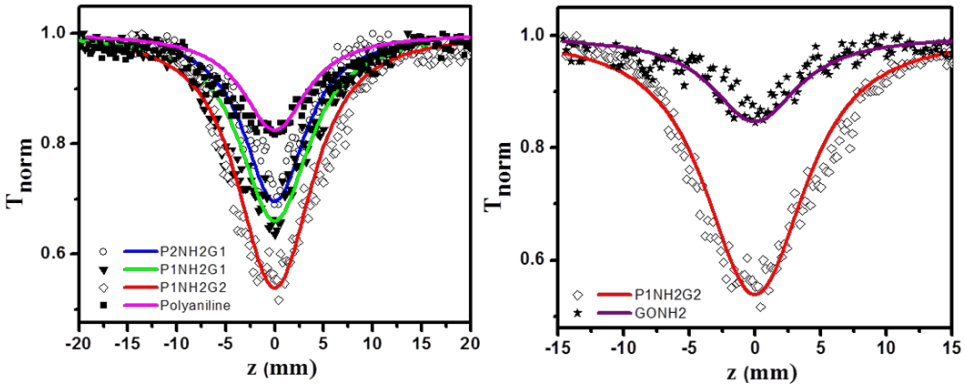

Figure 5.19 Open aperture Z scan plots of the samples

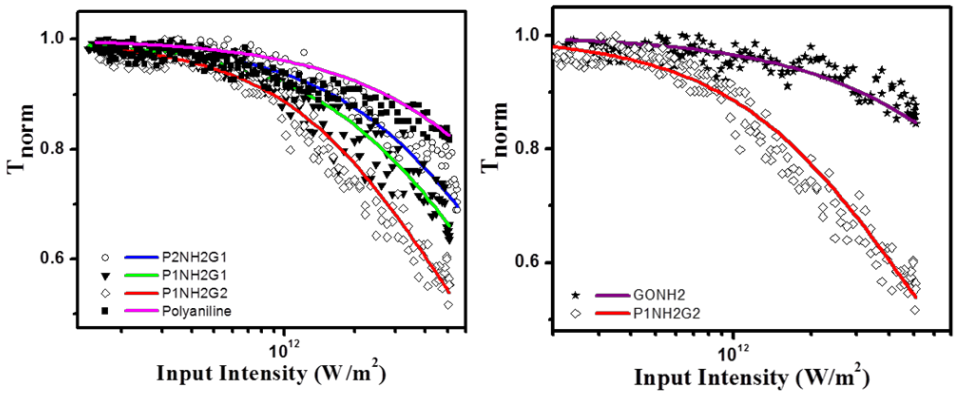

Figure 5.20 Optical limiting plots of the samples

The nonlinear absorption parameters of the samples derived from the theoretical fit of the Z scan data is listed in Table 5.1. P1NH2G2 shows the higher nonlinear absorption coefficient of 25 cm/GW with lower saturation intensity of 0.2 GW/cm^2. The improved optical limiting of the hybrids are attributed to the synergetic combination of NLO mechanisms of polyaniline and reduced graphene oxide facilitated by the covalent connections. At the same time, during the phenylene diamine functionalization and polymerization, the oxygen functionalities in GO are removed significantly and crystalline defects diminishes, which increases the conjugation network. The increase of lattice integrity of redued graphene oxide enhances its thermal transmission which can results in improved nonlinear scattering (Zhao, et al., 2013). The significant photoinduced electron transfer from the donor polyaniline to reduced graphene oxide may also play a major role in improving the optical limiting behaviour (Liu Z.-B. et al., 2009).

Table 5.1 Nonlinear absorption coefficient (β) and saturation intensity (I_{sat}) of the samples

Sample name	β (cm /GW)	I_{sat} (GW/cm^2)
Polyaniline	5.8	2.5
GONH2	4.8	3.7
P2NH2G1	12	0.6
P1NH2G1	15	0.5
P1NH2G2	25	0.2

5.3.4. DC conductivity and photocurrent generation studies

The dc-conductivity of the samples in the form of circular pellets are measured at room temperature using standard spring-loaded pressure contact four probe method. The probe spacing is 2 mm. The current from a dc-source meter (Keithley, 2182A) is allowed to pass through the outer probes of the four-probe

and voltage across the two inner probes is measured using nanovoltmeter (Keithley, 6221). The dc conductivity is calculated using the standard van der Pauw relation as described in Chapter 2 (Eq. 2.7). The thickness of the sample is taken as the average of three different measurements using a screw gauge. The conductivity values of the samples are given in Table 5.2. To investigate the effect of covalent functionalization in improving the conductivity, the conductivity of polyaniline-phenylene diamine functionalized reduced graphene oxide hybrids are compared with that of polyaniline/unfunctionalized GO hybrids.

Table 5.2 DC conductivity of the samples

Sample name	DC conductivity (S/cm)
Polyaniline	2
P2NH2G1	2.1
P1NH2G1	5.9
P1NH2G2	6.3
P2G1	0.33
P1G1	0.14
P1G2	0.03

The dc conductivity of pristine polyaniline is found to be 2 S/cm. The polyaniline-phenylene diamine functionalized reduced graphene oxide hybrids (P2NH2G1, P1NH2G1and P1NH2G2) shows increased conductivity compared to pure polyaniline. This may be because of the formation of direct conducting pathways due to the covalent bonds formed between polyaniline and GONH2. After functionalization with phenylene diamine, considerable reduction and exfoliation of GO occurs and hence GONH2 acts as conducting filler and promotes easier delocalization of electrons. So the hybrid with highest GONH2 percentage shows the highest dc conductivity of 6.3 S/cm. But in the case of polyaniline-unfunctionalized GO hybrids (P2G1, P1G1 and P1G2), the

conductivity decreases as the percentage of GO increases, because of the insulating nature of GO.

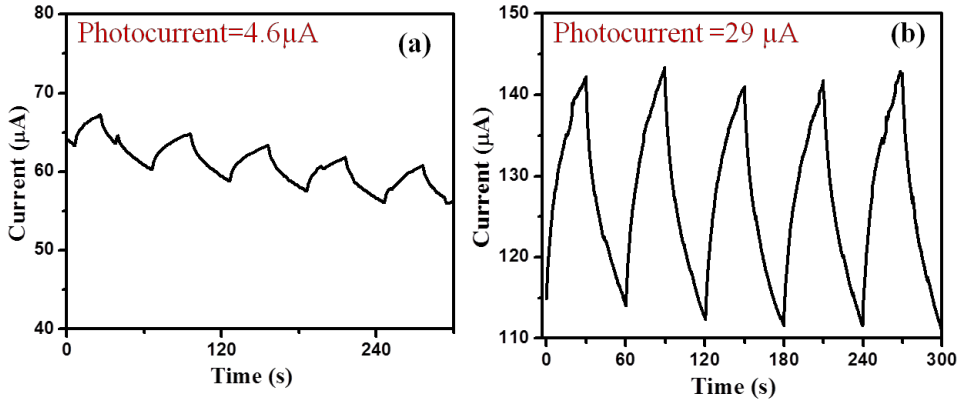

Figure 5.21 Photocurrent cycles of (a) polyaniline and (b) hybrid P1NH2G2

Fig. 5.21 shows the photocurrent cycles of polyanilne and P1NH2G2 by repetitive switching of the white light illumination (on/off) at an interval of 30 s. It is clear from the figure that photocurrent generation of the hybrid is high (29 μA) compared to that of pristine polyaniline (4.6 μA). The responsivity of the samples are calculated by the equation $(I_{light}-I_{dark})/I_{dark}$. Pure polyaniline shows a responsivity of 7.8%, while the hybrid shows an increased responsivity of 25.6%. Low exciton dissociation and immediate recombination of the photogenerated electrons and holes are responsible for the low photocurrent in polyaniline. But in the hybrid, the photogenerated exciton may easily be diffused into the interface between polyaniline and reduced graphene oxide and get dissociated. The electrons are transferred to reduced graphene oxide layers and the holes are delocalized along the polyaniline chain and results in large photocurrent. The efficient photocurrent generation of P1NH2G2 is due to the formation of direct conducting pathways because of the covalent linkage between polyaniline and reduced graphene oxide sheets. The photocurrent cycles of hybrids are more reproducible compared to polyaniline.

To get an insight into the process of photocurrent generation in this hybrid, energy level diagram of the photocurrent generating system is drawn as shown in Fig. 5.22.

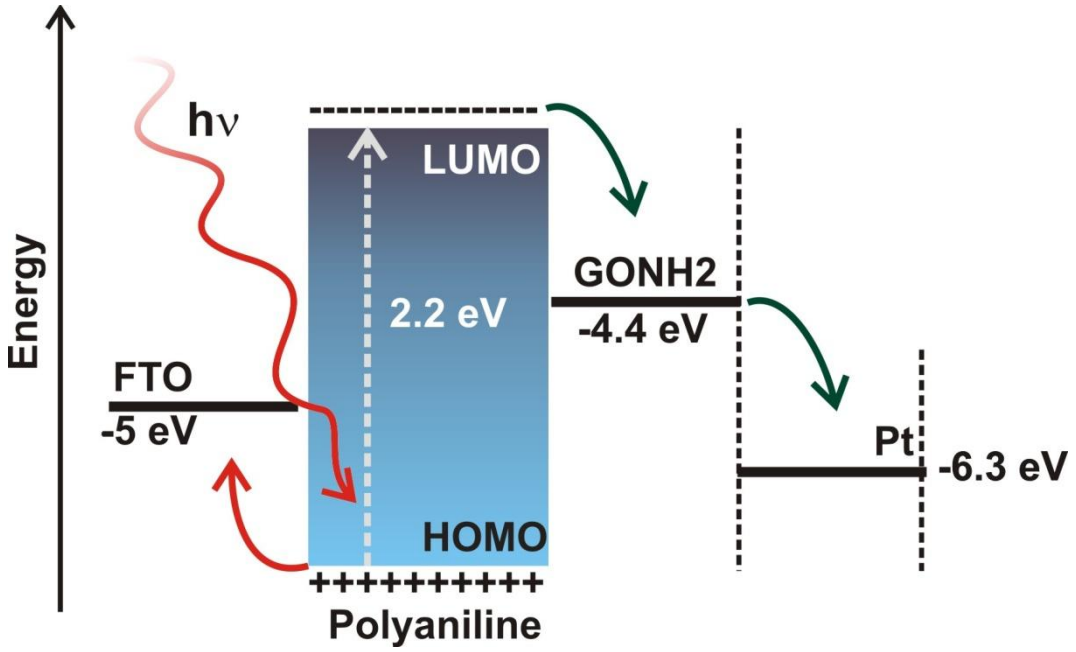

Fig. 5.22 Energy level diagram of the photocurrent generating system

The band gap of polyaniline in the hybrid (P1NH2G2) is calculated from the intercept on the abscissa of $(\alpha h\upsilon)^2$ vs. $h\upsilon$ plot (Fig. 5.23) drawn using Tauc relation as given in Eq. 5.1 (Tauc, J. 1970).

$$\alpha = \frac{B(h\upsilon - E_g)^n}{h\upsilon} \qquad (5.1.)$$

where, α is the absorption coefficient, B is the fitting parameter, h is the Planck's constant and υ is the photon frequency, E_g is the band gap and n corresponds to the different possible electronic transitions responsible for the light absorption. For polyaniline n is taken as ½ . From Fig. 5.23, the band gap of polyaniline in the hybrid is found to be 2.2 eV. The calculated workfuntion of graphene is reported as 4.42 eV (Chatterjee et al., 2013).

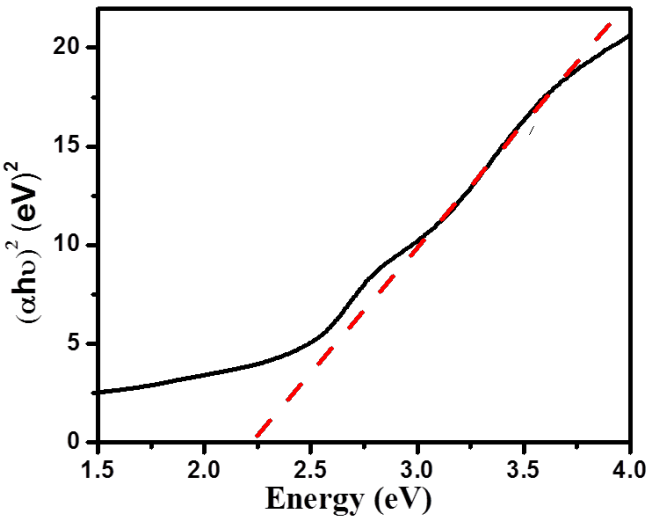

Figure 5.23 $(\alpha h\upsilon)^2$ vs. $h\upsilon$ plot (Tauc plot) of the hybrid P1NH2G2.

Therefore under white light illumination, electrons are excited from the highest occupied molecular orbital (HOMO) to the lowest unoccupied molecular orbital (LUMO) of polyaniline and leaves a hole in the HOMO of polyaniline. (Chatterjee et al., 2013). The excitons then diffuse to the interface between polyaniline and GONH2. Due to the difference in LUMO energy levels, a strong electric field exists at the interface between the polyaniline and GONH2, which allows the dissociation of the excitons at the interface. Reduced graphene oxide is having higher electron affinity, so naturally the dissociated electrons can relax to GONH2 and get transported away from polyaniline. The seperated holes can be delocalized along the polyaniline chain. The electrons and holes are then extracted out at cathode and anode respectively, supported by an internal electrical field generated mainly due to the difference in work function of the electrodes used. Hence the photocurrent generation has mainly 4 steps, light absorption and exciton generation, diffusion of excitons, dissociation of excitons, and transport of dissociated carriers to the respective electrodes (Blom et al., 2007).

5.3.5. Comparison of polyaniline-GONH2 hybrid with polyaniline-unfunctionalized GO hybrid

In situ polymerization of aniline in the presence of phenylene diamine functionalized reduced graphene oxide produces hybrids with covalent connections between polyaniline and GONH2, while the polymerization of aniline in presence of unfunctionalized GO produces hybrids with noncovalent interactions. The efficient reduction of GO is achieved during phenylene diamine functionalization. So polyaniline-GONH2 hybrids are having larger sp^2 domain and extended conjugation compared to polyaniline-GO hybrid. The photoluminescence quenching is more significant in P1NH2G2 (Fig. 5.17) than the corresponding unfunctionalized GO-polyaniline hybrid (P1G2, Fig. 4.19). This reveals the better electron transfer through the direct covalent linkage between polyaniline and GONH2 in P1NH2G2. The covalently connected hybrid P1NH2G2 shows better optical limiting behaviour (Table 5.1) compared to the corresponding polyaniline-GO hybrid (Table 4.1). The efficient photoinduced electron transfer and the combination of NLO mechanisms of polyaniline and GONH2 facilitated by covalent connections are contributing to the improved optical limiting of P1NH2G2 compared to P1G2. The dc conductivity of P1NH2G2 is around 200 times higher than that of P1G2 (Table 5.2). This large improvement in dc conductivity is also due to the formation of direct conducting pathways by the covalent connection between polyaniline and GONH2. Significant exfoliation and reduction of GO after functionalization also promote easier delocalization of electrons through the exfoliated and reduced graphene oxide sheets. But in P1G2, GO is acting as an insulating filler and hence the conductivity is decreased compared to polyaniline. Moreover, the hybrid P1NH2G2 shows a significant photocurrent of 29 μA (Fig. 5.21 (b)), where as the corresponding polyaniline-unfuctionalized hybrid P1G2 (9 μA, Fig.4.22) shows only slight improvement in photocurrent compared to pure polyaniline (4.6 μA, Fig. 5.21(a)). This large and stable photocurrent of P1NH2G2 is due to the efficient exciton dissociation due to the electron transfer between polyaniline and GONH2 and the easier transport of electrons through the reduced graphene oxide layers to electrodes.

5.4. Conclusions

Phenylene diamine functionalized reduced graphene oxide is designed, synthesized and characterized for the synthesis of polyaniline hybrids with covalent connections. The hybrids are synthesized by the *in situ* polymerization of aniline in the presence of synthesized GONH2. All the spectroscopic, microscopic and thermal characterization techiniques confirms the formation of polyaniline-GONH2 hybrid. Significant photoluminescence quenching is observed in the hybrid indicating the effective photoinduced electron transfer between polyaniline and reduced graphene oxide because of the formation of direct conducting pathways due to the covalent bonds. This class of hybrids show better optical limiting behaviour compared to individual components as well as the unfunctionalized GO-polyaniline hybrids. The improved optical limiting of the hybrids are attributed to the synergetic combination of NLO mechanisms of polyaniline and reduced graphene oxide facilitated by the covalent connections, better sp^2 conjugation and significant photoinduced electron transfer. These hybrids with large optical nonlinearity (β=25 cm/GW) and low limiting threshold (I_{sat}=0.2 GW/cm^2) apart from the unique structure and excellent electronic properties prove that they are good candidate for NLO device applications.

P1NH2G2 shows an electrical conductivity of 6.3 S/cm, which is around 3 times higher compared to pure polyaniline and around 200 times higher than unfunctionalized GO/polyaniline hybrid (PIG2). Considerable reduction and exfoliation of GO after phenylene diamine grafting and the covalent bonds between polyaniline and GONH2 are responsible for the better conductivity. The hybrid also produces large and stable photocurrent (29 μA) under white light irradiation, hence it is an ideal material for photosensing and photodetecting applications.

CHAPTER 6
STUDIES ON POLYANILINE-PHENYLENE DIAMINE FUNCTIONALIZED MULTIWALLED CARBON NANOTUBE HYBRID

This chapter presents the synthesis, characterization, optical limiting behaviour, dc conductivity and photocurrent generation of polyaniline-phenylene diamine functionalized MWNT hybrids. Photoluminescence quenching in the hybrid due to the photoinduced electron transfer between polyaniline and MWNT, band gap narrowing of the hybrid with respect to pure polyaniline, etc. are also discussed.

6.1. Introduction

Carbon nanotubes (CNTs), discovered by Iijima and Ichihashi (1993) have raised great interest among researchers in recent years due to their excellent electrical, optical, thermal and mechanical properties (Bhandari et al., 2008; Dresselhaus et al., 2004; Dresselhaus et al., 1995). However, the solubility and processability of the pristine carbon nanotubes have been challenging due to the presence of inter-tubular aromatic π-π interactions. Chemical functionalization at the tube-ends and sidewalls is one of the common ways to overcome this drawback of CNTs. The presence of oxygen functionalities like carboxyl and hydroxyl groups facilitates the separation of CNT bundles and increases the solubility in polar media. The chemical functionalization also favours the possibility of further modification of CNTs depending on the applications.

The studies on hybrids based on conducting polymers with CNTs are currently active areas of research in the field of material science. Many conducting polymers have been utilized for making hybrids with CNTs for various applications (Ferrer-Anglada et al., 2006; Wang F. et al., 2008; Wang and Musameh, 2005; Yuan et al., 2009). Among them polyaniline has achieved widespread importance because of its low cost, environmental stability and very

good electrical conductivity (Skotheim et al., 1997). Mainly there are two important approaches for the synthesis of polyaniline hybrids of CNTs, physical mixing of polyaniline with CNTs and *in situ* polymerization of aniline in the presence of CNTs. Studies shows that the latter method produces homogeneous nanocomposites (Zhang X. et al., 2005). But the insolubility of pristine CNTs reduces the compatibility with polymers. Functionalization of CNTs can increase the solubility; hence hybrids with better compatibility can be achieved by using functionalized CNTs during the *in situ* polymerization of aniline (Wu and Lin, 2006). The amine functionalization of CNTs increases the compatibility with aniline monomer and by the *in situ* polymerization of aniline in the presence of amine functionalized CNTs, nanocomposites with very good interactions can be achieved (Lafuente et al., 2008). It is also observed that the introduction of aniline monomer on the surface of CNTs not only increases the dispersion, but also join in the polymerization of aniline to impart chemical bonds between polyaniline and CNTs, and avoid microscopic phase separation in the nanocomposites (Philip et al., 2005; Xu J. et al., 2008; Xu J. et al., 2009; Yao et al., 2009).

The unique broadband (visible to NIR) optical limiting action of CNTs, has attracted researchers interest to utilize them as potential materials for the protection of human eyes and sensors. Currently researchers are trying to improve the nonlinear optical properties of CNTs by making composites with dyes having reverse saturable absorption. A cumulative optical limiting effect was observed by Izard et al. (2004) through a combination of SWNTs with two photon absorbing chromophore *stilbene 3.* Webster et al. (2005) observed an enhanced nonlinear transmittance by complementary nonlinear mechanisms between a reverse saturable absorbing dye (1,1′,3,3,3′,3′-hexamethylindotricarbocyanine iodide) with nonlinear-scattering carbon nanotubes. Ní Mhuircheartaigh et al. (2006) reported the superior optical limiting effect from a noncovalently linked tetraphenyl porphyrin–carbon nanotube composite. An enhanced optical limiting action is observed by Wang and Blau (2008) from stable solutions of physically blended phthalocyanine–single walled carbon nanotube composites.

Apart from carbon nanotube composites with noncovalent interactions, covalently connected hybrids of CNTs with materials showing complimentary nonlinear optical properties find greater interest for improving optical nonlinearity. Liu Z. B. et al. (2008) demonstrated the superior optical limiting performance of SWNTs covalently functionalized with porphyrins compared to the individual SWNT, porphyrins, and the bench mark material C_{60}. The improvement is attributed to the combined nonlinear mechanism and photoinduced electron or energy transfer between the porphyrin moiety and the SWNTs. Guo et al. (2006) synthesized novel covalently porphyrin-functionalized SWNTs by the reaction of SWNTs with *in situ* generated porphyrin diazonium compounds. They observed an enhancement in optical limiting due to the effective energy and electron transfer between the excited porphyrin moiety and the extended π-system of SWNTs facilitated by the direct covalent linkage. Phthalocyanine moieties are also grafted on CNTs for optical limiting applications. He et al. (2009) reported the preparation and optical limiting properties of MWNTs with π-conjugated metal-free phthalocyanine moieties. Feng et al. (2005) studied the enhancement of third-order optical nonlinearities for (poly[(3-octylthiophene-2,5-diyl)-(p-aminobenzylidenequinomethane)]-bonded multiwalled carbon nanotubes. Li et al. (2003) and Wu et al. (2003) observed efficient photoinduced electron transfer interactions and enhanced optical limiting in PVK bonded SWNTs.

CNT hybrids of various functional materials are also an interesting class of materials for optoelectronic and light harvesting applications. Cao et al. (2002) reported the photoconductive property of oxotitanium phthalocyanine physically doped with the chemically modified MWNTs and the results showed that the efficiency of charge carrier separation increases due to the photoinduced charge transfer between oxotitanium phthalocyanine and MWNT. Researchers from the same group studied the effect of covalent connections between CNTs and phthalocyanine moiety for improvement in photoconductivity (Yang et al., 2004). They covalently connected MWNT to 2,9,16,23-tetra amino manganese phthalocyanine and observed a photosensitivity better than that of individual

components and the corresponding physically blended sample. Yang et al. (2008) prepared 2,9,16-trilauryloxy-23-hexyloxy substituted copper phthalocyanine-multiwall carbon nanotubes hybrids by chemical functionalization method and presented the good solubility and enhanced photoconductivity of the hybrid material. The occurrence of photoinduced electron transfer in SWNTs bearing covalently linked phthalocyanines has been widely studied (Ballesteros et al., 2007; Chitta et al., 2007) which helps in improving the nonlinear optical response and photocurrent generation. Even though the covalently connected hybrids of CNTs with functional materials like, pthalocyanines, porphyrins, PVK, etc. are studied for photoinduced electron transfer and resulting improvement in optical limiting or photocurrent generation, the hybrids of polyaniline with CNT are not known for these applications.

With this background, polyaniline-MWNT hybrids are synthesized by the *in situ* polymerization of aniline in the presence of phenylene diamine functionalized MWNT. The aniline monomer is introduced on the surface of MWNT through phenylene diamine functionalization. Along with aniline monomer, the aniline moiety on the surface of MWNT also initiates the polymerization and acts as a covalent bridge between polyaniline and MWNT. The photoluminescence quenching in the hybrid due to the electron transfer between polyaniline and MWNT and the resulting improvement in optical limiting and photocurrent generation are also discussed in this chapter.

6.2. Experimental

6.2.1. Functionalization of MWNT

The MWNT (95 wt %, 5-15 nm diameter, 1-10 um length) is functionalized with phenylene diamine as per the synthesis route shown in Fig. 6.1. Carboxylation of MWNT is done by refluxing pristine MWNT with 60% HNO_3 at 120 ^oC for 6h. The acid functionalized MWNT is then filtered, washed with distilled water, and dried under vacuum at 80 ^oC. It is then redispersed in excess $SOCl_2$ and DMF and refluxed at 80 ^oC for 24 h to convert the carboxylic acid groups to acid chlorides. The excess $SOCl_2$ is removed by reduced pressure

distillation. Excess phenylene diamine and DMF is added to the suspension and the reaction mixture is refluxed at 120 ^{o}C for 72 h in nitrogen atmosphere. The resulting phenylene diamine functionalized MWNT (MWNTCONH2) is filtered washed, and dried under vacuum. The procedure for phenylenediamine grafting of acid functionalized MWNT is adapted from Xu J. et al. (2009).

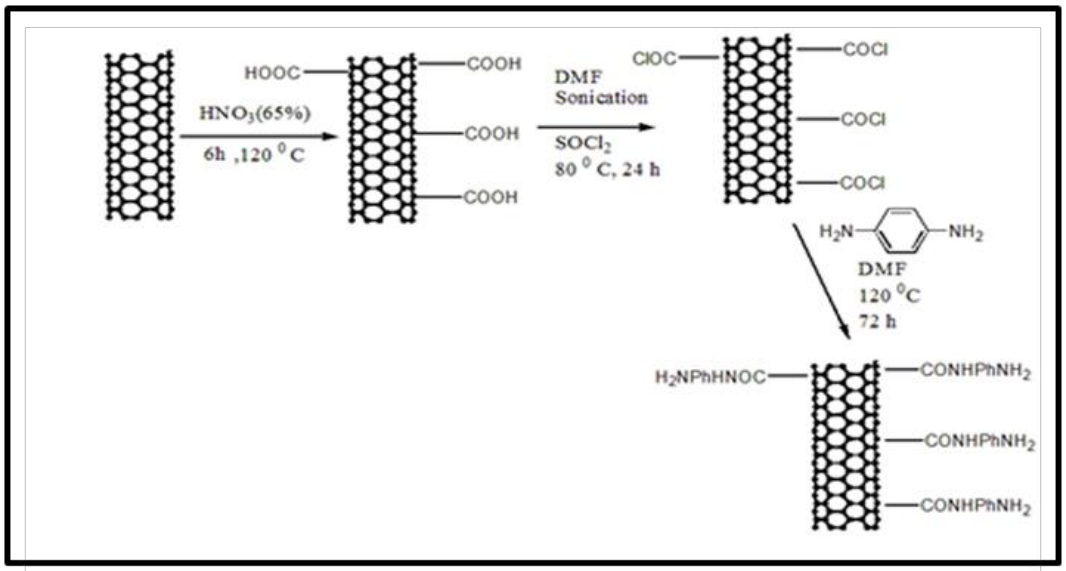

Figure 6.1 Scheme of the functionalization of MWNT

6.2.2. Synthesis of polyaniline-phenylene diamine functionalized MWNT hybrid

A schematic representation of the synthesis of polyaniline-MWNT hybrid is shown in Fig. 6.2. Weighed amount of MWNTCONH2 is dispersed in 1 M TSA by ultrasonication. Aniline monomer is added to it and stirred for 30 minutes to achieve adsorption of monomer on MWNTs. The interaction between aniline monomer and functionalized MWNTs causes adsorption of aniline molecules on MWNTs. Freshly prepared aqueous solution of ammonium persulfate is dropped slowly into the solution and polymerization is carried out for 9 h with constant stirring. The resulting green coloured solution is filtered, washed with distilled water and methanol and dried under vacuum at 80^{o} C. The aniline: MWNTCONH2 ratios chosen for the polymerization are 2:1, 1:1 and 1:2, and the samples are named as P2NH2C1, P1NH2C1 and P1NH2C2.

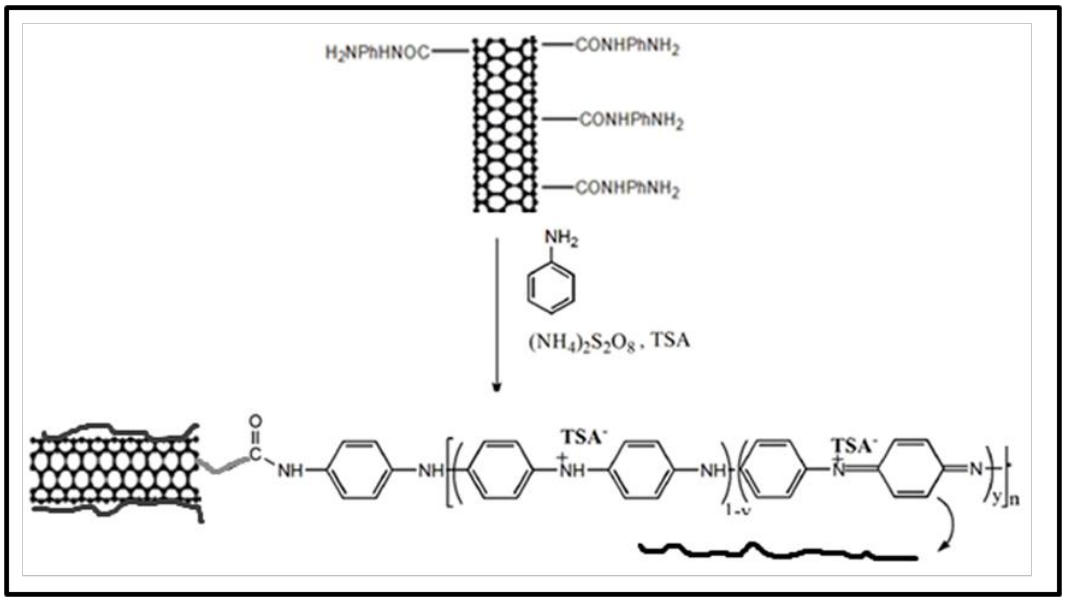

Figure 6.2 Scheme of the synthesis of polyaniline-phenylene diamine functionalized MWNT hybrid

As shown in Fig. 6.2, phenylene diamine groups are grafted on the defective sites at the side walls and tube ends of MWNT by amide bonds. During the polymerization reaction, two types of cation radicals can be formed after the addition of initiator. The aniline radical cation physically adsorbed on MWNT and phenylene diamine radical cation which is covalently grafted on MWNT. Both these radicals initiate the polymerization reaction. But it is reported that the chains initiated by the phenylene diamine radical cations dominates in the formation of inner layer coating of polyaniline on MWNT (Philip, et al., 2005). As time proceeds the aniline monomer also joins in the polymerization reaction and some of the chains formed get connected to polyaniline chains initiated by phenylene diamine radical cations and thus get covalently grafted on MWNT. Other chains physically cover the MWNT and form outer layers of polyaniline on MWNT.

6.3. Results and Discussion

6.3.1. Characterization of functionalized MWNT

FTIR spectra of pristine MWNT, MWNTCOOH and MWNTCONH2 are shown in Fig. 6.3. In the spectra of MWNTCOOH, the peak observed at

1736 cm^{-1} is attributed to the C=O stretching vibrations of –COOH groups. After phenylene diamine functionalization, this peak shifts to 1722 cm^{-1} due to the formation of amide bonds between phenylene diamine and MWNT. The characteristic –NH bending vibrations are seen at 1555 cm^{-1}.

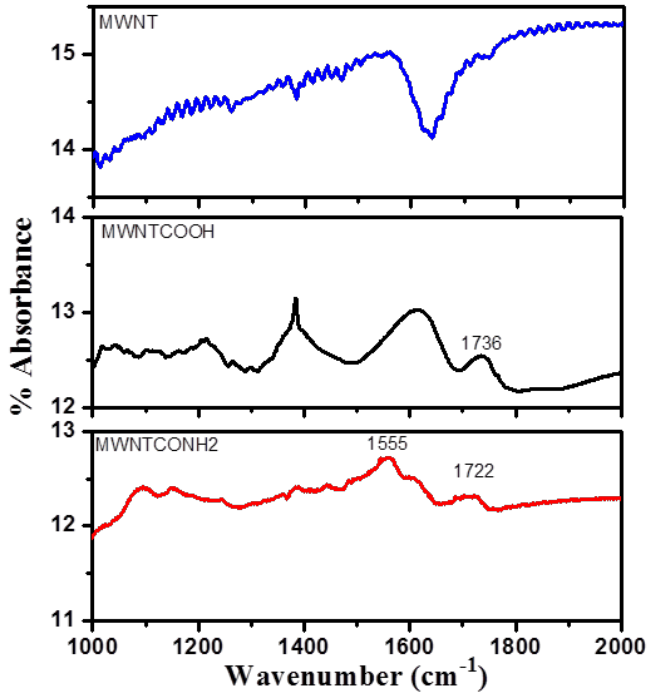

Figure 6.3 FTIR spectra of MWNT, MWNTCOOH and MWNTCONH2

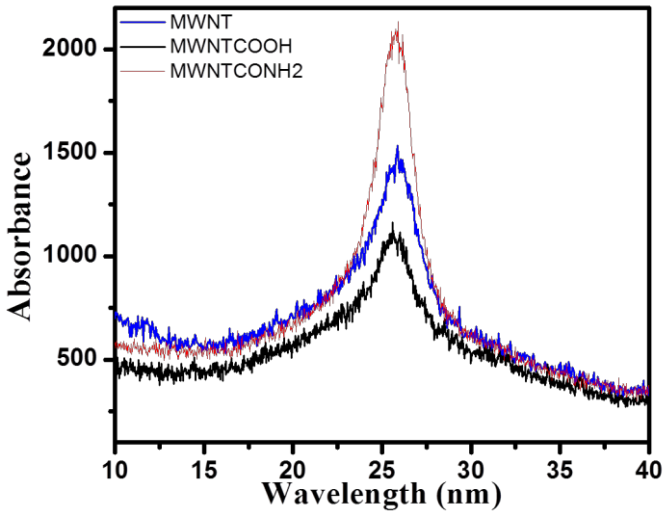

Figure 6.4 XRD spectra of MWNT, MWNTCOOH and MWNTCONH2

Fig. 6.4 shows the XRD spectra of pristine MWNT, MWNTCOOH and MWNTCONH2. All the spectra show the characteristic graphitic peak at $2\theta=25.7^{o}$ corresponding to (002) planes of MWNT (Huiqun et al., 2006) revealing that the treatment with nitric acid and thionyl chloride does not affect the graphitic structure of MWNT.

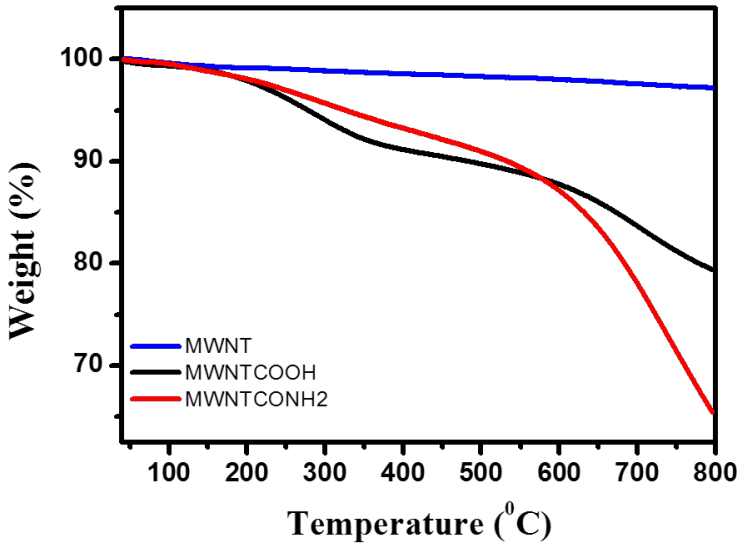

Figure 6.5 TGA patterns of MWNT, MWNTCOOH and MWNTCONH2

Thermal stability of the samples is studied by thermo gravimetric analysis as shown in Fig. 6.5. Pristine MWNT is found to be stable in the temperature range studied. The major weight loss (7%) observed in MWNTCOOH in the temperature range 150-350 ^{o}C is due to the decomposition of carboxylic acid group. The gradual weight loss observed in MWNTCONH2 in the temperature range 150-550 ^{o}C attributed to the decomposition of phenylene diamine groups. The steep weight loss after 550 ^{o}C observed both in MWNTCOOH and MWNTCONH2 is due to the decomposition of amorphous carbon formed after functionalization.

Fig. 6.6 shows the XPS spectra of acid functionalized and phenylene diamine functionalized MWNTs. MWNTCOOH shows 17% oxygen content and 83% carbon content. After functionalization with phenylene diamine, the percentage of oxygen reduces to 8 and a new peak at 400 eV corresponding to N

1s appears due to the introduction of phenylene diamine groups through amide bonds.

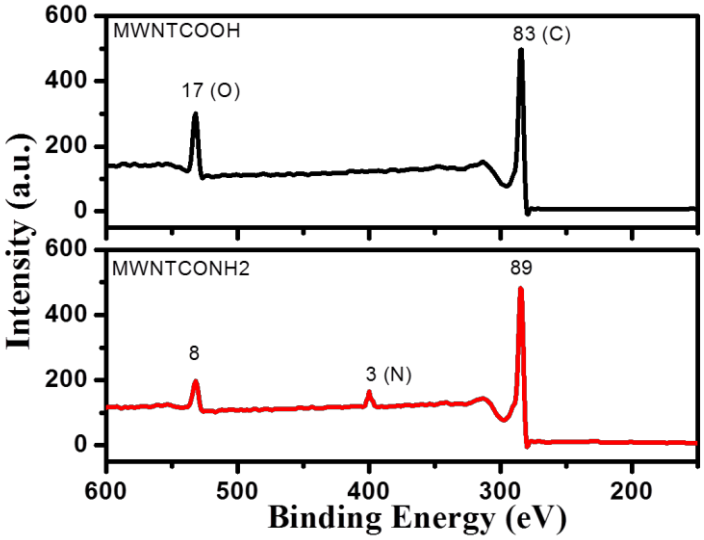

Figure 6.6 XPS spectra of MWNTCOOH and MWNTCONH2

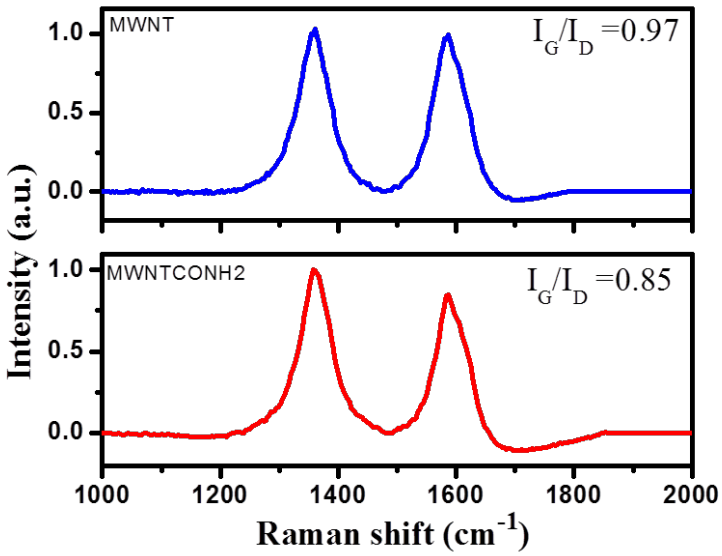

Figure 6.7 Raman spectra of MWNT and MWNTCONH2

Fig. 6.7 shows the Raman spectrum of MWNT before and after phenylene diamine functionalization. The spectrum of MWNT shows a broad G band at 1583 cm^{-1} which is Raman allowed phonon high frequency Raman mode and a defect induced D band at 1357 cm^{-1}. The intensity ratio of the G band to D

band gives a measure of disorder. Pristine MWNT shows I_G/I_D ratio of 0.97. But after chemical functionalization, the I_G/I_D ratio decreases to 0.85 due to the introduction of defects in the sidewalls and tube ends of MWNT.

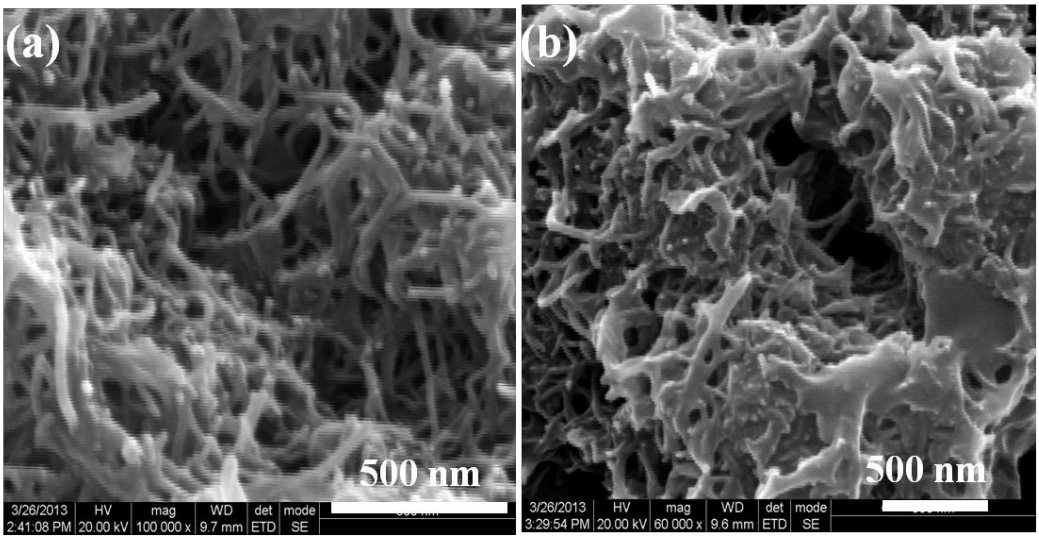

Figure 6.8 SEM images of MWNT at a magnification of 100000x and MWNTCONH2 at a magnification of 60000x

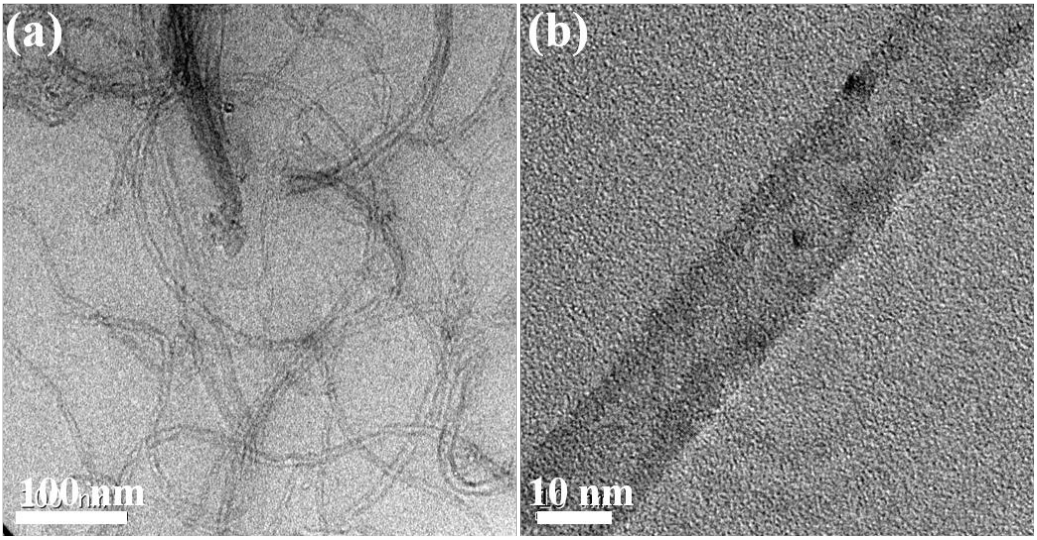

Figure 6.9 (a) TEM image and (b) HRTEM image of MWNTCONH2

Fig. 6.8 shows the morphology of MWNT before and after phenylene diamine functionalization studied using SEM analysis. Fig. 6.8 (a) shows the entangled pristine MWNTs with integrate and smooth sidewalls due to the

ordered graphene fragments of the outer shell. But in Fig. 6.8 (b) the sidewalls of MWNT are observed to be rough and hence indicate the introduction of phenylene diamine groups on the surface of MWNT after functionalization. The presence of amorphous prominences of phenylene diamine in MWNTCONH2 is observed with HRTEM analysis as shown in Fig. 6.9 (b)

6.3.2. Characterization of polyaniline-MWNTCONH2 hybrid

The structure of the hybrid is characterized using FTIR spectrum. As shown in Fig, 6.10, the hybrid P1NH2C2 shows all the characteristic peaks of polyaniline.

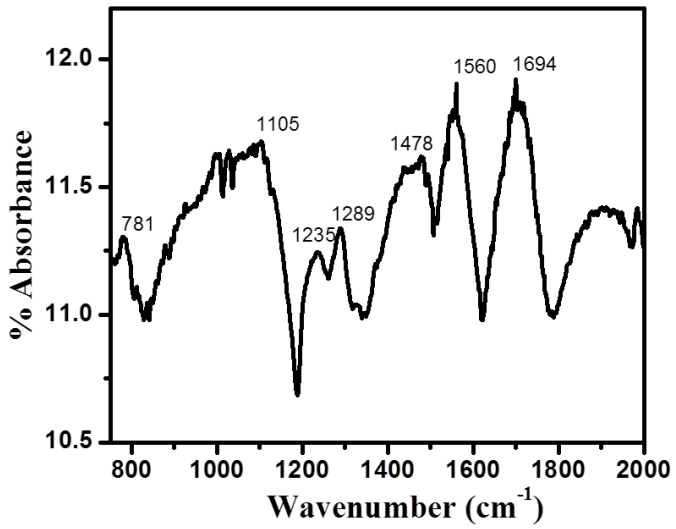

Figure 6.10 FTIR spectrum of the hybrid (P1NH2C2)

The absorption peaks at 1560 and 1478 cm^{-1} are attributed to the C=C stretching vibrations of quinonoid and benzenoid rings respectively. The bands at 1235 and 1289 cm^{-1} indicates polaronic and non-polaronic C-N stretching vibrations respectively. Aromatic C-H in-plane and out-of-plane bending vibrations are observed at 1105 and 781 cm^{-1} respectively. The peak at 1694 cm^{-1} is due to the C=C stretching vibrations of the functionalized MWNT. It is interesting to note that the hybrid exhibits an increased intensity ratio of quinonoid to benzenoid C=C stretching vibrations (I_q/I_b) compared to that of pure polyaniline (Fig. 4.10). These observations reveal that polyaniline in the hybrid is

richer in quinonoid rings than benzenoid rings. This increased intensity ratio compared to the pure polyaniline can be attributed to the site selective interaction between MWNTs and quinonoid rings of polyaniline (Cochet et al., 2001). The percentage of quinonoid ring is a measure of degree of delocalization, and the increase in relative intensity indicates an increase in the effective degree of electron delocalization (Quillard et al., 1994). The site selective interaction of CNT to quinonoid rings may facilitate charge-transfer processes between the two components of the system and thus influence the transport properties of the hybrid system.

Fig.6.11 shows the XRD spectrum of the hybrid P1NH2C2. The characteristic peaks of polyaniline are at 15, 20, and 25^{o} corresponding to the (011), (020), and (200) planes respectively. The intensity of the peak at 25^{o} due to the periodicity perpendicular to polymer chain is increased when compared to polyaniline (Fig. 4.11 (a)) and it is merged with graphitic peaks of MWNTs. But the intensity of the peaks at 15 and 20^{o} is reduced drastically due to the less ordering in the parallel directions of polymer chain due to the better π-π interactions between polyaniline and MWNTs.

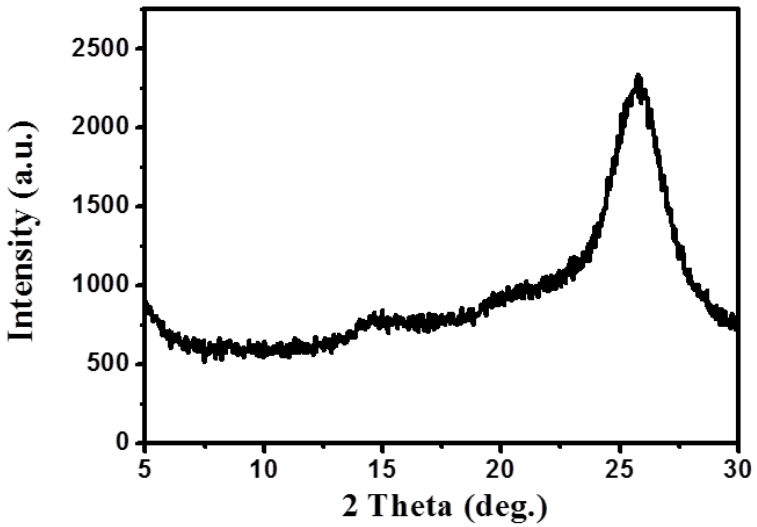

Figure 6.11 XRD spectrum of the hybrid (P1NH2C2)

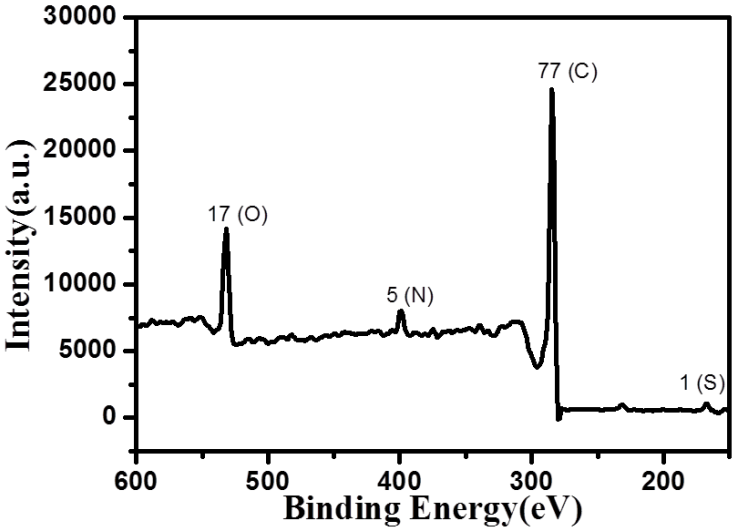

Figure 6.12 XPS spectrum of the hybrid (P1NH2C2)

Elemental composition of the hybrid P1NH2C2 is studied by XPS analysis and the spectrum is given in Fig. 6.12. It shows peaks at 532, 399, 285 and 168 eV corresponding to O1s, N1s, C1s, and S2p respectively. The hybrid shows 17 % oxygen, 5 % nitrogen, 77 % carbon and 1% sulphur.

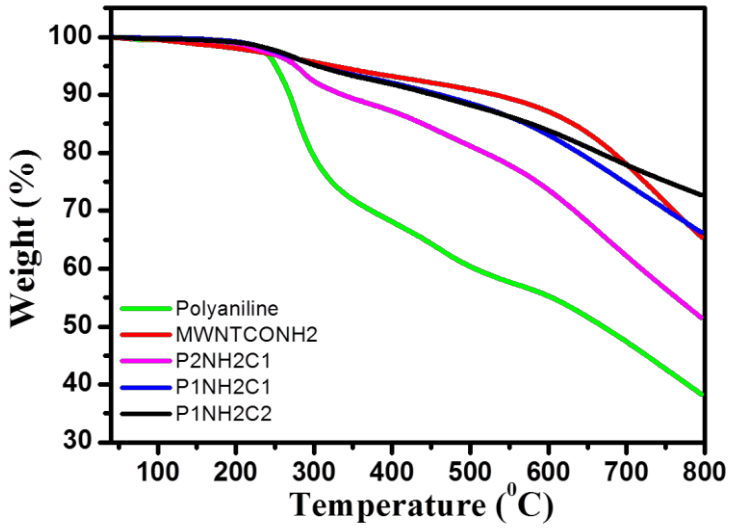

Figure 6.13 TGA patterns of the samples

The decomposition patterns of the samples are recorded by thermo gravimetric analysis as shown in Fig.6.13. In the thermograms of polyaniline and hybrids, first weight loss is observed from 250 ^{o}C, which is attributed to the loss

of dopants from polyaniline and the hybrids. Second weight loss is observed in the temperature range 350-550 ^{o}C and is assumed to be the main chain degradation of polyaniline. The steep decomposition observed after 550 ^{o}C indicates the decomposition of the backbone and ring opening of benzene. Compared to pristine polyaniline, all the hybrids show more residues at 800 ^{o}C.

As shown in Fig. 6.14, Raman spectrum of the hybrid P1NH2C2 exhibits similar pattern of the spectrum of MWNTCONH2 (Fig. 6.7), except the increase in I_G/I_D ratio (0.94). This increased I_G/I_D ratio signifies the reduced defects in the hybrid compared to the functionalized MWNT. Some of the defects are getting repaired during polymerization with aniline and leads to the formation of extended conjugation and larger sp^2 domain.

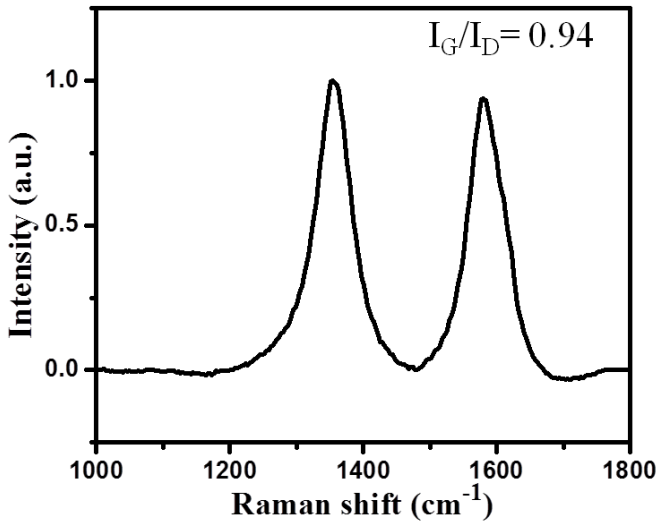

Figure 6.14 Raman spectrum of the hybrid (P1NH2C2)

SEM and TEM images of the hybrid P1NH2C2 is shown in Figs. 6.15 and 6.16 respectively. These images illustrate a uniform coating of polyaniline on MWNT. Individual polyaniline agglomerates are not observed because of the template like action and participation of MWNTCONH2 in the polymerization reaction and core-shell structures of approximately 20 nm diameter are formed. This is in agreement with the previous report showing uniform and complete coating of conducting polymer on CNTs (Konyushenko et al., 2006).

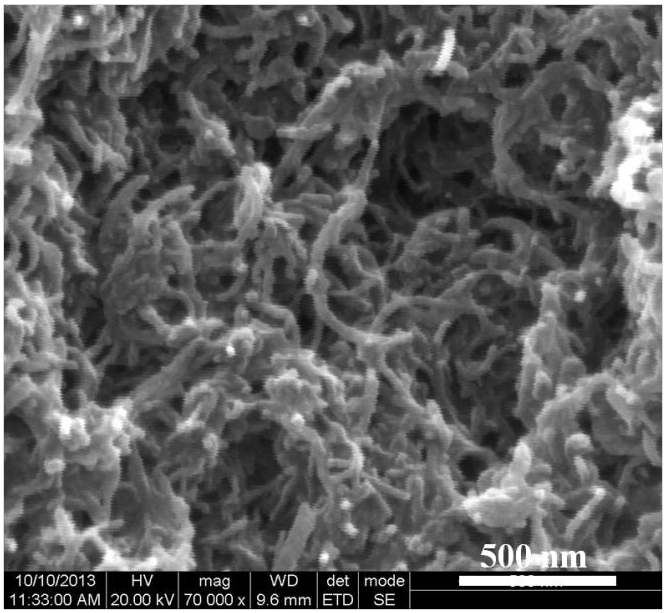

Figure 6.15 SEM image of the hybrid (P1NH2C2) at a magnification of 70000x

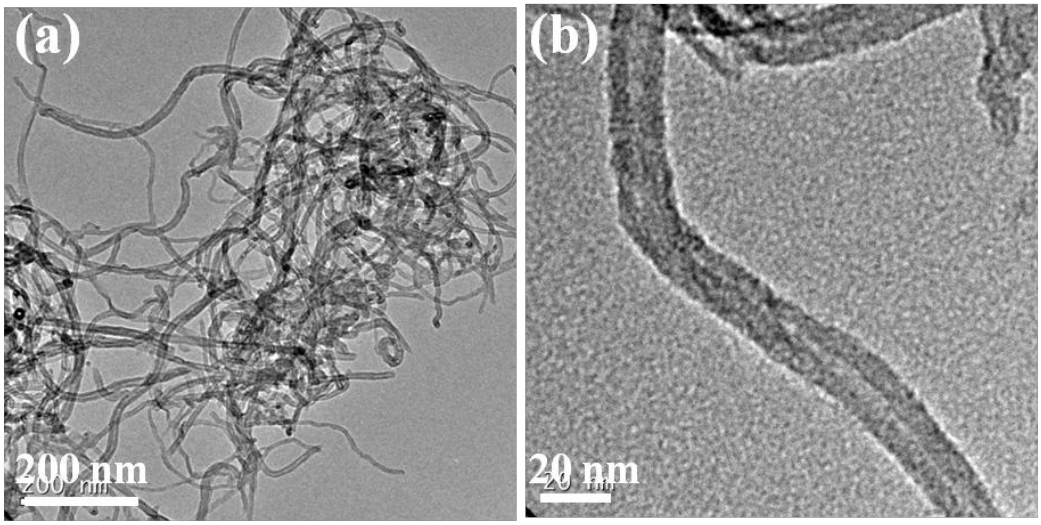

Figure 6.16 TEM images of the hybrid (P1NH2C2)

Fig. 6.17 (a) shows the UV-visible spectra of polyaniline, MWNTCONH2, and the hybrid P1NH2C2 recorded in 2-propanol. The spectrum of MWNTCONH2 shows a peak at 260 nm corresponding to the π-π* transition of C=C bond. The hybrid shows all the three characterestics features of polyaniline; λ_{max} at 338nm, shoulder around 435 nm and a free carrier tail extending to the NIR region corresponding to π-π* and polaron transitions,

respectively. The hybrid also shows peak corresponding to MWNTCONH2 at 260 nm.

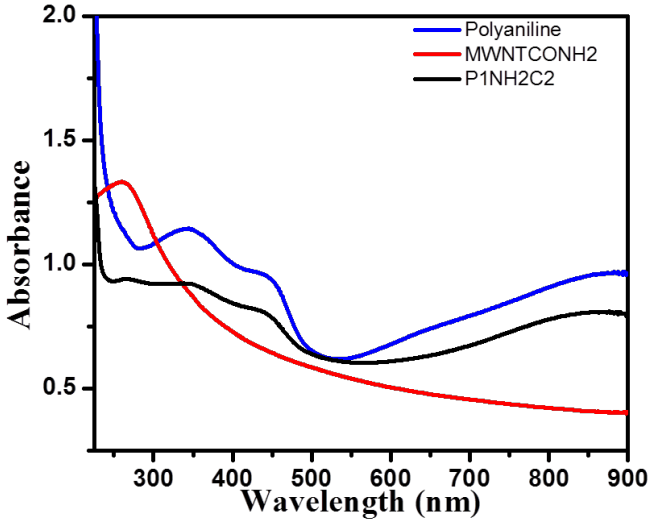

Figure 6.17 UV-visible spectra of polyaniline, MWNTCONH2 and the hybrid

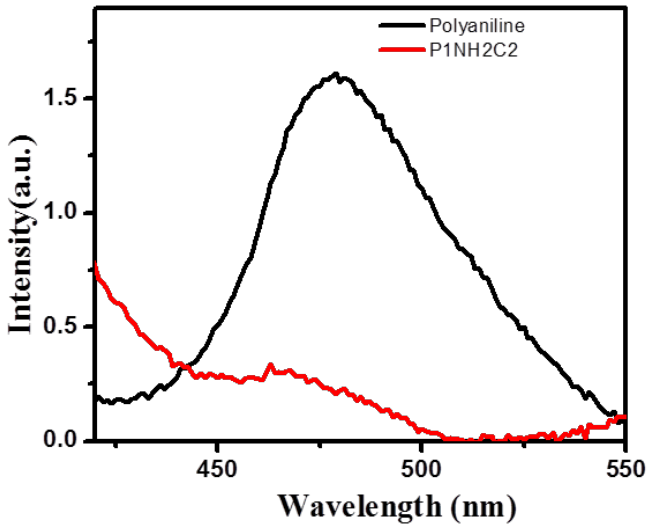

Figure 6.18 Photoluminescence spectra of polyaniline and the hybrid (P1NH2C2)

Fig.6.18 shows the photoluminescence spectra of polyaniline and the hybrid P1NH2C2 in 2-propanol (1 mg in 5 ml) excited at 360 nm. A notable quenching of photoluminescence is observed in the hybrid compared to pure polyaniline. This can be attributed to the photoinduced electron transfer between polyaniline and MWNTCONH2. This electron transfer will produce charge

separated excited state, which can influence the nonlinear optical properties as well as the photocurrent generation. Similar observations are reported in CNT hybrids of phthalocyanines (Ballesteros, et al., 2007; Wang and Blau, 2008), porphyrins (Chitta, et al., 2007; Ní Mhuircheartaigh, et al., 2006), PVK (Li, et al., 2003; Wu, et al., 2003), etc.

6.3.3 Optical limiting properties

The open aperture Z scan plots and optical limiting curves of the hybrid samples at 532 nm, compared with those of pure polyaniline and MWNTCONH2 are depicted in Fig. 6.19.

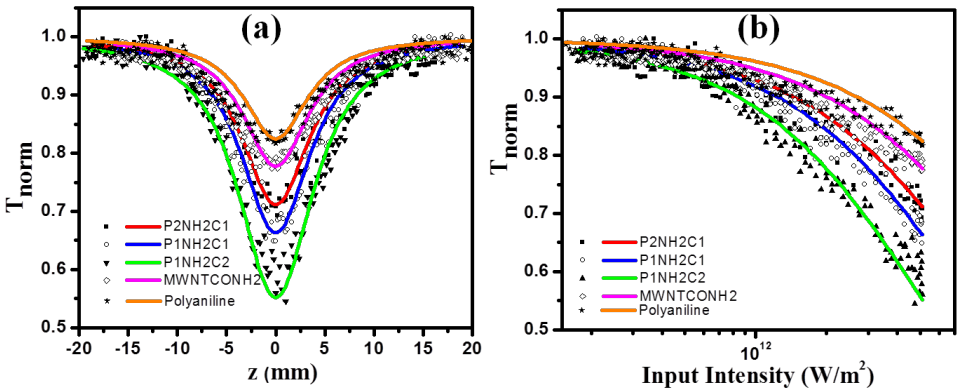

Figure 6.19 (a) Open aperture Z scan plot and (b) optical limiting curves of the samples

For a comparison, the nonlinear absorption coefficient and the saturation intensity of the samples are extracted from the theoretical fit and are listed in Table 6.1. All the samples exhibit a normalized transmittance valley with respect to the sample position. Pure polyaniline shows a β value of 5.8 cm/GW and saturation intensity of 2.5 GW/cm^2, while a remarkable increase in nonlinear absorption coefficient with low saturation intensity is observed in the hybrid samples compared to pure polyaniline and MWNTCONH2. The optical limiting of MWNT arises due to the thermally induced nonlinear scattering. On the other hand, the optical limiting of polyaniline originates from the reverse saturable absorption and two photon absorption. So the enhanced optical limiting of the polyaniline-MWNT hybrids is attributed to the photoinduced electron transfer and

the combination of NLO mechanisms of polyaniline and MWNT facilitated by the direct covalent interactions between polyaniline and MWNTCONH2.

Table 6.1 Nonlinear absorption coefficient (β) and saturation intensity (I_{sat}) of the samples

Sample name	β (cm /GW)	I_{sat} (GW/cm^2)
Polyaniline	5.8	2.5
MWNTCONH2	7.5	3.3
P2NH2C1	11	1.2
P1NH2C1	14.5	0.6
P1NH2C2	23	0.3

6.3.4. DC conductivity and photocurrent generation studies

The electrical conductivities measured by standard four probe method at room temperature of the hybrid samples are listed in Table 6.2.

Table 6.2 DC conductivity of the samples

Sample name	DC conductivity (S/cm)
Polyaniline	2
P2NH2C1	2.1
P1NH2C1	5.1
P1NH2C2	5.9

The phenylene diamine functionalized MWNT is acting as conducting filler and increases the conductivity of the hybrid as the concentration of

MWNTCONH2 increases. Pristine polyaniline shows a DC conductivity of 2 S/cm, whereas the hybrid samples P2NH2C1, P1NH2C1 and P1NH2C2 show conductivities of 2.1, 5.1 and 5.9 S/cm respectively. The direct covalent connection facilitates electron delocalization between polyaniline and MWNT and increases the conductivity.

The photocurrent generated in the samples under white light irradiation is studied as per the experimental set up given in chapter 2 (section 2.3.7). Fig. 6.20 shows the photocurrent cycles of polyaniline and the hybrid P1NH2C2. Pure polyaniline shows a photocurrent of 4.6 µA, where as the hybrid under the same experimental conditions exhibits a photocurrent of 10 µA.

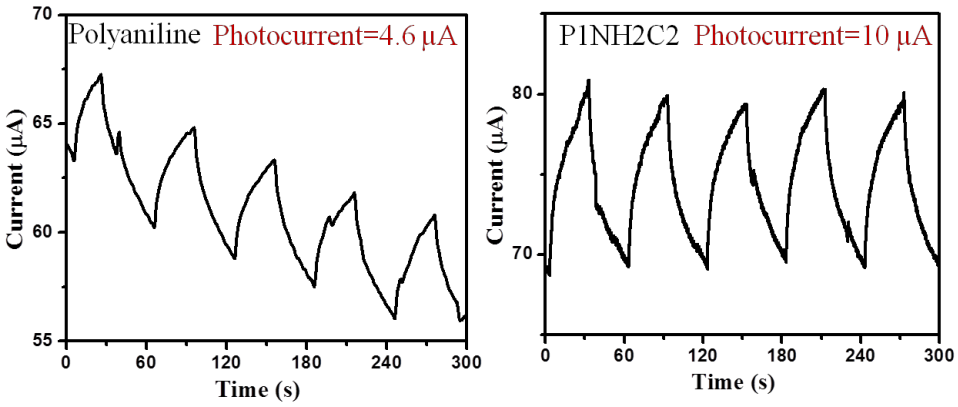

Figure 6.20 Photocurrent cycles of the samples

This improved photocurrent may be due to the better exciton dissociation due to the electron transfer between polyaniline and MWNTCONH2 and the easier transport of carriers to the respective electrodes because of the better conductivity of the hybrid due to the direct covalent connections.

6.4. Conclusions

Multiwalled carbon nanotube is functionalized with phenylene diamine and it is grafted on polyaniline by *in situ* chemical oxidative polymerization. The introduction of phenylene diamine group on MWNT through amide bond is confirmed with FTIR, XPS, SEM and TEM analysis. The hybrids with aniline to

MWNTCONH2 ratios of 2:1, 1:1 and 1:2 are synthesized and characterized in detail. Even though phenylene diamine functionalization introduces surface defects on MWNT, the defects are getting repaired after hybrid formation with polyaniline as evident from the Raman spectra. The hybrid shows significant photoluminescence quenching due to electron transfer between polyaniline and MWNTCONH2, facilitated by the direct covalent connections. The dc-conductivity of the hybrid (5.9 S/cm) is highly improved compared to pure polyaniline (2 S/cm) owing to the covalent interaction between polyaniline and MWNT. The optical limiting behaviour of the hybrid samples is compared with individual components by open aperture Z scan technique. The hybrids exhibit large nonlinear absorption coefficient with low limiting threshold compared to pure polyaniline and is attributed to the combination of NLO mechanisms of polyaniline (two photon absorption and reverse saturable absorption) with the nonlinear scattering of MWNTs. The hybrid shows large and stable photocurrent (10 μA) under white light illumination compared to pure polyaniline (4.6 μA). The photoinduced electron transfer interactions between polyaniline and MWNT also contribute significantly to the improved optical limiting as well as the photocurrent generation. This hybrid system with large optical nonlinearities and very good photocurrent generation is a promising candidate for future electronic and photonic applications.

CHAPTER 7
STUDIES ON CUBE-LIKE POLYANILINE GRAFTED ON REDUCED GRAPHENE OXIDE

This chapter deals with the covalent grafting of synthesized cube-like polyaniline on reduced graphene oxide (rGO) layers through a one step methodology. The detailed characterization of the hybrid, photoluminescence quenching due to the electron transfer between polyaniline and rGO, improved optical limiting behavior, dc-conductivity and photocurrent generation in the hybrid compared to cube-like polyaniline, are also discussed.

7.1. Introduction

The synthesis, characterization, improved nonlinear optical properties and photocurrent generation of two different classes of polyaniline-graphene hybrids were discussed in Chapters 4 and 5. The covalent interaction between polyaniline and graphene materials were found to increase the photoinduced electron transfer thereby improving the optical limiting behaviour and photocurrent generation, compared to individual components and hybrids with noncovalent interactions. An et al. (2012) grafted synthesized polyaniline nanofibers to GO sheets for supercapacitor applications through amide linkages. They observed that grafting of synthesized polyaniline nanofibers on GO produces higher specific capacitance compared to similar material synthesized by the *in situ* chemical oxidative grafting of polyaniline on reduced graphene oxide reported by Kumar et al. (2012). The electron densities of the polyaniline-graphene hybrid were computed by first-principle calculations and clarified the key role of amide group in the formation of π-conjugated structure.

In Chapter 3, we discussed the synthesis of easily processable cube-like polyaniline by inverse microemulsion polymerization technique. This synthesized cube-like polyaniline is grafted on reduced graphene oxide layers through the formation of amide bonds. Initially, carboxylic acid groups in GO is converted

into acid chlorides by the reaction with $SOCl_2$. This acyl chloride is then reacted with dedoped cube-like polyaniline to form amide groups between polyaniline and reduced graphene oxide. The hybrid (polyaniline-g-rGO) shows improved optical limiting behaviour compared to pure polyaniline. To explore and compare the optical limiting applications of this material with pure cube-like polyaniline, thin films in PMMA host are fabricated at the same linear transmittance of the cube-like polyaniline-PMMA film with highest polyaniline loading (chapter 3). The film showed large improvement in optical limiting behaviour compared to cube-like polyaniline at 45 μJ. The hybrid material also exhibit significant improvement in dc-conductivity and photocurrent generation.

7.2. Experimental

7.2.1. Dedoping of cube-like polyaniline

The cube like polyaniline (100 mg) is treated with NH_4OH (1M, 50 ml) and stirred at room temperature for 24 h to get dedoped polyaniline. The reaction mixture is filtered, washed with distilled water till neutral pH, and dried under vacuum at 80 ^oC for 12 h.

7.2.2. Grafting of cube-like polyaniline on reduced graphene oxide

The grafting of cube-like polyaniline is schematically represented in Fig. 7.1. GO (500 mg) is synthesized by low temperature modified Hummers method as described in section 4.2.1. The GO powder is then dispersed in catalytic amount of dry DMF and excess amount of freshly distilled $SOCl_2$ under nitrogen atmosphere and refluxed at 80 ^oC for 24 h. After the conversion of carboxylic acid groups to acid chlorides, the excess $SOCl_2$ is removed by reduced pressure distillation. The dedoped cube-like polyaniline (500 mg) is dispersed in excess dry DMF and refluxed with acylated GO at 120 ^oC for 72 h under inert atmosphere. The obtained mixture is filtered using Millipore 0.45 μm filter, washed with DMF, distilled water and methanol, and dried under vacuum at 80 ^oC for 24 h.

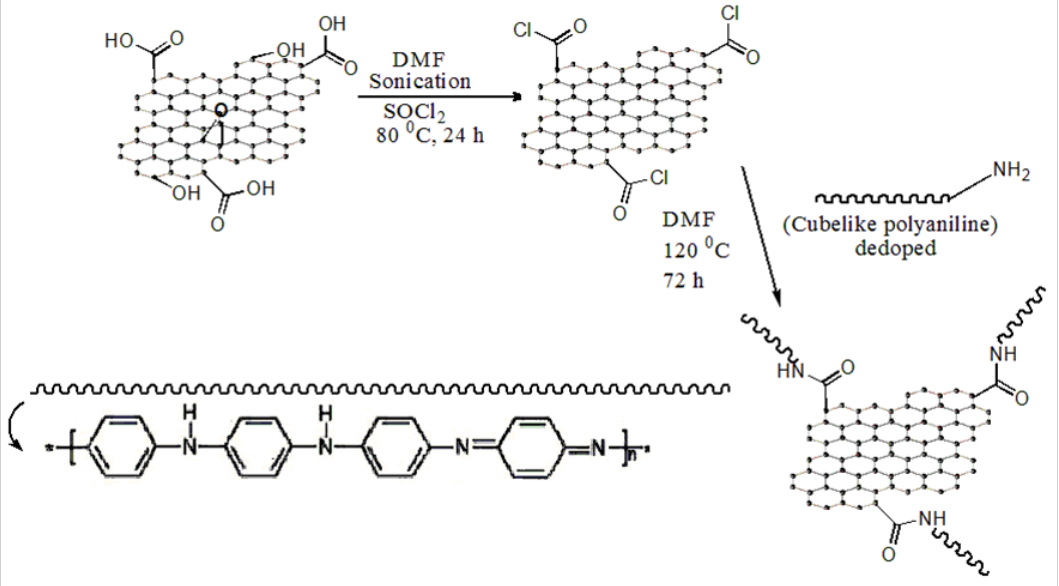

Figure 7.1 Scheme of the covalent grafting of cube-like polyaniline on reduced graphene oxide

7.3. Results and Discussion

7.3.1. Characterization of the hybrid

The structure of the hybrid is characterized using FTIR spectrum as shown in Fig. 7.2.

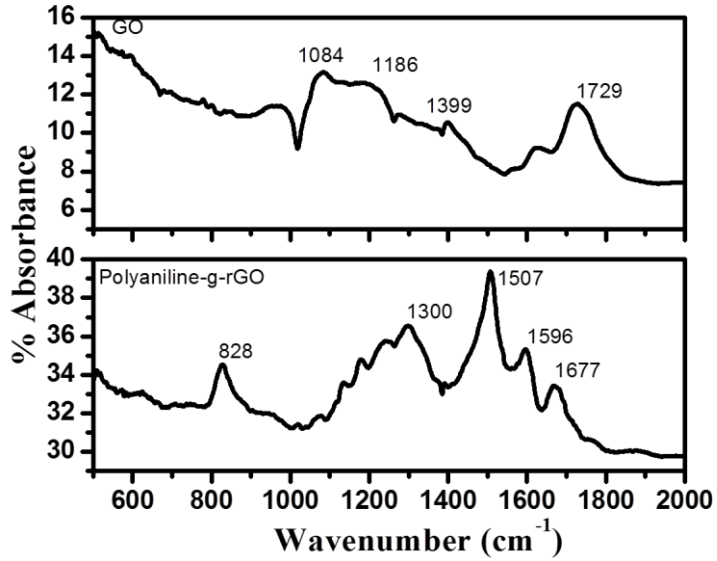

Figure 7.2 FTIR spectra of GO and the hybrid

The hybrid shows characteristic amide C=O stretching vibrations at 1677 cm^{-1}. C=O stretching vibration of GO at 1729 cm^{-1} is shifted to 1677 cm^{-1} due to the formation of amide linkages between polyaniline and GO. In addition to this, hybrid shows characteristic peaks of polyaniline. The peak at 1596 and 1507 cm^{-1} is due to the C=C stretching vibrations of the quinonoid and benzenoid rings respectively. The peaks at 1300 and 828 cm^{-1} are attributed to C-N stretching and out-of-plane bending vibrations of polyaniline respectively.

Fig. 7.3 shows the XRD spectra of GO and hybrid. After the anchoring of polyaniline, the peak at $2\theta=10.3^{o}$ in GO disappears and a new broad peak appears at $2\theta=25^{o}$, suggesting that a significant portion of GO is reduced and exfoliated during covalent grafting. Broadening of the peak indicates the poor ordering in the stacking direction, hence suggesting destacking of the graphene sheets in GO after polyaniline grafting.

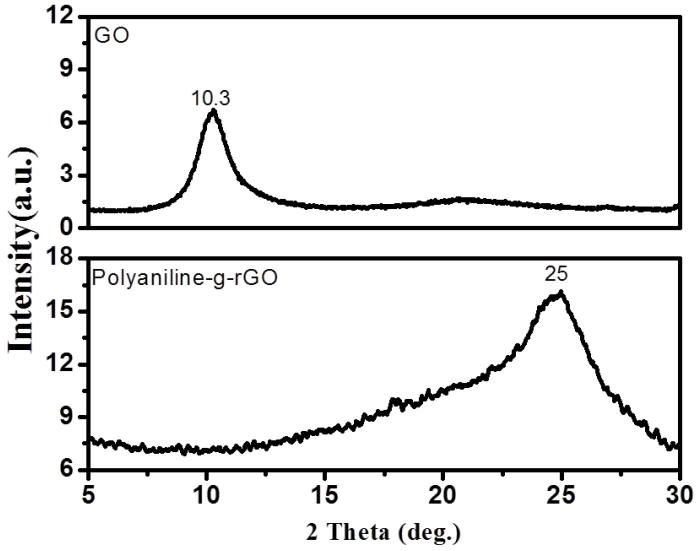

Figure 7.3 XRD spectra of GO and the hybrid

The decomposition pattern of GO and the hybrid measured using TGA is shown in Fig. 7.4. As evident from the spectrum, GO loses 42% of its weight from 150 to 200 ^{o}C, whereas the hybrid starts considerable weight loss only after 250 ^{o}C indicating removal of most of the oxygen containing groups during grafting of polyaniline.

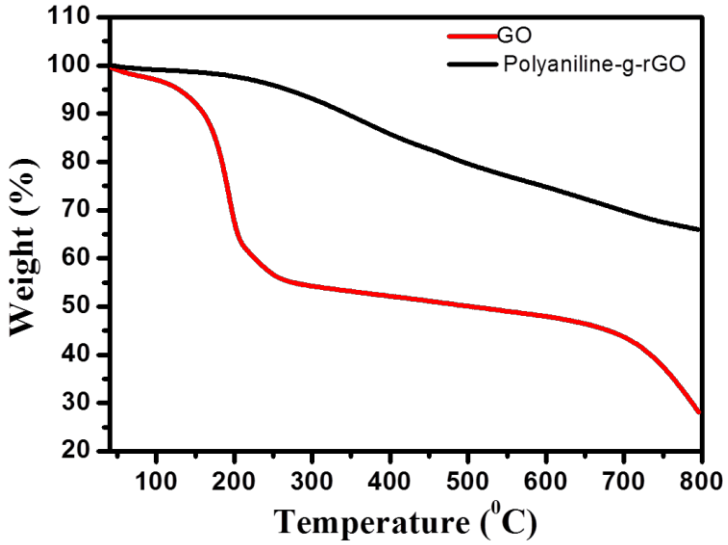

Figure 7.4 TGA pattern of GO and the hybrid

Fig. 7.5 shows the XPS spectra of the GO and the hybrid. As prepared GO shows the presence of 47% oxygen and 53% carbon content. When it is grafted with polyaniline, the oxygen content reduces drastically to 4% and the carbon content increases to 86%. Also a new peak corresponding to N 1s appears due to the anchoring of polyaniline on reduced graphene oxide layers. Drastic lowering of oxygen species and increased carbon content indicates the significant reduction of GO during grafting of polyaniline.

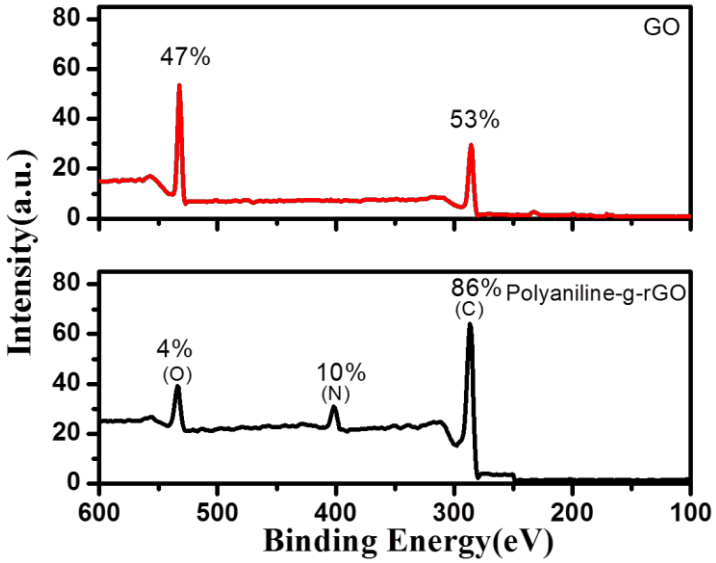

Figure 7.5 XPS spectra of GO and the hybrid

As shown Fig. 7.6, the Raman spectrum of the hybrid shows characteristic G and D bands at 1577 and 1363 cm^{-1} respectively. The I_G/I_D ratio is found to be 1.08, which is higher than that of GO (0.91). This indicates the restoration of sp^2 domains due to the reduction of GO after grafting with polyaniline.

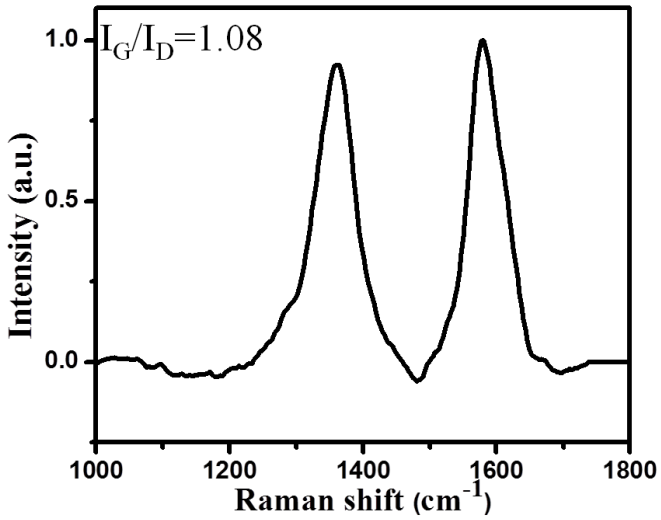

Figure 7.6 Raman spectrum of the hybrid

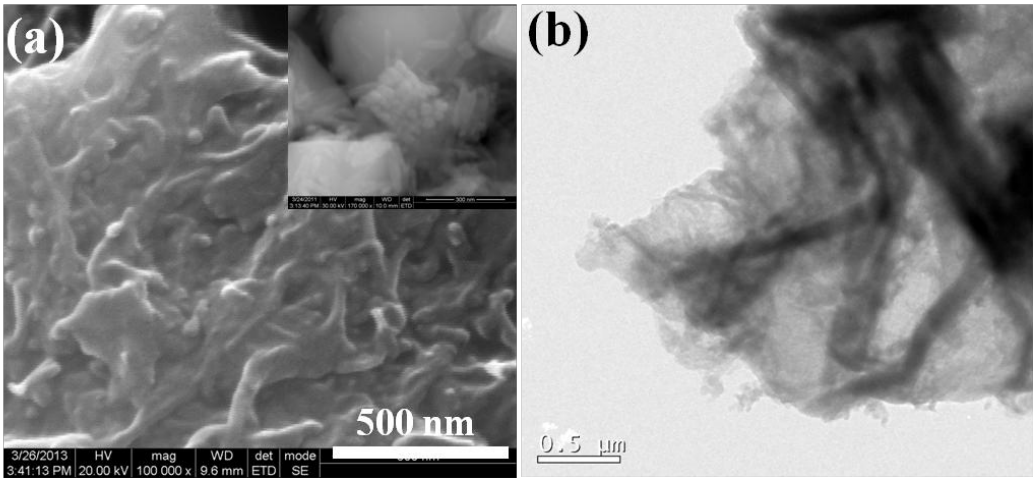

Figure 7.7 (a) SEM image and (b) TEM image of the hybrid. Inset shows SEM image of the cube-like polyaniline. Magnification of SEM image in (a) is 100000x

As shown in Fig. 7.7, SEM and TEM images of the hybrid indicate that the layered morphology of GO is disturbed after grafting of polyaniline. This

gives further evidence for the exfoliation of graphene sheets during grafting of the polyaniline. Moreover the introduction of graphene layers disrupts the π-π stacking and H-bonding interactions between polyaniline nanorods and the self assembly is disturbed.

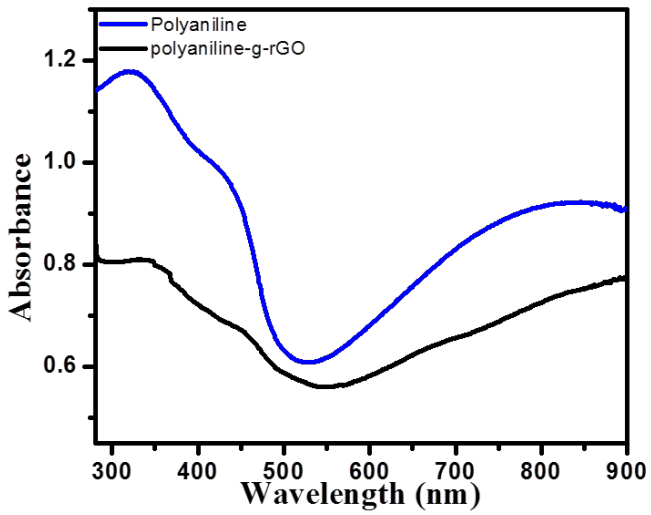

Figure 7.8 UV-visible spectra of polyaniline and the hybrid

The UV-visible spectra of cube-like polyaniline and the hybrid doped with toluene sulphonic acid is recorded in 2-propanol and it is shown in Fig. 7.8 (a). Polyaniline shows λ_{max} at 325 nm, a shoulder around 435 nm and a free carrier tail extending to NIR region corresponding to π-π* and polaron transitions respectively. The hybrid also shows the characteristic peaks of polyaniline.

Photoluminescence spectra of polyaniline and the hybrid dispersed in 2-propanol (1mg in 5 ml) excited at 360 nm is shown in Fig. 7.9. Polyaniline shows a broad emission centered at 480 nm. The hybrid shows photoluminescence quenching compared to pure polyaniline may be due to the efficient electron transfer from polyaniline to reduced graphene oxide sheets facilitated by the amide linkages.

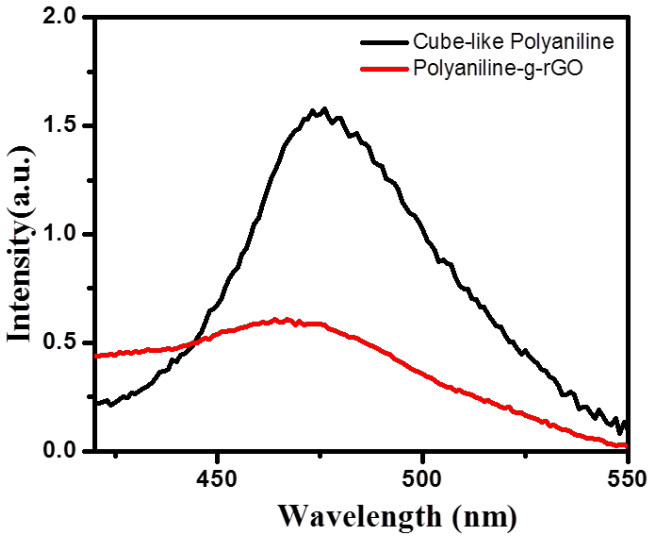

Figure 7.9 Photoluminescence spectra of cube-like polyaniline and the hybrid

7.3.2 Optical limiting properties

Open aperture Z scan technique as described in chapter 2 is employed to measure the nonlinear optical properties of the samples in DMF with 75% linear transmittance. Laser energy used is 25 μJ. The Z scan plots given in Fig. 7.10 (a) show normalized transmittance valley indicating optical limiting behaviour. Input intensity versus normalized transmittance graph is also drawn to study the optical limiting behaviour and is given in Fig.7.10 (b).

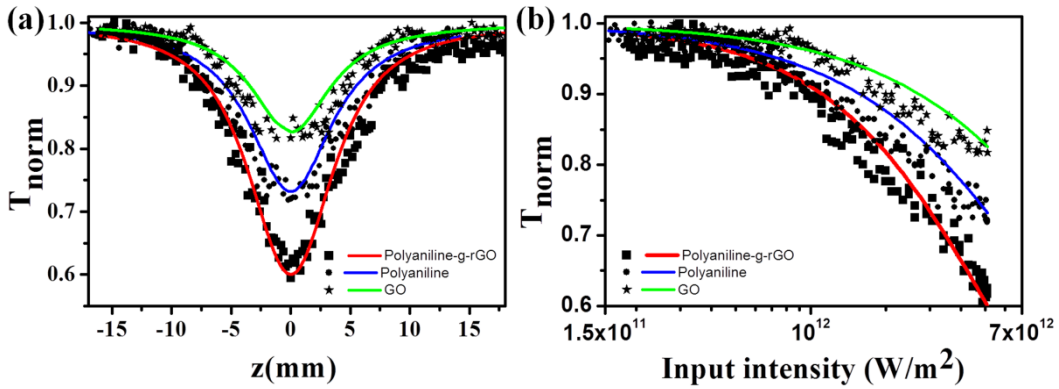

Figure 7.10 (a) Open aperture Z scan plot and (b) optical limiting curves of the samples

The experimental data is fitted with two photon absorption theoretical plot and the nonlinear optical parameters like nonlinear absorption coefficient and

saturation intensity are extracted from the theoretical fit. The details are listed in Table 7.1.

Table 7.1 Nonlinear absorption coefficient (β) and saturation intensity (I_{sat}) of the samples

Sample name	β (cm/GW)	I_{sat} (GW/cm^2)
Cube-like Polyaniline	5.5	3.5
GO	9.5	2
Polyaniline-g-rGO	20	0.25

There is a significant increase in β value, when polyanline is grafted to reduced graphene oxide as compared to individual counterparts due to the combination of the NLO mechanisms of both polyaniline and GO, namely reverse saturable absorption, two photon absorption and nonlinear scattering. Excited state absorption and nonlinear scattering are the dominant NLO mechanisms of graphene while RSA and 2PA is the dominant mechanism of polyaniline. During grafting, the oxygen functionalities are removed significantly and crystalline defects diminish which increases the conjugation network. So the resultant hybrid structure will transfer crystal lattice vibrations more rapidly and leads to enhanced optical limiting effect (Zhao et al., 2013). Low limiting threshold is one of the desirable attributes of a good optical limiter and the limiting threshold is significantly decreased when polyaniline is grafted to reduced graphene oxide (Remyamol et al., 2013).

In order to study the optical limiting behaviour in the film form, thin films of the hybrid in transparent PMMA matrix is fabricated as per the procedure given in section 3.2.2. The hybrid concentration is selected in such a way to get the same linear transmittance of the cube-like polyaniline-PMMA film with

highest polyaniline loading. Fig. 7.11 shows the open aperture Z-can plots of polyaniline-g-rGO-PMMA film at different laser pulse energies.

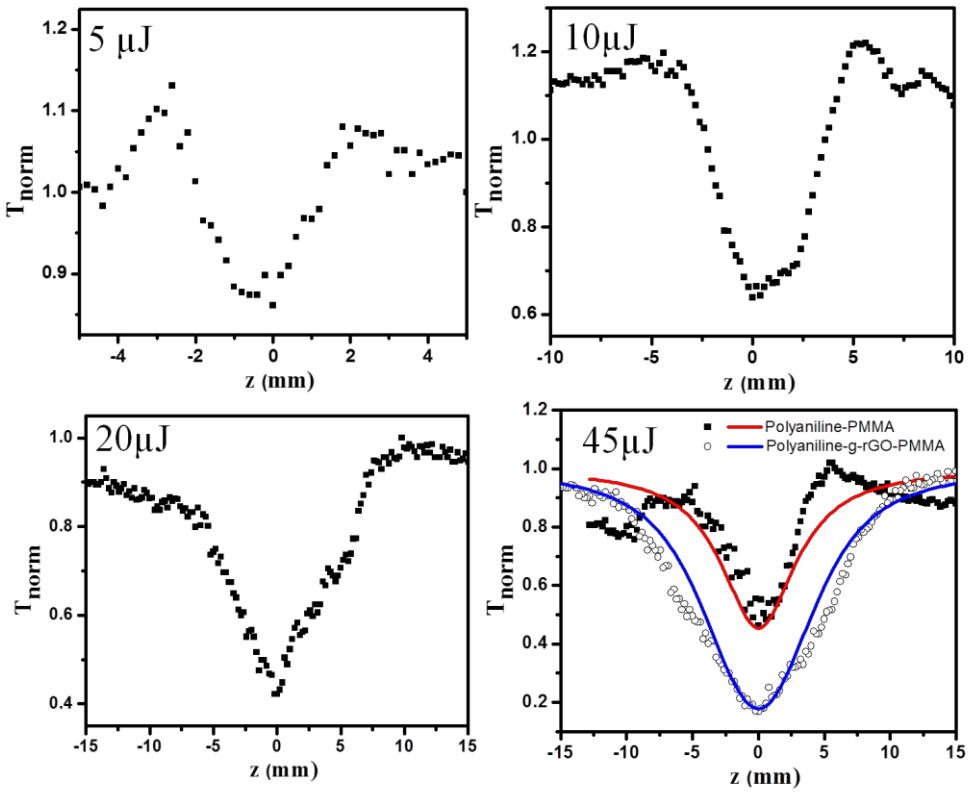

Figure 7.11 Open aperture Z scan plot of polyaniline-g-rGO-PMMA film at different energies

At 5 µJ laser energy of, the film shows a transmittance valley with two humps. The valley corresponds to reverse saturable absorption and the humps indicate saturable absorption. Unlike the cube-like polyaniline-PMMA film, which shows only saturable absorption at 5 µJ (Fig. 3.21), this hybrid film shows significant contribution of reverse saturation absorption at low laser energy of 5 µJ. In Fig.7.11, the open aperture Z scan plots of cube-like polyaniline-PMMA film and the hybrid-PMMA film is compared at the laser energy of 45 µJ. The nonlinear optical parameters are extracted from the theoretical fit. The hybrid-PMMA film shows high nonlinear absorption coefficient (320 cm/GW) and low saturation intensity (0.2 GW/cm^2) compared to that of cube-like polyaniline-PMMA film (β=70 cm/GW, I_{sat}=3 GW/cm^2). So this hybrid film with high

nonlinear absorption coefficient and low limiting threshold can be used as potential optical limiting material.

7.3.3. DC conductivity and photocurrent generation studies

The electrical conductivities of circular pellets of cube-like polyaniline and the hybrid is measured using standard four probe method. Before the electrical conductivity measurement, the hybrid is redoped with toluene sulphonic acid. The cube-like polyaniline shows dc conductivity of 1.9 S/cm, while the hybrid shows conductivity of 6.6 S/cm. This increased conductivity may be attributed to the covalent connection between polyaniline and reduced graphene oxide.

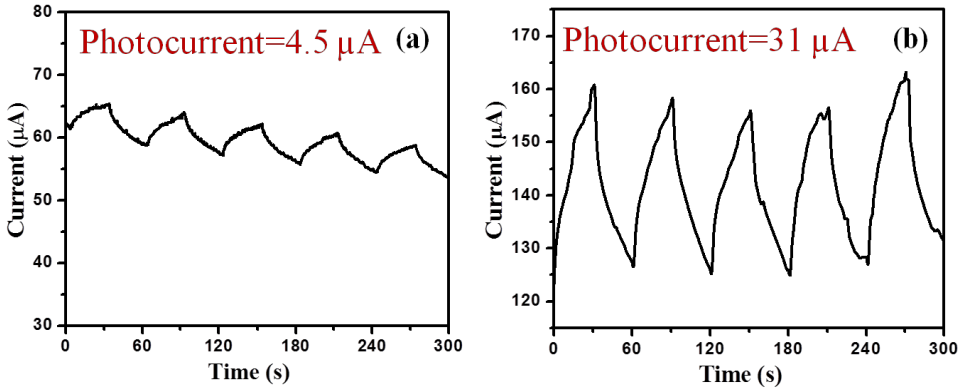

Figure 7.12 Photocurrent cycles of (a) cube-like polyaniline and (b) polyaniline-g-rGO

Fig. 7.12 shows the photocurrent cycles of cube-like polyaniline and the hybrid. The films for the measurements are prepared as discussed in section 2.2.2 and the measurement details are described in the section 2.3.7. As clear from the figure, the polyaniline grafted reduced graphene oxide hybrid shows large increase in photocurrent compared to pure cube-like polyaniline. The hybrid shows photocurrent of 31 µA, whereas pure polyaniline shows only a photocurrent of 4.5 µA. This increased photocurrent generation of the hybrid is due to the efficient exciton dissociation at the interface (Liu Z. et al., 2008) between polyaniline and reduced graphene oxide and the photoinduced electron

transfer from polyaniline to reduced graphene oxide, facilitated by the covalent connections.

7.4. Conclusions

The synthesized processable cube-like polyaniline is covalently grafted on reduced graphene oxide through the formation of amide linkages between acylated graphite oxide and polyaniline. The amide bond formation is confirmed using FTIR and XPS analysis. The reduction and exfoliation of GO during the grafting of polyaniline is proved using spectroscopic and microscopic analysis. The hybrid shows significant photoluminescence quenching due to the photoinduced electron transfer from polyaniline to reduced graphene oxide layers. Significant improvement in nonlinear absorption coefficient (20 cm/GW) and low limiting threshold (0.25 GW/cm^2) is achieved by covalent grafting of the polyaniline on reduced graphene oxide compared to the individual components. The photoinduced electron transfer interactions and the synergetic combination of NLO mechanisms of polyaniline and reduced graphene oxide by covalent connections are attributed to the enhanced optical limiting behaviour of the hybrid. The hybrid film in PMMA matrix shows significant contribution of reverse saturable absorption at lower laser energy 5 μJ, whereas cube-like polyaniline-PMMA film shows only saturable absorption at the same laser energy. The hybrid film shows large improvement in optical limiting behaviour (β=320 cm/GW, I_{sat}=0.2 GW/cm^2) compared to the cube-like polyaniline-PMMA film (β=70 cm/GW, I_{sat}=3 GW/cm^2) at laser pulse energy of 45 μJ, hence a promising candidate for optical limiting applications. Moreover, the polyaniline-reduced graphene oxide hybrid shows large increase in dc conductivity (6.6 S/cm) and photocurrent generation (31 μA) compared to pure cube-like polyaniline (1.9 S/cm, 4.5 μA). So this hybrid can be a versatile material for optical and optoelectronic applications.

CHAPTER 8
CONCLUSIONS

This thesis explores the synthesis of nano cube-like polyaniline and its hybrids with graphene and multiwalled carbon nanotube as well as their optical limiting and photocurrent generation properties. The main contributions of this thesis are (1) synthesis and characterization of cube-like nano polyaniline by a novel inverse microemulsion route (2) synthesis and characterization of polyaniline/graphene and polyaniline/MWNT hybrids through *in situ* polymerization technique and covalent grafting technique (3) fabrication of cube-like polyaniline and its graphene hybrid in transparent polymer matrix and (4) optical limiting and photocurrent generation studies in all the materials synthesized and fabricated.

An overall review on polyaniline, graphene, carbon nanotubes, hybrid materials, etc. is given in chapter 1. Structural properties and important applications, mainly optical limiting and photocurrent generation are also elaborated in this chapter. The materials used and experimental methods adopted for the thesis work is included in chapter 2 along with an overall idea about the principle and working of various characterization tools.

In chapter 3, the synthesis of easily processable cube-like nanostructures of polyaniline by a novel inverse microemulsion polymerization technique using ammonium oleate as the surfactant and toluene sulphonic acid as the dopant is described. The cube-like polyaniline is characterized using FTIR, XRD, XPS, TGA, UV-visible absorption spectrum, photoluminescence spectrum, SEM and TEM. The mechanism for the formation of novel cube-like polyaniline nanostructures by the self assembly of nanorods inside inverse micelles of ammonium oleate is proposed based on experimental evidences. Open aperture Z scan studies of the synthesized polyaniline in DMF show suitability of the material for optical limiting applications. Various films of cube-like polyaniline in transparent PMMA matrix are fabricated by *in situ* free radical polymerization

of methyl methacryate in the presence of weighed amount of synthesized polyaniline. The nonlinear absorption coefficient of the film increases with decrease of saturation intensity as the percentage of polyaniline in the film increases. The film with highest polyaniline loading (0.1 wt% with respect to monomer) is selected as a representative sample for energy dependant nonlinear optical studies. It shows a switchover from saturable absorption to reverse saturable absorption as the energy of the laser beam increases. At lower laser energy of 5 μJ, the film shows pure saturable absorption and at higher laser energy of 100 μJ, it shows pure reverse saturable absorption and strong optical limiting. The photocurrent generation by cube-like polyaniline is studied using Autolab electrochemical work station in a conventional three electrode electrochemical cell. Photocurrent growth and decay are recorded by repetitive switching (on/off) of the white light illumination (intensity 100 mW/cm^2) for 30 second duration. The photocurrent is calculated from the difference between current generated after illumination of the film for 30 seconds and the dark current. The cube-like polyaniline shows an average photocurrent of 4.5 μA.

In order to improve the optical limiting properties and photocurrent generation in polyaniline, hybrids with graphene and CNT are studied. First attempt is the synthesis of polyaniline-graphite oxide hybrid with non covalent interactions which is discussed in chapter 4. GO is synthesized by modified Hummers method (commonly used $NaNO_3$ is avoided and carried out the reaction at low temperature) and it is characterized in detail by spectroscopic, thermal and microscopic techniques. Hybrids are synthesized by simple *in situ* polymerization of aniline in the presence of weighed amount of synthesized GO. The aniline to GO ratio is selected as 4:1, 2:1, 1:1, and 1:2 and the samples are named as P4G1, P2G1, P1G1 and P1G2, respectively. Both optical limiting behaviour and photocurrent generation increases with increase in GO loading. The hybrid P1G2 is the best optical limiter (β=19 cm/GW, I_{sat}=0.4 GW/cm^2) among this class of hybrids and the same sample shows the highest photocurrent (9.1 μA). The considerable photoluminescence quenching of the hybrid indicates the photoinduced electron transfer between polyaniline and GO. The improved optical

limiting behaviour is due the synergetic combination of NLO mechanisms of polyaniline and GO, and light induced electron transfer within the hybrid. The efficient dissociation of excitons at the interface between polyaniline and GO and the photoinduced electron transfer to GO before recombination of the dissociated carriers are contributing to the increased photocurrent of the hybrid compared to pure polyaniline.

In order to further improve the interaction between polyaniline and graphene material, polyaniline is connected covalently with graphene. Phenylene diamine functionalized reduced graphene oxide (GONH2) is designed and synthesized so that simple *in situ* polymerization of aniline in the presence of GONH2 can form covalent bonds between polyaniline and reduced graphene oxide. The synthesis and characterization of GONH2 and the hybrids of polyaniline with GONH2 are discussed in chapter 5. Phenylene diamine functionalization leads to significant reduction and exfoliation of GO along with the introduction of aniline monomer on reduced graphene oxide layers. The polymerization of aniline along with GONH2 produces hybrids with covalent connections. The photoluminescence quenching is more significant in these hybrids compared to polyaniline-unfunctionalized GO hybrids. This class of hybrids show better optical limiting behaviour (β=25 cm/GW, I_{sat}=0.2 GW/cm^2), increased dc conductivity (6.3 S/cm), and photocurrent generation (29 μA) compared to pure polyaniline as well as the unfunctionalized GO-polyaniline hybrids. Considerable photoinduced electron transfer from polyaniline to GONH2 plays a major role in improving the nonlinear optical properties and photocurrent generation. Considerable reduction and exfoliation of GO after phenylene diamine grafting and the covalent bonds between polyaniline and GONH2 are responsible for the increased electrical conductivity in this hybrid.

Polyaniline-MWNT hybrids with covalent connections are also synthesized by the *in situ* polymerization of aniline in the presence of phenylene diamine functionalized MWNT and it is discussed in chapter 6. The photoluminescence quenching in the hybrid due to the electron transfer between

polyaniline and MWNT and the resulting improvement in optical limiting and photocurrent generation are also discussed in chapter 6.

Finally the synthesized cube-like polyaniline is directly grafted on reduced graphene oxide layers through the formation of amide linkages between acylated graphite oxide and polyaniline. During grafting, considerable reduction and exfoliation of graphite is achieved and it is proved using spectroscopic and microscopic techniques. The cube-like polyaniline grafted reduced graphene oxide hybrid shows photoluminescence quenching compared to pristine cube-like polyaniline. Significant improvement in optical limiting behaviour (β=20 cm/GW, I_{sat}=0.25 GW/cm^2) , dc conductivity (6.6 S/cm) and photocurrent generation (31 μA) are achieved after covalent grafting of polyaniline on reduced graphene oxide layers compared to pristine cube-like polyaniline. This is due to the synergetic combination of polyaniline and reduced graphene oxide through direct covalent connections and the significant photoinduced electron transfer interactions between polyaniline and reduced graphene oxide. Film of the hybrid in PMMA matrix is fabricated for nonlinear optical studies. Compared to cube-like polyaniline-PMMA film, the hybrid-PMMA film shows significant contribution of reverse saturable absorption at lower laser energy of 5μJ. The hybrid film shows large improvement in optical limiting behaviour (β=320 cm/GW, I_{sat}=0.2 GW/cm^2) compared to the cube-like polyaniline-PMMA film (β=70 cm/GW, I_{sat}=3 GW/cm^2) at laser pulse energy of 45 μJ, hence a promising candidate for optical limiting applications.

FUTURE OUTLOOK

The hybrids of polyaniline with graphene and MWNT with covalent connections show good potential for optical limiting and photocurrent generation applications. Freestanding and flexible films of the hybrid materials in PMMA matrix without compromising on the nonlinear optical properties and transparency can be easily achieved by simple *in situ* polymerization of methyl methacrylate in the presence of the NLO active materials, hence the practical optical limiting device fabrication using these hybrid materials can be thought of. Moreover, these

hybrid materials show excellent conductivity and photocurrent generation, hence an ideal material for organic solar cell applications. The photocurrent generation of these hybrid materials can also be utilized for photo detector applications.

REFERENCES

1. Admassie, S., Zhang, F., Manoj, A. G., Svensson, M., Andersson, M. R., and Inganäs, O. (2006). A polymer photodiode using vapour-phase polymerized PEDOT as an anode. *Solar Energy Materials and Solar Cells*, 90(2): 133-141.

2. Ago, H., Petritsch, K., Shaffer, M. S. P., Windle, A. H., and Friend, R. H. (1999). Composites of Carbon Nanotubes and Conjugated Polymers for Photovoltaic Devices. *Advanced Materials*, 11(15): 1281-1285.

3. Akhtar, M., Weakliem, H. A., Paiste, R. M., and Gaughan, K. (1988). Polyaniline thin film electrochromic devices. *Synthetic Metals*, 26 (3): 203-208.

4. Ali, S. R., Ma, Y., Parajuli, R. R., Balogun, Y., Lai, W. Y. C., and He, H. (2007). A Nonoxidative Sensor Based on a Self-Doped Polyaniline/Carbon Nanotube Composite for Sensitive and Selective Detection of the Neurotransmitter Dopamine. *Analytical Chemistry, 79*(6): 2583-2587.

5. Alvi, F., Ram, M. K., Basnayaka, P. A., Stefanakos, E., Goswami, Y., and Kumar, A. (2011). Graphene–polyethylenedioxythiophene conducting polymer nanocomposite based supercapacitor. *Electrochimica Acta, 56*(25): 9406-9412.

6. Ameen, S., Akhtar, M. S., and Shin, H. S. (2012). Hydrazine chemical sensing by modified electrode based on in situ electrochemically synthesized polyaniline/graphene composite thin film. *Sensors and Actuators B: Chemical, 173*: 177-183.

7. An, J., Liu, J., Zhou, Y., Zhao, H., Ma, Y., Li, M., et al. (2012). Polyaniline-Grafted Graphene Hybrid with Amide Groups and Its Use in Supercapacitors. *The Journal of Physical Chemistry C, 116*(37): 19699-19708.

8. An, X., Simmons, T., Shah, R., Wolfe, C., Lewis, K. M., Washington, M., et al. (2010). Stable Aqueous Dispersions of Noncovalently Functionalized Graphene from Graphite and their Multifunctional High-Performance Applications. *Nano Letters, 10*(11): 4295-4301.

9. Anglaret, E., Riehl, D., Hache, F., and Vivien, L. (2000). Nonlinear scattering origin in carbon nanotube suspensions. *Journal of Nonlinear Optical Physics & Materials,* 09(03): 297-307.

10. Ansari, M. O., Khan, M. M., Ansari, S. A., Amal, I., Lee, J., and Cho, M. H. (2014). Enhanced thermoelectric performance and ammonia sensing properties of sulfonated polyaniline/graphene thin films. *Materials Letters, 114*: 159-162.

11. Bai, H., Xu, Y., Zhao, L., Li, C., and Shi, G. (2009). Non-covalent functionalization of graphene sheets by sulfonated polyaniline. *Chemical Communications* (13): 1667-1669.

12. Balapanuru, J., Yang, J.-X., Xiao, S., Bao, Q., Jahan, M., Polavarapu, L., Wei, J., Xu, Q.-H., and Loh, K. P. (2010). A Graphene Oxide–Organic Dye Ionic Complex with DNA-Sensing and Optical-Limiting Properties. *Angewandte Chemie International Edition*, 122(37): 6699-6703.

13. Ballesteros, B., de la Torre, G., Ehli, C., Aminur Rahman, G. M., Agulló-Rueda, F., Guldi, D. M., and Torres, T. (2007). Single-Wall Carbon Nanotubes Bearing Covalently Linked Phthalocyanines-Photoinduced Electron Transfer. *Journal of the American Chemical Society, 129*(16): 5061-5068.

14. Band, Y. B., Harter, D. J., and Bavli, R. (1986). Optical pulse compressor composed of saturable and reverse saturable absorbers. *Chemical Physics Letters*, 126(3–4): 280-284.

15. Berger, C., Song, Z., Li, X., Wu, X., Brown, N., Naud, C., Mayou, D., Li, T., Hass, J., Marchenkov, A. N., Conrad, E. H., First, P. N., and de Heer, W. A. (2006). Electronic Confinement and Coherence in Patterned Epitaxial Graphene. *Science, 312*(5777): 1191-1196.

16. Bhadra, J., and Sarkar, D. (2009). Self-assembled polyaniline nanorods synthesized by facile route of dispersion polymerization. *Materials Letters, 63*(1): 69-71.

17. Bhandari, S., Deepa, M., Srivastava, A. K., Lal, C., and Kant, R. (2008). Poly(3,4-ethylenedioxythiophene) (PEDOT)-Coated MWCNTs Tethered to Conducting Substrates: Facile Electrochemistry and Enhanced Coloring Efficiency. *Macromolecular Rapid Communications, 29*(24): 1959-1964.

18. Binnig, G., and Quate, C. F. (1986). Atomic Force Microscope. *Physical Review Letters*, 56(9): 930-933

19. Blake, P., Brimicombe, P. D., Nair, R. R., Booth, T. J., Jiang, D., Schedin, F., et al. (2008). Graphene-Based Liquid Crystal Device. *Nano Letters, 8*(6): 1704-1708.

20. Blom, P. W. M., Mihailetchi, V. D., Koster, L. J. A., and Markov, D. E. (2007). Device Physics of Polymer:Fullerene Bulk Heterojunction Solar Cells. *Advanced Materials, 19*(12): 1551-1566.

21. Bolotin, K. I., Sikes, K. J., Hone, J., Stormer, H. L., and Kim, P. (2008). Temperature-Dependent Transport in Suspended Graphene. *Physical Review Letters, 101*(9): 096802.

22. Bourlinos, A. B., Bakandritsos, A., Liaros, N., Couris, S., Safarova, K., Otyepka, M., and Zbořil, R. (2012). Water dispersible functionalized graphene fluoride with significant nonlinear optical response. *Chemical Physics Letters, 543*(0): 101-105.

23. Bragg, W. L. (1912). The Specular Reflexion of X-rays. *Nature,* 90 (2250): 410.

24. Braun, D., and Heeger, A. J. (1991). Visible light emission from semiconducting polymer diodes. *Applied Physics Letters, 58*(18): 1982-1984.

25. Bredas, J. L., and Street, G. B. (1985). Polarons, bipolarons, and solitons in conducting polymers. *Accounts of Chemical Research, 18*(10): 309-315.

26. Bubb, D. M., O'Malley, S. M., Antonacci, C., Belmont, R., McGill, R. A., and Crimi, C. (2005). Observation of persistent photoconductivity in conducting polyaniline thin films. *Applied Physics A, 81*(1): 119-125.

27. Bunch, J. S., van der Zande, A. M., Verbridge, S. S., Frank, I. W., Tanenbaum, D. M., Parpia, J. M., Craighead, H. G., and McEuen, P. L. (2007). Electromechanical Resonators from Graphene Sheets. *Science, 315*(5811): 490-493.

28. Burroughes, J., Bradley, D., Brown, A., Marks, R., Mackay, K., Friend, R., Burns, P., and Holmes, A. (1990). Light-emitting diodes based on conjugated polymers. *Nature, 347*(6293): 539-541.

29. Cançado, L. G., Pimenta, M. A., Neves, B. R. A., Dantas, M. S. S., and Jorio, A. (2004). Influence of the Atomic Structure on the Raman Spectra of Graphite Edges. *Physical Review Letters, 93*(24): 247401.

30. Cao, A., Liu, Z., Chu, S., Wu, M., Ye, Z., Cai, Z., Chang, Y., Wang, S., Gong, Q., and Liu, Y. (2010). A Facile One-step Method to Produce Graphene–CdS Quantum Dot Nanocomposites as Promising Optoelectronic Materials. *Advanced Materials, 22*(1): 103-106.

31. Cao, L., Chen, H., Wang, M., Sun, J., Zhang, X., and Kong, F. (2002). Photoconductivity Study of Modified Carbon Nanotube/Oxotitanium Phthalocyanine Composites. *The Journal of Physical Chemistry B, 106*(35): 8971-8975.

32. Cao, Y., Smith, P., and Heeger, A. J. (1992). Counter-ion induced processibility of conducting polyaniline and of conducting polyblends of polyaniline in bulk polymers. *Synthetic Metals, 48*(1): 91-97.

33. Capan, I., Tarimci, C., and Tanrisever, T. (2007). Self assembled thin films of poly (methylmethacrylate) for gas sensing. *Sensor Letters*, 5:533-537.

34. Cappella, B., and Dietler, G. (1999). Force-distance curves by atomic force microscopy. *Surface Science Reports,* 34 (1-3): 1-104.

35. Castro Neto, A. H., Guinea, F., Peres, N. M. R., Novoselov, K. S., and Geim, A. K. (2009). The electronic properties of graphene. *Reviews of Modern Physics, 81*(1): 109-162.

36. Chan, H. S. O., Ho, P. K. H., Khor, E., and Tan, M.M. (1989). Preparation of polyanilines doped in mixed protonic acids: Their characterization by X-ray photoelectron spectroscopy and thermogravimetry. *Synthetic Metals*, 31 (1): 95-108.

37. Chan, H. S. O., Ho, P. K. H., Ng, S. C., Tan, B. T. G., and Tan, K. L. (1995). A New Water-Soluble, Self-Doping Conducting Polyaniline from Poly(o-aminobenzylphosphonic acid) and Its Sodium Salts: Synthesis and Characterization. *Journal of the American Chemical Society, 117*(33): 8517-8523.

38. Chandrasekar, A., and Pradeep, T. (2012). Luminescent Silver Clusters with Covalent Functionalization of Graphene. *The Journal of Physical Chemistry C, 116*(26): 14057-14061.

39. Chang, C.-H., Huang, T.-C., Peng, C.-W., Yeh, T.-C., Lu, H.-I., Hung, W.-I., Weng, C.-J., Yang, T.-I., and Yeh, J.-M. (2012). Novel anticorrosion coatings prepared from polyaniline/graphene composites. *Carbon, 50*(14): 5044-5051.

40. Charlier, J. C., Gonze, X., and Michenaud, J. P. (1991). First-principles study of the electronic properties of graphite. *Physical Review B, 43*(6): 4579-4589.

41. Chatterjee, S., Layek, R. K., and Nandi, A. K. (2013). Changing the morphology of polyaniline from a nanotube to a flat rectangular nanopipe by polymerizing in the presence of amino-functionalized reduced graphene oxide and its resulting increase in photocurrent. *Carbon, 52*: 509-519.

42. Chen, B., Yu, L., Liu, B., Feng, J., Liu, Z., Ying, L., Li Y., and Yang, W. (2014). Efficient π-conjugated interrupted host polymer by metal-free polymerization for blue/green phosphorescent light-emitting diodes. *Journal of Polymer Science Part A: Polymer Chemistry*: 52(7):1037-1046.

43. Chen, F., Liu, P., and Zhao, Q. (2012). Well-defined graphene/polyaniline flake composites for high performance supercapacitors. *Electrochimica Acta, 76*: 62-68.

44. Chen, P. (1999). Electronic structure and optical limiting behavior of carbon nanotubes. *Physical Review Letters, 82*: 2548-2551.

45. Chen, S., Zhu, J., Wu, X., Han, Q., and Wang, X. (2010). Graphene Oxide−MnO_2 Nanocomposites for Supercapacitors. *ACS Nano, 4*(5): 2822-2830.

46. Chen, S.-A., Chuang, K.-R., Chao, C.-I., and Lee, H.-T. (1996). White-light emission from electroluminescence diode with polyaniline as the emitting layer. *Synthetic Metals, 82*(3): 207-210.

47. Chen, W.-C., Jenekhe, S. A., Meth, J. S., and Vanherzeele, H. (1994). Refractive index and nonlinear optical properties of polyaniline derivatives. *Journal of Polymer Science Part B: Polymer Physics*, 32(1): 195-200.

48. Chen, Z., Cai, P., Chen, J., Liu, X., Zhang, L., Lan, L., Peng, J., Ma, Y., and Cao, Y. (2014). Low Band-Gap Conjugated Polymers with Strong Interchain Aggregation and Very High Hole Mobility Towards Highly Efficient Thick-Film Polymer Solar Cells. *Advanced Materials*, DOI: 10.1002/adma.201305092.

49. Chiou, N.-R., Lee, L. J., and Epstein, A. J. (2007). Self-Assembled Polyaniline Nanofibers/Nanotubes. *Chemistry of Materials, 19*(15): 3589-3591.

50. Chitta, R., Sandanayaka, A. S. D., Schumacher, A. L., D'Souza, L., Araki, Y., Ito, O., and D'Souza, F. (2007). Donor−Acceptor Nanohybrids of Zinc Naphthalocyanine or Zinc Porphyrin Noncovalently Linked to Single-Wall Carbon Nanotubes for Photoinduced Electron Transfer. *The Journal of Physical Chemistry C, 111*(19): 6947-6955.

51. Choi, E.-Y., Han, T. H., Hong, J., Kim, J. E., Lee, S. H., Kim, H. W., and Kim, S. O. (2010). Noncovalent functionalization of graphene with end-functional polymers. *Journal of Materials Chemistry, 20*(10): 1907-1912.

52. Coats, A. W., and Redfern, J. P. (1963). Thermogravimetric Analysis: A Review. *Analyst,* 88: 906–924.

53. Cochet, M., Maser, W. K., Benito, A. M., Callejas, M. A., Martinez, M. T., Benoit, J.-M., Schreiber, J., and Chauvet, O. (2001). Synthesis of a new polyaniline/nanotube composite: "in-situ" polymerisation and charge transfer through site-selective interaction. *Chemical Communications,* 16: 1450-1451.

54. Cooper, E. C., and Vincent, B. (1989). Electrically conducting organic films and beads based on conducting latex particles. *Journal of Physics D: Applied Physics, 22*(11): 1580.

55. Curran, S. A., Ajayan, P. M., Blau, W. J., Carroll, D. L., Coleman, J. N., Dalton, A. B., Davey, A. P., Drury, A., McCarthy, B., Maier, S., and Strevens, A. (1998). A Composite from Poly(m-phenylenevinylene-co-2,5-dioctoxy-p-phenylenevinylene) and Carbon Nanotubes: A Novel Material for Molecular Optoelectronics. *Advanced Materials*, 10(14): 1091-1093.

56. de Souza, J. M., Petrov, D. V., Gomes, A. S. L., de Azevedo, W. M., de Melo, J. V., de Araújo, C. B., and Diniz, F. B. (1995). Nonlinear-optical properties of a poly(vinylalcohol)/polyaniline interpenetrating polymer network. *Optics Letters*, 20(6): 554-556.

57. Desilvestro, J., and Haas, O. (1991). Electrocatalytic behavior of polyaniline in the dark and under illumination. *Electrochimica Acta, 36*(2): 361-367.

58. Dhand, C., Das, M., Sumana, G., Srivastava, A. K., Pandey, M. K., Kim, C. G., Datta, M., and Malhotra, B. D. (2010). Preparation, characterization and application of polyaniline nanospheres to biosensing. *Nanoscale, 2*(5): 747-754.

59. Ding, S., Mao, H., and Zhang, W. (2008). Fabrication of DBSA-doped polyaniline nanorods by interfacial polymerization. *Journal of Applied Polymer Science, 109*(5): 2842-2847.

60. Domingues, S. H., Salvatierra, R. V., Oliveira, M. M., and Zarbin, A. J. G. (2011). Transparent and conductive thin films of graphene/polyaniline nanocomposites prepared through interfacial polymerization. *Chemical Communications, 47*(9): 2592-2594.

61. Dong, L., Deng, C., He, C., Shi, L., Fu, Y., Zhu, D., Cao, H., He, Q., and Cheng, J (2013). Highly sensitive vapor detection of amines with fluorescent conjugated polymer: A novel lasing turn-on sensory mechanism. *Sensors and Actuators B: Chemical, 180*: 28-34.

62. Dong, Y.-P., Zhang, J., Ding, Y., Chu, X.-F., and Chen, J. (2013). Electrogenerated chemiluminescence of luminol at a polyaniline/graphene modified electrode in neutral solution. *Electrochimica Acta, 91*: 240-245.

63. Dresselhaus, M., Dresselhaus, G., and Jorio, A. (2004). Unusual properties and structure of carbon nanotubes. *Annual Review of Materials Reserach, 34*: 247-278.

64. Dresselhaus, M. S., Dresselhaus, G., and Saito, R. (1995). Physics of carbon nanotubes. *Carbon, 33*(7): 883-891.

65. Du, Y., Shen, S. Z., Yang, W., Donelson, R., Cai, K., and Casey, P. S. (2012). Simultaneous increase in conductivity and Seebeck coefficient in a polyaniline/graphene nanosheets thermoelectric nanocomposite. *Synthetic Metals, 161*(23–24): 2688-2692.

66. Eda, G., Fanchini, G., and Chhowalla, M. (2008). Large-area ultrathin films of reduced graphene oxide as a transparent and flexible electronic material. *Nature Nano, 3*(5): 270-274.

67. Englebienne, P., and Van Hoonacker, A. (2005). Gold–conductive polymer nanoparticles: A hybrid material with enhanced photonic reactivity to environmental stimuli. *Journal of Colloid and Interface Science, 292*(2): 445-454.

68. Englert, J. M., Dotzer, C., Yang, G., Schmid, M., Papp, C., Gottfried, J. M., et al. (2011). Covalent bulk functionalization of graphene. *Nature Chemistry, 3*(4): 279-286.

69. Fan, W., Zhang, C., Tjiu, W. W., Pramoda, K. P., He, C., and Liu, T. (2013). Graphene-Wrapped Polyaniline Hollow Spheres As Novel Hybrid Electrode Materials for Supercapacitor Applications. *ACS Applied Materials & Interfaces, 5*(8): 3382-3391.

70. Fan, Y., Liu, J.-H., Yang, C.-P., Yu, M., and Liu, P. (2011). Graphene–polyaniline composite film modified electrode for voltammetric determination of 4-aminophenol. *Sensors and Actuators B: Chemical, 157*(2): 669-674.

71. Fang, M., Wang, K., Lu, H., Yang, Y., and Nutt, S. (2009). Covalent polymer functionalization of graphene nanosheets and mechanical properties of composites. *Journal of Materials Chemistry, 19*(38): 7098-7105.

72. Feng, M., Zhan, H., and Chen, Y. (2010). Nonlinear optical and optical limiting properties of graphene families. *Applied Physics Letters, 96*: 033107.

73. Feng, W., Bai, X. D., Lian, Y. Q., Liang, J., Wang, X. G., and Yoshino, K. (2003). Well-aligned polyaniline/carbon-nanotube composite films grown by in-situ aniline polymerization. *Carbon, 41*(8): 1551-1557.

74. Feng, W., Yi, W., Wu, H., Ozaki, M., and Yoshino, K. (2005). Enhancement of third-order optical nonlinearities by conjugated polymer-bonded carbon nanotubes. *Journal of Applied Physics, 98*(3): 034301

75. Feng, X.-M., Li, R.-M., Ma, Y.-W., Chen, R.-F., Shi, N.-E., Fan, Q.-L., and Huang, W. (2011). One-Step Electrochemical Synthesis of Graphene/Polyaniline Composite Film and Its Applications. *Advanced Functional Materials, 21*(15): 2989-2996.

76. Feng, Y., Liu, H., Luo, W., Liu, E., Zhao, N., Yoshino, K., and Feng, W. (2013). Covalent functionalization of graphene by azobenzene with molecular hydrogen bonds for long-term solar thermal storage. *Scientific Reports, 3*:3260.

77. Ferrari, A. C., and Robertson, J. (2000). Interpretation of Raman spectra of disordered and amorphous carbon. *Physical Review B, 61*(20): 14095-14107.

78. Ferrer-Anglada, N., Kaempgen, M., and Roth, S. (2006). Transparent and flexible carbon nanotube/polypyrrole and carbon nanotube/polyaniline pH sensors. *physica status solidi (b), 243*(13): 3519-3523.

79. Freshour, G. B. (1995). Chapter 7. In Masson, J. C. (Ed.). *Acrylic Fibre technology and applications* (p. 197). Marcel Dekker: New York .

80. Friend, R. H., Denton, G. J., Halls, J. J. M., Harrison, N. T., Holmes, A. B., Köhler, A., Lux, A., Moratti, S. C., Pichler, K., Tessler, N., Towns, K., and Wittmann, H. F. (1997). Electronic excitations in luminescent conjugated polymers. *Solid State Communications, 102*(2–3): 249-258.

81. Fu, G. D., Zhao, J. P., Sun, Y. M., Kang, E. T., and Neoh, K. G. (2007). Conductive Hollow Nanospheres of Polyaniline via Surface-Initiated Atom Transfer Radical Polymerization of 4-Vinylaniline and Oxidative Graft Copolymerization of Aniline. *Macromolecules, 40*(6): 2271-2275.

82. Gao, C., Ai, M., Li, X., and Xu, Z. (2011). Basic amino acid assisted-fabrication of rectangular nanotube, circular nanotube, and hollow microsphere of polyaniline: Adjusting and controlling effect of pH value. *Journal of Polymer Science Part A: Polymer Chemistry, 49*(10): 2173-2182.

83. Gao, Y., Chang, Q., Ye, H., Jiao, W., Song, Y., Wang, Y., and Qin, J. (2007). Saturable and reverse saturable absorption of a linear polymer in dimethylformamide. *Applied Physics B, 88*(2): 255-258.

84. Gardiner, D.J. (1989). *Practical Raman spectroscopy*. Springer-Verlag.

85. Geim, A. K., K. S. Novoselov. (2007). The rise of graphene. *Nature Materials, 6*(3): 183 - 191.

86. Gilje, S., Han, S., Wang, M., Wang, K. L., and Kaner, R. B. (2007). A Chemical Route to Graphene for Device Applications. *Nano Letters, 7*(11): 3394-3398.

87. Giuliano, C. R., and Hess, L. D. (1967). Nonlinear absorption of light: Optical saturation of electronic transitions in organic molecules with high intensity laser radiation. *IEEE Journal of Quantum Electronics, 3*(8): 358-367.

88. Goldstein, G. I., Newbury, D. E., Echlin, P., Joy, D. C., Fiori, C., and Lifshin, E. (1981). *Scanning electron microscopy and X-ray microanalysis*. New York: Plenum Press.

89. Gómez, H., Ram, M. K., Alvi, F., Villalba, P., Stefanakos, E., and Kumar, A. (2011). Graphene-conducting polymer nanocomposite as novel electrode for supercapacitors. *Journal of Power Sources, 196*(8): 4102-4108.

90. Gopalakrishnan, D., and Dichtel, W. R. (2013). Direct Detection of RDX Vapor Using a Conjugated Polymer Network. *Journal of the American Chemical Society, 135*(22): 8357-8362.

91. Goswami, S., Maiti, U. N., Maiti, S., Nandy, S., Mitra, M. K., and Chattopadhyay, K. K. (2011). Preparation of graphene–polyaniline composites by simple chemical procedure and its improved field emission properties. *Carbon, 49*(7): 2245-2252.

92. Griffiths, P., and de Hasseth, J.A. (2007). *Fourier Transform Infrared Spectrometry* (2nd ed.). Wiley-Blackwell.

93. Gross, L., Mohn, F., Moll, N., Liljeroth, P., and Meyer, G. (2009). The Chemical Structure of a Molecule Resolved by Atomic Force Microscopy. *Science,* 325 (5944): 1110-1114.

94. Guo, C. X., Wang, M., Chen, T., Lou, X. W., and Li, C. M. (2011). A Hierarchically Nanostructured Composite of MnO_2/Conjugated Polymer/Graphene for High-Performance Lithium Ion Batteries. *Advanced Energy Materials, 1*(5): 736-741.

95. Guo, H.-L., Wang, X.-F., Qian, Q.-Y., Wang, F.-B., and Xia, X.-H. (2009). A Green Approach to the Synthesis of Graphene Nanosheets. *ACS Nano, 3*(9): 2653-2659.

96. Guo, S., Dong, S., and Wang, E. (2009). Three-Dimensional Pt-on-Pd Bimetallic Nanodendrites Supported on Graphene Nanosheet: Facile Synthesis and Used as an Advanced Nanoelectrocatalyst for Methanol Oxidation. *ACS Nano, 4*(1): 547-555.

97. Guo, Z., Du, F., Ren, D., Chen, Y., Zheng, J., Liu, Z., and Tian, J. (2006). Covalently porphyrin-functionalized single-walled carbon nanotubes: a novel photoactive and optical limiting donor-acceptor nanohybrid. *Journal of Materials Chemistry, 16*(29): 3021-3030.

98. Gupta, V., and Miura, N. (2006). High performance electrochemical supercapacitor from electrochemically synthesized nanostructured polyaniline. *Materials Letters, 60*(12): 1466-1469.

99. Gurudas, U., Brooks, E., Bubb, D. M., Heiroth, S., Lippert, T., and Wokaun, A. (2008). Saturable and reverse saturable absorption in silver nanodots at 532 nm using picosecond laser pulses. *Journal of Applied Physics, 104*(7): 073107-073108.

100. Gustafsson, G., Cao, Y., Treacy, G., Klavetter, F., Colaneri, N., and Heeger, A. (1992). Flexible light-emitting diodes made from soluble conducting polymers. *Nature, 357*(6378): 477-479.

101. Hai Binh, N., Van Chuc, N., Van Tu, N., Thi Thanh Tam, N., Ngoc Thinh, N., Thi Thu Huyen, D., et al. (2012). Graphene patterned polyaniline-based biosensor for glucose detection. *Advances in Natural Sciences: Nanoscience and Nanotechnology, 3*(2): 025011.

102. Han, G., and Shi, G. (2004). Conducting polymer electrochemical actuator made of high-strength three-layered composite films of polythiophene and polypyrrole. *Sensors and Actuators B: Chemical, 99*(2–3): 525-531.

103. He, F., Fan, J., Ma, D., Zhang, L., Leung, C., and Chan, H. L. (2010). The attachment of Fe_3O_4 nanoparticles to graphene oxide by covalent bonding. *Carbon, 48*(11): 3139-3144.

104. He, H., Klinowski, J., Forster, M., and Lerf, A. (1998). A new structural model for graphite oxide. *Chemical Physics Letters, 287*(1–2): 53-56.

105. He, N., Chen, Y., Bai, J., Wang, J., Blau, W. J., and Zhu, J. (2009). Preparation and Optical Limiting Properties of Multiwalled Carbon Nanotubes with π-Conjugated Metal-Free Phthalocyanine Moieties. *The Journal of Physical Chemistry C, 113*(30): 13029-13035.

106. Heeger, A. J. (2001). Semiconducting and Metallic Polymers: The Fourth Generation of Polymeric Materials (Nobel Lecture). *Angewandte Chemie International Edition, 40*(14): 2591-2611.

107. Hoppe, H., Niggemann, M., Winder, C., Kraut, J., Hiesgen, R., Hinsch, A., Meissner, D., and Sariciftci, N. S. (2004). Nanoscale Morphology of Conjugated Polymer/Fullerene-Based Bulk- Heterojunction Solar Cells. *Advanced Functional Materials, 14*(10): 1005-1011.

108. Hu, H., Wang, X., Wang, J., Liu, F., Zhang, M., and Xu, C. (2011). Microwave-assisted covalent modification of graphene nanosheets with chitosan and its electrorheological characteristics. *Applied Surface Science, 257*(7): 2637-2642.

109. Hua, J., Qu, Y., Zhang, X., Wu, Y., and Li, F. (2014). Fluorescent conjugated polymer based on thiocarbonyl quinacridone for sensing mercury ion and bioimaging. *Polymer Chemistry,*
DOI: 10.1039/C4PY00014E.

110. Huang, H., Zhou, N., Ortiz, R. P., Chen, Z., Loser, S., Zhang, S., Guo, X., Casado, J., López Navarrete, J. T., Yu, X., Facchetti, A., and Marks, T. J. (2014). Alkoxy-Functionalized Thienyl-Vinylene Polymers for Field-Effect Transistors and All-Polymer Solar Cells. *Advanced Functional Materials*, DOI: 10.1002/adfm.201303219.

111. Huang, J., and Kaner, R. B. (2003). A General Chemical Route to Polyaniline Nanofibers. *Journal of the American Chemical Society, 126*(3): 851-855.

112. Huang, J., Virji, S., Weiller, B. H., and Kaner, R. B. (2002). Polyaniline Nanofibers:Facile Synthesis and Chemical Sensors. *Journal of the American Chemical Society, 125*(2): 314-315.

113. Huang, J., Virji, S., Weiller, B. H., and Kaner, R. B. (2004). Nanostructured Polyaniline Sensors. *Chemistry – A European Journal, 10*(6): 1314-1319.

114. Huang, K., and Wan, M. (2002). Self-Assembled Polyaniline Nanostructures with Photoisomerization Function. *Chemistry of Materials*, 14(8): 3486-3492.

115. Huang, X., Qi, X., Boey, F., and Zhang, H. (2012). Graphene-based composites. *Chemical Society Reviews, 41*(2): 666-686.

116. Huang, X., Zhou, X., Wu, S., Wei, Y., Qi, X., Zhang, J., et al. (2010). Reduced Graphene Oxide-Templated Photochemical Synthesis and in situ Assembly of Au Nanodots to Orderly Patterned Au Nanodot Chains. *Small, 6*(4): 513-516.

117. Huiqun, C., Meifang, Z., and Yaogang, L. (2006). Decoration of carbon nanotubes with iron oxide. *Journal of Solid State Chemistry*, 179(4): 1208-1213.

118. Hummers, W.S., and Offeman, R. E. (1958). Preparation of graphitic oxide, *Journal of the American Chemical Society*, 80(6): 1339.

119. Huynh, W. U., Dittmer, J. J., and Alivisatos, A. P. (2002). Hybrid Nanorod-Polymer Solar Cells. *Science, 295*(5564): 2425-2427.

120. Iijima, S., and Ichihashi, T. (1993). Single-shell carbon nanotubes of 1-nm diameter. *Nature, 363*(6430): 603-605.

121. Izard, N., Ménard, C., Riehl, D., Doris, E., Mioskowski, C., and Anglaret, E. (2004). Combination of carbon nanotubes and two-photon absorbers for broadband optical limiting. *Chemical Physics Letters, 391*(1–3): 124-128.

122. Jager, E. W. H., Smela, E., and Inganäs, O. (2000). Microfabricating Conjugated Polymer Actuators. *Science, 290*(5496): 1540-1545.

123. Jang, J., Ha, J., and Kim, S. (2007). Fabrication of polyaniline nanoparticles using microemulsion polymerization. *Macromolecular Research, 15*(2): 154-159.

124. Jeon, S. S., Kim, C., Lee, T. H., Lee, Y. W., Do, K., Ko, J., and Im, S. S. (2012). Camphorsulfonic Acid-Doped Polyaniline Transparent Counter Electrode for Dye-Sensitized Solar Cells. *The Journal of Physical Chemistry C*, 116(43): 22743-22748.

125. Jiang, X.-F., Polavarapu, L., Neo, S. T., Venkatesan, T., and Xu, Q.-H. (2012). Graphene Oxides as Tunable Broadband Nonlinear Optical Materials for Femtosecond Laser Pulses. *The Journal of Physical Chemistry Letters, 3*(6): 785-790.

126. Jianhua, L., Junwei, A., Yecheng, Z., Yuxiao, M., Mengliu, L., Mei, Y., and Songmei, L. (2012). Preparation of an Amide Group-Connected Graphene–Polyaniline Nanofiber Hybrid and Its Application in Supercapacitors. *ACS Applied Materials & Interfaces, 4*(6): 2870-2876.

127. Kai, S., Carl, N., Anders, F., Ragnar, N., Kjell, H., Jan, H., et al. (1967). *ESCA: Atomic, Molecular and Solid State Structure Studied by Means of Electron Spectroscopy*. Almqvist and Wiksells Boktryckeri AB.

128. Kane, M., and Krafcik, K. (2013). Nanostructured soluble conducting polyaniline produced by emulsion polymerization. *Synthetic Metals*, 181: 129-135.

129. Karami, H., Mousavi, M. F., and Shamsipur, M. (2003). A new design for dry polyaniline rechargeable batteries. *Journal of Power Sources, 117*(1–2): 255-259.

130. Karousis, N., Sandanayaka, A. S. D., Hasobe, T., Economopoulos, S. P., Sarantopoulou, E., and Tagmatarchis, N. (2011). Graphene oxide with covalently linked porphyrin antennae: Synthesis, characterization and photophysical properties. *Journal of Materials Chemistry, 21*(1): 109-117.

131. Katsnelson, M. I., Novoselov, K. S., and Geim, A. K. (2006). Chiral tunnelling and the Klein paradox in graphene. *Nature Physics, 2*(9): 620-625.

132. Kavitha, M. K., John, H., Gopinath, P., and Philip, R. (2013). Synthesis of reduced graphene oxide-ZnO hybrid with enhanced optical limiting properties. *Journal of Materials Chemistry C, 1*(23): 3669-3676.

133. Kazaoui, S., Minami, N., Nalini, B., Kim, Y., and Hara, K. (2005). Near-infrared photoconductive and photovoltaic devices using single-wall carbon nanotubes in conductive polymer films. *Journal of Applied Physics*, 98(8): 084314.

134. Kemp, K. C., Vimlesh, C., Muhammad, S., and Kwang, S. K. (2013). Reversible CO_2 adsorption by an activated nitrogen doped graphene/polyaniline material. *Nanotechnology, 24*(23): 235703.

135. Kilmartin, P. A., and Wright, G. A. (1996). Photoeffects at a polyaniline film electrode. *Electrochimica Acta, 41*(10): 1677-1687.

136. Kim, Y., Cook, S., Tuladhar, S. M., Choulis, S. A., Nelson, J., Durrant, J. R., Bradley, D. D. C., Giles, M., McCulloch, I., Ha, C.-S., and Ree, M. (2006). A strong regioregularity effect in self-organizing conjugated polymer films and high-efficiency polythiophene:fullerene solar cells. *Nature Materials, 5*(3): 197-203.

137. Kong, B.-S., Geng, J., and Jung, H.-T. (2009). Layer-by-layer assembly of graphene and gold nanoparticles by vacuum filtration and spontaneous reduction of gold ions. *Chemical Communications* (16): 2174-2176.

138. Konyushenko, E. N., Stejskal, J., Trchová, M., Hradil, J., Kovářová, J., Prokeš, J., et al. (2006). Multi-wall carbon nanotubes coated with polyaniline. *Polymer, 47*(16): 5715-5723.

139. Koul, S., Chandra, R., and Dhawan, S. K. (2000). Conducting polyaniline composite for ESD and EMI at 101 GHz. *Polymer, 41*(26): 9305-9310.

140. Krishna, M. B. M., Kumar, V. P., Venkatramaiah, N., Venkatesan, R., and Rao, D. N. (2011). Nonlinear optical properties of covalently linked graphene-metal porphyrin composite materials. *Applied Physics Letters*, 98(8): 081106.

141. Krishna, M. B. M., Venkatramaiah, N., Venkatesan, R., and Narayana Rao, D. (2012). Synthesis and structural, spectroscopic and nonlinear optical measurements of graphene oxide and its composites with metal and metal free porphyrins. *Journal of Materials Chemistry, 22*(7): 3059-3068.

142. Kuik, M., Wetzelaer, G.-J. A. H., Nicolai, H. T., Craciun, N. I., De Leeuw, D. M., and Blom, P. W. M. (2014). 25th Anniversary Article: Charge Transport and Recombination in Polymer Light-Emitting Diodes. *Advanced Materials, 26*(4): 512-531.

143. Kuila, B. K., Nandan, B., Bohme, M., Janke, A., and Stamm, M. (2009). Vertically oriented arrays of polyaniline nanorods and their super electrochemical properties. *Chemical Communications,* 38: 5749-5751.

144. Kumar, M., Singh, K., Dhawan, S. K., Tharanikkarasu, K., Chung, J. S., Kong, B.-S., et al. (2013). Synthesis and characterization of covalently-grafted graphene–polyaniline nanocomposites and its use in a supercapacitor. *Chemical Engineering Journal, 231*: 397-405.

145. Kumar, N. A., Choi, H.-J., Shin, Y. R., Chang, D. W., Dai, L., and Baek, J.-B. (2012). Polyaniline-Grafted Reduced Graphene Oxide for Efficient Electrochemical Supercapacitors. *ACS Nano, 6*(2): 1715-1723.

146. Kurmaev, E. Z., Katsnelson, M. I., Moewes, A., Magnuson, M., Guo, J. H., Butorin, S. M., et al. (2001). Spectroscopic observation of polaron-lattice band structure in the conducting polymer polyaniline. *Journal of Physics: Condensed Matter, 13*(17): 3907.

147. Kymakis, E., Alexandrou, I., and Amaratunga, G. A. J. (2003). High open-circuit voltage photovoltaic devices from carbon-nanotube-polymer composites. *Journal of Applied Physics, 93*(3): 1764-1768.

148. Kymakis, E., and Amaratunga, G. A. J. (2002). Single-wall carbon nanotube/conjugated polymer photovoltaic devices. *Applied Physics Letters, 80*(1): 112-114.

149. Kymakis, E., Servati, P., Tzanetakis, P., Koudoumas, E., Kornilios, N., Rompogiannakis, I., Franghiadakis, Y., and Amaratunga, G. A. J. (2007). Effective mobility and photocurrent in carbon nanotube–polymer composite photovoltaic cells. *Nanotechnology, 18*(43): 435702.

150. Lafuente, E., Callejas, M. A., Sainz, R., Benito, A. M., Maser, W. K., Sanjuán, M. L., Saurel, D., de Teresa, J. M., and Martínez, M. T. (2008). The influence of single-walled carbon nanotube functionalization on the electronic properties of their polyaniline composites. *Carbon, 46*(14): 1909-1917.

151. Landi, B. J., Castro, S. L., Ruf, H. J., Evans, C. M., Bailey, S. G., and Raffaelle, R. P. (2005a). CdSe quantum dot-single wall carbon nanotube complexes for polymeric solar cells. *Solar Energy Materials and Solar Cells,* 87(1–4): 733-746.

152. Landi, B. J., Raffaelle, R. P., Castro, S. L., and Bailey, S. G. (2005b). Single-wall carbon nanotube–polymer solar cells. *Progress in Photovoltaics: Research and Applications, 13*(2): 165-172.

153. Lee, S. H., Dreyer, D. R., An, J., Velamakanni, A., Piner, R. D., Park, S., Zhu, Y., Kim, S. O., Bielawski, C. W., and Ruoff, R. S. (2010). Polymer Brushes via Controlled, Surface-Initiated Atom Transfer Radical Polymerization (ATRP) from Graphene Oxide. *Macromolecular Rapid Communications, 31*(3): 281-288.

154. Lei, Z., Zhao, M., Dang, L., An, L., Lu, M., Lo, A.-Y., Yu, N., and Liu, S.-B. (2009). Structural evolution and electrocatalytic application of nitrogen-doped carbon shells synthesized by pyrolysis of near-monodisperse polyaniline nanospheres. *Journal of Materials Chemistry, 19*(33): 5985-5995.

155. Lerf, A., He, H., Forster, M., and Klinowski, J. (1998). Structure of graphite oxide revisited. *The Journal of Physical Chemistry B, 102*: 4477-4482.

156. Li, C., Liu, C., Li, F., and Gong, Q. (2003). Optical limiting performance of two soluble multi-walled carbon nanotubes. *Chemical Physics Letters, 380*(1–2): 201-205.

157. Li, D., and Kaner, R. B. (2005). Processable stabilizer-free polyaniline nanofiber aqueous colloids. *Chemical Communications* (26): 3286-3288.

158. Li, D., Muller, M. B., Gilje, S., Kaner, R. B., and Wallace, G. G. (2008). Processable aqueous dispersions of graphene nanosheets. *Nature Nanotechnology, 3*(2): 101-105.

159. Li, J., Xie, H., Li, Y., Liu, J., and Li, Z. (2011). Electrochemical properties of graphene nanosheets/polyaniline nanofibers composites as electrode for supercapacitors. *Journal of Power Sources, 196*(24): 10775-10781.

160. Li, P.-P., Chen, Y., Zhu, J., Feng, M., Zhuang, X., Lin, Y., and Zhan, H. (2011). Charm-Bracelet-Type Poly(N-vinylcarbazole) Functionalized with Reduced Graphene Oxide for Broadband Optical Limiting. *Chemistry – A European Journal, 17*(3): 780-785.

161. Li, Q., Wu, J., Tang, Q., Lan, Z., Li, P., Lin, J., and Fan, L. (2008). Application of microporous polyaniline counter electrode for dye-sensitized solar cells. *Electrochemistry Communications, 10*(9): 1299-1302.

162. Li, W., Furlan, A., Roelofs, W. S. C., Hendriks, K. H., van Pruissen, G. W. P., Wienk, M. M., and Janssen, R. A. J. (2014). Wide band gap diketopyrrolopyrrole-based conjugated polymers incorporating biphenyl units applied in polymer solar cells. *Chemical Communications, 50*(6): 679-681.

163. Li, X., Cai, W., An, J., Kim, S., Nah, J., Yang, D., Piner, R., Velamakanni, A., Jung, I., Tutuc, E., Banerjee, S. K., Colombo, L., and Ruoff, R. S. (2009). Large-Area Synthesis of High-Quality and Uniform Graphene Films on Copper Foils. *Science, 324*(5932): 1312-1314.

164. Li, X., Zhuang, T., Wang, G., and Zhao, Y. (2008). Stabilizer-free conducting polyaniline nanofiber aqueous colloids and their stability. *Materials Letters, 62*(8–9): 1431-1434.

165. Li, Y., Peng, H., Li, G., and Chen, K. (2012). Synthesis and electrochemical performance of sandwich-like polyaniline/graphene composite nanosheets. *European Polymer Journal, 48*(8): 1406-1412.

166. Li, Z.-F., Zhang, H., Liu, Q., Liu, Y., Stanciu, L., and Xie, J. (2014). Covalently-grafted polyaniline on graphene oxide sheets for high performance electrochemical supercapacitors. *Carbon*, http://dx.doi.org/10.1016/j.carbon.2014.01.037.

167. Liang, Y., Wang, H., Zhou, J., Li, Y., Wang, J., Regier, T., and Dai, H. (2012). Covalent Hybrid of Spinel Manganese–Cobalt Oxide and Graphene as Advanced Oxygen Reduction Electrocatalysts. *Journal of the American Chemical Society, 134*(7): 3517-3523.

168. Liao, H.-C., Hsu, C.-P., Wu, M.-C., Lu, C.-F., and Su, W.-F. (2013). Conjugated Polymer/Nanoparticles Nanocomposites for High Efficient and Real-Time Volatile Organic Compounds Sensors. *Analytical Chemistry, 85*(19): 9305-9311.

169. Lijuan, Z., and Meixiang, W. (2002). Synthesis and characterization of self-assembled polyaniline nanotubes doped with D-10-camphorsulfonic acid. *Nanotechnology, 13*(6): 750.

170. Lim, G.-K., Chen, Z.-L., Clark, J., Goh, R. G. S., Ng, W.-H., Tan, H.-W., Friend, R. H., Ho, P. K. H., and Chua, L.-L. (2011). Giant broadband nonlinear optical absorption response in dispersed graphene single sheets. *Nature Photonics, 5*(9): 554-560.

171. Liu, C.-Y., Huang, K.-C., Chung, P.-H., Wang, C.-C., Chen, C.-Y., Vittal, R., et al. (2012). Graphene-modified polyaniline as the catalyst material for the counter electrode of a dye-sensitized solar cell. *Journal of Power Sources, 217*: 152-157.

172. Liu, Q., Liu, Z., Zhang, X., Yang, L., Zhang, N., Pan, G., et al. (2009). Polymer Photovoltaic Cells Based on Solution-Processable Graphene and P3HT. *Advanced Functional Materials, 19*(6): 894-904.

173. Liu, Y., Zhou, J., Zhang, X., Liu, Z., Wan, X., Tian, J., et al. (2009). Synthesis, characterization and optical limiting property of covalently oligothiophene-functionalized graphene material. *Carbon, 47*(13): 3113-3121.

174. Liu, Z., He, D., Wang, Y., Wu, H., and Wang, J. (2010). Solution-processable functionalized graphene in donor/acceptor-type organic photovoltaic cells. *Solar Energy Materials and Solar Cells, 94*(7): 1196-1200.

175. Liu, Z., Liu, Q., Huang, Y., Ma, Y., Yin, S., Zhang, X., Sun, W., and Chen, Y. (2008). Organic Photovoltaic Devices Based on a Novel Acceptor Material: Graphene. *Advanced Materials, 20*(20): 3924-3930.

176. Liu, Z., Wang, Y., Zhang, X., Xu, Y., Yongsheng, C., and Tian, J. (2009). Nonlinear optical properties of graphene oxide in nanosecond and picosecond regimes. *Applied Physics Letters, 94*(2): 021902-021903.

177. Liu, Z., Zhu, Y., Wang, L., Ding, C., Wang, N., Wan, M., and Jiang, L. (2011). Polyaniline Microtubes with a Hexagonal Cross-Section and pH-Sensitive Fluorescence Properties. *Macromolecular Rapid Communications, 32*(6): 512-517.

178. Liu, Z. B., Tian, J. G., Guo, Z., Ren, D. M., Du, F., Zheng, J. Y., and Chen, Y. S. (2008). Enhanced Optical Limiting Effects in Porphyrin-Covalently Functionalized Single-Walled Carbon Nanotubes. *Advanced Materials, 20*(3): 511-515.

179. Liu, Z.-B., Xu, Y.-F., Zhang, X.-Y., Zhang, X.-L., Chen, Y.-S., and Tian, J.-G. (2009). Porphyrin and Fullerene Covalently Functionalized Graphene Hybrid Materials with Large Nonlinear Optical Properties. *The Journal of Physical Chemistry B, 113*(29): 9681-9686.

180. MacDiarmid, A. G. (2001). "Synthetic Metals": A Novel Role for Organic Polymers (Nobel Lecture). *Angewandte Chemie International Edition, 40*(14): 2581-2590.

181. Maiman, T. H. (1960). Stimulated Optical Radiation in Ruby. *Nature, 187*(4736): 493-494.

182. Marks, R. N., Halls, J. J. M., Bradley, D. D. C., Friend, R. H., and Holmes, A. B. (1994). The photovoltaic response in poly(p-phenylene vinylene) thin-film devices. *Journal of Physics: Condensed Matter, 6*(7): 1379.

183. Marrucci, L., Paparo, D., Abbate, G., Santamato, E., Kreuzer, M., Lehnert, P., and Vogeler, T. (1998). Enhanced optical nonlinearity by photoinduced molecular orientation in absorbing liquids. *Physical Review A*, 58(6): 4926-4936.

184. Mattes, B. R., Knobbe, E. T., Fuqua, P. D., Nishida, F., Chang, E. W., Pierce, B. M., et al. (1991). Polyaniline sol-gels and their third-order nonlinear optical effects. *Synthetic Metals*, 43(1–2): 3183-3187.

185. Mattevi, C., Kim, H., and Chhowalla, M. (2011). A review of chemical vapour deposition of graphene on copper. *Journal of Materials Chemistry, 21*(10): 3324-3334.

186. McAllister, M. J., Li, J.-L., Adamson, D. H., Schniepp, H. C., Abdala, A. A., Liu, J., et al. (2007). Single Sheet Functionalized Graphene by Oxidation and Thermal Expansion of Graphite. *Chemistry of Materials, 19*(18): 4396-4404.

187. McQuade, D. T., Pullen, A. E., and Swager, T. M. (2000). Conjugated Polymer-Based Chemical Sensors. *Chemical Reviews, 100*(7): 2537-2574.

188. Miller, A. J., Hatton, R. A., and Silva, S. R. P. (2006). Water-soluble multiwall-carbon-nanotube-polythiophene composite for bilayer photovoltaics. *Applied Physics Letters, 89*(12): 123115

189. Mishra, A. K., and Ramaprabhu, S. (2012). Nanostructured polyaniline decorated graphene sheets for reversible CO_2 capture. *Journal of Materials Chemistry, 22*(9): 3708-3712.

190. Murugan, A. V., Muraliganth, T., and Manthiram, A. (2009). Rapid, Facile Microwave-Solvothermal Synthesis of Graphene Nanosheets and Their Polyaniline Nanocomposites for Energy Strorage. *Chemistry of Materials, 21*(21): 5004-5006.

191. Nair, R. R., Blake, P., Grigorenko, A. N., Novoselov, K. S., Booth, T. J., Stauber, T., Peres, N. M. R., and Geim, A. K. (2008). Fine Structure Constant Defines Visual Transparency of Graphene. *Science, 320*(5881): 1308.

192. Nalwa, H.S. (2007). *Handbook of Organic Conductive Molecules and Polymers*, Wiley: Chichester.

193. Narasimhan, M., Hagler, M., Cammarata, V., and Thakur, M. (1998). Junction devices based on sulfonated polyaniline. *Applied Physics Letters, 72*(9): 1063-1065.

194. Nayak, P., Anbarasan, B., and Ramaprabhu, S. (2013). Fabrication of Organophosphorus Biosensor Using ZnO Nanoparticle-Decorated Carbon Nanotube–Graphene Hybrid Composite Prepared by a Novel Green Technique. *The Journal of Physical Chemistry C, 117*(25): 13202-13209.

195. Nguyen, C. H., Alici, G., and Wallace, G. G. (2012). Modelling trilayer conjugated polymer actuators for their sensorless position control. *Sensors and Actuators A: Physical, 185*: 82-91.

196. Ní Mhuircheartaigh, É. M., Giordani, S., and Blau, W. J. (2006). Linear and Nonlinear Optical Characterization of a Tetraphenylporphyrin−Carbon Nanotube Composite System. *The Journal of Physical Chemistry B, 110*(46): 23136-23141.

197. Niyogi, S., Bekyarova, E., Itkis, M. E., McWilliams, J. L., Hamon, M. A., and Haddon, R. C. (2006). Solution Properties of Graphite and Graphene. *Journal of the American Chemical Society, 128*(24): 7720-7721.

198. Notaras, E. G. A., Fazekas, M., Doyle, J. J., Blau, W. J., and Senge, M. O. (2007). A2B2-type push-pull porphyrins as reverse saturable and saturable absorbers. *Chemical Communications,* 21: 2166-2168.

199. Novoselov, K. S., Geim, A. K., Morozov, S. V., Jiang, D., Katsnelson, M. I., Grigorieva, I. V., Dubonos, S. V., and Firsov, A. A. (2005). Two-dimensional gas of massless Dirac fermions in graphene. *Nature, 438*(7065): 197-200.

200. Novoselov, K. S., Geim, A. K., Morozov, S. V., Jiang, D., Zhang, Y., Dubonos, S. V., et al. (2004). Electric Field Effect in Atomically Thin Carbon Films. *Science, 306*(5696): 666-669.

201. O'Flaherty, S. M., Murphy, R., Hold, S. V., Cadek, M., Coleman, J. N., and Blau, W. J. (2003). Material Investigation and Optical Limiting Properties of Carbon Nanotube and Nanoparticle Dispersions. *The Journal of Physical Chemistry B*, 107(4): 958-964.

202. Osaheni, J. A., Jenekhe, S. A., Vanherzeele, H., Meth, J. S., Sun, Y., and MacDiarmid, A. G. (1992). Nonlinear optical properties of polyanilines and derivatives. *The Journal of Physical Chemistry, 96*(7): 2830-2836.

203. Österholm, J. E., Cao, Y., Klavetter, F., and Smith, P. (1993). Emulsion polymerization of aniline. *Synthetic Metals*, 55(2–3): 1034-1039.

204. Paloheimo, J., Kuivalainen, P., Stubb, H., Vuorimaa, E., and Yli-Lahti, P. (1990). Molecular field-effect transistors using conducting polymer Langmuir–Blodgett films. *Applied Physics Letters, 56*(12): 1157-1159.

205. Pandey, R. K., Sandeep, C. S. S., Philip, R., and Lakshminarayanan, V. (2009). Enhanced Optical Nonlinearity of Polyaniline−Porphyrin Nanocomposite. *The Journal of Physical Chemistry C*, 113(20): 8630-8634.

206. Philip, B., Xie, J., Abraham, J. K., and Varadan, V. K. (2005). Polyaniline /carbon nanotube composites: starting with phenylamino functionalized carbon nanotubes. *Polymer Bulletin, 53*(2): 127-138.

207. Philip, R., Ravindra Kumar, G., Sandhyarani, N., and Pradeep, T. (2000). Picosecond optical nonlinearity in monolayer-protected gold, silver, and gold-silver alloy nanoclusters. *Physical Review B*, 62(19):13160-13166.

208. Pouget, J. P., Jozefowicz, M. E., Epstein, A. J., Tang, X., and MacDiarmid, A. G. (1991). X-ray structure of polyaniline. *Macromolecules, 24*(3): 779-789.

209. Pramoda, K. P., Hussain, H., Koh, H. M., Tan, H. R., and He, C. B. (2010). Covalent bonded polymer–graphene nanocomposites. *Journal of Polymer Science Part A: Polymer Chemistry, 48*(19): 4262-4267.

210. Price, S. C., Stuart, A. C., Yang, L., Zhou, H., and You, W. (2011). Fluorine Substituted Conjugated Polymer of Medium Band Gap Yields 7% Efficiency in Polymer−Fullerene Solar Cells. *Journal of the American Chemical Society, 133*(12): 4625-4631.

211. Qiu, H., Wan, M., Matthews, B., and Dai, L. (2001). Conducting Polyaniline Nanotubes by Template-Free Polymerization. *Macromolecules, 34* (4): 675-677.

212. Qiu, J.-D., Shi, L., Liang, R.-P., Wang, G.-C., and Xia, X.-H. (2012). Controllable Deposition of a Platinum Nanoparticle Ensemble on a Polyaniline/Graphene Hybrid as a Novel Electrode Material for Electrochemical Sensing. *Chemistry – A European Journal, 18*(25): 7950-7959.

213. Quillard, S., Louarn, G., Lefrant, S., and Macdiarmid, A. G. (1994). Vibrational analysis of polyaniline: A comparative study of leucoemeraldine, emeraldine, and pernigraniline bases. *Physical Review B, 50*(17): 12496-12508.

214. Rånby B. (1993). Chapter 3. In W. R. Salaneck, I. Lundström and B. Rånby (Eds.) *Conjugated Polymers and Related Materials: The Interconnection of Chemical and Electronic Structures*. Oxford University Press, Oxford.

215. Remyamol, T., Honey, J., and Pramod, G. (2013). Grafting of self assembled polyaniline nanorods on reduced graphene oxide for nonlinear optical appication. *Synthetic Metals*, 185-186:38-44.

216. Remyamol, T., Honey, J., Reji, P., and Pramod, G. (2014). Energy dependent saturable and reverse saturable absorption in cube-like polyaniline/polymethyl methacrylate film. *Materials Chemistry and Physics*, http://dx.doi.org/10.1016/j.matchemphys.2014.02.040

217. Robert, W. (1990). *Chromatography/Fourier transform infrared spectroscopy and its applications.* Marcel Dekker.

218. Roncali, J. (1997). Synthetic Principles for Bandgap Control in Linear π-Conjugated Systems. *Chemical Reviews, 97*(1): 173-206.

219. Ruiz, J., Gonzalo, B., Dios, J. R., Laza, J. M., Vilas, J. L., and León, L. M. (2013). Improving the Processability of Conductive Polymers: The Case of Polyaniline. *Advances in Polymer Technology, 32*(S1): E180-E188.

220. Sansiñena, J. M., Gao, J., and Wang, H. L. (2003). High-Performance, Monolithic Polyaniline Electrochemical Actuators. *Advanced Functional Materials, 13*(9): 703-709.

221. Sapurina, I., Mokeev, M., Lavrentev, V., Zgonnik, V., Trchová, M., Hlavatá, D., and Stejskal, J. (2000). Polyaniline complex with fullerene C_{60}. *European Polymer Journal, 36*(11): 2321-2326.

222. Schedin, F., Geim, A. K., Morozov, S. V., Hill, E. W., Blake, P., Katsnelson, M. I., and Novoselov, K. S. (2007). Detection of individual gas molecules adsorbed on graphene. *Nature Materials, 6*(9): 652-655.

223. Schniepp, H. C., Li, J.-L., McAllister, M. J., Sai, H., Herrera-Alonso, M., Adamson, D. H., Prud'homme, R. K., Car, R., Saville, D. A., and Aksay, I. A. (2006). Functionalized Single Graphene Sheets Derived from Splitting Graphite Oxide. *The Journal of Physical Chemistry B, 110*(17): 8535-8539.

224. Sessolo, M., Tordera, D., and Bolink, H. J. (2013). Ionic Iridium Complex and Conjugated Polymer Used To Solution-Process a Bilayer White Light-Emitting Diode. *ACS Applied Materials & Interfaces, 5*(3): 630-634.

225. Sezer, A., Gurudas, U., Collins, B., McKinlay, A., and Bubb, D. M. (2009). Nonlinear optical properties of conducting polyaniline and polyaniline–Ag composite thin films. *Chemical Physics Letters*, 477(1–3): 164-168.

226. Sheik-Bahae, M., Said, A. A., Wei, T. H., Hagan, D. J., and Van Stryland, E. W. (1990). Sensitive measurements of optical nonlinearities using a single beam. *IEEE Journal of Quantum Electronics*, 26(4): 760-769.

227. Shimano, J. Y., and MacDiarmid, A. G. (2001). Polyaniline, a dynamic block copolymer: key to attaining its intrinsic conductivity? *Synthetic Metals*, 123(2): 251-262.

228. Shirakawa, H. (2001). The Discovery of Polyacetylene Film: The Dawning of an Era of Conducting Polymers (Nobel Lecture). *Angewandte Chemie International Edition, 40*(14): 2574-2580.

229. Shirakawa, H., Louis, E. J., MacDiarmid, A. G., Chiang, C. K., and Heeger, A. J. (1977). Synthesis of electrically conducting organic polymers: halogen derivatives of polyacetylene, (CH). *Journal of the Chemical Society, Chemical Communications*(16): 578-580.

230. Si, Y., and Samulski, E. T. (2008). Synthesis of Water Soluble Graphene. *Nano Letters, 8*(6): 1679-1682.

231. Sirringhaus, H., Wilson, R. J., Friend, R. H., Inbasekaran, M., Wu, W., Woo, E. P., Grell, M., and Bradley, D. D. C. (2000). Mobility enhancement in conjugated polymer field-effect transistors through chain alignment in a liquid-crystalline phase. *Applied Physics Letters, 77*(3): 406-408.

232. Skoog, D. A., Holler, F. J., and Crouch, S. R. (2007). *Principles of Instrumental Analysis* (6th ed.). Belmont, CA: Thomson Brooks/Cole. pp. 169-173.

233. Skotheim, T. A., Elsenbaumer, R. L., Reynolds, J. R. (1997) *Handbook of conducting polymers*. New York.

234. Snook, G. A., Kao, P., and Best, A. S. (2011). Conducting-polymer-based supercapacitor devices and electrodes. *Journal of Power Sources, 196*(1): 1-12.

235. Sotzing, G. A., Phend, J. N., Grubbs, R. H., and Lewis, N. S. (2000). Highly Sensitive Detection and Discrimination of Biogenic Amines Utilizing Arrays of Polyaniline/Carbon Black Composite Vapor Detectors. *Chemistry of Materials, 12*(3): 593-595.

236. Sreekumar, G., Frobel, P. G. L., Muneera, C. I., Sathiyamoorthy, K., Vijayan, C., and Chandrachur, M. (2009). Saturable and reverse saturable absorption and nonlinear refraction in nanoclustered Amido Black dye–polymer films under low power continuous wave He–Ne laser light excitation. *Journal of Optics A: Pure and Applied Optics, 11*(12): 125204.

237. Stankovich, S., Dikin, D. A., Dommett, G. H. B., Kohlhaas, K. M., Zimney, E. J., Stach, E. A., Piner, R. D., Nguyen, S. T., and Ruoff, R. S. (2006b). Graphene-based composite materials. *Nature, 442*(7100): 282-286.

238. Stankovich, S., Dikin, D. A., Piner, R. D., Kohlhaas, K. A., Kleinhammes, A., Jia, Y., Wu, Y., Nguyen, S. T., and Ruoff, R. S. (2007). Synthesis of graphene-based nanosheets via chemical reduction of exfoliated graphite oxide. *Carbon, 45*(7): 1558-1565.

239. Stankovich, S., Piner, R. D., Nguyen, S. T., and Ruoff, R. S. (2006a). Synthesis and exfoliation of isocyanate-treated graphene oxide nanoplatelets. *Carbon, 44*(15): 3342-3347.

240. Stejskal, J., and Sapurina, I. (2004). On the origin of colloidal particles in the dispersion polymerization of aniline. *Journal of Colloid and Interface Science, 274*(2): 489-495.

241. Stejskal, J., Kratochvíl, P., and Radhakrishnan, N. (1993). Polyaniline dispersions 2. UV—Vis absorption spectra. *Synthetic Metals*, 61(3): 225-231.

242. Su, Q., Pang, S., Alijani, V., Li, C., Feng, X., and Müllen, K. (2009). Composites of Graphene with Large Aromatic Molecules. *Advanced Materials, 21*(31): 3191-3195.

243. Su, S., Chen, B., He, M., Hu, B., and Xiao, Z. (2014). Determination of trace/ultratrace rare earth elements in environmental samples by ICP-MS after magnetic solid phase extraction with Fe3O4@SiO2@polyaniline–graphene oxide composite. *Talanta, 119*: 458-466.

244. Sun, M., Tang, Q., Zhang, T., and Wang, G. (2014). Rational synthesis of novel π-conjugated poly(1,5-diaminoanthraquinone) for high-performance supercapacitors. *RSC Advances, 4*(15): 7774-7779.

245. Sun, X., Xiong, Y., Chen, P., Lin, J., Ji, W., Lim, J. H., ang, S. S., Hagan, D. J., and Van Stryland, E. W. (2000). Investigation of an Optical Limiting Mechanism in Multiwalled Carbon Nanotubes. *Applied Optics, 39*(12): 1998-2001.

246. Sun, W., Shi, S., and Yao, T. (2011). Graphene oxide-Ru complex for label-free assay of DNA sequence and potassium ions via fluorescence resonance energy transfer. *Analytical Methods*, 3(11): 2472-2474.

247. Sutherland, R. L. (2003). *Handbook of Nonlinear Optics* (2nd ed.). Marcel Dekker: New York.

248. Tadros, P., Armes, S. P., and Luk, S. Y. (1992). Preparation and characterisation of polyaniline colloids using a monodisperse poly(ethylene oxide)-based steric stabiliser. *Journal of Materials Chemistry, 2*(1): 125-130.

249. Tang, C. W. (1986). Two-layer organic photovoltaic cell. *Applied Physics Letters, 48*(2): 183-185.

250. Tang, J., Niu, L., Liu, J., Wang, Y., Huang, Z., Xie, S., et al. (2014). Effect of photocurrent enhancement in porphyrin–graphene covalent hybrids. *Materials Science and Engineering: C, 34*: 186-192.

251. Tauc, J. (1970) In A. Abeles (ed.). *Optical properties of solids* (p. 227) Amsterdam: North Holland.

252. Tsai, K.-W., Guo, T.-F., Jen, A. K. Y., and Wen, T.-C. (2014). Role of self-assembled tetraoctylammonium bromide on various conjugated polymers in polymer light-emitting diodes. *Journal of Materials Chemistry C, 2*(2): 272-276.

253. Tseng, H.-R., Phan, H., Luo, C., Wang, M., Perez, L. A., Patel, S. N., Ying, L., Kramer, E. J., Nguyen, T.-Q., Bazan, G. C., and Heeger, A. J. (2014). High-Mobility Field-Effect Transistors Fabricated with Macroscopic Aligned Semiconducting Polymers. *Advanced Materials*, DOI: 10.1002/adma.201305084.

254. Tuan Anh, P., Byung Choon, C., and Yeon Tae, J. (2010). Facile covalent immobilization of cadmium sulfide quantum dots on graphene oxide nanosheets: preparation, characterization, and optical properties. *Nanotechnology, 21*(46): 465603.

255. Tutt, L. W., and Boggess, T. F. (1993). A review of optical limiting mechanisms and devices using organics, fullerenes, semiconductors and other materials. *Progress in Quantum Electronics, 17*(4): 299-338.

256. Valdes, L. B. (1954). Resistivity Measurements on Germanium for Transistors, In *Proc. IRE*, 1954, pp. 420-427.

257. Varshney, S., Ohlan, A., Jain, V. K., Dutta, V. P., and Dhawan, S. K. (2014). Synthesis of ferrofluid based nanoarchitectured polypyrrole composites and its application for electromagnetic shielding. *Materials Chemistry and Physics, 143*(2): 806-813.

258. Vivien, L., Anglaret, E., Riehl, D., Hache, F., Bacou, F., Andrieux, M., Lafonta, F., Journet, C., Goze, C., Brunet, M., and Bernier, P. (2000a). Optical limiting properties of singlewall carbon nanotubes. *Optics Communications, 174*(1–4): 271-275.

259. Vivien, L., Lançon, P., Riehl, D., Hache, F., and Anglaret, E. (2002). Carbon nanotubes for optical limiting. *Carbon, 40*(10): 1789-1797.

260. Vivien, L., Riehl, D., Anglaret, E., and Hache, F. (2000b). Pump-probe experiments at 1064 nm in singlewall carbon nanotube suspensions., *IEEE Journal of Quantum Electronics, 36*(6): 680-686.

261. Wang, A., Long, L., Zhao, W., Song, Y., Humphrey, M. G., Cifuentes, M. P., Wu, X., Fu, Y., Zhang, D., Li, X., and Zhang, C (2013). Increased optical nonlinearities of graphene nanohybrids covalently functionalized by axially-coordinated porphyrins. *Carbon*, 53: 327-338.

262. Wang, F., Gu, H., and Swager, T. M. (2008). Carbon Nanotube/Polythiophene Chemiresistive Sensors for Chemical Warfare Agents. *Journal of the American Chemical Society, 130*(16): 5392-5393.

263. Wang, G., Xing, W., and Zhuo, S. (2012a). The production of polyaniline/graphene hybrids for use as a counter electrode in dye-sensitized solar cells. *Electrochimica Acta, 66*: 151-157.

264. Wang, G., Yang, Z., Li, X., and Li, C. (2005). Synthesis of poly(aniline-co-o-anisidine)-intercalated graphite oxide composite by delamination/reassembling method. *Carbon, 43*(12): 2564-2570.

265. Wang, G., Zhuo, S., and Xing, W. (2012b). Graphene/polyaniline nanocomposite as counter electrode of dye-sensitized solar cells. *Materials Letters, 69*: 27-29.

266. Wang, H., Hao, Q., Yang, X., Lu, L., and Wang, X. (2009). Graphene oxide doped polyaniline for supercapacitors. *Electrochemistry Communications, 11*(6): 1158-1161.

267. Wang, J. (2009). Broadband nonlinear optical response of graphene dispersions. *Advanced Materials., 21*: 2430-2435.

268. Wang, J., and Blau, W. J. (2008). Linear and nonlinear spectroscopic studies of phthalocyanine-carbon nanotube blends. *Chemical Physics Letters, 465*(4–6): 265-271.

269. Wang, J., and Musameh, M. (2005). Carbon-nanotubes doped polypyrrole glucose biosensor. *Analytica Chimica Acta, 539*(1–2): 209-213.

270. Wang, X., Zhi, L., and Mullen, K. (2007). Transparent, Conductive Graphene Electrodes for Dye-Sensitized Solar Cells. *Nano Letters, 8*(1): 323-327.

271. Wang, Y., and Jing, X. (2005). Intrinsically conducting polymers for electromagnetic interference shielding. *Polymers for Advanced Technologies, 16*(4): 344-351.

272. Webster, S., Reyes-Reyes, M., Pedron, X., López-Sandoval, R., Terrones, M., and Carroll, D. L. (2005). Enhanced Nonlinear Transmittance by Complementary Nonlinear Mechanisms: A Reverse-Saturable Absorbing Dye Blended with Nonlinear-Scattering Carbon Nanotubes. *Advanced Materials, 17*(10): 1239-1243.

273. Wei, Z., Zhang, L., Yu, M., Yang, Y., and Wan, M. (2003). Self-Assembling Sub-Micrometer-Sized Tube Junctions and Dendrites of Conducting Polymers. *Advanced Materials*, 15(16): 1382-1385.

274. Wei, Z., Zhang, Z., and Wan, M. (2002). Formation Mechanism of Self-Assembled Polyaniline Micro/Nanotubes. *Langmuir, 18*(3): 917-921.

275. Williams, J. R., DiCarlo, L., and Marcus, C. M. (2007). Quantum Hall Effect in a Gate-Controlled p-n Junction of Graphene. *Science, 317*(5838): 638-641.

276. Wu, C.-G., and Bein, T. (1994). Conducting Polyaniline Filaments in a Mesoporous Channel Host. *Science, 264*(5166): 1757-1759.

277. Wu, G., Li, L., Li, J.-H., and Xu, B.-Q. (2005). Polyaniline-carbon composite films as supports of Pt and PtRu particles for methanol electrooxidation. *Carbon, 43*(12): 2579-2587.

278. Wu, T.-M., and Lin, Y.-W. (2006). Doped polyaniline/multi-walled carbon nanotube composites: Preparation, characterization and properties. *Polymer, 47*(10): 3576-3582.

279. Wu, W., Zhang, S., Li, Y., Li, J., Liu, L., Qin, Y., Guo, Z.-X., Dai, L., Ye, C., and Zhu, D. (2003). PVK-Modified Single-Walled Carbon Nanotubes with Effective Photoinduced Electron Transfer. *Macromolecules, 36*(17): 6286-6288.

280. Xiaoming, W., Huaqiang, C., Baojun, L., and Gui, Y. (2011). The synthesis and fluorescence quenching properties of well soluble hybrid graphene material covalently functionalized with indolizine. *Nanotechnology, 22*(7): 075202.

281. Xiong, S., Yang, F., Jiang, H., Ma, J., and Lu, X. (2012). Covalently bonded polyaniline/fullerene hybrids with coral-like morphology for high-performance supercapacitor. *Electrochimica Acta, 85*: 235-242.

282. Xu, J., Wang, K., Zu, S.-Z., Han, B.-H., and Wei, Z. (2010). Hierarchical Nanocomposites of Polyaniline Nanowire Arrays on Graphene Oxide Sheets with Synergistic Effect for Energy Storage. *ACS Nano, 4*(9): 5019-5026.

283. Xu, J., Yao, P., Li, X., and He, F. (2008). Synthesis and characterization of water-soluble and conducting sulfonated polyaniline/para-phenylenediamine-functionalized multi-walled carbon nanotubes nano-composite. *Materials Science and Engineering: B, 151*(3): 210-219.

284. Xu, J., Yao, P., Wang, Y., He, F., and Wu, Y. (2009). Synthesis and characterization of HCl doped polyaniline grafted multi-walled carbon nanotubes core-shell nano-composite. *Journal of Materials Science: Materials in Electronics, 20*(6): 517-527.

285. Xu, Y., Bai, H., Lu, G., Li, C., and Shi, G. (2008). Flexible Graphene Films via the Filtration of Water-Soluble Noncovalent Functionalized Graphene Sheets. *Journal of the American Chemical Society, 130*(18): 5856-5857.

286. Xu, Y., Liu, Z., Zhang, X., Wang, Y., Tian, J., Huang, Y., Ma, Y., Zhang, X., and Chen, Y. (2009). A Graphene Hybrid Material Covalently Functionalized with Porphyrin: Synthesis and Optical Limiting Property. *Advanced Materials, 21*(12): 1275-1279.

287. Yan, J., Wei, T., Shao, B., Fan, Z., Qian, W., Zhang, M., and Wei, F. (2010). Preparation of a graphene nanosheet/polyaniline composite with high specific capacitance. *Carbon, 48*(2): 487-493.

288. Yang, C.-H., Chih, Y.-K., Cheng, H.-E., and Chen, C.-H. (2005). Nanofibers of self-doped polyaniline. *Polymer*, 46(24): 10688-10698.

289. Yang, H. (2012). "Saturable absorption and two photon absorption in graphene" Ph. D. thesis, National University of Singapore, Singapore.

290. Yang, H., Li, F., Shan, C., Han, D., Zhang, Q., Niu, L., and Ivaska, A. (2009b). Covalent functionalization of chemically converted graphene sheets via silane and its reinforcement. *Journal of Materials Chemistry, 19*(26): 4632-4638.

291. Yang, H., Shan, C., Li, F., Han, D., Zhang, Q., and Niu, L. (2009a). Covalent functionalization of polydisperse chemically-converted graphene sheets with amine-terminated ionic liquid. *Chemical Communications*(26): 3880-3882.

292. Yang, W., Chen, G., Shi, Z., Liu, C.-C., Zhang, L., Xie, G., Cheng, M., Wang, D., Yang, R., Shi, D., Watanabe, K., Taniguchi, T., Yao, Y., Zhang, Y., and Zhang, G. (2013). Epitaxial growth of single-domain graphene on hexagonal boron nitride. *Nature Materials, 12*(9): 792-797.

293. Yang, Z.-L., Chen, H.-Z., Cao, L., Li, H.-Y., and Wang, M. (2004). Synthesis and photoconductivity study of carbon nanotube bonded by tetrasubstituted amino manganese phthalocyanine. *Materials Science and Engineering: B, 106*(1): 73-78.

294. Yang, Z., Pu, H., Yuan, J., Wan, D., and Liu, Y. (2008). Phthalocyanines–MWCNT hybrid materials: Fabrication, aggregation and photoconductivity properties improvement. *Chemical Physics Letters, 465*(1–3): 73-77.

295. Yao, P., Xu, J., Wang, Y., and Zhu, C. (2009). Preparation and characterization of soluble and DBSA doped polyaniline grafted multi-walled carbon nanotubes nano-composite. *Journal of Materials Science: Materials in Electronics, 20*(9): 891-898.

296. Yong-Xi, L., Jinhui, Z., Yu, C., Jinjuan, Z., Jun, W., Bin, Z., Ying, H., and Werner, J. B. (2011). Synthesis and strong optical limiting response of graphite oxide covalently functionalized with gallium phthalocyanine. *Nanotechnology, 22*(20): 205704.

297. Yu, D., Yang, Y., Durstock, M., Baek, J.-B., and Dai, L. (2010). Soluble P3HT-Grafted Graphene for Efficient Bilayer−Heterojunction Photovoltaic Devices. *ACS Nano, 4*(10): 5633-5640.

298. Yuan, W. Z., Lam, J. W. Y., Shen, X. Y., Sun, J. Z., Mahtab, F., Zheng, Q., and Tang, B. Z. (2009). Functional Polyacetylenes Carrying Mesogenic and Polynuclear Aromatic Pendants: Polymer Synthesis, Hybridization with Carbon Nanotubes, Liquid Crystallinity, Light Emission, and Electrical Conductivity. *Macromolecules, 42*(7): 2523-2531.

299. Yue, J., Wang, Z. H., Cromack, K. R., Epstein, A. J., and MacDiarmid, A. G. (1991). Effect of sulfonic acid group on polyaniline backbone. *Journal of the American Chemical Society, 113*(7): 2665-2671.

300. Zhang, B., Chen, Y., Ren, Y., Xu, L.-Q., Liu, G., Kang, E.-T., Wang, C., Zhu, C.-X., and Neoh, K.-G. (2013). In Situ Synthesis and Nonvolatile Rewritable-Memory Effect of Polyaniline-Functionalized Graphene Oxide. *Chemistry – A European Journal, 19*(20): 6265-6273.

301. Zhang, F., Johansson, M., Andersson, M. R., Hummelen, J. C., and Inganäs, O. (2002). Polymer Photovoltaic Cells with Conducting Polymer Anodes. *Advanced Materials, 14*(9): 662-665.

302. Zhang, K., Zhang, L. L., Zhao, X. S., and Wu, J. (2010). Graphene/Polyaniline Nanofiber Composites as Supercapacitor Electrodes. *Chemistry of Materials, 22*(4): 1392-1401.

303. Zhang, L., and Wan, M. (2005). Chiral polyaniline nanotubes synthesized via a self-assembly process. *Thin Solid Films, 477*(1–2): 24-31.

304. Zhang, L., and Wan, M. (2003). Self-Assembly of Polyaniline—From Nanotubes to Hollow Microspheres. *Advanced Functional Materials, 13*(10): 815-820.

305. Zhang, L., Long, Y., Chen, Z., and Wan, M. (2004). The Effect of Hydrogen Bonding on Self-Assembled Polyaniline Nanostructures. *Advanced Functional Materials, 14*(7): 693-698.

306. Zhang, Q., Sun, H., Wang, X., Zhu, Z., Liang, W., Li, A., Wen, S., and Deng, W. (2013). Conjugated Microporous Polymer-Derived Porous Hard Carbon as High-Rate Long-Life Anode Materials for Lithium Ion Batteries. *Energy Technology, 1*(12): 721-725.

307. Zhang, W. L., Liu, Y. D., and Choi, H. J. (2012). Fabrication of semiconducting graphene oxide/polyaniline composite particles and their electrorheological response under an applied electric field. *Carbon, 50*(1): 290-296.

308. Zhang, X., Goux, W. J., and Manohar, S. K. (2004). Synthesis of Polyaniline Nanofibers by "Nanofiber Seeding". *Journal of the American Chemical Society, 126*(14): 4502-4503.

309. Zhang, X., Liu, Z., Huang, Y., Wan, X., Tian, J., Ma, Y., and Chen, Y. (2009a). Synthesis, Characterization and Nonlinear Optical Property of Graphene-C_{60} Hybrid. *Journal of Nanoscience and Nanotechnology, 9*(10): 5752-5756.

310. Zhang, X., Zhang, J., and Liu, Z. (2005). Tubular composite of doped polyaniline with multi-walled carbon nanotubes. *Applied Physics A, 80*(8): 1813-1817.

311. Zhang, X.-L., Zhao, X., Liu, Z.-B., Liu, Y.-S., Chen, Y.-S., and Tian, J.-G. (2009b). Enhanced nonlinear optical properties of graphene-oligothiophene hybrid material. *Optics Express, 17*(26): 23959-23964.

312. Zhang, Y.-S., Xu, W.-H., Yao, W.-T., and Yu, S.-H. (2009). Oxidation−Reduction Reaction Driven Approach for Hydrothermal Synthesis of Polyaniline Hollow Spheres with Controllable Size and Shell Thickness. *The Journal of Physical Chemistry C, 113*(20): 8588-8594.

313. Zhao, X., Yan, X.-Q., Ma, Q., Yao, J., Zhang, X.-L., Liu, Z.-B., and Tian, J.-G. (2013). Nonlinear optical and optical limiting properties of graphene

hybrids covalently functionalized by phthalocyanine. *Chemical Physics Letters, 577*: 62-67.

314. Zheng, C., Ye, X. Y., Cai, S. G., Wang, M. J., and Xiao, X. Q. (2010). Observation of nonlinear saturable and reverse-saturable absorption in silver nanowires and their silica gel glass composite. *Applied Physics B, 101*(4): 835-840.

315. Zhou, M., Wang, Y., Zhai, Y., Zhai, J., Ren, W., Wang, F., and Dong, S. (2009). Controlled Synthesis of Large-Area and Patterned Electrochemically Reduced Graphene Oxide Films. *Chemistry – A European Journal, 15*(25): 6116-6120.

316. Zhou, S., Zhang, H., Zhao, Q., Wang, X., Li, J., and Wang, F. (2013). Graphene-wrapped polyaniline nanofibers as electrode materials for organic supercapacitors. *Carbon, 52*: 440-450.

317. Zhou, X., Cao, Y., Wang, X.-Y., Guo, Z.-H., Wang, J.-Y., and Pei, J. (2014). Tuning the Charge-Transport Property of Pyromellitic Diimide-Based Conjugated Polymers towards Efficient Field-Effect Transistors. *Asian Journal of Organic Chemistry, 3*(2): 209-215.

318. Zhu, C., Guo, S., Fang, Y., and Dong, S. (2010). Reducing Sugar: New Functional Molecules for the Green Synthesis of Graphene Nanosheets. *ACS Nano, 4*(4): 2429-2437.

319. Zhu, J., Chen, M., Qu, H., Zhang, X., Wei, H., Luo, Z., Colorado, H. A., Wei, S., and Guo, Z. (2012). Interfacial polymerized polyaniline/graphite oxide nanocomposites toward electrochemical energy storage. *Polymer, 53*(25): 5953-5964

320. Zhu, J., Li, Y., Chen, Y., Wang, J., Zhang, B., Zhang, J., and Blau, W. J. (2011). Graphene oxide covalently functionalized with zinc phthalocyanine for broadband optical limiting. *Carbon*, 49(6): 1900-1905.

321. Zhu, Y., Higginbotham, A. L., and Tour, J. M. (2009). Covalent Functionalization of Surfactant-Wrapped Graphene Nanoribbons. *Chemistry of Materials, 21*(21): 5284-5291.